A new design methodology for composite materials exposed to humid, high temperature environments.

Adams, Richard

A thesis submitted for the degree of Doctor of Phillosophy in the Faculty of Engineering, Swansea University

2010

Swansea University
Prifysgol Abertawe

A NEW DESIGN METHODOLOGY FOR COMPOSITE MATERIALS EXPOSED TO HUMID, HIGH TEMPERATURE ENVIRONMENTS

By

Mr Richard Adams BEng (Hons) MRes CEng MIMMM GradWeldI
Stress Group Leader, Composite Boxes Research, Airbus Operations Ltd.

AIRBUS OPERATIONS: AN EADS COMPANY

ABSTRACT

Moisture ingress and thermal effects on carbon fibre reinforced plastic is a well understood phenomenon. For aircraft structures where safety is paramount this results in the use of worst case material properties, known as HOT/WET properties. In reality most structures are not fully saturated and are therefore penalised by using these worst case properties. This project attempts to fully understand the environmental effect on mechanical performance and accurately model a structures exposure to the environment, while still maintaining conservatism, to realise structural weight savings for aircraft. From the literature study it appears that this is the first attempt to link the mechanical property degradation brought about by environment, to classical laminate theory. By modelling individual ply property performance, based on each ply's level of saturation and linking it to a bespoke set of materials properties generated within the project, it is possible to accurately model the mechanical performance of a component. The model and modelling process derived within this project have been successfully validated by structural testing.

ACKNOWLEDGMENTS

The author would like to express gratitude to the academic supervisor Professor Steve Brown, for his invaluable support with this PhD and also the running of the EMOC programme between Airbus Operations, Swansea University and EADS Innovation Works. Secondly to Airbus Operations for agreeing to sponsor this PhD and its ongoing support to the EMOC project. Additional thanks to Mr Russell Older, Dr Matt Jevons & Mr Rob Ferguson (Airbus Operations).

Special thanks to my family for their support throughout the project, especially to my wife Rhiannon who has had to look after my son on her own while completing this thesis and also to my son William, who has had to make do without me whilst writing up.

TABLE OF CONTENTS

LIST OF FIGURES

LIST OF TABLES

GLOSSARY OF ABBREVIATIONS

A/C:	Aircraft
AD:	Anderson Darling
AECMA:	European Association of Aerospace Industries
AISP:	Airbus Industrie Specification
AITM:	Airbus Industrie Test Method
ALCAS:	Advanced Low Cost Aircraft Structure (EU framework 6 project)
ASTM:	American Society for the Testing of Materials
ATL:	Automatic Tape Layer
BVID:	Barely Visible Impact Damage
CAD:	Computer Aided Design
CAI:	Compression after Impact
CAT 2:	Fully traceable documentation of testing
CFRP:	Carbon Fibre Reinforced Plastic
CLA:	Classical Laminate Theory
COLD/WET:	Low Temperature (typically -55/60°C)/fully saturated material
DLB:	Double Lap Bearing
EKDF:	Environmental Knock-Down Factor
ELAP:	Environmental Laminate Analysis Program
ELAP 1D:	Environmental Laminate Analysis Program one dimensional model
EMOC:	Environmental Modelling of Composites (Airbus/Swansea project)
ESDU:	Engineering Science Data Unit
FD	Finite Difference
FE:	Finite Element
FEA:	Finite Element Analysis
FHC:	Filled-Hole Compression
GFEM:	Global Finite Element Model
GUI:	Graphical User Interface
HOT/WET:	High Temperature (typically 90°C)/fully saturated material
HTP:	Horizontal Tail Plane
HTS	High Tensile Strength
IPSS:	In-Plane Shear Strength
LAP:	Laminate Analysis Program
LVDT:	Linear Variable Displacement Transducer
LE:	Leading Edge

LG:	Landing Gear
MRes:	Master of Research
NASA:	National Aeronautical Space Administration
MNR:	Maximum Normal Residual
OHC:	Open-Hole Compression
OHT:	Open-Hole Tension
OSL:	Observed Level of Significance
PEEK:	Polyether Ether Ketone
PPS:	Polyphenylene Sulfide
PR1:	Supporting PhD Project 1
PR2:	Supporting PhD Project 2
PSM	Parallel Stiffness Model
RA:	Research Assistant
RBE:	Rigid Body Element
RF:	Reserve Factor
RH:	Relative Humidity
RT:	Room Temperature (typically 21-23^{o}C)
RT/DRY:	Room Temperature/ Dry material
SLB:	Single Lap Bearing
TANGO:	Technology Application to the Near-Term Business Goals and Objectives (EU framework 6 project)
TE:	Trailing Edge
UD:	Unidirectional (with respect to composite ply orientation)
USAF:	United States Air Force
VTP:	Vertical Tail Plane

1. INTRODUCTION

1.1 Operating Environment

Carbon Fibre Reinforced Plastics (CFRP) must be designed to operate in various environments. For metallic materials general operating temperatures can be relatively high, in excess of 400°C depending on the material being used. In contrast, composite components are made up of fibres and a polymeric matrix (depending on the resin system, a polymeric material typically cured at 180°C) and cannot withstand temperatures in excess of their cure temperature.

A typical airliner has a large environmental envelope in which it has to operate; this is typically between –60°C & 150°C. At these temperature extremes a human being would be unable to survive, especially if one considers the air density of the atmosphere throughout the flight cycle. A typical example of these extremes would be the wing skin of an aircraft parked on an Apron in a tropical country where solar loading effects could cause localised surface temperatures to reach this limit. As temperature increases the resin stiffness and subsequent strength decreases. In addition aircraft structures operate in varying humidities from 0-100%. Here 0% represents a dry environment containing no moisture in the air, whereas 100% humidity would represent submersion in water. The critical point here is that the matrix resins used in construction of these aircraft components are subject to moisture ingress. As moisture is absorbed by the structure it reduces the stiffness of the component and therefore reduces its strength. In addition moisture ingress damages the structure, as it may react at a chemical level with the resin, permanently altering the molecular structure of the matrix. If the effects of moisture ingress and temperature are combined there is a significant reduction in material strength.

Furthermore, although we have now defined the upper limit of the hostile environment it is also necessary to consider the low temperature extreme. In flight the aircraft operates in the upper atmosphere where temperatures can be as low as –60°C. The humidity here can be very low. In a lower temperature environment the matrix will become very stiff and can become brittle, showing that these components must be designed to withstand both extremes.

Although the example above is specific to aerospace similar operating conditions can be found across British industry e.g. oil pipelines that see high and low temperatures,

exposed to 100% humidity and also deep sea marine environments where components can be subjected to full saturation in low temperature sea water operating at high pressures.

1.2 Innovation

Again using aircraft structures as an example, structural components have to be designed with a safety factor to ensure that they do not fail in service. Typically the worst case material properties can be assumed to be those arising from the reduction in stiffness brought about by high temperature and full saturation by moisture, known as HOT/WET design allowables. Use of these conservative material properties was valid in the past, as composite structures were relatively thin and used in low loaded secondary structures, therefore likely to reach full saturation when exposed to elevated temperatures. However use of composite materials in high loaded primary structure components with greater thickness has steadily increased. Moisture transport through the structure can be considered to be a relatively slow process and Airbus considers structures with a thickness greater than 8mm, never to reach saturation. With thicknesses in excess of 100mm saturation will never be achieved with only a small percentage of the outer plies of the component becoming saturated. Clearly, designing to full saturation is too conservative. At present there is no tool or modelling capability available to be able to predict mechanical properties of composites exposed to varying environmental conditions and therefore accurate stress prediction for components is not possible. This inevitably results in over engineered structures, which are inefficient.

Such a tool is being developed by the author (accounting for Airbus Operations's involvement), in association with Swansea University. The development of such a tool would represent highly significant innovation. It would permit a more realistic, more efficient and less conservative design approach. Moreover, where safety is considered the key driver, the tool will provide more confidence.

This project is specifically designed to evaluate and further develop the proposed tool for aerospace structural components. The focus will be on airliner wing, primary structural components. The definition of primary structure is being high loaded, critical structure, designed to carry the main forces on the wing imposed in flight. The tool will be used to predict moisture levels and subsequent material strengths allowing stress analysis to be carried out. Once the analysis has been carried out the results will be compared to the current design approach. Reductions in component thickness are

expected and subsequent weight savings will be the result. An example of this is provided in section 1.3.

1.3 Introduction to the Approach

It is known that the level of saturation in a component is thickness related. Thus, the thicker the component the larger the potential weight saving, as thick structures have mechanical properties closer to dry material than the HOT/WET mechanical properties. To illustrate this potential weight saving consider figure 1. Here a comparison is made to room temperature dry material properties and HOT/WET material properties. In terms of weight it can be seen that there is up to a 30% increase in weight for all components when designing using the HOT/WET criterion. There is a potentially enormous weight saving that could be made. If the novel design approach proposed here is successful it should deliver very significant weight savings (≤30%) for thick laminates.

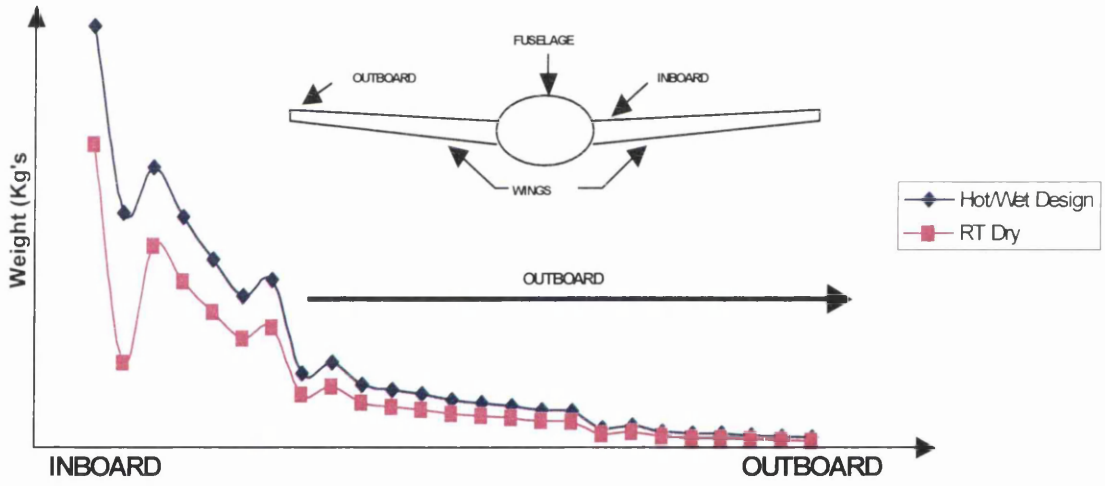

Figure 1 Comparison Between Hot/Wet & Room Temperature (RT) Dry Materials Properties in Terms of Rib Weight for a Typical Airliner Wing

An example is illustrated by figure 1: For an inboard (inboard is the point at which the wing attaches to the fuselage and outboard is at the wing tip) thick section wingbox component, the weight saving could be up to 30%. If this were the case for all wingbox components an estimated weight saving of 30% would result in a reduction in excess of 5% saving in fuel consumption. For an A330 size aircraft flying from London to New York, this could result in reduced fuel burn in excess of 1800kg per flight, equivalent to in excess of ~5 tonnes of CO_2/per flight. In short, reduced economic running costs for

the operator, significantly reduced environmental effects and reduced material usage in manufacture may all be attainable.

2. LITERATURE REVIEW

2.1 Carbon Fibre Reinforced Plastics

The definition of a composite material is that it is formed by the combination of two or more distinct materials to form a new material with enhanced properties. This can be a material such as concrete, which combines cement and rock/stone components to form a material having similar characteristics to a rock yet being easily moulded into different and sometimes complex shapes, which would take significantly longer to fabricate from solid rock. Typically composites are made of fibres with a binder that holds the fibres together. The oldest composite material could be considered to be wood, which consists of cellulose fibres in a lignin matrix. Similarly a human bone is made up of fibre like osteons imbedded in an interstitial bone matrix [1]. A more modern example of composites could be considered to be fibreglass boats, being typically made up of a polyester resin, which is reinforced by glass fibres. A further variation on this basic concept could include sandwich structures where a light core material is sandwiched between two faces of strong stiff material [1]. This sandwich structure if often found on Airbus aircraft, generally applicable to secondary structures, where it provides a light weight, strong solution compared to a conventional metallic approach.

Fibre reinforcement is a generally preferred form for composite materials as most materials are stronger in fibre form than in their bulk form. For example glass typically has fewer defects in its fibre form than in its bulk form. The high strength of polymeric fibres, such as aramid, is attributed to the alignment of the polymer chains along the fibre as opposed to the randomly entangled arrangement in the bulk polymer [1].

The main factor that drives the use of composites in aerospace is weight reduction, however composites also have advantages in their corrosion resistance, part count reduction, wear resistance, enhanced fatigue life, thermal acoustical insulation, low thermal expansion, low or high thermal conductivity etc. However, weight is the key for Airbus aircraft and any aerospace application. Typically these materials provide a lower weight solution, as their constituent parts are low density but more significantly fibres have higher values of strength-to-weight and stiffness to weight ratios than most materials. Figure 2, shows typical composite materials, comparing specific strength and stiffness of composite materials and metals.

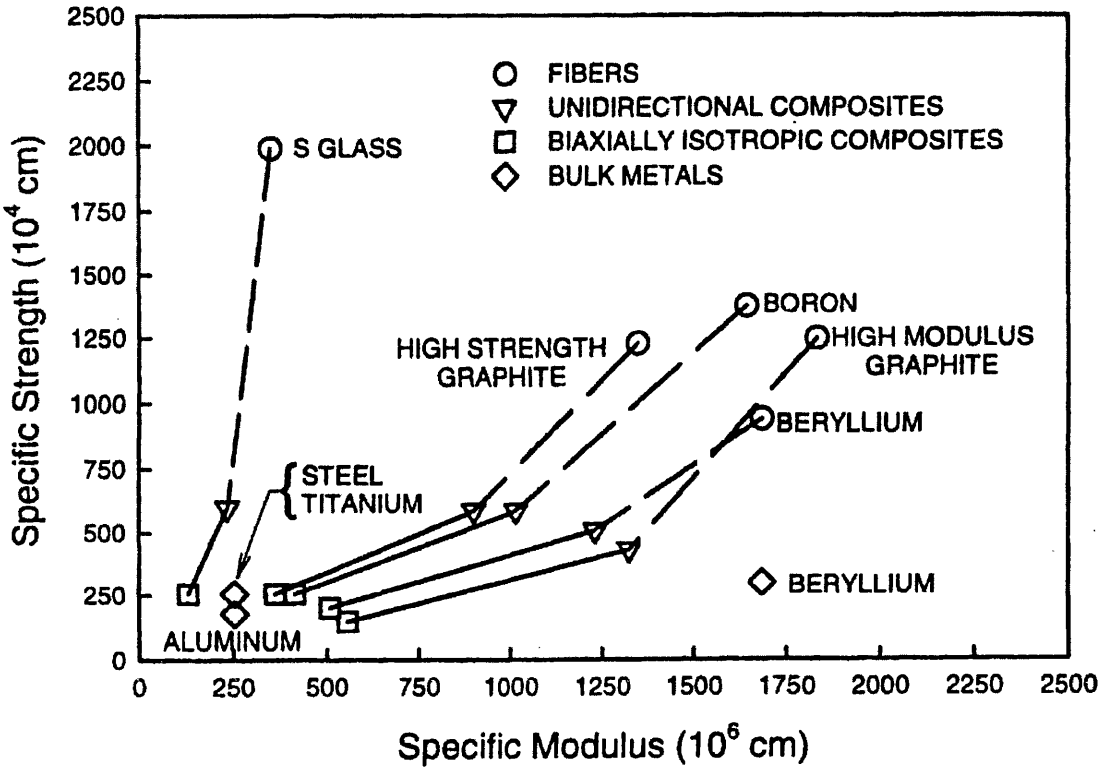

Figure 2 Comparison of Specific Strength and Stiffness of Composite Materials & Metals [1]

Generally speaking it is difficult to draw up a table of materials characteristics in order to assess the relative strengths and weaknesses of different materials, due to the fact that there are general families of materials, all having a broad range of mechanical and physical properties. Overall some more obvious advantages and disadvantages are [2]:

- Plastics are low density and generally have good short term chemical resistance but they lack thermal stability and only have moderate resistance to environmental degradation. They have relatively poor mechanical properties but are easily moulded, fabricated and joined.
- Ceramics can be low density, have excellent thermal stability and are resistant to most forms of chemical attack. Although intrinsically very rigid and strong because of their chemical bonding, they are brittle and are formed and shaped with relative difficulty.
- Metals are mostly of medium density, with only the likes of metals such as Aluminium competing with plastics in this respect. They generally have high toughness and good mechanical properties and they also have good thermal stability and can be made corrosion resistant through the use of alloying.

From an aerospace perspective the most commonly used composites are carbon and graphite, Kevlar and boron. Generally speaking as the fibre modulus increases the tensile strength decreases. Overall carbon fibre is generally considered to be the most versatile of the advanced reinforcements and the most widely used on aircraft structures. Typically carbon products are available in pre-impregnated unidirectional woven tapes or cloth or alternatively as dry fibres using resin films or resin injection processes to add the matrix during manufacture [3]. The matrices can be made of a variety of materials from plastics, metals and even ceramic materials, however with aerospace components epoxy resin (thermosetting polymer) is generally the benchmark matrix system used. With all thermosetting polymers the matrix is cured by means of time, temperature and pressure into a dense, low void content structure in which the fibre reinforcement is aligned in the direction of the predicted loads [3].

2.2 Composite versus Metallic

Composite materials from early demonstration could produce weight savings of 25-35% over Aluminium alloy construction, with the addition of fewer parts required for each application making composites appear extremely attractive. These basic advantages have placed pressure on the Aluminium manufacturers to improve the materials performance through advanced alloy systems such as Aluminium-Lithium alloys which have the advantage that they only require existing infrastructure to produce. In fact it is this lower cost that hampers composites, which have a high acquisition cost compared to Aluminium. Composites traditionally have labour intensive construction techniques and generally require large capital equipment outlay in order to set up a manufacturing facility. These labour intensive manufacturing processes represent an area where major research is being carried out to reduce costs and manufacturing time of components. An example of this is an automated tape laying machine (ATL), which can significantly cut the time and cost of producing composite components by a factor of ten or more [3]. ATL technology is extensively used within Airbus to manufacture horizontal and vertical tail planes (HTP & VTP respectively).

The use of composite materials began in the US in the early 1970 for the United States Air Force (USAF) with the National Aeronautics Space Administration (NASA) instigating a series of programmes to develop composite technology with the outcome of utilising composite materials in both primary and secondary structural designs in commercial services. This has resulted in aircraft manufacturers becoming more

comfortable with composite materials and associated efficient construction techniques. As demand increased the costs of the materials have been reduced [3].

Polycrystalline metals are isotropic in nature, having structural properties which are usually uniform in all directions (if you ignore certain metallic materials that have directed grain orientations etc.). Composites however are typically anisotropic, where a single ply has very high strength and stiffness in the axial direction but has marginal properties in the crosswise or transverse direction. This is represented in figure 3, which compares metals to composites.

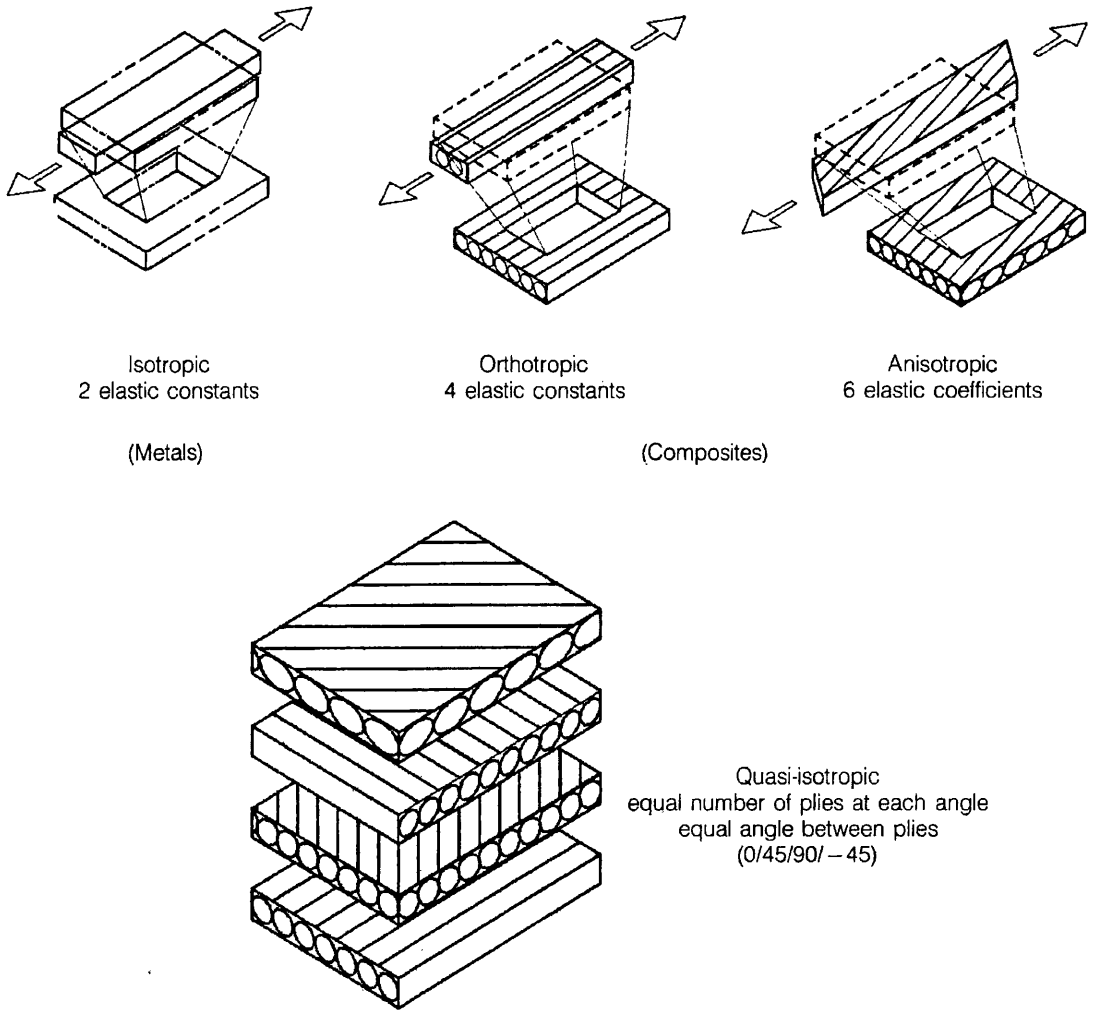

Figure 3 Composites versus Metallic [3]

Some general comparisons of Aluminium Alloy and composite characteristics and the relative advantages of thermosets, thermoplastics and metal are shown in tables 1 & 2. Composites differ from metals as their properties are not uniform in all directions, the

strength and stiffness can be tailored to the loading direction and they possess a greater variety of mechanical properties.

Table 1 Composite versus Metallic Mechanical Properties [3]

Condition		Composite Behaviour Relative to Metals
Load-Strain relationship		More Linear Strain to Failure
Notch Sensitivity	Static	Greater Sensitivity
	Fatigue	Less Sensitivity
Transverse Properties		Weaker
Mechanical Properties Variability		Higher
Sensitivity to Aircraft Hydrothermal Environment		Greater
Damage Growth Mechanism		In-Plane Delamination instead of through-thickness cracks

Table 2 Relative Advantages of Composite Thermoplastics, Composites Thermosets & Metallic [3]

Material Properties	Relative Advantage		
	Thermoplastics	Thermosets	Metal
Corrosion Resistance	XXX	XXX	X
Creep	XXX	XXX	X
Damage Resistance	XX	X	XXX
Design Flexibility	XXX	XXX	X
Fabrication	XX	XX	X
Fabrication Time	XXX	XX	X
Final Part Cost	XXX	XX	X
Finished Part Cost	XXX	XX	X
Moisture Resistance	XX	X	XXX
Physical Properties	XXX	XXX	XXX
Processing Cost	XXX	XX	X
Raw Material Cost	X	XX	XXX
Reusable Scrap	XX	-	XXX
Shelf Life	XXX	X	XXX
Solvent Resistance	XXX	XX	X
Specific Strength	XXX	XXX	X
Strength	XXX	XXX	X
Weight Saving	XXX	XX	0

Note: *XXX equals best, X equals worst and 0 equals baseline for comparison.*

The varying mechanical properties of different fibres are shown in figure 4 showing a comparison to Aluminium. The Aluminium material is significantly weaker than all of the composite fibres. Composites have a greater sensitivity to their environment, hence the need in this project to predict the properties under different environments. Typically strength and modulus is reduced as temperature and humidly increase. Composites are most often created in a two dimensional form, while metals may be utilised in billets, bars, forgings, castings etc. As mentioned previously composites generally have a better resistance to fatigue, an example of this is shown in figure 5, comparing typical

composite material fatigue behaviour to Aluminium. It can be seen that the composite materials typically have a flat 'SN' curve, meaning that increased cycles has little effect on the strength of the material over time. Finally propagation of damage through de-lamination occurs rather than classical through-thickness cracks exhibited in metals.

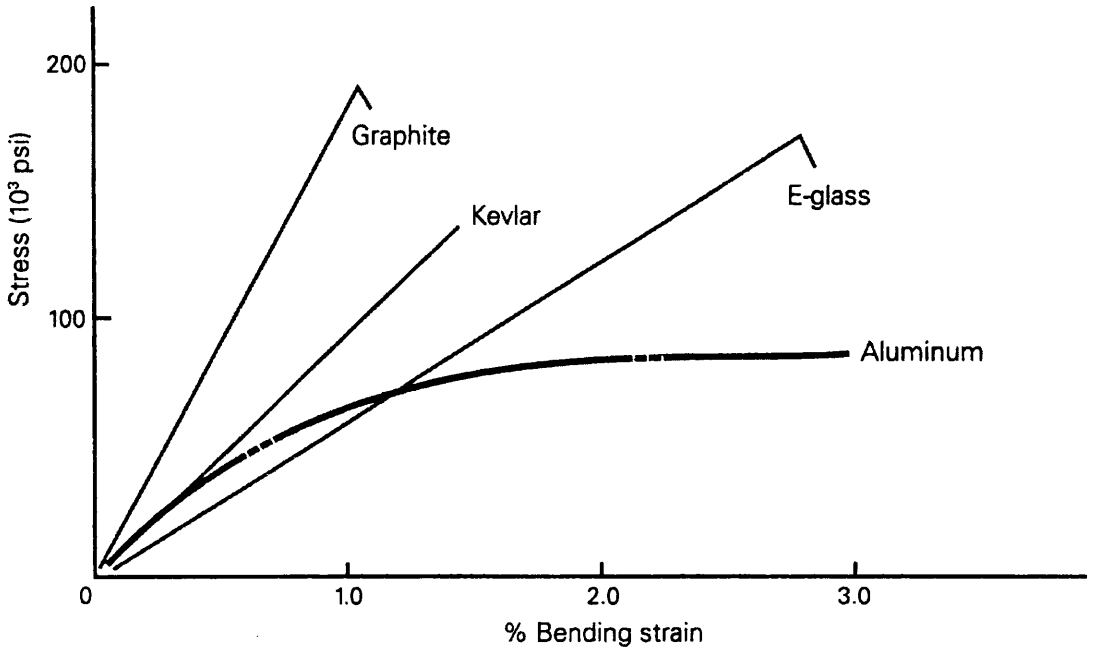

Figure 4 Epoxy Unidirectional Tapes Composites versus Metallic Stress Strain Curves Comparison [3]

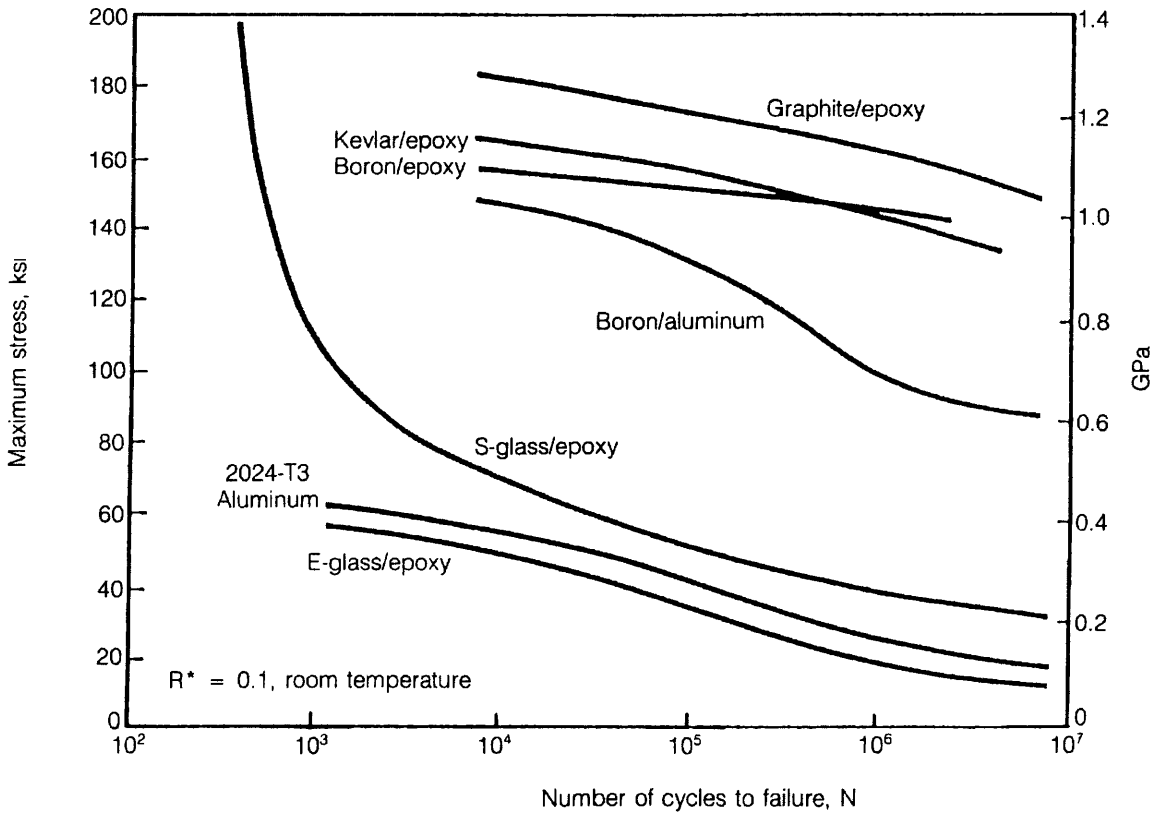

Figure 5 Fatigue Behaviour of Unidirectional Composites versus Aluminium [3]

There are however a number of disadvantages of using composites as opposed to metallic material. These are summarised below:

- Expensive Material Cost
- Lack of Established design allowables – typically for every new configuration matrix fibre combination design allowables will need to be generated.
- Corrosion problems can result from improper coupling to metals especially when carbon and graphite are used. In this case sealing the dissimilar material become essential.
- Degradation of mechanical properties at elevated temperature and humidities.
- Poor energy absorption and impact damage. This is shown in figure 6. This aspect is of particular importance as structures made of composite are difficult to repair and often impact damage cannot be seen by the naked eye.
- Require lightening strike protection for lateral wing boxes.
- Complicated and expensive inspection methods need to be employed. Coupled to this the ability to detect substandard bonds within the structure is difficult.
- Defects can and do occur within the structure yet it is difficult to know their location.

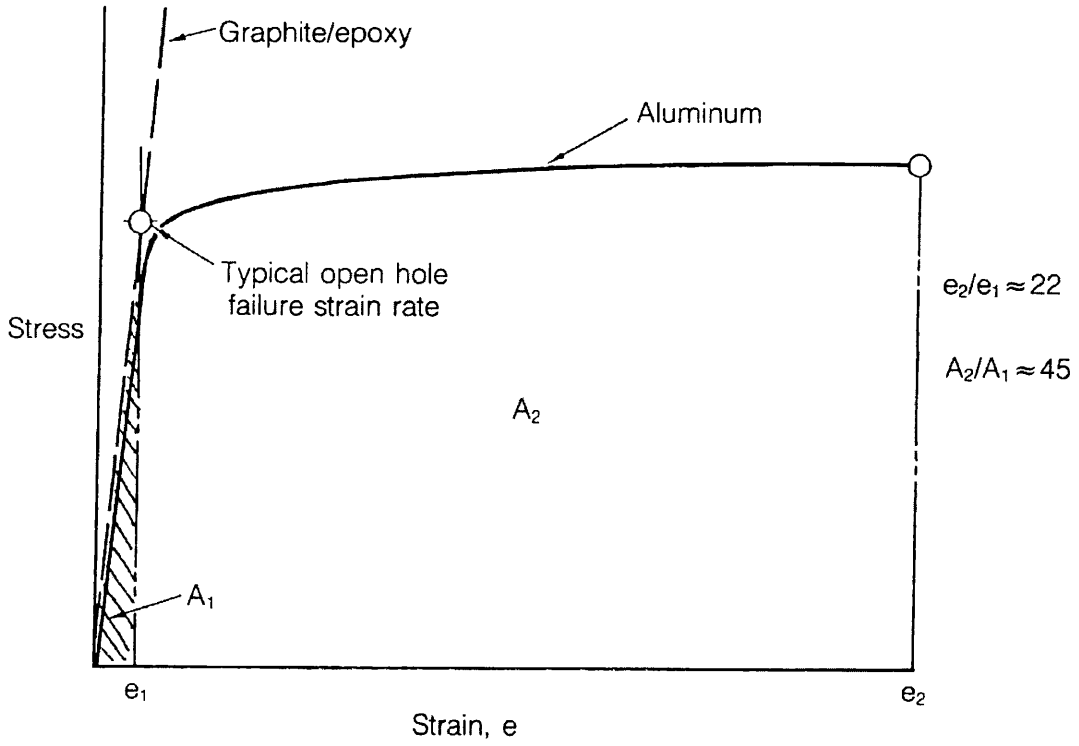

Figure 6 Stress/ Strain Relationship of Graphite/Epoxy & Aluminium [3]

The ability to preferentially orientate the properties of carbon fibre materials is one of the material's biggest advantages. This is where the laminate is orientated so that the majority of the fibres are orientated in the direction of loading and the proportion of transverse fibres is determined by the relative values of the biaxial loading components or torsional stiffness requirements. The quantification of these extreme directional characteristics is shown in table 3, which shows the range of weight reduction potentials of five classes of composite materials compared to an Aluminium Alloy.

Table 3 Comparison of Aluminium & Composite Materials Properties [3]

Material	Units		F^{tu} Ksi	F^{ty*} Ksi	F^{cu} Ksi	F^{cy*} Ksi	E^{c} Msi	F^{su**} Ksi	G^{**} Msi
7075-T6 Al. sheet, (B), ϱ=.101			80	73	—	72	10.5	48	3.9
Boron/Epoxy V_f = .5 ϱ = .0725	Uni-directional	Absolute	180	164	400	364	30	13/67	.7/7.8
		ratio	.319	.319	—	.142	.251	2.65/.514	/.359
	Quasi-isotropic	Absolute	55	50	146	133	10.8	21	2.5
		ratio	1.044	1.048	—	.389	.698	1.641	1.120
High strength C/EP V_f = .6 ϱ = .056	Uni-directional	Absolute	180	164	180	164	21	12/65	.65/5.5
		ratio	.246	.247	—	.243	.277	2.22/.409	/.393
	Quasi-isotropic	Absolute	65	59	65	59	7.6	22	1.88
		ratio	.682	.686	—	.677	.766	1.210	1.150
High Modulus C/EP V_f = .6 ϱ = .058	Uni-directional	Absolute	110	100	100	91	25	9/43	.65/6.5
		ratio	.418	.419	—	.454	.241	3.06/.641	/.344
	Quasi-isotropic	Absolute	39	35	36	33	8.7	14	2.1
		ratio	1.178	1.198	—	1.253	.693	1.969	1.066
Ultra-high Modulus C/EP V_f = .6 ϱ = .061	Uni-directional	Absolute	84	76	80	73	40	6/40	.6/10.1
		ratio	.575	.580	—	.596	.159	4.83/.725	/.233
	Quasi-isotropic	Absolute	30	27	28	25	14.1	21	5.4
		ratio	1.611	1.633	1.739	.450	1.380	1.380	.436
Intermediate Modulus C/EP V_f = .6 ϱ=.055	Uni-directional	Absolute	160	145	160	145	17	10/50	.65/4.5
		ratio	.272	.274	—	.270	.336	2.61/.523	/.472
	Quasi-isotropic	Absolute	60	54	60	54	63	18	1.6
		ratio	.726	.736	—	.726	.908	1.452	1.327

For shear strength or stiffness 100% of ±45 laminate properties are shown, as they represent the upper limit for shear properties. The ratio of specific shear strength or stiffness of Aluminium to that for the extremes of the composite properties are also shown. The average of these is identified as the mean ratio. The mean ratio represents the most likely measure of weight reduction to be expected from the use of composite material [3].

2.3 Resin Systems & the Matrix

The composition of the matrix, which binds the fibres together, is an important element in determining the material's mechanical behaviour. The selected matrix formulation will determine the material cure cycle and will affect such properties as creep, compressive & shear strengths, thermal resistance, moisture sensitivity and, ultraviolet

sensitivity all of which are resin dominated material properties affect the composite's long term stability. A summary of typical characteristics of a selection of composite matrices include [3]:

EPOXY

- Most Widely Used.
- Generally best structural characteristics.
- Temperature range typically up to 100°C.
- Easy to Process.
- Toughened versions are available.

BISMALEIMIDE

- Operating temperature up to 180°C.
- Easy to Process.
- Toughened version available.

POLYAMIDE

- Variety of matrix types.
- Can be used up to 320°C.
- Difficult to process.
- Expensive.

POLYESTER

- Relatively poor structural characteristics limiting usage to non structural parts.
- Easy to process.

PHENOLIC

- Same limitations as polyesters.
- More difficult to process.
- Better temperature capabilities than epoxies and polyesters.
- Low smoke generation.

THERMOPLASTICS

- Greater improved toughness.
- Unique Processing capabilities.
- Have processing difficulties.

Generally thermoplastics have a higher operating temperature and a shorter fabrication cycle reducing cost, combined with no need for a chemical cure. There is no refrigeration required for storage. They have increased fracture toughness and have a greater resistance to moisture absorption [3].

2.4 Thermoset Matrices

A thermoset matrix is formed by an irreversible chemical transformation of the resin system into an amorphous cross linked polymer matrix. Thermoset resins have low viscosity, which allows for excellent impregnation of the fibre reinforcement and higher processing speed, hence they tend to be the most commonly used resin systems. These systems do however have a limited shelf life and must be refrigerated. These shelf lives will vary depending on the resin system and can be determined experimentally using ASTM (American Society for the Testing of Materials) methods. These times will vary from minutes to hours depending on the choice of catalyst being used. The choice of catalyst will also determine the cure temperature, which can be at high temperature or room temperature. The chemical reaction that takes place during curing is an exothermic one, with rapid gelation. Gelation occurs when the resin has reached a point where the viscosity has increased so that it will barely move. Once cured the mixture thickens, releases heat, solidifies and then shrinks. For epoxy this shrinkage is typically around 4%. The fibres within the composite do not shrink and it should be noted that this can result in induced stresses, which may cause cracking, fibre misalignment, as well as dimensional inaccuracy and surface roughness [1].

Overall the epoxy resin systems are considered to be 'high performance' due to their superior mechanical properties compared to other thermosets. The most common thermoset resins are polyesters, vinyl ester, epoxy and phenolics, however only epoxy resins will be discussed henceforth as they are most applicable to this project.

Besides having superior mechanical properties epoxies also exhibit a lower percentage of shrinkage than other thermosets, which also provides them with excellent bonding characteristics when used as adhesives. Epoxies are also less affected by heat and moisture than other thermosets and are favoured for their simple cure process at any temperature between 5-180^{o}C. Being typically used in aerospace applications they can be used for honeycomb structures, as laminating resins, for filament wound structures and for tooling. Some typical mechanical properties of epoxies are given in table 4.

Table 4 Mechanical Properties of Thermoset Matrices [1]

Thermosets	Tensile Modulus [GPa]	Tensile Strength [MPa]	Compress. Strength [MPa]	Shear Strength [MPa] (°)	Tensile Elong. [%]	Flexural Modulus [GPa]	Flexural Strength [MPa]	Thermal Expansion [10^{-6}/°C]	Heat Deflect. Temp. [°C]	Poisson Ratio	Tg [°C]	Density [gr/cc]
Polyester												
Orthophthalic	3.4	55.2	–	–	2.1	6.9	220.7	–	79.4	0.38	–	–
Isophthalic	3.4	75.9	117.2	75.9	3.3	7.6	241.4	30	90.6	0.38	–	–
BPA Fumarate	2.8	41.4	103.5	–	1.4	9	158.6	–	129.4	0.38	–	–
Chlorendic	3.4	20.7	103.5	–	–	9.7	193.1	–	140.6	0.38	–	–
Vinyl Ester												
Derakane 411-45	3.4	82.7	117.1	82.7	5-6	3.1	124	–	104	0.38	–	–
Epoxy												
9310/9360 @23°C	3.12	75.8	–	–	4	–	–	54	–	0.38	185	1.2
9310/9360 @149°C	1.4	26.2	–	–	5.2	–	–	–	–	–	185	1.2
9420/9470(A) @23°C	2.66	57.2	–	–	3.1	–	–	–	–	–	195	1.162
9420/9470(B) @23°C	2.83	77.2	–	–	5.2	–	–	–	–	–	155	1.158
HPT1072/1062-M @23°C	3.383	–	–	–	–	3.383	131	–	–	–	239	–
Bismaleimide												
796/TM-123 @24°C	3.582	–	–	–	–	3.582	132	–	–	–	260	–
796/TM-123 @249°C	–	–	–	–	–	2.48	90	–	–	–	260	–

Epoxy matrices can be used at operating temperature up to 125-175°C depending on the exact resin system being used. To increase the toughness of the resin and hence the composite, the basic thermoset epoxy resins are toughened with additives, including the addition of thermoplastics. If the system is toughened in such a way, then normally its service temperature is reduced too. The operating temperature of all epoxies is always below the glass transition temperature of the material, which is high for brittle epoxies and lower for toughened epoxies [1].

2.5 Thermoplastic Matrices

A thermoplastic polymer does not undergo any chemical transformation during processing. In this case during processing the polymer is softened from the solid state by the application of heat, returning to solid post processing when the temperature is reduced. Thermoplastics have a very high viscosity at high temperatures meaning that they are harder to process. To induce flow of the thermoplastic means that high shear stresses are induced, which can often damage the fibres resulting in a reduction in fibre length. This is one of the main areas of research in trying to improve the process-ability of thermoplastic matrix systems [1].

Thermoplastics do not require refrigerated storage and have no shelf or pot life and are also better in terms of repair, as they can be heated and remoulded without any

degradation to material strength. A common thermoplastic used is PEEK, having high fracture toughness, which is generally used for high performance applications such as aerospace where damage tolerance is an important factor. PEEK is a semi-crystalline thermoplastic which absorbs moisture at a relatively low rate at room temperature (≤0.5% of weight of material), which is superior to epoxies. PPS, polyphenylene sulphide, also a semi-crystalline thermoplastic has the advantage of excellent chemical resistance. An example of an amorphous thermoplastic is PSUL, polysulfone which has a very high elongation to failure and excellent stability under hot/wet conditions. Table 5, summarises some typical material properties for these materials [1].

Table 5 Typical Properties of Thermoplastic Matrices [1]

Material	Tensile Modulus (GPa)	Tensile Strength (MPa)	Poissons Ratio	Glass Transition Tg (°C)	Fracture Toughness G^{1c} (kJ/m^2)	Density (gr/cc)
PEEK	3.24	100	0.4	143	4.03	1.32
PPS	3.3	82.7	0.37	90	-	1.36
PSUL	2.48	70.3	0.37	190	2.45	1.24
PEI	3	10.5	0.37	217	2.8	1.27
PAI	2.756	89.57	0.37	243	3.5	1.4
K-III	3.76	102	0.365	250	1.9	1.31
LARC-TPI	3.72	119	0.36	264	1	1.37

2.6 Fibre Types

The strength of any ceramic or glass is determined by the size of the largest crack or defect, which the material contains. Roughly, the strength is proportional to the inverse square root of the length of the largest flaw, a relationship developed in the thermodynamic argument by Griffith. In its simplest form the equation is as follows (Equation 1) [2]:

$$\sigma_{max} = \sqrt{\frac{2E\gamma_f}{\pi a}} \qquad \textbf{(Equation 1)}$$

σ_{max} is the strength of the material, E is its elastic stiffness (Young's modulus), γ_f is the work required to fracture the sample, a is the flaw size. This model is of limited practical value due to the spread and location of the flaws varying in every sample of material. If the flaw size is reduced the strength of the material increases and the variability is also reduced. It is the reinforcing fibres which provide the composite material with high

strength and stiffness, combined with low density. A summary of some typical fibre types is shown in table 6.

Table 6 Typical Properties of Some Reinforcing Fibres [2]

Material	Trade Name	Density, 10^3 kg.m^{-3}	Fibre Diameter, μm	Young's Modulus, GPa	Tensile Strength, GPa
High-carbon steel wire	e.g., piano wire	7.8	250	210	2.8
Short Fibres:					
α-Al_2O_3 (whisker crystals)		3.96	1 - 10	450	20
δ-Al_2O_3 + SiO_2 (discontinuous)	Saffil (U.K.)	2.1	3	280	1.5
Continuous Fibres: (inorganic)					
α-Al_2O_3	FP (U.S.A.)	3.9	20	385	1.8
Al_2O_3 + SiO_2 + B_2O_3 (Mullite)	Nextel 480 (U.S.A.)	3.05	11	224	2.3
Al_2O_3 + SiO_2	Altex (Japan)	3.3	10 - 15	210	2.0
Boron (CVD on tungsten)	VMC (Japan)	2.6	140	410	4.0
Carbon (PAN precursor)	T300 (Japan)	1.8	7	230	3.5
Carbon (PAN precursor)	T800 (Japan)	1.8	5.5	295	5.6
Carbon (pitch precursor)	Thornel P755 (U.S.A.)	2.06	10	517	2.1
SiC (+O)	Nicalon (Japan)	2.6	15	190	2.5 - 3.3
SiC (low O)	Hi-Nicalon (Japan)	2.74	14	270	2.8
SiC (+O+Ti)	Tyranno (Japan)	2.4	9	200	2.8
SiC (monofilament)	Sigma (U.K.)	3.1	100	400	3.5
Silica (E glass)		2.5	10	70	1.5 - 2.0
Silica (S or R glass)		2.6	10	90	4.6
Silica (quartz)		2.2	3 - 15	80	3.5
Continuous Fibres: (organic)					
Aromatic polyamide	Kevlar 49 (U.S.A.)	1.5	12	130	3.6
Polyethylene (UHMW)	Spectra 1000 (U.S.A.)	0.97	38	175	3.0

2.7 Glass Fibres an Overview

Overall fibre glass provides low cost, light weight and high strength characteristics. Historically fibre glass parts have been used in aerospace for components that do not carry heavy load or operate under heavy stress. For example fuselage interior parts such as window surrounds and storage compartments, as well as wing fairings and wing fixed trailing edge panels [3]. Glass fibres are manufactured by drawing molten glass into very fine threads and then immediately protecting them from contact with the atmosphere or with hard surfaces in order to protect the defect free structure that is created during the drawing process. Glass fibres are as strong as many of the newer inorganic fibres but lack the rigidity on account of their molecular structure; they can be modified to a limited extent by changing the chemical composition of the glass [2].

The two most common grades of fibreglass are 'E' glass, used for electrical board and 'S' glass, high strength for structural use. 'E' glass has a high strength to weight ratio, good fatigue resistance, excellent dielectric properties, retention of 50% tensile strength up to 320°C and an excellent environmental resistance. This material has been proven in secondary structures in aircraft, but where superior mechanical properties are required S glass is utilised. S glass has up to a 25% higher compressive strength, 40% higher tensile strength, 20% higher modulus and a 4% lower density, albeit at a higher cost [3].

There are other types of glass, A, B, C and D, however their mechanical properties are such that they are not suitable for structural applications.

2.8 Carbon Fibres an Overview

In a single crystal of graphite the carbon atoms are arranged in hexagonal arrays stacked in a regular sequence with atoms being held together by strong covalent bonds, with week van der Waals forces between them. The basic crystals are highly anisotropic having in plane modulus of ~1000GPa and perpendicular modulus of 35GPa both Carbon and Graphite fibres are based on this structure. If the layers stack with three-dimensional order then the material is defined as graphite. Where there is only 2D dimensional order the material is known as Carbon [4,5].

Carbon fibres are typically around 8μm in diameter and consist of small crystallites of 'Turbostratic' graphite, which closely resembles graphite single crystals except the

layers are not regularly packed. To achieve a high axial modulus alignment of the basal planes is critical [5].

Overall carbon fibres offer a significantly higher modulus with lower density than glass fibres, making them an obvious choice for high stiffness low weight applications such as airframe structures. The fibres do not suffer from stress corrosion or stress rupture failures at room temperature and at higher temperatures offer the same outstanding performance for both strength and modulus.

2.9 Mechanical Properties of Unidirectional Material & Their Generation

To be discussed in section 2.11.1 the prediction of laminate properties, is dependent on knowing the properties of each individual ply. Internationally and within Airbus there are many standardised test methods, which are known to produce accurate properties for lamina. In most cases these tests are actually generated from laminates, which typically have a unidirectional lay-up. It is not within the scope of this thesis to propose or investigate novel test methods. To validate the EMOC modelling process it is only necessary to demonstrate that wherever possible standardised methods for generating mechanical properties have been adhered to. This is of paramount importance if the modelling tool is to be eventually adopted within Airbus, as it must satisfy Airbus requirements, which have been designed to meet certification requirements.

The test methods discussed here are for tension, compression and shear. Specifically the 0^0 and perpendicular 90^o lamina properties are discussed. For all test methods it is necessary to follow set procedures for the control and testing of materials. These include the production and preparation of test panels prior to testing [6,7] and standardised procedures for the conditioning of coupons prior to testing [8], which have been further modified within the scope of this project, see section 4. Finally there is the procedure for determining the effect on the material during the conditioning process [9]. Airbus generally does not need to generate its own lamina properties, as this is typically done by the material supplier, who follows Airbus methods and procedures to produce statistically robust lamina properties, known as qualification values. These qualification values typically cover the full operating environment, which includes conditioning tests all carried out at 75^oC with a relative humidity (RH) of 85%. Tests are conducted at room temperature, -55^oC and 90^oC for both dry (often known as 'as received') and conditioned specimens.

2.9.1 Tensile Strength & Modulus

For both the 0° and 90° mechanical properties in tension and compression, method [10] may be used, however typically the method described in [11] is used for the perpendicular direction. Both test types allow both strength and modulus values to be obtained. In both cases this is by a uni-axial strain gauge, which is placed at the centre of the specimen, on both sides (to verify that no bending is taking place that would invalidate the test). Unsurprisingly, the tensile strength in the 0° specimens is high compared to other materials and other fibre orientations and as such the laminates used for this test are 1mm thick and 15mm in width, compared to the 90° perpendicular test that has a thickness of 2mm and 25mm width. Typically cure ply thickness of the specimens is 0.184-0.254mm and the number of plies used is therefore determined using the thickness required by the standard. Both tests require the use of end tabs to aid load transfer. It should be noted that the 90° specimens are particularly sensitive to the surface finish, with any surface imperfections leading to localised stress concentration, which can lead to a large degree of scatter between the results [12].

In both cases the stress at failure is simply determined by the area the load is distributed across. Modulus for the 0° loading direction is determined by equation 2, with terms defined in figure 7 where 0° modulus is E_{11}:

$$E_{11} = \frac{\sigma_2 - \sigma_1}{\varepsilon_2 - \varepsilon_1}$$ **(Equation 2)**

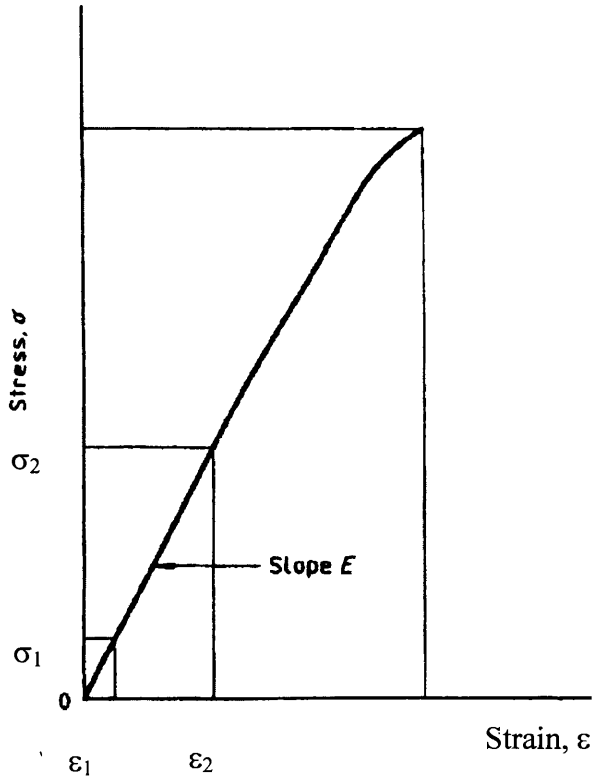

Figure 7 Stress Strain Curve of 0° Tensile Test [10]

Equation 3 is used to determine the 90° modulus, known as E_{22}, where F_R is the load at failure (N), b is the width (mm), h the thickness (mm), $(\varepsilon_{22})_A$ is the strain perpendicular to the fibre direction corresponding to $F_R/10$ and $(\varepsilon_{22})_B$ is the strain corresponding to the fibre direction corresponding to $F_R/2$ (see figure 8):

$$E_{22} = \frac{0.4F_R}{b \cdot h[(\varepsilon_{22})_B - (\varepsilon_{22})_A]} \qquad \textbf{(Equation 3)}$$

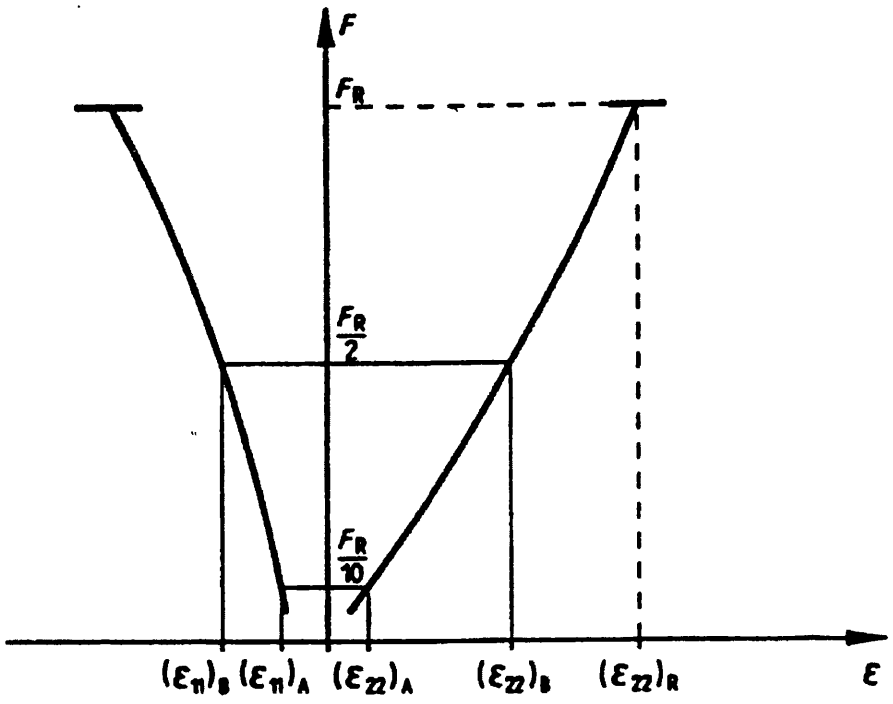

Figure 8 Load/strain recording for 90° Tension Test [10]

2.9.2 Compressive Strength & Modulus

As with the tension tests previously discussed, it is necessary to determine the lamina strength in both the 0° fibre direction and also perpendicular to the fibre direction. The test method used in the EMOC project for determination of the 0° & 90° compressive strengths is an AECMA (European Association of Aerospace Industries) standard [13]. There are two methods within this standard with method 'A' being used for the 0° fibre direction and method 'B' for the 90° direction. The decision to use this particular test method was made by the Airbus methods group that provided some overall guidance to the project. The fixtures for both method 'A' & 'B' are different and so is that of the load introduction, where in method 'A' the load is transferred by the end tabs and in method 'B' the load is transferred by direct end loading of the coupon. It should be noted that the determination of modulus for method B requires a separate set of coupons to be manufactured having no end tabs. In both test cases the test is only valid if failure occurs in the gauge section of the specimen. A schematic of the required test fixtures is shown in figure 9 & 10.

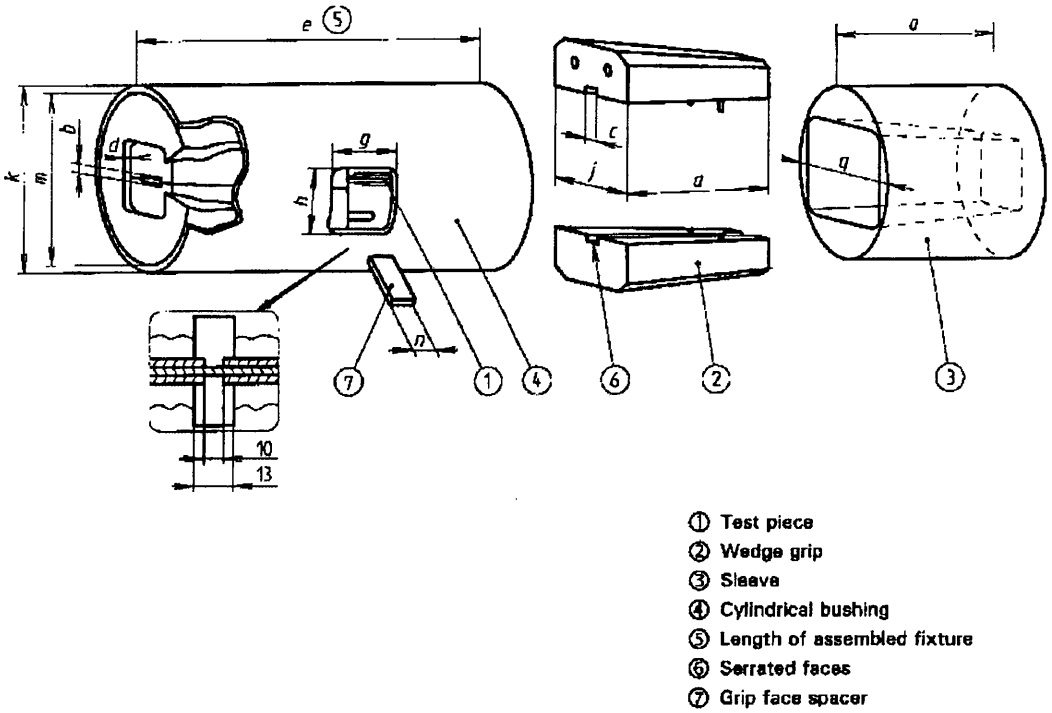

Figure 9 Basic Schematic of Method 'A' Test Fixture [13]

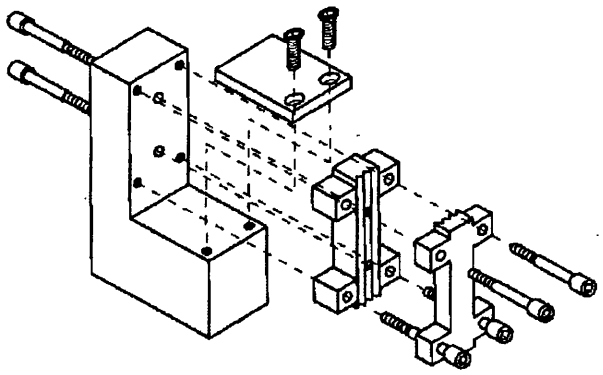

Figure 10 Basic Schematic of Method 'B' Test Fixture [13]

When conducting the tests the strains are continually monitored to detect any tendency for the coupon to buckle, which would inevitably invalidate the test. These strains are determined using strain gauges located on both faces of the gauge section of the specimen, both should track strains of similar magnitude, unless buckling begins to occur. The stress at failure is calculated by taking into account the cross sectional area of the specimen over which the forced is induced. The modulus E_{11} is derived from equation 4 and figure 11. There are two ways to calculate the modulus, force based and strain based. The preferred method is strain based is discussed here:

$$E_{c11}(\alpha,\beta)=\frac{P_\beta - P_\alpha}{bh[\beta-\alpha]}$$ **(Equation 4)**

Where 'α' is the lower limit of strain parallel to the axis of the test piece, 'β' is the upper limit of the strain parallel to the test piece, 'P_α' is the load corresponding to 'α' (N), 'P_β' is the load corresponding to 'β' (N), 'b' the coupon width (mm), 'h' the thickness (mm).

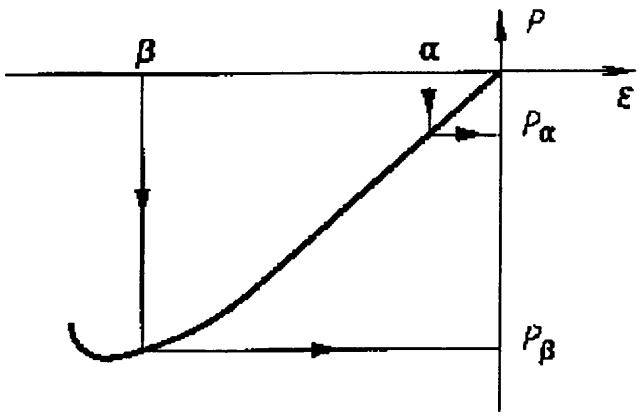

Figure 11 Load/Strain Relationships for the Determination of Compressive Modulus [13]

2.9.3 Shear Strength (In-plane & Interlaminar) & Modulus

The in-plane shear strength and interlaminar shear strength are both resin dominated properties, however it is the use of in-plane shear that is typically used in laminate analysis. The in-plane shear strength is determined using AITM 1-0002 (Airbus Industrie Test Method) [14], which is essentially the same test as defined by the British standard equivalent [15]. This test uses a laminate of 8 plies orientated at $+45^0$ & -45^o to the loading direction, which is designed to impose a state of shear between the 2 fibre orientations. The test method gives a relative value for shear strength and modulus, but it is not a true reading of the shear strength as the test is in fact a laminate and not a unidirectional coupon where shear is induced between 1 ply [12]. As with the tension test methods the coupon requires end tabs to aid load introduction into the specimen and is typically of similar geometry to the 90^o tension coupons, having a gauge width of 25mm. Because of the fibre orientation relative to the loading, to determine modulus it is necessary to use bi-axial strain gauges to measure the strains in both the loading axis and perpendicular to it. The strain in each direction is

considered to be the average strain measure on the face of the specimen. Again it is standard practice to measure strains on both faces to ensure no bending occurs during testing.

Shear Modulus G is defined by equation 5, where 'ΔP', is the difference in tensile loads (N) at longitudinal strains $(\varepsilon_o)_1 = 500X10^{-6}$ & $(\varepsilon_o)_2 = 2500X10^{-6}$, $\Delta\tau$ is the difference in shear (see figure 12) stress (N/mm^2) at $(\varepsilon_o-\varepsilon_{90})_2 = 4500X10^{-6}$ & $(\varepsilon_o-\varepsilon_{90})_1 = 900X10^{-6}$, $\Delta\varepsilon_0$ - $\Delta\varepsilon_{90}$ $(\varepsilon_0-\varepsilon_{90})_2$ - $(\varepsilon_0-\varepsilon_{90})_1 = 3600X10^{-6}$, 'w', is the width (mm), 't' is the thickness of 8 plies (in mm, dependent on the cure ply thickness), $\Delta\varepsilon_0$ is the difference in longitudinal strains $(\varepsilon_0)_2$ - $(\varepsilon_0)_1 = 2000X10^{-6}$, $\Delta\varepsilon_{90}$ is the difference in transverse strains $(\varepsilon_0)_2 = 2500X10^{-6}$ & $(\varepsilon_0)_1 = 500X10^{-6}$.

$$G = \frac{\Delta P}{2wt(\Delta\varepsilon_0 - \Delta\varepsilon_{90})} = \frac{\Delta\tau}{(\Delta\varepsilon_0 - \Delta\varepsilon_{90})} \qquad \textbf{(Equation 5)}$$

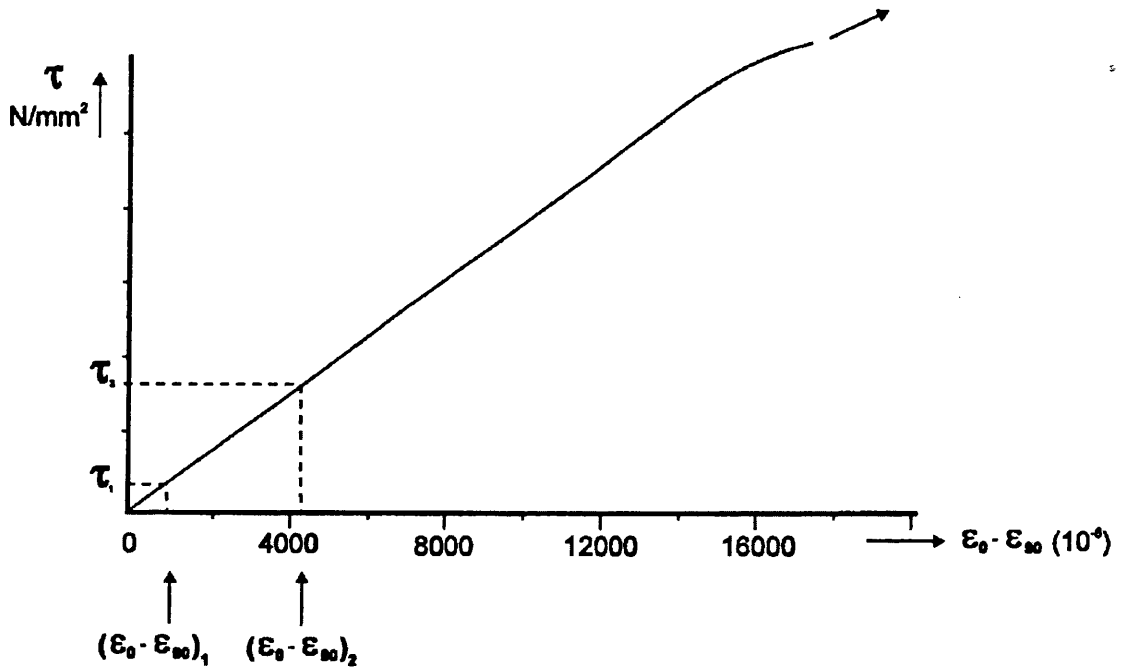

Figure 12 τ - ε Curve for the ± 45 Shear Test Determination of Shear Modulus [14]

Both references [16,17] detail three point bend tests, which are essentially the same test method. This method can be applied to both unidirectional coupons and woven materials and directed lay-ups. To determine the shear strength between the plies within the laminate a coupon is placed in flexure on two supports and load is then applied at the centre of the specimen. The shear strength measured is the 'apparent'

interlaminar shear strength, calculated at half thickness of the specimen at the moment of first failure. It should therefore be noted that the first failure may not always occur around the specimen centreline. Using this method it is not possible to determine the shear modulus and this test only provides an indication of strength. A schematic of the test set up is shown in figure 13.

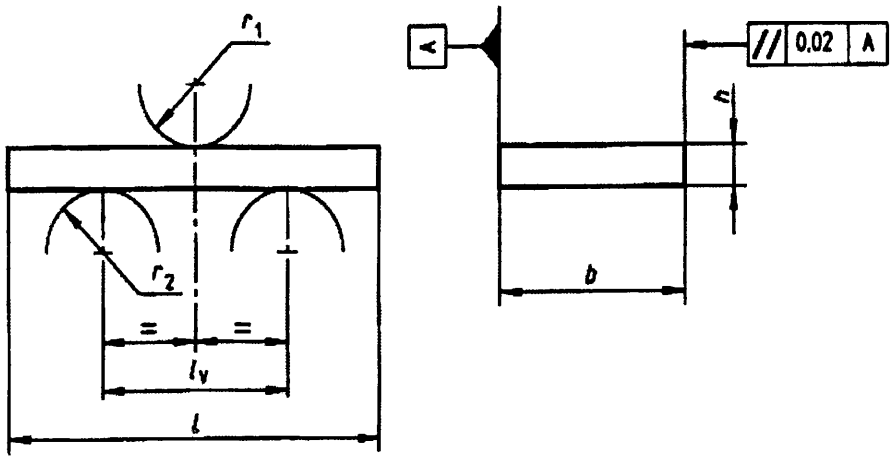

Figure 13 Schematic of 3 Point Bend Test Showing Critical Dimensions with respect to Support & Load Introduction Points [16]

For qualification values (i.e. during the qualification of a new material), it is necessary to position the supports as determined by equation 6 (c.f. figure 13):

$$l_v = (5 \cdot h) \pm 0.1 \qquad \textbf{(Equation 6)}$$

Where 'l_v' is the distance between supports in (mm) & 'h' is the arithmetic mean thickness of specimens (mm). The apparent interlaminar shear strength is then calculated by equation 7:

$$\tau = \frac{3 \cdot P_R}{4 \cdot b \cdot h} \qquad \textbf{(Equation 7)}$$

'P_R' is the maximum load at the moment of first failure (N), 'τ' is the apparent interlaminar shear strength (MPa), 'b' is the width of the specimen (mm) and 'h' is the thickness of the specimen (mm).

2.9.4 *Bearing Strength*

The bearing strength of a material is affected by a number of factors and it is therefore hard to predict the exact bearing strength of a joint. These factors include the strength of the fasteners and resistance to shear and bolt bending, the torque applied to the fasteners before loading and the type of joint arrangement, which is typically a single or double lap shear joint. Furthermore the quality of the joint must also be considered e.g. the tolerances of the hole itself. Airbus determines the bearing strength of components, as laid out by [18], which allows bearing strength using either bolted fasteners of pin bearing to be determined. A typical bearing plot for a bolted joint is shown in figure 14.

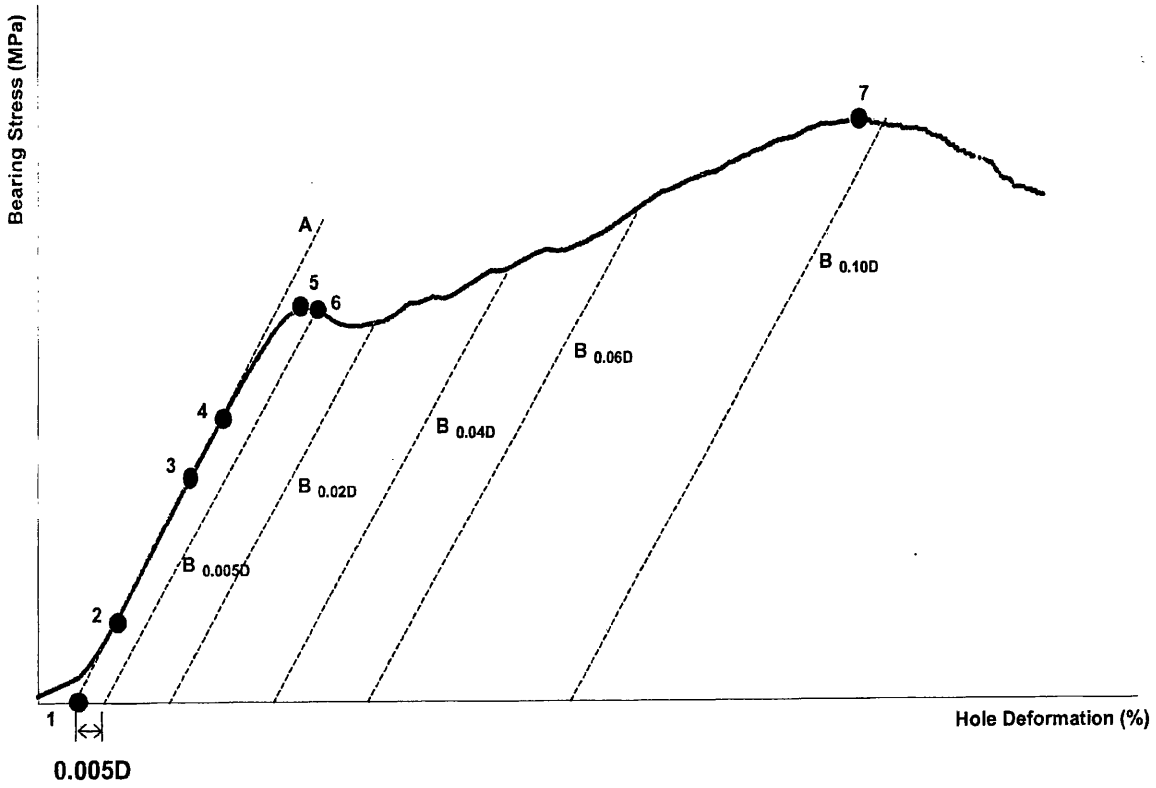

Figure 14 Illustrating a Typical Bolt Bearing Curve[18]

The determination of bearing strength is dependent on what defines 'bearing failure'. Typically bearing strength is measured at 6% hole deformation. This offset bearing strength can then be determined by equation 8, the ultimate bearing strength by equation 9 and initial peak bearing strength by equation 10:

$$\sigma_y = \frac{P_y}{dt_n} \quad \text{(MPa)} \qquad \textbf{(Equation 8)}$$

$$\sigma_u = \frac{P_u}{dt_n} \quad \text{(MPa)} \qquad \textbf{(Equation 9)}$$

$$\sigma_i = \frac{P_i}{dt_n} \quad \text{(MPa)} \qquad \textbf{(Equation 10)}$$

Where 'P_y' is the offset load (N) corresponding to the specified offset value, 'P_u' is the maximum load (N) sustained by the specimen during test, 'P_i' is the load (N) at initial peak/inflection point on the bolt bearing test curve, 'd' is the nominal bolt diameter (mm), 't_n' is the cure ply thickness multiplied by the number of plies (mm).

2.9.5 Compression Strength after Impact (CAI)

To meet certification requirements it is necessary to consider damage to a structure whilst in service. The philosophy governing the amount of damage and how it is accounted for within a structure by Airbus is a classified policy, which cannot be described in detail in this thesis. However the general principle is to estimate for a specific piece of structure the energy it may receive from an impact. This can either be based on a worst case maximum energy criterion or by determining BVID (barely visible impact damage). Where BVID is used it is assumed that this damage can be within the structure and the structure must be able to operate safely with no damage growth. Once the energy has be determined to cause BVID, then a test method can use an impact event to determine the strength of the coupon after it has been subjected to an impact (causing BVID). At the point of failure the maximum strain can be recorded and used in design. The structure is then stressed so that the strains within it do not exceed the maximum strain at failure, which thereby ensures that the structure can operate with an undetected amount of damage without any risk of the damage growing and causing a failure to the structure [19].

The compression after impact test is an Airbus method [20] where much of the technical work is in the impact event itself, which follows the same methodology as that highlighted in [21]. A flat rectangular plate of the composite to be tested is constructed and then impacted at the centre of its gauge length. All edges of the coupon are supported (fully supported boundary condition). A schematic of the impact frame is shown in figure 15:

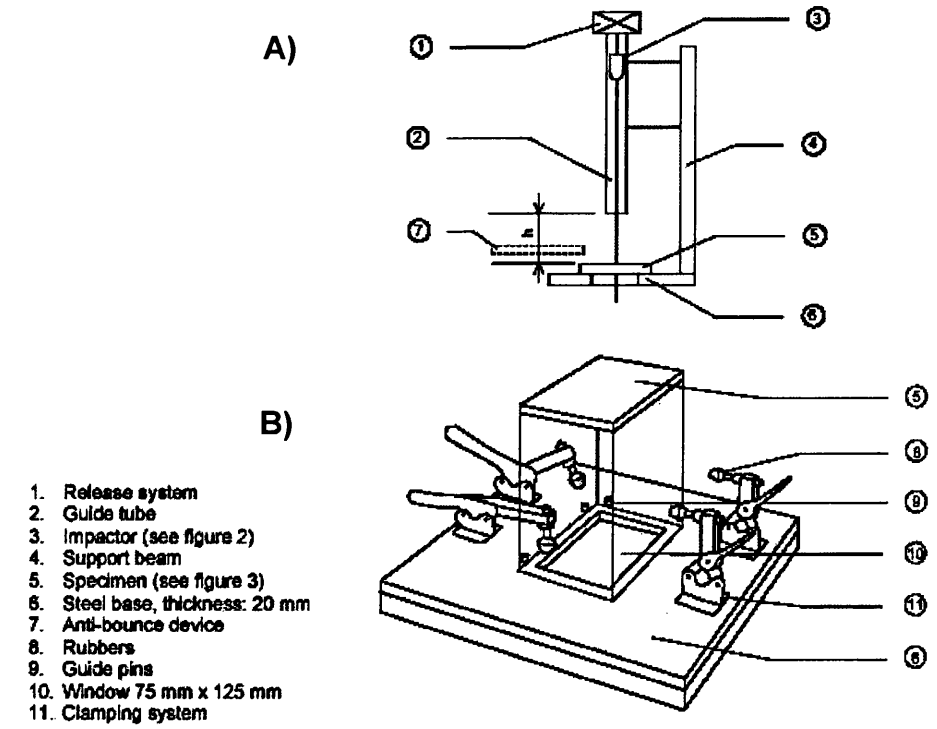

Figure 15 A) Schematic of Drop Weight over Specimen B) Schematic of Specimen Support Structure [20]

Once the coupons have undergone the impact event, they can then be tested in compression, or conditioned and then tested in compression post conditioning. Strain can be determined simplistically and the maximum strain at failure can then be set as the maximum strain limit of the structure. A schematic of the compression test fixture for this test is shown in figure 16.

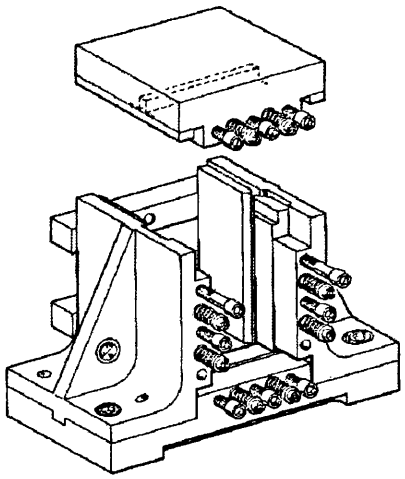

Figure 16 Example of a Typical Test Frame for Carrying out Compression Testing Post Impact [20]

The impact energy 'E' can be expressed in joules (J) using equation 11, which allows the parameters for a specific impact energy requirement to be determined:

$E = mgh$ or $E = mv^2/2$ **(Equation 11)**

Where 'm' is the impactor mass (kg), 'g' = 9.81 (m/s^2), 'h' is the drop height (m) and 'v' is the velocity at impact (m/s).

The normalised (allowing for cure ply thickness) compression strength (MPa) after impact at a specific energy 'E' is then derived from equation 12:

$\sigma_r(E) = P_r/(w.t_n)$ **(Equation 12)**

Where 'P_r is the load at failure (N), 'w' is the specimen width (mm) and t_n' is the cured ply thickness specific to the material being used, multiplied by the number of plies used.

2.9.6 Compression/ Tension Strength of Plain, Open Hole & Filled Hole Laminates

When carrying out structural assessment of wing structure, the tensile and compressive strength of the laminate containing a hole is often required. These values are relevant to bolted joint areas where fastener spacing may lead to a failure between fasteners. These test methods allow both the strength and modulus of the material to be determined. Both methods [22,23] follow a similar principle for deriving strength and modulus. As we are considering resin dominated properties, the determination of compressive strength and modulus will be briefly described here.

Plain, open hole and filled-hole Compression Strength is defined by equation 13, noting that although the equation remains the same the notation changes, with plain strength notation being shown here:

$\sigma_{cu} = P_u/(t_n w)$ (MPa) **(Equation 13)**

Where 'P_u' is the maximum load (N), 'w' is the specimen width (mm), 't_n' is the nominal thickness (cure ply thickness in mm).

The normalised compression modulus 'E_c' is the mean of the strains recorded on both sides of the specimen. For each specimen it is necessary to plot a curve of the load, displacement, where the definition of load increase is given by equation 14:

$$\Delta P = (P_u / 2) - (P_u / 10) \qquad \textbf{(Equation 14)}$$

Normalised compression modulus is then given by equation 15:

$$E_c = \Delta P / w t_n \Delta \varepsilon_x \qquad \textbf{(Equation 15)}$$

Notch factors are required for open and filled-hole compression.

2.10 Generation of Mean & 'B-Basis' Design Allowables

Composite materials can have extensive variability with regard to their mechanical properties, due to their in-homogeneity, anisotropy and also the basic brittleness of the fibres and the matrix that often suffer from property mismatch between the components. Statistical analysis of these materials is more complex than traditional metallic materials. A basis property is a stress value that is determined so that there is a specified probability of the strength exceeding this value with 95% confidence in assertion. Survival probabilities are in the 99th percentile for A-basis and 90th percentile for B-basis. B-basis is typically used by Airbus to determine material allowables for use in design [4,24].

When assessing the methodology for deriving B-basis properties, it is important to consider the batch size, the number of batches and differences among the batches. This leads to the selection of an appropriate statistical model. Statistical Models include the Lemon Method, k-sample Anderson Darling test, Weibull method, Normal method and the Non-parametric method. Figure 17, shows how to select the appropriate method that prevents the use of the wrong statistical method [4].

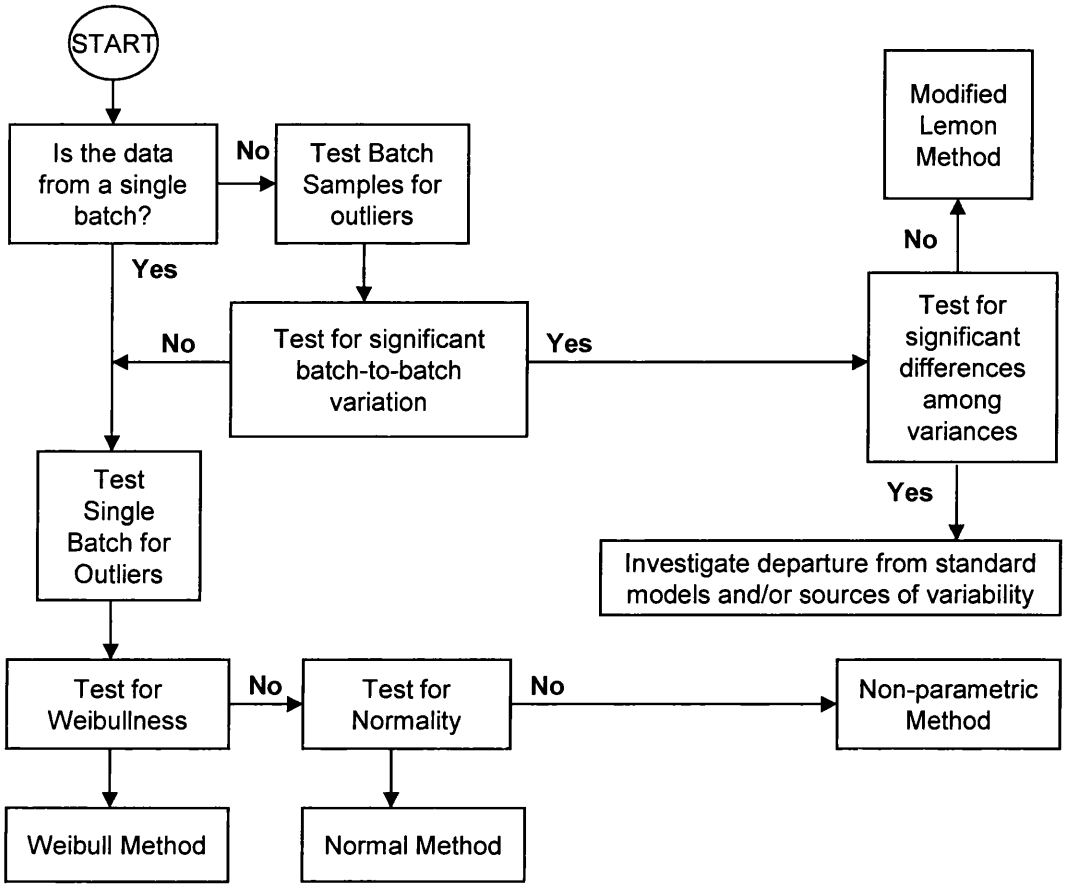

Figure 17 Procedures for Determination of Appropriate Statistical Method [4]

Increased batch size or the number of tests improves the precision of the estimates produced. For single batch cases, the data must be screened for outliers that may have occurred due to a fluctuation in the quality of the test specimen or discrepancies that may have occurred during test. For generation of B-basis properties for batches greater than one the equality of the populations must be investigated. Where there are three or more batches and pooling cannot be carried out due to differences between each batch additional tests would be required. A more detailed description of statistical methods can be found in Mil 17B [25].

If outliers are detected within batches they should either be corrected or removed from the batch. When detecting outliers it is first necessary to calculate the maximum normal residual (MNR) statistic. If x_1, x_2,...., x_n denote the data values in a samples size n, the MNR is defined as equation 16:

$$r_i = \frac{x_i - \bar{x}}{S}$$ **(Equation 16)**

Where i = 1,2...,n & $\bar{x}$ and S are the sample mean and sample standard deviation respectively. Normal residuals are scaled deviations from the centre of the data. The MNR statistic is the maximum of the absolute values of the normal residuals shown in equation 17:

$$MNR = \max_i |r_i|$$ **(Equation 17)**

The MNR statistic is then compared to the critical value for the sample size n. If the MNR is smaller than the critical value, then no outliers are detected. If larger than the critical value, the datum associated with the absolute normal residual is declared to be an outlier. When the sample size is small, values that appear to be outliers should be investigated. The critical values can be calculated using equation 18:

$$CV = \frac{n-1}{\sqrt{n}} \sqrt{\frac{t^2}{n-2+t^2}}$$ **(Equation 18)**

Where t is the 1 – α/(2n) quantile of the t distribution, with n-2 degrees of freedom. Values for this can be seen in table 7:

Table 7 Critical Values (CV) for the maximum Normal Residual Outlier Test [4]

n	CV α = .01	α = .05	α = .10
5	1.764	1.715	1.671
6	1.973	1.887	1.822
7	2.139	2.020	1.938
8	2.274	2.127	2.032
9	2.387	2.215	2.110
10	2.482	2.290	2.176
11	2.564	2.355	2.234
12	2.636	2.412	2.285
13	2.699	2.462	2.331
14	2.755	2.507	2.372
15	2.806	2.548	2.409
16	2.852	2.586	2.443
17	2.894	2.620	2.475
18	2.932	2.652	2.504
19	2.968	2.681	2.531
20	3.001	2.708	2.557
21	3.031	2.734	2.580
22	3.060	2.758	2.603
23	3.087	2.780	2.624
24	3.112	2.802	2.644
25	3.135	2.822	2.663
26	3.158	2.841	2.681
27	3.179	2.859	2.698
28	3.199	2.876	2.714
29	3.218	2.893	2.730
30	3.236	2.908	2.745

Only single batch data has been used in complimentary work and by this project specifically, thus only the single batch analysis is discussed in this literature review. Having first carried out the examination for outliers as previously discussed figure 17 is then used to attempt to identify an appropriate model. The Weibull model with the cumulative distribution function should be considered first. This is given by equation 19:

$$F_o(x) = 1 - e^{-(x/\alpha)^{\beta}} \qquad \textbf{(Equation 19)}$$

The Anderson –Darling (AD) goodness-of-fit test statistic is suggested for identifying a model as it is sensitive to discrepancies in the tail regions. This is the comparison between the cumulative distribution function of the data with the cumulative distribution function of the model. For the Weibull distribution this is shown in equation 20 [4].

$$Z_{(i)} = \left(\frac{x_{(i)}}{\alpha} \right)^{\beta}$$ **(Equation 20)**

Where i=1,....., n and α & β are the maximum likelihood estimates, the sample size is n, and the sample observations ordered from least to greatest $x_{(1)}$,....., $x_{(n)}$ The AD statistic is shown in equation 21 [4].

$$AD = \sum_{i=1}^{n} \frac{1 - Z_i}{n} \{ \ln[1 - \exp(-Z_{(i)})] - Z_{(n+1+i)} \} - n$$ **(Equation 21)**

The observed level of significance (OSL) is calculated from equation 22 [4]:

$$OSL = 1/1 + \{ \exp[-0.10 + 1.24 \ln(AD^*) + 4.48(AD^*)] \}$$ **(Equation 22)**

Where: $$AD^* = \left(\frac{1 + 0.2}{\sqrt{n}} \right) AD$$ **(Equation 23)**

The OSL measures the goodness of fit of the two-parameter Weibull fit to the data. The OSL is the probability of observing the AD statistic as extreme as the value calculated if the two-parameter Weibull distribution is in fact the correct model.

If the OSL ≤ 0.05, it can be concluded (5% risk of error) that the data is not a sample from the Weibull population. If the Weibull model is rejected, the AD procedure is applied to the normal distribution. It should be noted that for small sample sizes it is difficult to distinguish between the Weibull and normal distribution models, although the Weibull model should always be considered first for composite materials [4]. The normal distribution is shown in equation 24:

$$F_o(x) = \frac{1}{\sigma\sqrt{2\pi}} \int e^{\frac{-(t-\mu)^2}{2\sigma^2} dt}$$ **(Equation 24)**

The parameters are the mean μ and standard-deviation σ. These are estimated by the sample mean and standard-deviation, as shown in equation 25, which gives the sample mean and equation 26, which gives the standard deviation:

$$\bar{x} = \sum_{i=1}^{n} \frac{x_i}{n}$$ **(Equation 25)**

$$S = \sqrt{\sum_{i=1}^{n} \frac{\left(x_i - \bar{x}\right)^2}{n-1}}$$ **(Equation 26)**

The procedure for goodness of fit for the normal distribution is similar to the Weibull model, except for the definitions of $Z_{(i)}$ AD and the OSL where:

$$Z_{(i)} = \frac{x_i - \bar{x}}{S}$$ **(Equation 27)**

i = 1, ... n The AD statistic is then:

$$AD = \sum_{i=1}^{n} \left(\frac{1 - Z_i}{n} \right) \left[\ln F_o\left(Z_{(i)}\right) + \ln\left(1 - F_o\left(Z_{(n+1-i)}\right)\right) \right] - n$$ **(Equation 28)**

F_o is the standard normal distribution function and the OSL can be calculated via equation 29:

$$OSL = \frac{1}{\left\{1 + \exp\left[-0.48+).78\ln\left(AD^*\right) + 4.58\left(AD^*\right)\right]\right\}}$$ **(Equation 29)**

Where AD* is shown in equation 30:

$$AD^* = (1 + 4/n - 25/n^2)AD$$ **(Equation 30)**

The OSL measures the goodness of fit of the distribution. Again the OSL is a probability of observing an AD statistic as extreme as the value calculated, if the normal distribution is the correct model. If the OSL ≤ 0.5, it may be concluded (at 5% risk of error) that the data is not a sample from the normal distribution. If the Normal or Weibull distributions are not accepted by the Anderson-Darling (AD) test, then the non-parametric model must be used.

If the Weibull model has been accepted by the AD test then equation 31 can be used to calculate the B-basis value:

$$B = a[\ln(1/P_B)]^{1/b}$$ **(Equation 31)**

Where P_B is obtained from table 8, as a function of the sample size n.

Table 8 B-Basis Factors (P_B) for the Weibull Distribution [4]

n	P_B	n	P_B	n	P_B	n	P_B
5	0.9987	15	0.9771	25	0.9636	55	0.9453
6	0.9969	16	0.9754	26	0.9626	60	0.9435
7	0.9948	17	0.9738	27	0.9616	65	0.9420
8	0.9929	18	0.9723	28	0.9607	70	0.9406
9	0.9895	19	0.9708	29	0.9599	75	0.9393
10	0.9875	20	0.9695	30	0.9590	80	0.9381
11	0.9852	21	0.9682	35	0.9553	85	0.9371
12	0.9830	22	0.9669	40	0.9522	90	0.9361
13	0.9809	23	0.9658	45	0.9495	95	0.9352
14	0.9790	24	0.9647	50	0.9473	100	0.9344

Similarly for the Normal model the B-basis value can be calculated from equation 32:

$$B = \bar{x} - K_B S$$ **(Equation 32)**

Values for K_B can be taken from table 9:

Table 9 B-Basis Factors (K_B) for the Normal Distribution

n	K_B	n	K_B	n	K_B	n	K_B
1	...	11	2.275	21	1.905	35	1.732
2	20.581	12	2.210	22	1.886	40	1.697
3	6.155	13	2.155	23	1.869	45	1.669
4	4.162	14	2.109	24	1.853	50	1.646
5	3.407	15	2.068	25	1.838	55	1.626
6	3.006	16	2.033	26	1.824	60	1.609
7	2.755	17	2.002	27	1.811	70	1.581
8	2.582	18	1.974	28	1.799	80	1.559
9	2.454	19	1.949	29	1.788	90	1.542
10	2.355	20	1.926	30	1.777	100	1.527

If the previously discussed Weibull and Normal distributions are not valid, then the non-parametric model may be used. This model normally provides a more conservative B-basis value. The procedure to calculate the B-basis value varies depending on whether the sample size is greater than 28 or less than 29. For samples sizes greater than 28,

the data is sorted into order of increasing values. Table 10 is then used to determine the r value corresponding to the sample size n. Where the sample size is between the tabulated values, the r value associated with the largest sample size that is smaller than the actual n, should be used. The B-basis value is the r^{th} lowest observation in the ordered sample.

Table 10 Ranks (r) of Observation (n) for Determining B-Basis Values for an Unknown Distribution [4]

n	r	n	r	n	r
<29	See Table 11	129	8	227	16
29	1	142	9	239	17
46	2	154	10	251	18
61	3	167	11	263	19
76	4	179	12	275	20
89	5	191	13	298	21
103	6	203	14	321	22
116	7	215	15	345	23

For sample sizes smaller than 29, a similar approach is adopted. Order the values from smallest to largest and obtain values r & k corresponding to the sample size n from table 11.

Table 11 B-basis Values for Small Sample Sizes [4]

n	*r*	*k*
2	2	35.177
3	3	7.859
4	4	4.505
5	4	4.101
6	5	3.064
7	5	2.858
8	6	2.382
9	6	2.253
10	6	2.137
11	7	1.897
12	7	1.814
13	7	1.738
14	8	1.599
15	8	1.540
16	8	1.485
17	8	1.434
18	9	1.354
19	9	1.311
20	10	1.253
21	10	1.218
22	10	1.184
23	11	1.143
24	11	1.114
25	11	1.087
26	11	1.060
27	11	1.035
28	12	1.010

Equation 33 can then be used to calculate the B-value:

$$B = X_{(r)} - k\left(X_{(r)} - X_{(1)}\right) \qquad \textbf{(Equation 33)}$$

2.11 Structural Mechanics of Fibre Composites

2.11.1 Single Ply Stress-Strain Laws

Single ply stress-strain laws are generally less useful to the engineer as in most cases the structural application consists of complex stress states and in many cases more than a single uni-axial load. As a result of more than one load application in any given plane, it becomes necessary to create a laminate, where ply direction is optimised to give the greatest mechanical performance to resist the applied load. It should be noted that in many cases the mechanical properties of these UD composite materials are

used to predict the properties of directed laminates that will be discussed further on in the literature review.

The axis system for a single UD laminate will be used as a reference axis when translating the stress-strain laws of the laminate. Once a laminate is created the stress-strain laws for the individual plies are translated into a single stress-strain law for the laminate [26]. Figure 18 shows a rectangular block of material representing a single ply of carbon fibre material, which has had standard Cartesian coordinates assigned to it. The 1 axis denotes the fibre direction, 2 is perpendicular to the fibre direction and 2 perpendicular to the plane of the ply.

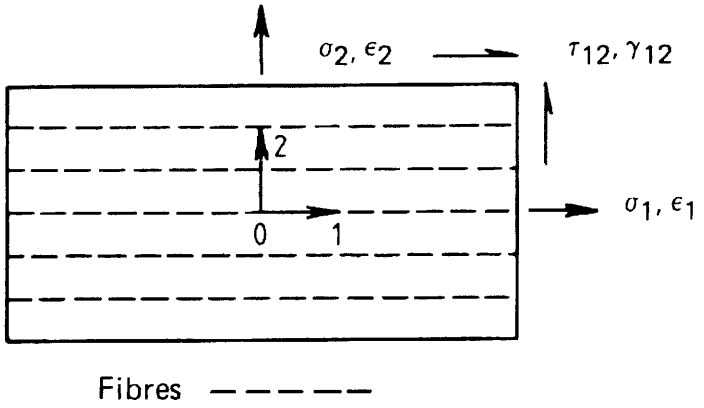

Figure 18 The Materials Axis system for a Single Ply [26]

For plane stress conditions the stresses can be referred to as σ_1, σ_2 & τ_{12} and the associated strains ε_1, ε_2 and γ_{12}. Planes 012, 023 and 031 are those of material symmetry. A material which has three mutually orthogonal planes of symmetry is known as orthotropic. The stress-strain law for an orthotropic material is denoted by equation 34 [26].

$$\begin{bmatrix} \varepsilon_1 \\ \varepsilon_2 \\ \gamma_{12} \end{bmatrix} = \begin{bmatrix} \frac{1}{E_1} & \frac{-\nu_{21}}{E_2} & 0 \\ \frac{-\nu_{12}}{E_1} & \frac{1}{E_2} & 0 \\ 0 & 0 & \frac{1}{G_{12}} \end{bmatrix} \begin{bmatrix} \sigma_1 \\ \sigma_2 \\ \tau_3 \end{bmatrix}$$

(Equation 34)

Where E_1, E_2 are equal to the Young's moduli in the 1 & 2 directions, respectively. ν_{12} is the Poissons ratio governing the contraction in the 2 direction for tension in the 1 direction, with ν_{21} having tension in the 2 direction and contraction in the 1 direction. G_{12} represents the in-plane shear modulus. The material has 5 constraints, 4 of which are independent because of the relationship shown in equation 35.

$$\frac{\nu_{12}}{E_1} = \frac{\nu_{21}}{E_2} \qquad \textbf{(Equation 35)}$$

E_1 will always be much larger than E_2 or G_{12} because E_1 is the fibre dominated direction, with the other two properties being dominated by the weaker matrix. These fundamental mechanics can be applied to unidirectional laminates, as thickness is not a function of the equations. It is these UD properties, which are then utilised to understand the mechanical properties of directed laminates. It is often more convenient to deal with equation 34 in its inverse form as shown in equation 36, where $Q_{ij}(0)$ is commonly known as the reduced stiffness coefficients. The use of Q simplifies the equations when dealing with complex 3 dimensional anisotropic problems. The reduced stiffness coefficients are given in equation 36.

$$\begin{bmatrix} \sigma_1 \\ \sigma_2 \\ \tau_{12} \end{bmatrix} = \begin{bmatrix} Q_{11}(0) & Q_{12}(0) & 0 \\ Q_{12}(0) & Q_{22}(0) & 0 \\ 0 & 0 & Q_{66}(0) \end{bmatrix} \begin{bmatrix} \varepsilon_1 \\ \varepsilon_2 \\ \gamma_{12} \end{bmatrix} \qquad \textbf{(Equation 36)}$$

$$Q_{11}(0) = \frac{E_1}{(1-\nu_{12}\nu_{21})}$$

$$Q_{22}(0) = \frac{E_2}{(1-\nu_{12}\nu_{21})} \qquad \textbf{(Equation 37)}$$

$$Q_{12}(0) = \frac{\nu_{12}E_1}{(1-\nu_{12}\nu_{21})}$$

$$Q_{66}(0) = G_{12}$$

Off-axis laminates now need to be considered. Figure 19, similar to 18, shows the structural axis for a single ply, where θ denotes the prescribed angle of the plies with reference axis fixed in the laminate. This angle shall be measured from the x-axis system. The angle is from the x-axis to the 1 axis and it positive in the anti-clockwise

direction. The y-axis is perpendicular to the x-axis and in the plane of the ply. All calculations are made using the xy, known as the structural axes. It is necessary to transform the stress strain law from the material axis to the x-axis.

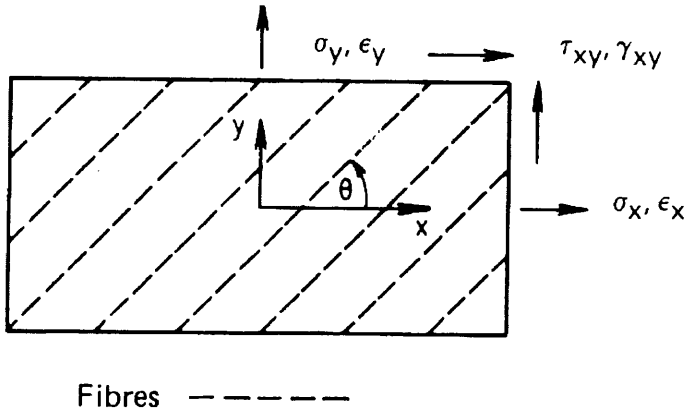

Figure 19 Structural Axes for a Single Ply [26]

If the stresses in the structural axes are denoted by σ_x, σ_y, and τ_{xy}, then these are related to the stresses referred to the material axes by the transformation shown in equation 38 [26]:

$$\begin{bmatrix} \sigma_x \\ \sigma_y \\ \tau_{xy} \end{bmatrix} = \begin{bmatrix} c^2 & s^2 & -2cs \\ s^2 & c^2 & 2cs \\ cs & -cs & c^2 - s^2 \end{bmatrix} \begin{bmatrix} \sigma_1 \\ \sigma_2 \\ \tau_{12} \end{bmatrix} \qquad \textbf{(Equation 38)}$$

c denotes cosθ and s, sinθ. The strains in the material axes are related to those in the structural axes, ε_x, ε_y, $\Upsilon_{xy,}$ which is the inverse transformation shown in equation 39 [26]:

$$\begin{bmatrix} \varepsilon_1 \\ \varepsilon_2 \\ \gamma_{12} \end{bmatrix} = \begin{bmatrix} c^2 & s^2 & cs \\ s^2 & c^2 & -cs \\ -2cs & 2cs & c^2 - s^2 \end{bmatrix} \begin{bmatrix} \varepsilon_x \\ \varepsilon_y \\ \gamma_{xy} \end{bmatrix} \qquad \textbf{(Equation 39)}$$

Substitutions can now be made for σ_1, σ_2, τ_{12}, ε_1, ε_2 and $\gamma_{12,}$ which gives equation 40 [26]:

$$\begin{bmatrix}\sigma_x\\ \sigma_y\\ \tau_{xy}\end{bmatrix}=\begin{bmatrix}Q_{11}(\theta) & Q_{12}(\theta) & Q_{16}(\theta)\\ Q_{12}(\theta) & Q_{22}(\theta) & Q_{26}(\theta)\\ Q_{12}(\theta) & Q_{26}(\theta) & Q_{66}(\theta)\end{bmatrix}\begin{bmatrix}\varepsilon_x\\ \varepsilon_y\\ \gamma_{xy}\end{bmatrix}$$ **(Equation 40)**

The direct stresses are dependent on the shear strains and the shear stress is dependent on the direct strains. Q_{ij} (θ) are related to Q_{ij} (0) by equation 41:

$$\begin{bmatrix}Q_{11}(\theta)\\ Q_{12}(\theta)\\ Q_{22}(\theta)\\ Q_{16}(\theta)\\ Q_{26}(\theta)\\ Q_{66}(\theta)\end{bmatrix}=\begin{bmatrix}c^4 & 2c^2s^2 & s^4 & 4c^2s^2\\ c^2s^2 & c^4+s^4 & c^2s^2 & -4c^2s^2\\ s^4 & 2c^2s^2 & c^4 & 4c^2s^2\\ c^3s & -cs(c^2-s^2) & -cs^3 & -2cs(c^2-s^2)\\ cs^3 & cs(c^2-s^2) & -c^3s & 2cs(c^2-s^2)\\ c^2s^2 & -2c^2s^2 & c^2s^2 & (c^2-s^2)^2\end{bmatrix}\times\begin{bmatrix}Q_{11}(0)\\ Q_{12}(0)\\ Q_{22}(0)\\ Q_{66}(0)\end{bmatrix}$$ **(Equation 41)**

Where values of θ are greater than zero the structural axis are not symmetric and with respect to the axis the material is not orthotropic. This theory is also valid for a laminate as well as a single ply provided that all plies are orientated in the same direction [26].

2.11.2 Laminate Theory

Plate theory relies on the assumption that the thickness of the component is very much smaller than the in-plane dimensions and therefore insignificant, allowing simplifications to be made when carrying out analyses [4]. In-plane loading can be analysed by plane stress elastic theory and bending can be analysed by classical plate bending theory. Analysing these two independently is possible because the two loadings are uncoupled and when both occur the result is given by superposition. For anisotropic laminates, in-plane loading and bending are usually coupled and must therefore be treated together. Uncoupling only generally occurs when a laminate is balanced and symmetric, which is the case for all Airbus laminated structure at the present time.

There are seven basic assumptions of laminate theory [3,4]:

- The structure is restricted to a thin plate or shell, where thickness is insignificant and very much smaller than the in-plane dimensions.
- The strains in the deformed plate are small compared to unity.

- Normal to the un-deformed plate surface remains normal to the deformed plate surface.
- Vertical deflection does not vary through the thickness.
- Stress normal to the plate surface remains negligible.
- The loading is assumed to be in-plane membrane stress and moment resultants.
- The two transverse shear stresses (τ_{zy} & τ_{yz}) are neglected to satisfy classic thin plate shell theory.

Consider Hooke's law; for a homogenous isotropic material in a one dimensional stress state the Hooke's law relationship can be written as:

$\sigma = E\,\varepsilon$ **(Equation 42)**

The proportionality constant, known as the Young's modulus, is the modulus of elasticity and ε is the strain. For a homogeneous isotropic material in a two dimensional stress state (Plane Stress) the relationship changes to equations 43-45:

$$\sigma_1 = (\varepsilon_1 + \nu\varepsilon_{2)})\frac{E}{1-\nu^2}$$ **(Equation 43)**

$$\sigma_2 = (\varepsilon_2 + \nu\varepsilon_1)\frac{E}{1-\nu^2}$$ **(Equation 44)**

$$\tau_{12} = (\gamma_{12})\frac{E}{2(1+\nu)}$$ **(Equation 45)**

The 1D & 2D stress states can be seen graphically in figure 20:

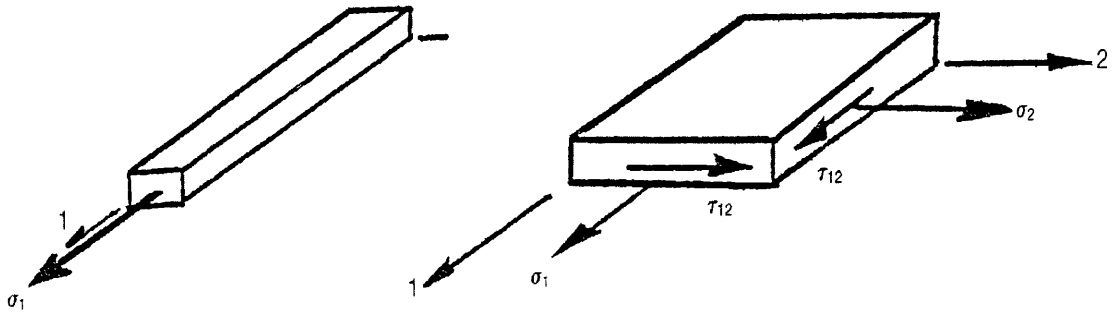

(a) One-dimensional (b) Two-dimensional

Figure 20 Showing 1D & 2D Stress States [3]

The equations can also be expressed in the matrix form, as shown in equation 46:

$$\begin{bmatrix}\sigma_1\\ \sigma_2\\ \tau_{12}\end{bmatrix}=\begin{bmatrix}C_{11} & C_{12} & 0\\ C_{12} & C_{22} & 0\\ 0 & 0 & C_{66}\end{bmatrix}\begin{bmatrix}\varepsilon_1\\ \varepsilon_2\\ \gamma_{12}\end{bmatrix} \qquad \textbf{(Equation 46)}$$

Where C terms can be described by equations 47-49:

$$C_{11}=C_{22}=E/(1-\nu^2) \qquad \textbf{(Equation 47)}$$

$$C_{21}=C_{12}=\nu E/(1-\nu^2) \qquad \textbf{(Equation 48)}$$

$$C_{66}=E/2(1+\nu)=G \qquad \textbf{(Equation 49)}$$

E & ν are two independent elastic constants and in addition G, the shear modulus, is a function of E & ν. Hooke's law relationships can be generalised for three dimensions for anisotropic materials, showing in figure 21:

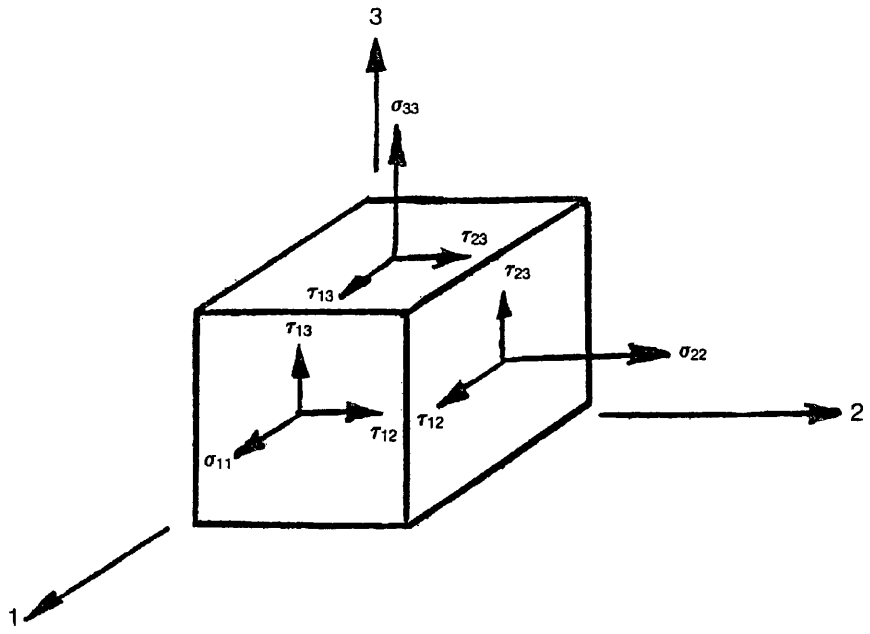

Figure 21 Hooke's Law Theory for Three Dimensions

The relationship to stress and strain is given by equation 50:

$$G=E/2(1+\nu) \qquad \textbf{(Equation 50)}$$

For isotropic materials only two elastic constants are necessary for two or three dimensional applications. For anisotropic materials the following can be generalised:

- There are 21 independent elastic constants for the Hooke's law relationship in three dimensional applications.
- For orthotropic material in three dimensions there are 9 independent elastic constants.
- For an orthotropic material in a two dimensional analysis, there are 4 independent elastic constants required.

The two dimensional stress/strain relationships are represented in figure 22:

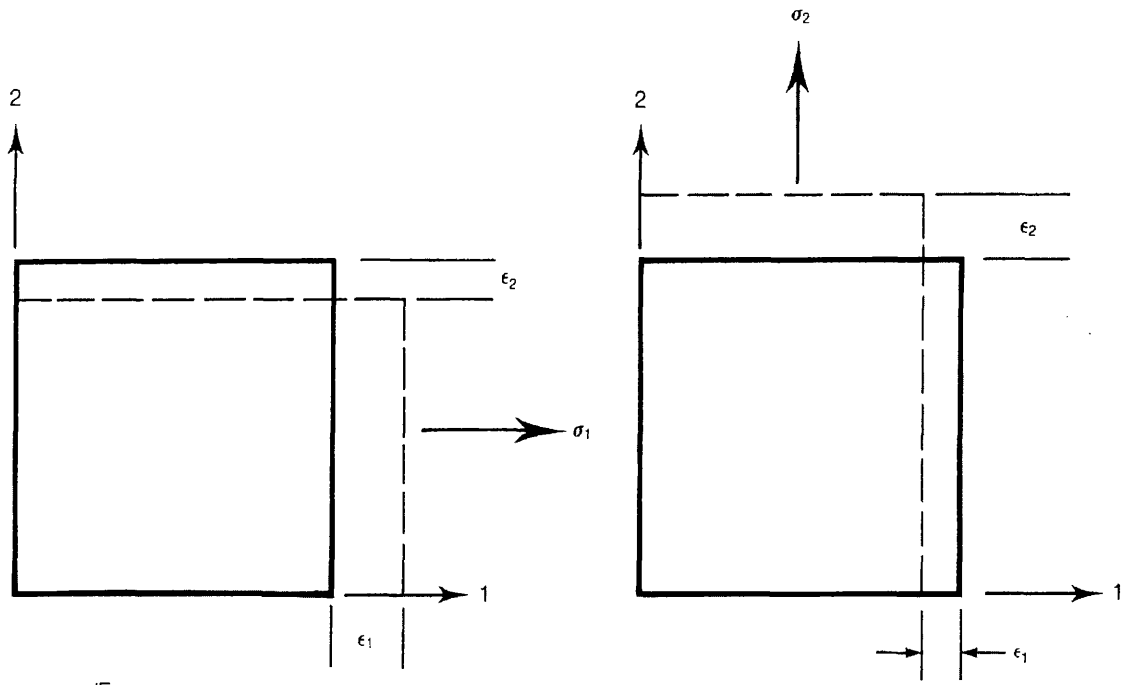

(a) Due to stress σ_1

(b) Due to stress σ_2

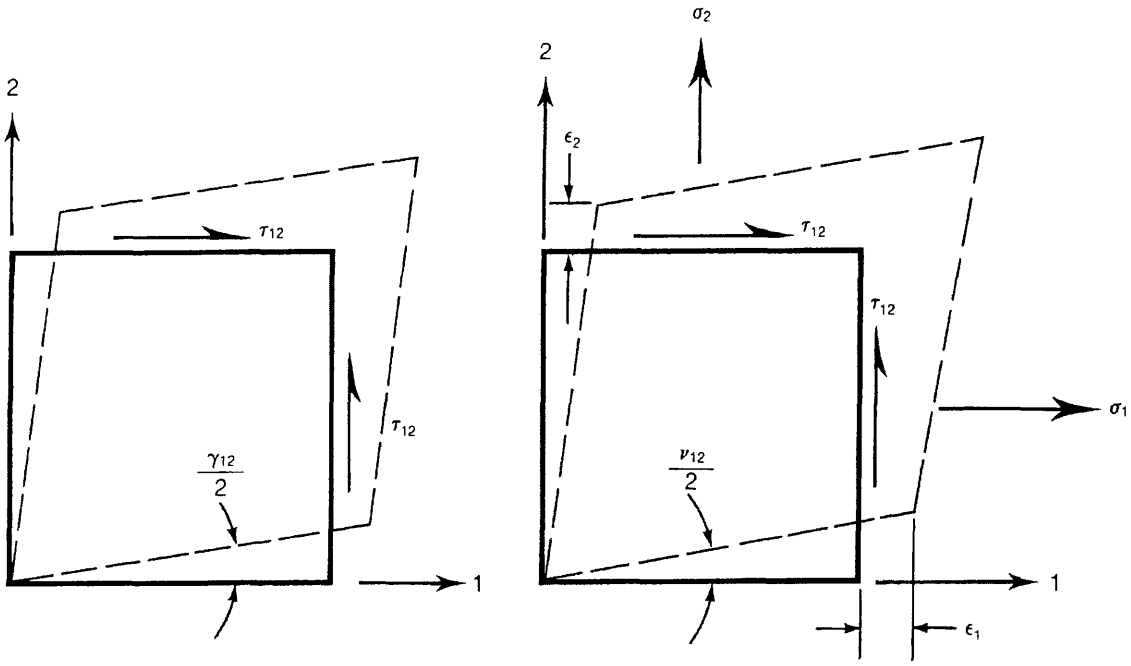

(c) Due to shear stress τ_{12}

(d) Due to combined stresses

Figure 22 Two Dimensional Stress/Strain Relationships [3]

Hooke's law can be written in matrix form as shown in equation 51, where C_{ij} is the stiffness matrix:

$$\begin{bmatrix} \sigma_{11} \\ \sigma_{22} \\ \sigma_{33} \\ \tau_{23} \\ \tau_{13} \\ \tau_{12} \end{bmatrix} = \begin{bmatrix} C_{11} & C_{12} & C_{13} & C_{14} & C_{15} & C_{16} \\ C_{12} & C_{22} & C_{23} & C_{24} & C_{25} & C_{26} \\ C_{13} & C_{23} & C_{33} & C_{34} & C_{35} & C_{36} \\ C_{14} & C_{24} & C_{34} & C_{44} & C_{45} & C_{46} \\ C_{15} & C_{25} & C_{35} & C_{45} & C_{55} & C_{56} \\ C_{16} & C_{26} & C_{36} & C_{46} & C_{56} & C_{66} \end{bmatrix} \begin{bmatrix} \varepsilon_{11} \\ \varepsilon_{22} \\ \varepsilon_{33} \\ \gamma_{23} \\ \gamma_{13} \\ \gamma_{12} \end{bmatrix} \quad \textbf{(Equation 51)}$$

For a plane stress state the equation can now be reduced to equation 52:

$$\begin{bmatrix} \sigma_{11} \\ \sigma_{22} \\ \tau_{12} \end{bmatrix} = \begin{bmatrix} C_{11} & C_{12} & 0 \\ C_{12} & C_{22} & 0 \\ 0 & 0 & C_{66} \end{bmatrix} \begin{bmatrix} \varepsilon_{11} \\ \varepsilon_{22} \\ \gamma_{12} \end{bmatrix} \quad \textbf{(Equation 52)}$$

The four elastic independent constants are expressed in equations 53-56:

$$C_{11} = \frac{E_{11}}{(1 - \nu_{12}\nu_{21})} \quad \textbf{(Equation 53)}$$

$$C_{12} = \nu_{12} C_{22} \quad \textbf{(Equation 54)}$$

$$C_{22} = \frac{E_{22}}{(1 - \nu_{12}\nu_{21})} \quad \textbf{(Equation 55)}$$

$$C_{66} = G_{12} \quad \textbf{(Equation 56)}$$

The elastic constraints can be transformed for an orthotropic material in two dimensions to the laminate axis x & y, for a plane stress state using the transformation matrix Q_{ij}, shown in equation 57:

$$\begin{bmatrix} \sigma_x \\ \sigma_y \\ \tau_{xy} \end{bmatrix} = \begin{bmatrix} Q_{11} & Q_{12} & Q_{16} \\ Q_{21} & Q_{22} & Q_{26} \\ Q_{61} & Q_{62} & Q_{66} \end{bmatrix} \begin{bmatrix} \varepsilon_x \\ \varepsilon_y \\ \gamma_{xy} \end{bmatrix} \quad \textbf{(Equation 57)}$$

The terms of Q can be defined by equations 58-63:

$$Q_{11} = C_{11}\cos^4\theta + 2(C_{12} + 2C_{66})\sin^2\theta\cos^2\theta + C_{22}\sin^4\theta \quad \textbf{(Equation 58)}$$

$$Q_{22} = C_{11}\sin^4\theta + 2(C_{12} + 2C_{66})\sin^2\theta\cos^2\theta + C_{22}\cos^4\theta \quad \textbf{(Equation 59)}$$

$$Q_{12} = (C_{11} + C_{22} - 4C_{66})\sin^2\theta\cos^2\theta + C_{12}(\sin^4\theta + \cos^4\theta) \quad \textbf{(Equation 60)}$$

$$Q_{66} = (C_{11} + C_{22} - 2C_{12} - 2C_{66})\sin^2\theta\cos^2\theta + C_{66}(\sin^4\theta + \cos^4\theta) \quad \textbf{(Equation 61)}$$

$$Q_{16} = (C_{11} - C_{12} - 2C_{66})\sin\theta\cos^3\theta + (C_{12} - C_{22} + 2C_{66})\sin^3\theta\cos\theta \quad \textbf{(Equation 62)}$$

$$Q_{26} = (C_{11} - C_{12} - 2C_{66})\sin^3\theta\cos^3\theta + (C_{12} - C_{22} + 2C_{66})\sin^3\theta\cos^3\theta \quad \textbf{(Equation 63)}$$

The equation for a thin laminated anisotropic plate is shown in equation 64:

$$\begin{bmatrix} N \\ M \end{bmatrix} = \begin{bmatrix} A & B \\ B & D \end{bmatrix} \begin{bmatrix} \varepsilon \\ \aleph \end{bmatrix} \quad \textbf{(Equation 64)}$$

This can be further shown in equation 65:

$$\begin{bmatrix} N_x \\ N_y \\ N_{xy} \\ M_x \\ M_y \\ M_{xy} \end{bmatrix} = \begin{bmatrix} A_{11} & A_{12} & A_{16} \\ A_{21} & A_{22} & A_{26} \\ A_{61} & A_{62} & A_{66} \\ B_{11} & B_{12} & B_{16} \\ B_{21} & B_{22} & B_{26} \\ B_{61} & B_{62} & B_{66} \end{bmatrix} \begin{bmatrix} \varepsilon_x \\ \varepsilon_y \\ \varepsilon_{xy} \end{bmatrix} + \begin{bmatrix} B_{11} & B_{12} & B_{16} \\ B_{21} & B_{22} & B_{26} \\ B_{61} & B_{62} & B_{66} \\ D_{11} & D_{22} & D_{16} \\ D_{21} & D_{22} & D_{26} \\ D_{61} & D_{62} & D_{66} \end{bmatrix} \begin{bmatrix} \aleph_x \\ \aleph_y \\ \aleph_{xy} \end{bmatrix} \quad \textbf{(Equation 65)}$$

Where:

$$A_{ij} = \sum_{k=1}^{n} (Q_{ij})_k (h_k - h_{k-1}) \quad \textbf{(Equation 66)}$$

$$B_{ij} = \sum_{k=1}^{n} (Q_{ij})_k (h_k{}^2 - h_{k-1}^2)/2 \quad \textbf{(Equation 67)}$$

$$D_{ij} = \sum_{k=1}^{n} (Q_{ij})_k (h_k{}^3 - h_{k-1}^3)/3 \quad \textbf{(Equation 68)}$$

A_{ij} is the extensional or membrane stiffness, D_{ij} is the flexural or bending stiffness, B_{ij} is responsible for the coupling between the membrane and bending behaviours. $\aleph$, is the forced curvature, which even within the limits of small deflection theory causes the induction of in-plane loads, N. In-plane strains, ε, induce curvatures in the laminate. This coupling is caused by the neutral axis and the mid-plane of the laminate not being coincident. There are procedures for simplifying the general equation. The one discussed here is to eliminate the coupling matrix B. This is done by creating a symmetric laminate about the mid-plane, which allows the equation to be reduced to that shown in equation 69:

$$[N] = [A][\varepsilon] \qquad \textbf{(Equation 69)}$$
$$[M] = -[D][\aleph]$$

If the laminate is constructed with equal number of pairs of lamina with symmetry then the A matrix become orthotropic in nature, with the B matrix remaining fully populated and anisotropic, as shown in equation 70:

$$[A] = \begin{bmatrix} A_{11} & A_{12} & 0 \\ A_{12} & A_{22} & 0 \\ 0 & 0 & A_{66} \end{bmatrix} \qquad \textbf{(Equation 70)}$$

2.11.3 Laminate Failure Criterion

The basis of laminate failure criteria requires mechanical property data for a single ply. It is a means by which strength of the laminate under plane stress conditions can be derived. Using laminate failure criterion it is possible to predict the first ply failure of a laminate as well as the ultimate failure load. It is possible to determine the stresses in individual plies within the laminate. It is also possible, using equation 38, to calculate the stresses at any point within a ply aligned to the material axis which makes the calculation of ultimate strength of a component possible. Failure criteria are well documented and can be found in references [3,5,26]. Work still continues with regard to failure criteria and it can be said that each criteria discussed has limitations. Airbus insists that the Hoffman Failure criterion should be used when carrying out failure analysis of composites structures, as the associated analysis procedures have been certified for aircraft use and can be considered to be a conservative method.

Before using the failure criterion, it is necessary to generate lamina data from tests for a given material (fibre & resin combination). The properties required are ultimate strength in tension and compression in the fibre direction (F_{1T} & F_{1C} respectively) & transverse direction (F_{2T} & F_{2C} respectively), followed by the in-plane ultimate shear strength (F_{12}).

2.11.3.1 Maximum Stress Criterion

The maximum stress criterion assumes that failure occurs only when one of the terms in equation 71 is violated. The criterion does not account for interaction between the stress components and therefore is considered to be an optimistic method.

$$-F_{1C} \leq \sigma_1 \leq F_{1T}$$
$$-F_{2C} \leq \sigma_2 \leq F_{2T} \qquad \textbf{(Equation 71)}$$
$$-F_{12} \leq \tau_{21} \leq F_{12}$$

2.11.3.2 Maximum Strain Criterion

Strains can be derived from test. The ultimate strain for a single ply can then be used as in equation 71. Again this method is thought to be optimistic.

2.11.3.3 Tsai-Hill/ Hoffman Criterion/ Tsai-Wu

This criterion begins with its original form proposed by Tsai-Hill, which did not specifically allow for the differences between the tensile and compressive strengths. It was Hoffman who modified the criterion to account for the different compressive and tensile strengths [26]. Failure can be considered to occur when equation 72 is violated:

$$\sigma_1^2/(F_{1T}F_{1C}) - \sigma_1\sigma_2/(F_{1T}F_{1C}) + \sigma_2^2/(F_{2T}F_{2C}) + (1/F_{1T} - 1/F_{1C})\sigma_1 + (1/F_{2T} - 1/F_{2C})\sigma_2 + \tau_{12}^2/F_{12}^2 \leq 1$$

(Equation 72)

The equation does not allow for stress interaction effects. A more refined criterion is known as the Tsai-Wu criterion, which is based on stress tensor theory. The previously discussed Hoffman criterion can be considered not to take into account these tensors,

which has led to many objecting to the Hoffman criterion. The Tsai-Wu criterion is subject to transformation and allows interaction between stresses [3]. Failure occurs when equation 73 is valid:

$K_iF_i + K_{ij}F_{ij}=1$ where $(i,j = 1, 2, 6)$ **(Equation 73)**

K_i & K_{ij} are the strength tensors (inverse) that require off-axis tests in order to evaluate them.

2.11.3.4 Other Failure Criteria

Additional failure criteria have been developed, that have not been discussed here. These are captured in [27] and include Yamada-Sun, Hashin, Hashin-Rotem and modified Puck. As these failure criteria were not part of the laminate analysis used by Airbus when this programme of work was started these criteria have not been discussed in detail, however they should be considered for future work.

2.12 Moisture Absorption in Carbon Fibre Reinforced Composites

2.12.1 The Effects of Environment on Composite Materials

The effects of environment on composite structures has been widely investigated and understood. As time progresses more and more composite materials are being utilised in airframe structures to include both primary and secondary structures. Classically composites were first used on military applications such as the F-14, F-15, F-16 & B-1 [28]. Being generally lightweight compared to their civil airliner counterparts, their structures tend to be relatively thin (due to the relatively lower loading) and therefore are affected by their environment to a greater extent, as the time to heat and saturate thin structures is less than that of thick structures. As composites are used to a greater extent within wingbox structures their thicknesses are ever increasing.

Primary environmental conditions encountered during the service life of an aircraft include temperature, humidity and cyclic loading. There are other environmental effects such as lightening strikes, acoustic fatigue, thermal spikes, ultraviolet radiation and aircraft fluids. None of these environmental effects are catastrophic and they can be easily measured and understood allowing the designer to account for them during design [28]. Within Airbus composites are generally designed using worst case material

properties to ensure conservatism, namely HOT/WET material properties are used where material strengths are generated assuming that they are fully saturated. This approach is essential for thin structures; however it comes into question where structures are becoming relatively thicker.

Very little research into strength degradation as a result of environment exists and to the author's knowledge the effect of varying saturation levels on the strength of thick structures to date has not been rigorously investigated. It is however well documented that moisture ingress and varying temperatures causes reductions in structural properties of the matrix [28,29,30,31,32,33,34]. Good design practice orients the fibres so that the matrix stresses are minimised and therefore the resulting designed component is well within design allowables produced by testing.

As previously mentioned the combined effect of temperature and humidity represent the most severe threat to structural integrity of composite structures. Epoxy systems have an affinity for the absorption of moisture which can occur during runway storage and various flight conditions, however early studies have shown that the fibres themselves are relatively unaffected [28]. When the structure absorbs moisture the material undergoes a physical change due to swelling and the glass transition temperature of the resin is lowered, resulting in a decrease in matrix controlled and interface controlled mechanical properties [31].

2.12.2 Mechanical Property Degradation

The reduction in performance of composite materials exposed to environment is well understood. At Airbus when qualifying new materials an extensive material test programme is produced, that explores the following conditions:

- Room Temperature Tested Dry Samples (RT/DRY)
- Room Temperature Wet Samples (RT/WET)
- High Temperature (90°C) Dry Samples (HOT/DRY)
- High Temperature Wet Samples (HOT/WET)
- Low Temperature (-55°C) Wet Samples (-55°C/WET)

Typically the worst case level of saturation is investigated i.e. 70°C 85%RH until saturation, followed by testing. From the literature many people have explored the

effects on performance of composite materials using similar criteria. However, none of these studies seriously attempts to quantify strength at different levels of saturation and/or the strength of laminates which were partially saturated.

Within the literature a number of people have studied the effects of moisture on the properties of composites [35,36,37,38,39]. In terms of following a similar approach [39] comes close to what is being attempted within this project. This research (at the University of Birmingham) looked at the compression strength of both unidirectional and directed laminates exposed to environment. The work followed a similar approach with regard to predicted mechanical property performance using classical laminate theory discussed in section 2.11.2. However in a similar way to Airbus they focused on one level of saturation, which in this case was 95% RH, where coupons were conditioned at 50°C. However they were able to link a 24% strength reduction for 0/90° laminates and 37.4% for a quasi-isotropic laminate. A similar study on 0° and 90^0 compression tests was carried out by [40], which showed a similar reduction in strength of up to 35%. This study initially looked like it had adopted the same approach, characterising strength as a function of moisture content. However, it was not clear from the published material how they achieved different moisture contents because all samples were immersed in water at different temperatures. Temperature affects rate and not moisture percentage thus one cannot draw any conclusions from this data at any point other than the fully saturated condition.

Although the tensile properties of the fibres are known to be insensitive to moisture absorption off axis loading leads to a reduction in strength, brought about by degradation of the matrix. 90° tensile strength is directly affected by moisture, quantified by the supporting research [41] and other literature [42] with [43] showing significant reductions in both strength & modulus. Similar findings are found in [44], where unidirectional and directed ($\pm 45^0$) laminates were studied in both tension compression and shear and a reported drop of 25-30% was seen in tensile strength for the 90^0 & $\pm 45^0$ laminates.

Within the literature several studies on the effect of shear strength have also been reported [45,46,47]. Adams & Singh [47] specifically looked at both interlaminar and in-plane shear, both of which are considered within the current EMOC project, utilising similar aerospace grade materials. In this study only full saturation at maximum humidity was considered with 100%RH being used to evaluate mechanical

performance. Both recorded that interlaminar and in-plane shear strength and stiffness were reduced by temperature and moisture, however it was also noted that once specimens were dried out there was no permanent affect on mechanical performance indicating that the effects of environment can be reversed. Reference [46] shows good agreement with the literature; however the Carall (Aluminium Carbon Fibre Laminates) material having a metallic barrier showed significantly reduced and slower uptake than standard carbon fibre laminates. Reference [48] studied interlaminar shear and found a 10% reduction in interlaminar shear strength after 33 days at 95%RH at 50°C and a further reduction of 35% when conditioning specimens over the same period by boiling them in water.

Studies on the fracture toughness of composites have also been documented [49,50]. Reference [50] reports a 25% higher fracture toughness for saturated material compared to dry samples. There was no effect reported of moisture on fracture toughness, however as temperature increased the strain energy release rate increased slightly for mode 1 uni-axial loading. In pure mode II (shear loading) the critical strain energy release rate drops with increased moisture and temperature. For mixed mode (mode 1 & 2), the strain energy release rate decreased with moisture but no dependency was observed with temperature. Further work was discovered that was able to assess transverse cracking in a simple lamina [51], where good correlation was made to temperature and humidity, although this did not extend the analysis of directed laminates.

As mentioned in section 2.9.5, where compression after impact is discussed, it is important to consider the effect of damage on structural integrity. One reference was found in the literature, which specifically linked moisture concentration and damage [52]. This source did not specifically damage their test specimen they simply evaluated the damage propagation of each ply layer under tensile loading. It was observed that the presence of moisture resulted in a decrease in modulus as a result of large scale edge de-lamination. It was further found that moisture reduced residual stresses, but the high temperatures overcame this benefit. The literature indicated that conditioning was carried out at different levels of saturation; although it is not stated what the conditioning parameters were, different moisture contents were simply quoted which were then tested at different temperatures.

In terms of actual structural tests, one reference was discovered [53] that discussed, what was essentially a filled hole compression/tension test, as described in 2.9.6. It

should be noted that the extreme environment was not just the presence of temperature and humidity, but also the use of a flight temperature of 127°C during supersonic flight and most of the degradation was attributed to the glass transition temperature being frequently exceeded by this high temperature cycle. It was observed that there was a link between absorbed moisture and the exceeded glass transition temperature, which increased absorption and as a result further degraded matrix dominated properties. The literature in this case also verified that there was no degradation in fibre dominated properties.

Attempts have been made by Airbus as well as other institutions to reduce the conditioning time during testing [54]. To achieve this the temperature was often raised well above 90°C often reaching the glass transition temperature of the material, while at the same time raising the humidity past that found in service. This leads to an artificially high moisture distribution at the outer most plies and an artificially low moisture profile within the thickness and in the author's opinion may worsen the affects on mechanical performance to high temperature degrading the matrix producing for example micro-cracks. These micro-cracks were found in research done in [55] where a glass epoxy material was used. It should be noted that the presence of micro-cracks after conditioning for the materials being considered by the EMOC programme were not found, with the appropriate limits placed on temperature to prevent this from occurring [41]. Finally [56] showed promise in modelling the properties of the material relative to moisture absorption and oxygen diffusivity using FEM techniques; however it made no attempt to change the individual lamina properties as a function of the modelled moisture values and or temperature. The modelling approach is worth considering as it may allow more accurate predictions of the moisture transport.

Fatigue is a consideration which has not been considered in EMOC as it is based on modelling the static strength of the composite and with a no crack and hence no crack growth philosophy it was not felt necessary to consider it. Composites are considered in terms of damage tolerance and in this instance strain limits are placed on the structure to prevent crack growth up to a point where the damage size is barely visible and therefore may go undetected. Any damage larger than this would lead to a repair to the airframe. Within the literature a study on the fatigue performance at elevated temperatures was found [57], although this was not linked to moisture. It was observed that the softening of the matrix resulted in lower fatigue strengths and they also considered temperatures above the glass transition temperature, which lead to a more rapid degradation in performance as would be expected.

2.12.3 *Accounting for Moisture in Composite Structures*

Material allowable strengths are derived from statistics [4], where a percentage of the population (95% or 99%) of the specimens are expected to exceed the quoted allowable strength with 95% confidence. Due to the scatter in results and the application of statistics it is often necessary to perform a significant amount of testing for each material, which will account for variations in manufacturing processes etc.

There are two methods for determining HOT/WET environmental knock-downs as described by Springer [58]. The first method determines reduced allowables for lamina properties, based on large and expensive test campaigns, where the worst case temperature is applied when generating the allowables. These allowables can then be used when deriving laminate strengths using the HOT/WET allowable strengths. Damage tolerance factors may also be applied, as is the case with Airbus policy, where coupons such as those described in 2.1.7.5 are tested under HOT/WET conditions. The second methodology is to apply a single strength/strain factor to the composite component, based on actual tests. An example of where Airbus would apply this would be to bearing specimens, where large test programmes are required for each joint configuration, requiring exponentially large test programmes to generate HOT/WET properties for each joint. These applied factors are typically extremely conservative but offer a good balance between cost and structural efficiency.

2.12.4 *Fickian Diffusion & Modelling Moisture Ingress*

Diffusion of moisture into a composite material can be described by a mathematical model based on standard diffusion equations and provides a fundamental grounding for which diffusion of both moisture (Fick's 2nd Law) and heat (Fourier equation) into the material can be predicted. Within Airbus three computer-based mathematical tools exist for calculating one dimensional (1D) absorption of moisture into a composite material. These tools were all based on the work Springer [59] conducted in the early 1980's where he constructed a simple computer code based on a Fourier Transform equation to calculate the rate of moisture uptake. This basic model was designed for use on a simple hand held calculator and the code had been bought from Springer for use by Airbus in the 1990's.

There are essentially two basic ways in which diffusion can be described. An analogy could be two bulbs connected by a long thin capillary, as shown in figure 23. The bulbs are under constant temperature and pressure and have equal volumes. One bulb contains Carbon Dioxide, the other Nitrogen.

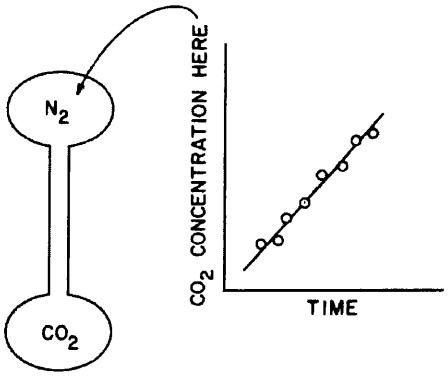

Figure 23 A Simple Diffusion Experiment of Two Bulbs Filled with Different Gases [60]

The concentration of Carbon Dioxide is measured in the bulb filled with Nitrogen. These measurements are made when only a trace of the gas has been transferred and it is observed that the concentration of Carbon Dioxide increases linearly with time and therefore it is known the amount transferred per unit of time is known. To analyse the amount transferred it is necessary to first define the 'flux', shown by equation 74:

$$CO_2\,flux = \left(\frac{Amount\ of\ gas\ removed}{time(cross\ sectional\ area\ capillary)} \right) \qquad \textbf{(Equation 74)}$$

If the cross sectional area is doubled the amount transported must also double. The next step is to consider the flux proportional to the gas concentration, shown by equation 75:

$$CO_2 flux = k\ (CO_2\ concentration\ difference) \qquad \textbf{(Equation 75)}$$

The proportionality constant k is called a mass transfer coefficient. Its introduction is one of the two basic models of diffusion. If the capillary's length is increased, the flux will decrease as shown in equation 76:

$$CO_2\,flux = D\left(\frac{\Delta CO_2 concentration}{capillary\ length} \right) \qquad \textbf{(Equation 76)}$$

D (m^2s^{-1}) is a new proportionality constant known as the diffusion coefficient, this is the second model of diffusion, known as Fick's law. Both methods may be unsuccessful due to the assumptions made when developing them e.g. the flux may not be proportional to the concentration difference if the capillary is very thin or if the two gases react. These cases are however exceptions and in most cases the models work well as practical solutions [60].

The choice between each model often comes down to experimental resources required to calculate a diffusion coefficient 'D'. The mass transfer coefficient will only provide an average concentration ignoring the fact that the concentration may be fully saturated at a material surface, while the centre of the material may not have experienced any increase in mass. The diffusion method often assumes 'D' to be constant and concentration will vary with time and position.

To improve both methods experiments can be conducted to measure the uptake rate and then correlate the measurements as mass transfer coefficients. The average concentration versus time is then known. This can then be included in the diffusion model previously defined, Equation 77, where '*l*' is the distance over which diffusion occurs [60].

$$CO_2\,flux = D\left(\frac{(CO_2 concentration\ \ at\ z=0) - (CO_2 concentration\ at\ z=l)}{(thickness\ at\ z=l) - (thickness\ at\ z=0)}\right)$$

(Equation 77)

It is normal to assume the distance '*l*' to be very small. This relationship is written symbolically in equation 78. This relationship correlates the diffusion coefficient 'D'. From this it is possible to correctly predict uptake over time and the concentration of the diffusing substance in the material for all positions and times.

$$D\lim_{l\to 0}\frac{c_1|z=z-c_1|z=z+1}{z|z+1-z|z} = -D\frac{\partial c_1}{\partial z}$$

(Equation 78)

2.12.5 *George Springer's Moisture Absorption Model*

The theory based on Fick's law is essentially the same as that discussed in section 2.12.4. Springer considered the problem to be a one dimensional plate of known thickness 'h', exposed on both sides to a moist environment. He set the model to consider a plate consisting of one or more materials where 'n', describes a solid single plate or an 'n' laminate of thickness h_1, h_2, h_3..... h_n etc, as shown in figure 24:

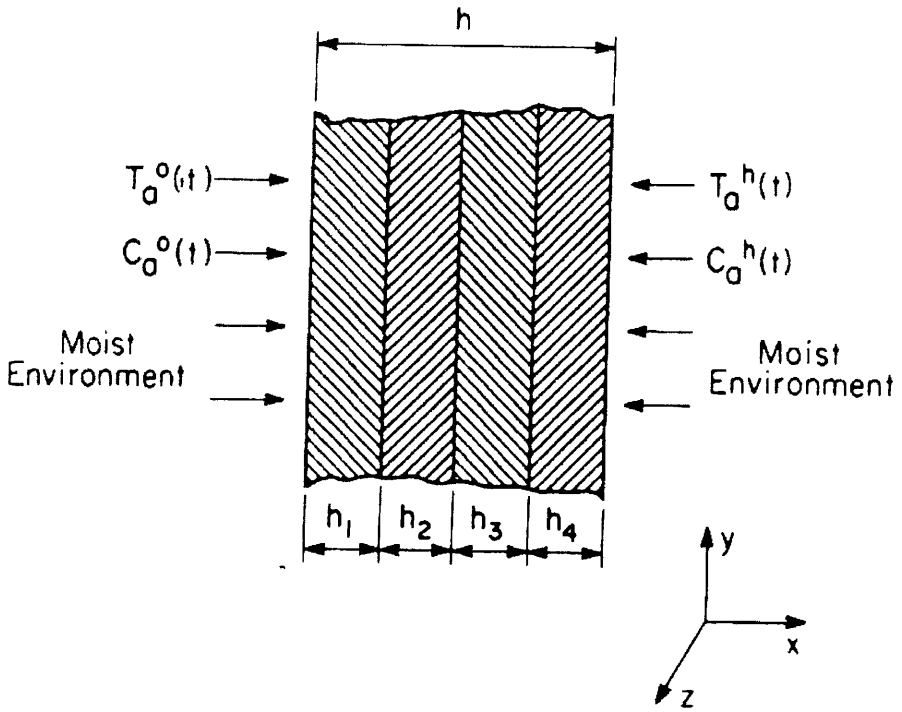

Figure 24 Description of Springer's Mathematical Problem for a Plate of Dissimilar Material [59]

For the other dimensions of the laminate the plate is considered to be infinite i.e. the 'y' & 'z' directions, which allows variation of temperature and moisture content in the 'x' direction only. At time less than 0 the temperature 'T_i' and the moisture concentration 'C_i' are specified. At time equal to zero the sides of the plate are exposed to the moisture for which the temperature T_a and the moisture concentration C_a are given as a function of time. The objective is to determine the temperature 'T' and moisture distribution 'C' inside the plate as a function of both position and time and the moisture content (weight or mass gain) of the material 'm' as a function of time. As with the Airbus models the temperature and moisture diffusion are described by the Fourier and Fick equations shown in equation 79 & 80 respectively. 'ρ' is the density of the material (kg/m^3), 'c' the specific heat (J/(kg.K)), 'k_x' the thermal conductivity (W/(m.K)) and 'D_x' the diffusivity of the material (mm^2/s) [59].

$$\rho c \frac{\partial T}{\partial t} = \frac{\partial}{\partial x}\left(k_x \frac{\partial T}{\partial x} \right)$$ **(Equation 79)**

$$\frac{\partial C}{\partial t} = \frac{\partial}{\partial x}\left(D_x \frac{\partial C}{\partial x} \right)$$ **(Equation 80)**

Equations 79 & 80 (with potentially non-constant k & D parameters) are subjected to initial boundary conditions. For multilayered laminates, two or more conditions must be specified at the interface of each layer. The theory assumed here is incorporated into both the 'Wet Aging' & Swansea University tool discussed in section 2.12.4 & 2.12.5. Springer utilised FORTRAN computer code to create the first moisture model, known as 'W8GAIN'. The derivation of the moisture method and a full list of the 'W8GAIN' code can be found in reference [59].

2.12.6 Airbus/EADS Wet Ageing Model

Airbus Germany modified the 'W8GAIN' code to allow graphical outputs to be produced from the original FORTRAN code to show moisture uptake over time and the levels of moisture (in terms of percentage weight increase) through the thickness of the 1D laminate. At the time Airbus was not a unified company and a parallel activity was carried out in Airbus Spain. Near the end of the 1990s, early 2000, Airbus France created a superior tool, again mathematically all of these tools were fundamentally the same, however this new tool known as 'Wet Aging', had the advantage of a superior graphical User Interface (GUI) and could be run from any windows based operating system providing result output files which could be utilised by standard Microsoft Software (e.g. Microsoft Excel via text files). During this time the Author commissioned Swansea University to undertake a similar modelling exercise but to build on the existing capability by allowing a three dimensional (3D) modelling capability to be adopted. This 3D model would allow moisture diffusion coefficients to be entered in each dimension further increasing the functionality of the model.

Since 2001 Airbus has become a single entity. This has highlighted the fact that each industrial site across Europe has it own tools and methods for assessing composite structures and in the case of moisture absorption 3 different tools existed. To ensure best practice a number of harmonisation activities were taken place to ensure a unified

Airbus can exploit optimal methods and tools. The moisture ingress methodology was one of the methods that were to be harmonised. Headed up by the author a multi-national Airbus team was brought together to benchmark the different sites tools. Together with the Airbus tools the Swansea University Tool was also benchmarked against the existing Airbus tools as validation. As a result of the harmonisation process the Airbus France Tool known as 'Wet Aging' was selected as the harmonised Airbus method for predicting moisture ingress into carbon fibre laminates.

The harmonisation process established that the predictions of all models including the Swansea University Model were the same. This was established by running a number of different test cases including different materials, cyclic and varying environmental conditions. The 'Wet Aging Tool' was chosen as it provided a Windows based solution with the advantage of having a user friendly GUI. There are two main objectives of 'Wet Aging' software firstly computation of the local and total predictive calculation of the water concentration of a laminate for a given thickness and secondly, allowing varying material properties to be taken into account (single and multiphase) for constant and variable hydrometrical loading.

Diffusion is three-dimensional problem, but the tool only considers a 1D problem because for a sufficiently large plate it can be considered that the diffusion of water only occurs through the thickness of the material. This means that Fick's 2nd law is only utilised in the 1D form represented in equation 81 [61]:

$$\frac{\partial C \times t}{\partial t} = D \frac{\partial^2 C \times t}{\partial x^2} \qquad \textbf{(Equation 81)}$$

Where '*C*' represents the local mass water concentration inside the composite and '*D*' the coefficient of diffusion. In addition to the coefficient of diffusion *'D',* which characterises the rate of penetration of water, a second parameter named '*Ms*' (saturation weight) represents the maximum quantity of water which the composite can absorb. It often is expressed as a percentage. Mathematically Ms is given in equation 82, where M_{dry} is the dry mass (g) and M_{wet} the final mass after diffusion (g) [61]:

$$Ms = \frac{M_{wet} - M_{dry}}{M_{dry}} \times 100\% \qquad \textbf{(Equation 82)}$$

Ms is not explicitly present in Fick's law, but it appears in certain boundary conditions. Indeed, it is considered that locally, on the edge of a plate, one has a local concentration equal to the mass with saturation, which supposes that the edge of plate is saturated with moisture instantaneously. Therefore it is possible to neglect all the local phenomena of transfer of moisture between the outside media and the plate. Instead the major dependence with the first order is the sensitivity of the parameters with respect to the external conditions, namely the temperature 'T' and the relative humidity '%rh'. As a first approximation, it is considered that the coefficient of diffusion is dependent only on the temperature. In this case an Arrhenius law is used where 'R' is the perfect gas constant, 'T' temperature (K), shown in equation 83 [61]:

$$D = D_0 e^{-\frac{Q}{RT}} \qquad \textbf{(Equation 83)}$$

In addition, the relative humidity 'RH' significantly influences the maximum moisture content at saturation. Its effect is modelled by equation 84, indicating non-linearity between humidity and level of water mass in the material. Where 'a' and 'b' are constants given by test results of specimens with percentage of fibre, v_f.

$$Ms = g \times v_f \times a \times RH^b \qquad \textbf{(Equation 84)}$$

To improve the correlation between tests results and the calculated asymptotic weight, the percentage of fibres is taken into account modifying equation 84 to give 85 as follows:

$$Ms = \frac{-v_f}{-v_{fref}} a \times RH^b \qquad \textbf{(Equation 85)}$$

It is important to note that the coefficients used will vary for cyclic temperatures and humidities. The modelling exercise is dependent on the material test data available to accurately mimic material behaviour using the model. Essentially the diffusion coefficient needs to be derived from testing. It is derived from monitoring the uptake of moisture over time until the laminate is fully saturated and no longer increases in weight.

Now to calculate the mass concentration of the water in the laminate utilising equations 81 to 85, equation 86 is produced, where m is moisture concentration, m_i the dry concentration and m_∞ is asymptotic concentration, 't' is time (s) 'n' is the length (m) & 'h' is the thickness (m) of the modelled laminate:

$$\frac{m-m_i}{m_\infty-m_i}=-\frac{8}{\pi^2}\sum_{n=0}^{\infty}\frac{1}{(2n+1)^2}e^{-D(2n+1)^2\pi^2 t/h^2} \qquad \textbf{(Equation 86)}$$

In the same way that the mass concentration is calculated the variation of water concentration along the thickness of the laminate can be calculated as shown in equation 87. The terms are the same as equation 86 with the exception of C, which is concentration:

$$\frac{C-C_i}{C_\infty-C_i}=-\frac{4}{\pi}\sum_{n=0}^{\infty}\frac{(-1)^n}{2n+1}e^{-D(2n+1)^2+\pi^2 t/h^2} \qquad \textbf{(Equation 87)}$$

These equations can then be further modified to take into account cyclic thermal/humidity loadings. In this case it is not enough to only know the initial condition of the laminate in terms of concentration and temperature it is necessary to find time intervals with a snap-shot of moisture content and diffusion coefficient at precise moments in time [61].

The next challenge that the tool must overcome is the consideration of two dissimilar composite materials forming a laminate i.e. a co-bonded structure may have the same composite material type but be bonded together by a different resin system. For a single material Fick's law is solved by understanding the conditions at either end of the plate. In the multi-phase (two plus material case) it is necessary to solve Fick's law for each material where the concentrations at the ends of each material may not be known. These new unknowns complicate the situation further and the necessary solutions are drawn from equations to resolve the behaviour of the water at the interface or boundary [61].

The water at the interface will obey thermodynamic laws and therefore be in balance. A good analogy of this is to consider a material constructed of a metal and a sponge. In a wet environment the mass concentration will be zero in the metal whereas it will be high in the sponge. The standard Fickian law needs special boundary conditions to

model such a situation. This is based on mass transfer by means of diffusion of the local concentration as it would result in the same level of concentration in both the materials at the end of an infinite time. The water will go into the material which has the greatest affinity for it, explained by the fact that there must be uniformity of the chemical potential of water between the two materials. The chemical potential (v) is not directly related to the mass concentration (C) but to the mass fraction (M_s) of concentration compared to saturation as shown in equation 88:

$$v = \frac{C}{Ms} \qquad \textbf{(Equation 88)}$$

This state is not considered to be accurate for high levels of humidity and therefore it is apparent that there is a difference with thermal equivalence, where the thermodynamic balance implies the uniformity of the temperatures directly. In this multi-material case the original variable of resolution 'v' and the concentration 'C' brings together an interface, 'i' equation, 89:

$$v^{+} + i = v^{-} i \qquad \textbf{(Equation 89)}$$

Finally continuity of flow is considered at the interface which is the final missing equation as a result of the relationship between flow and the interface. Continuity of flow for concentration and variable of resolution is expressed as (equation 90 a & b):

a) $$Di\frac{dCi}{dx}right = Di + \frac{dCi+}{dx}left$$ and **b)** $$DiMsi\frac{dvi}{dx}right = di + Msi + \frac{dvi+}{dx}left$$

(Equations 90 a & b)

2.12.7 Swansea University Finite Difference Model

This model has been developed using the same physics described in section 2.11.2, however it adopts a true finite difference (FD) approach to solving moisture content with respect to diffusion. Benchmarked against existing Airbus tools and methods this FD code forms the starting point of the FE project supporting this project as specified by the author who is the main project manager. The key innovation with respect to the FE project will be to link the moisture diffusion predictions to the mechanical properties, which are typically degraded as moisture ingress occurs. This model utilises Fick's 2nd

law but in this case different diffusion coefficients can be assigned in 3D i.e. in the 'x', 'y', and 'z' dimensions. As with the wet aging tool an initial moisture content inside the plate is specified, 'C_i'. Starting with time 't' equal to zero the faces of the plate are exposed to known relative humidity 'RH', for which the temperature, 'T_a' and the moisture concentration, 'C_a' are given as a function of time. A schematic of the material to be modelled is shown in figure 25 [62].

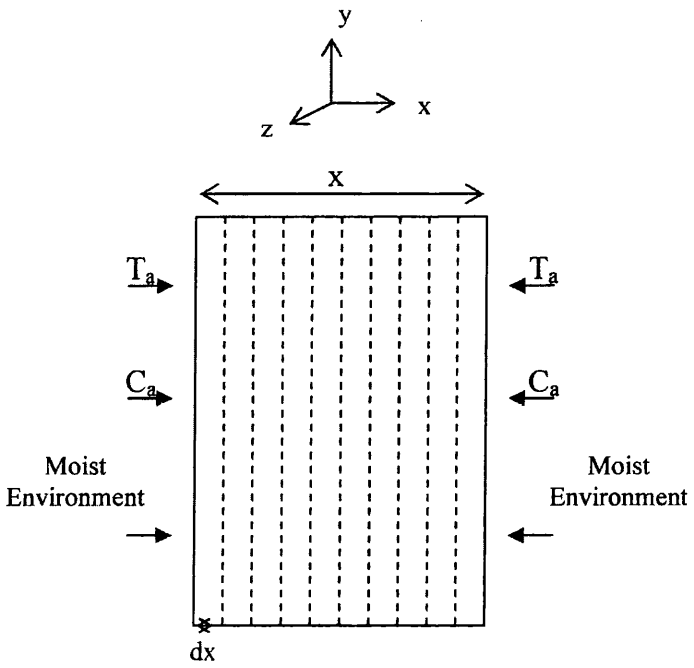

Figure 25 Imposed Concentrations & Temperatures on the Faces of the Plate in the 'X' Direction [62]

The 3D FD model requires Fick's law in 3D as expressed in equation 91.

$$\frac{\partial C}{\partial t} = \frac{\partial}{\partial x}\left(Dx\frac{\partial C}{\partial x}\right) + \frac{\partial}{\partial y}\left(Dy\frac{\partial C}{\partial y}\right) + \frac{\partial}{\partial z}\left(Dz\frac{\partial C}{\partial z}\right) \qquad \textbf{(Equation 91)}$$

Where 'C' represents the local mass water concentration inside the composite (g/mm^3), 't' is the time in seconds, 'x', 'y', 'z' are distances (mm) and D_x, D_y & D_z the coefficients of diffusion in each of the three dimensions. As with the 'Wet Ageing' Tool it is assumed that the diffusion coefficient is only dependent on the temperature and can therefore be modelled using an Arrhenius equation as shown in equation 83. 'R' is the universal gas constant (J/mol.K), 'Q' the activation energy for diffusion (J/mol) & 'T' the temperature (K).

It is known that any composite material reaches a saturated state after a certain period of time in an environment where humidity and temperature remain constant. It is important to define this equilibrium point, known as the equilibrium moisture content 'M_m'. This maximum amount that the material can contain is expressed as a percentage of the dry material mass. Equation 82 (from section 2.12.6 in this case using different notation) shows the equation for 'M_m', where 'M_{sat}' is the mass at saturation (g), 'M_{dry}' the dry specimen mass (g).

$$M_m = \frac{M_{sat} - M_{dry}}{M_{dry}} \times 100\% \qquad \textbf{(Equation 82)}$$

'M_m' does not form part of Fick's law, however it is utilised to determine the boundary conditions. Locally at the faces of the plate, the moisture concentration is equal to the equilibrium moisture content. It is assumed that at time 't' equal to zero the faces of the plate are instantaneously saturated with moisture. The level of humidity will also affect the equilibrium moisture content. The effect can be modelled using the empirical relationship shown in equation 92, where 'a' & 'b' are empirical constants and 'RH' the relative humidity.

$$M_m = a(RH)^b \qquad \textbf{(Equation 92)}$$

Equation 91 can now be solved making a number of assumptions. Firstly the ambient temperature and moisture content are the same at all faces of the material. The concentration of moisture at the surface of the material is equal to the equilibrium moisture content M_m. The temperature inside the material approaches equilibrium much faster than the moisture concentration and the temperature inside the material is taken to be the same as the ambient temperature. Initially the moisture distribution through the material is considered to be uniform. The mass diffusivity is only dependent on the temperature and is independent of moisture concentration and stress level inside the material [62]. The temperature inside the material is uniform from these assumptions:

$T=T_i=Ta \qquad 0 \leq x \leq X \qquad t \geq 0$

Equation 93 describes the concentration with the initial conditions and boundary conditions:

$$C = Ci\begin{Bmatrix} 0 \le x \le X \\ 0 \le y \le Y \\ 0 \le z \le Z \end{Bmatrix} at \cdot t = 0$$

(Equation 93)

As the initial concentration is equal to 'M_m', the expression can now be written as:

$$C = Ca = M_m for\begin{Bmatrix} x < 0; x > X \\ y < 0; y > Y \\ z < 0; z > Z \end{Bmatrix} at \cdot t \ge 0$$

(Equation 94)

In finite difference terms equation 94 can now be approximated using the second derivative in space and the first derivative in time. The computer model uses the discretisation of space and time, so that the concentrations are calculated with the nodes for each time step. Each node is characterised by three indices 'i','j' & 'k' and is bounded by six walls. Each wall is denoted by North, South, East, West, Fore & Aft. The model uses a 3D array to set up the nodes at the plate. Equations 95 to 97, show the solutions for equation 94 in each direction.

$$\frac{\partial^2 C}{\partial x^2} \cong \frac{C^n_{i+1,j,k} - 2C^n_{i,j,k} + C^n_{i-1,j,k}}{\Delta x^2}$$

(Equation 95)

$$\frac{\partial^2 C}{\partial y^2} \cong \frac{C^n_{i+1,j,k} - 2C^n_{i,j,k} + C^n_{i-1,j,k}}{\Delta y^2}$$

(Equation 96)

$$\frac{\partial^2 C}{\partial z^2} \cong \frac{C^n_{i+1,j,k} - 2C^n_{i,j,k} + C^n_{i-1,j,k}}{\Delta z^2}$$

(Equation 97)

and

$$\frac{\partial C}{\partial t} \cong \frac{C^{n+1}_{i,j,k} - C^n_{i,j,k}}{\Delta t}$$

(Equation 98)

Equations 95-98 indicate the present moisture concentration value and n+1, the future value at Δt.

The model was then further developed to account for dissimilar materials. Dissimilar materials can be created through two differing materials being cured together, a resin bond line or the application of a surface coating to a component such as paint. The mathematical solution is essentially the same as previously discussed however in this case the diffusion coefficients for each material type must be known. Secondly, it is important to analyse the boundary condition at the interface between the dissimilar materials. This requires extra terms to be created to account for changes in flux due to the presence of a different material. The problem is solved by a number of linear equations where J_w is the flux through the west wall, J_e, the flux through the east wall etc. These linear equations are forward-difference and backward-difference approximations based on Fick's 1st law. The general expression is shown in equation 99:

$$J = -D\frac{\partial C}{\partial x} \qquad \textbf{(Equation 99)}$$

The changes in flux due to different materials can be taken into account by:

$$\frac{C^{(n)}_{i,j,k}}{C\infty_{i,j,k}} \cdot \frac{C\infty_{i,j,k} - C\infty_{i,j,k+1}}{\partial z} = 0 \qquad \textbf{(Equation 100)}$$

If the material node (i-1,j,k):$m1_{i-1,j,k}$ is the same as node (i,j,k):$m2_{i,j,k}$ then the equation is simple Fick's first law. If $m1_{i-1,j,k}$ is different from $m2_{i-1,j,k}$ then there will be a difference in the equilibrium concentration between the two materials and a value is derived which changes the flux in that direction.

2.13 Literature Review Conclusions

- A general introduction to composite materials shows the benefits of carbon fibre with an epoxy matrix for aerospace applications over other resin systems and fibre types.
- Composites generally offer a 25-30% weight saving over their metallic counterparts, with weight saving potential set to increase as analysis methods for composite structures improve. However advances in metallic materials such

as Aluminium-Lithium Alloys prevent the gap in performance between metallic and composites growing significantly.

- Composites are generally less sensitive to fatigue than metals, although they have much greater notch sensitivity.
- The generation of lamina properties has been discussed based on test methods used by the composites industry and Airbus, which form the basis for the test methods used within the EMOC project.
- Bolted joint test methods and open and filled-hole compression test have been discussed, which are important due to the notch sensitivity, along with compression after impact, which provides strain limits to prevent damage growth in service.
- The methods for generating statistical B-basis material allowables are discussed, which are used by the EMOC project via the small sample and Weibull methods to assess test data generated.
- Structural analysis methods for single plies and laminates are discussed for both strength and stiffness, which is utilised by Airbus for predicting the mechanical performance of laminates, the theory of which is used by the EMOC project and associated models that have been developed.
- Effects on mechanical performance due to the environment have been captured from many literature sources, although no evidence was found to suggest that the methodology developed within this project has been done before.
- The basis of Fickian diffusion is discussed along with how it is used by Airbus via the Airbus 'Wet Aging Tool' and also previous work commissioned by Airbus with Swansea University to model moisture ingress in composites, which provides the starting point for this project.

3. CONVENTIONAL WINGBOX STRUCTURAL DESIGN

3.1 Introduction

Wingbox design varies depending on the aircraft type and its requirements. Airbus aircraft utilise what is known as a cantilever Wingbox design, which is considered to be the most efficient for high speed efficient airliners comprising a 'thick box beam - multi-spar box' structure for lower aspect ratio wings. The outline of the wing, both in plan form and the cross sectional shape, must be suitable for housing a structure which is capable of carrying out its purpose. Once the basic wing shape has been defined a preliminary layout of the Wingbox structure is created, which must be capable of providing sufficient strength, stiffness and light weight structure with the added consideration of manufacturability [63].

It is important to classify the main wingbox components to aid the discussion within this section. Figure 26 shows a schematic of the ALCAS demonstrator wingbox, with each key structural component labelled.

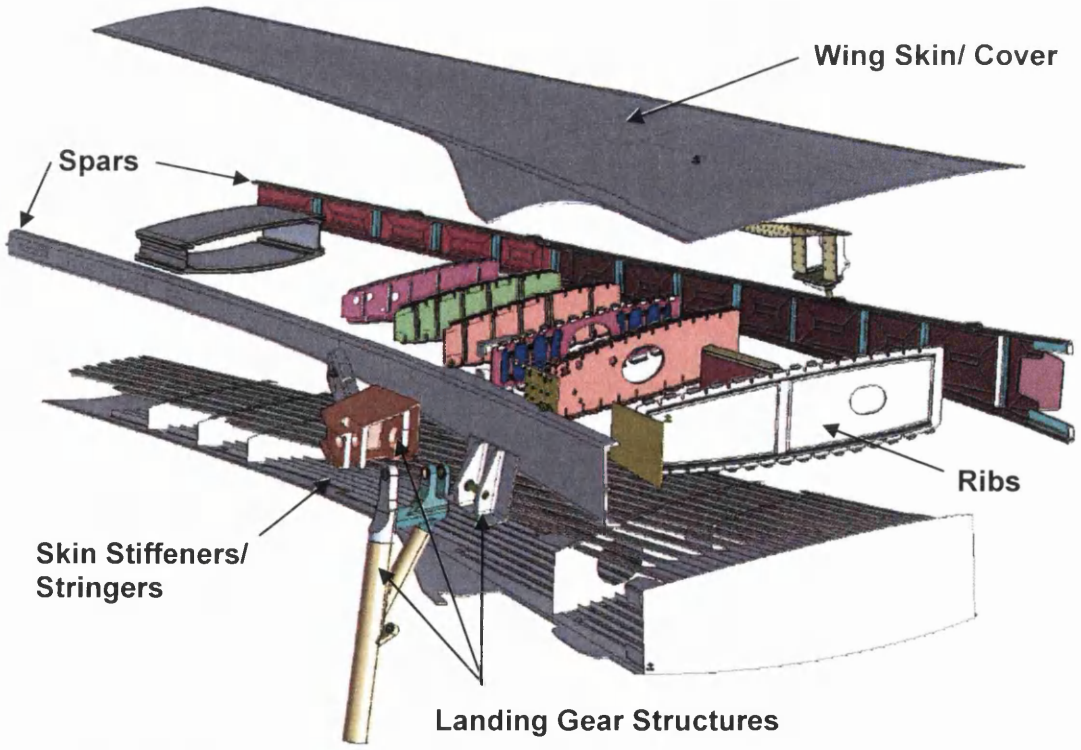

Figure 26 ALCAS Research Project Lateral Wingbox and Key Structural Components

The wing is essentially a beam which transmits and gathers all applied air-load through the Wingbox root joint, through into the centre Wingbox and surrounding fuselage structure. For preliminary structural sizing and load purposes it is generally assumed that the total wing load equals the weight of the aircraft times the limit load factor, times a safety factor of 1.5. In addition to this applied load it is also necessary to take into account other loads that the Wingbox structure will be subjected to [63]. This may include:

- Internal Fuel Pressures (both static and dynamic), which may influence structural design.
- Landing Gear attachment loads.
- Wing Leading Edge (LE) & Trailing Edge (TE) loads.

These loads are generally considered as secondary loads when designing the Wingbox structure with the primary loads resulting from the applied airload. Secondary loads may require the careful positioning of a rib or other such component to allow the effective load distribution into the surrounding Wingbox structure. The applied airloads result in increasing shear and bending moments towards the wing root [63].

The shear load is carried by the Wingbox spars and the bending moment by the Wingbox covers. Wingbox covers typically account for around 70% of the weight of the Wingbox and therefore it is critical to the wing design that these be designed as efficiently as possible from both a cost and weight standpoint. The lower cover is loaded primarily in tension and has a generally straightforward design. It requires careful material selection, assessing material tensile strength to density ratio combined with good fracture toughness and fatigue life. Generally the upper cover design is a lot more complex and configuration dependent. The upper cover is primarily loaded in compression and its performance is generally rated on how well it is able to resist buckling. There are various methods to aid the covers resistance to buckling one typically employed in airliner wings is the use of stringers. The ribs are also affected by the use of the stringers, requiring a pitch close enough to prevent the stiffeners failing as a column [63].

3.2 Advanced Aerofoil

Studies have shown that supercritical airfoils can provide greater performance gains by increasing airfoil thickness and/or decreasing wing sweep while maintaining the same cruise Mach number, rather than by increasing cruise speed. A 30% increase in wing depth can alone improve wing weight, it has been determined that the greatest benefit is achieved by a combination of increased depth, reduced sweep and increased aspect ratio. The difference between a conventional airfoil shape and a supercritical wing are shown in figure 27.

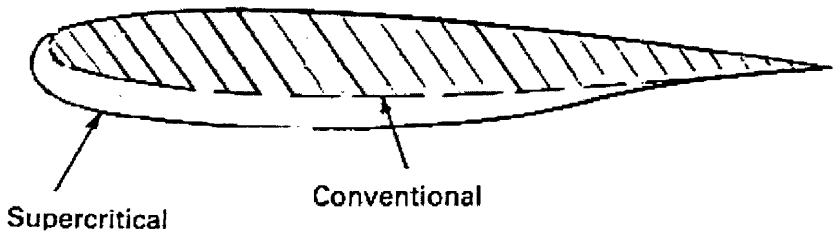

Figure 27 – Schematic of Conventional and Supercritical Aerofoil [63]

There are however disadvantages to the supercritical wing:

- The incompatibility of the sharply 'undercut' trailing edge with extensive flaps.
- The extremely close tolerances required to maintain laminar flow over the wing surfaces.

There is however a third aerofoil option available. This design is know as aeroelastic tailoring. Here the wing flexibility is tailored so that the aerodynamic loads can be used to flex it to the proper size and shape for the performance envelope in which it is operating. For example, the wing might be structured so that it normally assumes the correct aerodynamic shape for take off and landing. As the aircraft becomes airborne, the aerodynamic forces on the wing should be sufficient to flex it to the shape best suited to the cruise [63].

3.3 Wingbox Loading

All Airbus Aircraft to date have been constructed with a low set cantilever wing and podded engines, slung below and ahead of the wing. Figure 28 illustrates a typical

airliner arrangement and shows the principal forces acting upon it during normal (1g) level flight. The structural weight of the aircraft in addition to the mass of the engine and the passengers/payload act to 'pull down' the aircraft, as does the fuel weight. The first group, labelled Aircraft Weight in figure 28, should not vary during flight and as such may be taken as a constant value. Fuel Weight however, decreases as the aircraft travels along its course and as such it is desirable to label it separately The Airload refers to the wing lift, and during level flight this must be equal to the Aircraft Weight + Fuel Weight. Together these are the main forces applied to an aircraft wing but they are not the only ones [63].

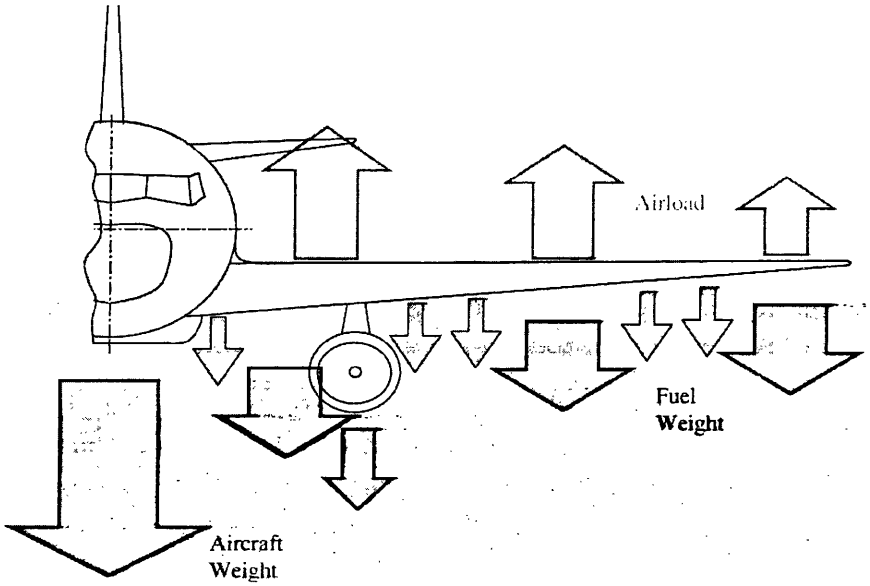

Figure 28 Schematic of Global Loads Acting on a Cantilever Wing [63]

Figure 29 shows some of the other forces applied. The engine Thrust is the force that propels the aircraft forward and is transferred to the wingbox via the engine pylon. The location and design of the engine installation has a major effect upon the loads transmitted through the wing. By placing the mass of the engine and the thrust it produces ahead and below the wing it produces a clockwise torque pitching the leading edge up.

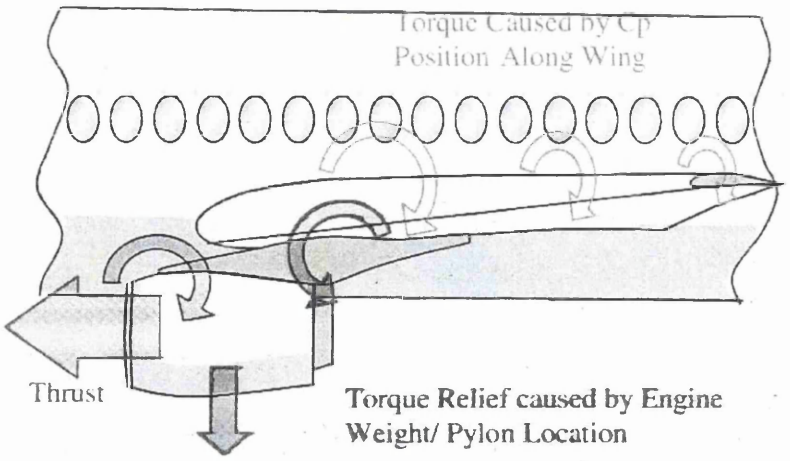

Figure 29 Schematic of Cantilever Wing Showing Engine Induced Forces [63]

Figure 30 shows a typical aerofoil section and the pattern of lift around it. The centre of pressure is a term used to define a point along the wing where the resultant lift would act. It may be described as the "aerodynamic balancing point" of the wing for idealised purposes, and is used to represent the point through which the lift is said to act. This point is usually between 1/4 and 1/3 of the chord of the wing and this location gives rise to a clockwise torque, pitching the aircraft nose up [63].

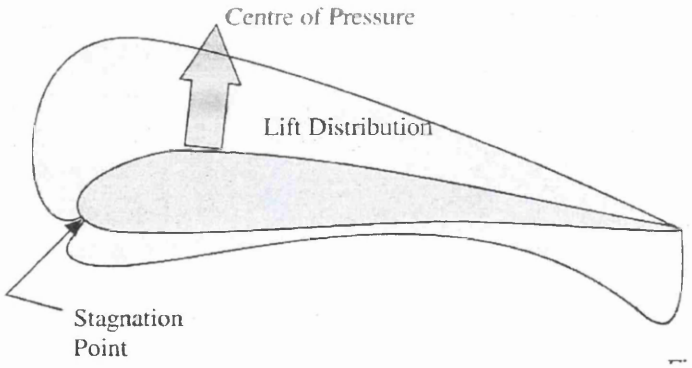

Figure 30 Schematic of Cantilever Wing Showing Typical Aerofoil Section and Pattern of Lift Around it [63]

All the loads and forces acting upon the wing can be simplified into 4 basic components for the purpose of designing the structure; these are shown in Figure 31. The loading of a wing refers to the load applied by the lift at points along the span. From an aerodynamic point of view it is best to maintain an elliptical loading pattern because this produces uniform downwash which leads to low trailing edge drag. This loading imparts shear along the wing, which increases as you approach the root because each

section of wing not only transfers the load produced at that section but everything outboard of it as well. This shear force also results in a large bending moment being produced and this is normally measured at each rib bay. The torque along the wing is also illustrated and shows the effect of mounting the engines ahead and below the wing. It is important to note that these are only illustrative diagrams; there are a number of other loads/torques etc. applied along the wing at such areas as flap attachment points [63].

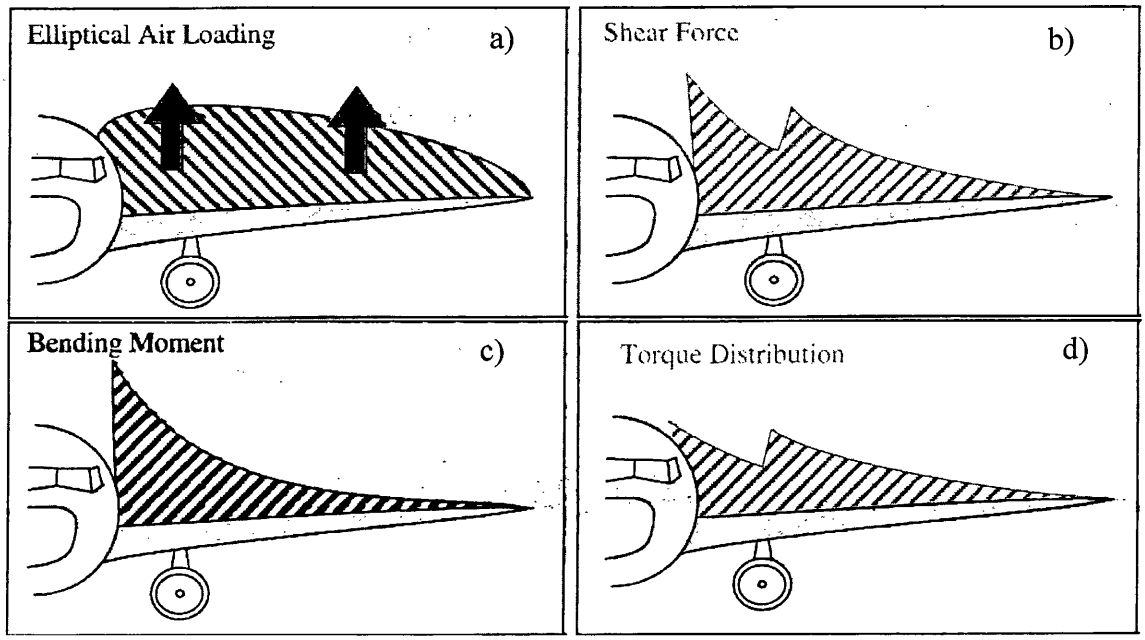

Figure 31 Schematic of Cantilever Wing; a) Elliptical Air Loading Distribution; b) Bending Moment; c) Shear Force Distribution; d) Torque Distribution [63]

Figure 32 shows a Simplified Bending diagram used to represent a typical modern wing design. It illustrates the effect on the wing all the forces mentioned above have in raising the tip of the wing. Also illustrated is one of the ways that designers use the weight to their advantage. By storing as much fuel as possible in the wing and by using the fuel from the centre outwards it is possible to reduce the bending moment. By moving the weight of the fuel from the fuselage out to the wings you are reducing the load on the wing roots and producing a distributed load which in effect 'pulls down' the wing and reduces bending.

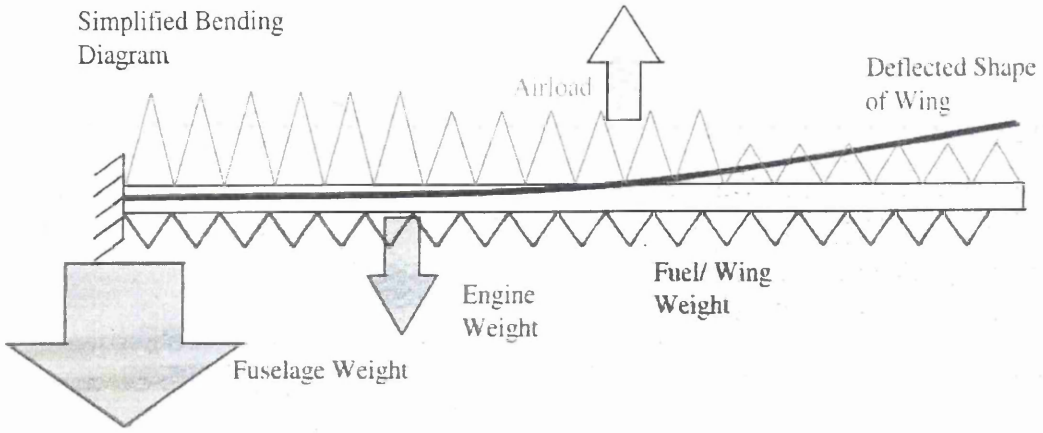

Figure 32 Simplified Bending Diagram Representative of Modern Wing Design [63]

Another important scenario is that related to during landing and ground manoeuvres. Figure 33 a, illustrates how, prior to flight, the full fuel tanks no longer have a beneficial effect because the wing weight is no longer supported by the lift it produces. In these cases the whole weight of the aircraft is concentrated at the landing gear attachment points. Generally speaking, due to wing sweep, centre of gravity considerations and the location of fuel tanks the main gear is usually situated towards the rear of the wing and this produces a new set of loads to contend with, illustrated in figure 33b. When on the ground the weight of the aircraft is reacted by the main landing gear leg and the location of this produces an anti-clockwise torque on the wing. This is opposite to the flight case and is worsened by the torque generated by the engine thrust.

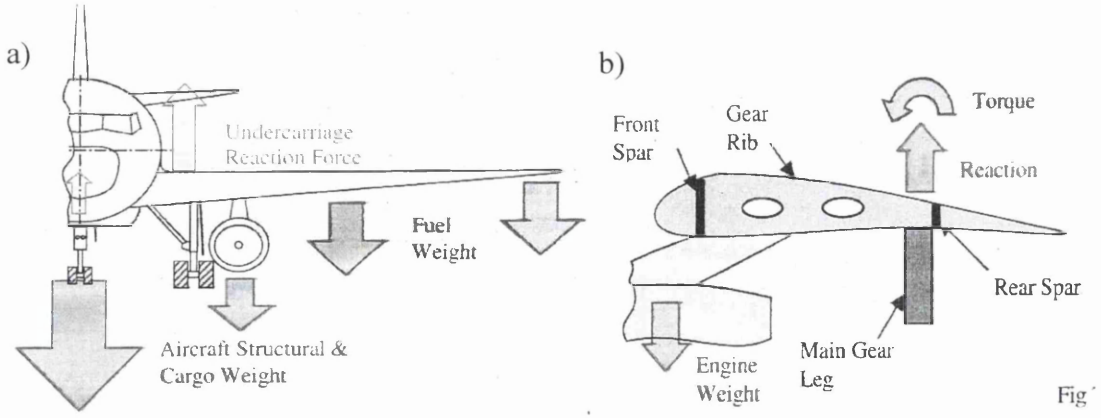

Figure 33 a) Fuel Tank Effects Prior to Flight; b) Concentration of Weight at the landing Gear Attachment Points [63]

Fig 34 shows the effect that the undercarriage has on the wing and it is important to consider these factors in addition to the flight cases. The Gear rib, supporting the

undercarriage has to be designed for these loads. It is cantilevered from the rear spar and is a very important structural item [63].

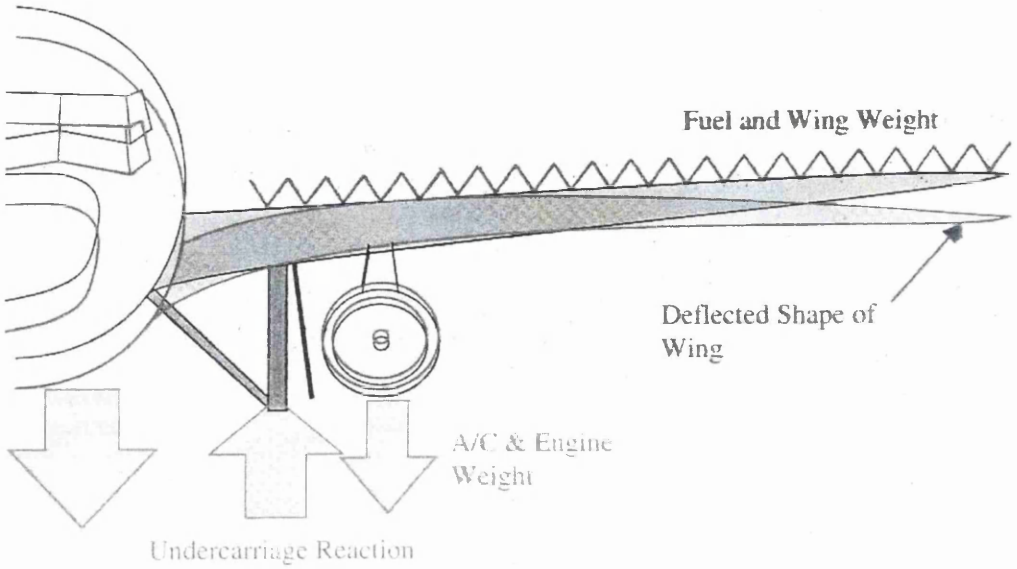

Figure 34 Undercarriage Effects on the Wing [63]

3.4 Wingbox Design

The main issues with Wingbox design of primary structural components are with regard to layout of components. For example whether a larger percentage of the wing bending shall be carried by the spars, or whether the cover should be utilized to a large extent. It is obvious that the cover should be utilised to a large percentage of the bending material. This is true as torsional rigidity is required, and since it is, this same torsion material may as well be utilised for both primary bending and torsional material. Spanwise stiffeners spaced close together are required as a consequence to keep the buckling of the bending material down to a minimum [63].

The direction of the wing ribs also needs to be considered with many designs having the ribs directed in line with the flight path of the aircraft, the aim being to ensure the correct aerodynamic profile of the wing between the spars is maintained. This arrangement does however have a number of disadvantages although can be considered a variable solution. Furthermore, when carrying out initial weight estimations of the aircraft, the weight of the wing root rib bulkhead must not be neglected. Spar locations have to be established very early in the design process and before any mathematical evaluation of the design is carried out. Rear spar position is also of great importance and must leave adequate room for flaps, ailerons, spoilers and

associated actuation. A rearward shift in the spar increases cross section area and as a consequence increases fuel storage space but results in a structure less efficient in bending. This is also similar for the Front Spar [63].

Generally speaking the wing arrangement is generally:

- Front Spar located at around 15% chord.
- Rear Spar at about 55-60% chord.
- 5-10% chord should be reserved for the control system elements.
- Centre part of wing between spars takes the loads from nose & rear sections. and carries them to the fuselage, together with its own loads.
- Primary wing structure is an integral fuel tank.

3.5 Wing Layout

There are many factors associated with wing design such as spar and stringer location, landing-gear attachment & retraction, power plant, ailerons, flaps etc. Preliminary studies should be made to take into account all of these features. A general guide to the design of a two spar wing is as follows [63]:

- Draw wing planform, to scale with appropriate dimensions to satisfy aspect ratio, area and sweepback.
- Determine mean geometric chord and check the relationship between fuselage and wing to ensure centre of gravity lies in the lateral plain perpendicular to the mean geometric chord at the mean aerodynamic centre.
- Locate front spar at a constant percentage of the chord from root to tip.
- Locate the rear spar in a similar way.
- Mark out the aileron. The leading edge of the aileron may be parallel to the rear spar.
- Ribs are likely to be located at each aileron and flap hinge. Rib spacing is determined from panel size considerations. Reinforced ribs are also required for engine mounting attachments and landing gear.
- Spanwise stringers may be located, parallel to each other or at a constant percentage of the wing chord. Stringer run out can occur as the chord width reduces further outboard.

3.6 Spars

For strength and weight efficiency, the beam (or spar) cap should be designed to make the radius of gyration of the beam section as large as possible and at the same time maintain a cap section which will have a high local stress. Cap sections for large cantilever beams, frequently used in wing designs, should be of such shape to enable tapering and reduction of section as the beam extends outboard. Figure 35 shows typical beam cap sections for a typical metallic wing cover construction, where additional stringers and skins are used to provide bending resistance. The beam web is typically composed of a flat sheet reinforced with vertical stiffeners shown in figure 36.

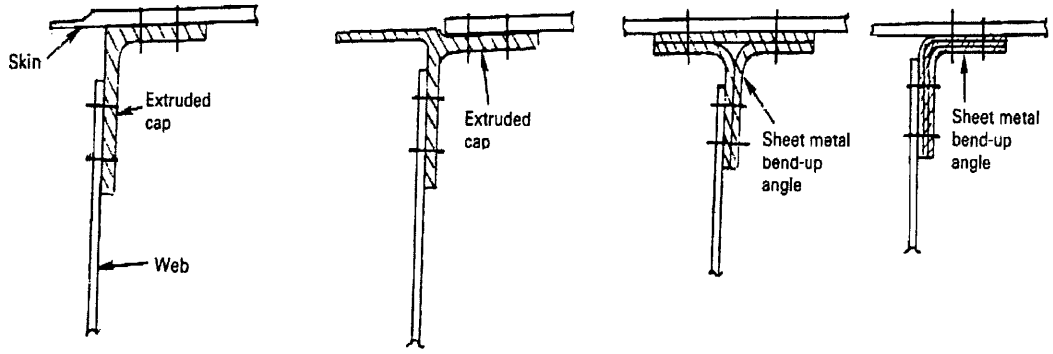

Figure 35 Schematic of Typical Metallic Spar Cap Solutions [63]

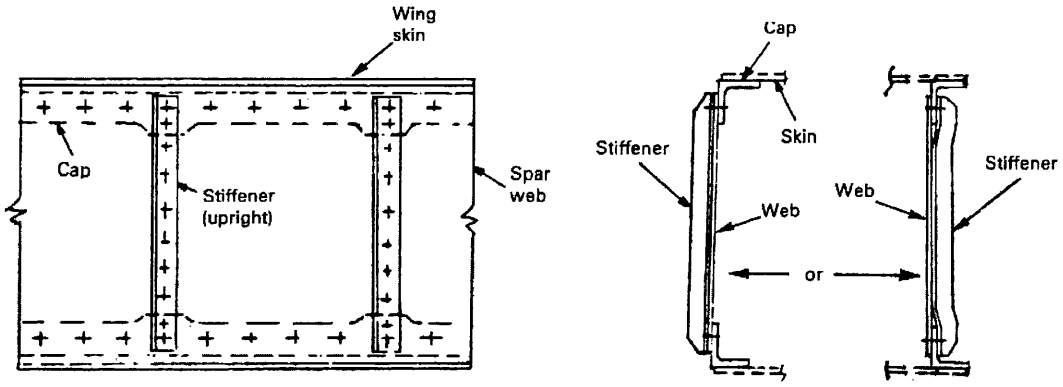

Figure 36 Schematic of Typical Metallic Spar Construction Comprising of Shear Webs Reinforced with Stiffeners [63]

The air loads act directly on the wing cover, which transmit loads in shear to the ribs. The ribs transmit the loads in shear to the spar webs and distribute the load between them in proportion to the web stiffness. In the past it has been customary to design wings with three or more spars. The use of additional spars elevate the loads

transmitted to the ribs, while at the same time providing better support for the Spanwise bending material. As with Airbus aircraft two or more spars are typically used in Wingbox construction. The two spar wing construction consists of front and rear spars. The front spar locates the leading edge structure (slats) and the rear spar the trailing edge structure (flaps, aileron, spoiler, associated hinge brackets etc.). When the covers are added this creates what is known as a torsion resistant box, serving as an integral fuel tank. Typical spar beam construction is shown in figure 37. Spars can be divided into two basic types, shear web type and truss type. It is possible to have varying spar types, such designs can allow buckling of the structure to occur, while other designs are shear resistant, allowing for no buckling in the structure, the latter being of typical Airbus configuration.

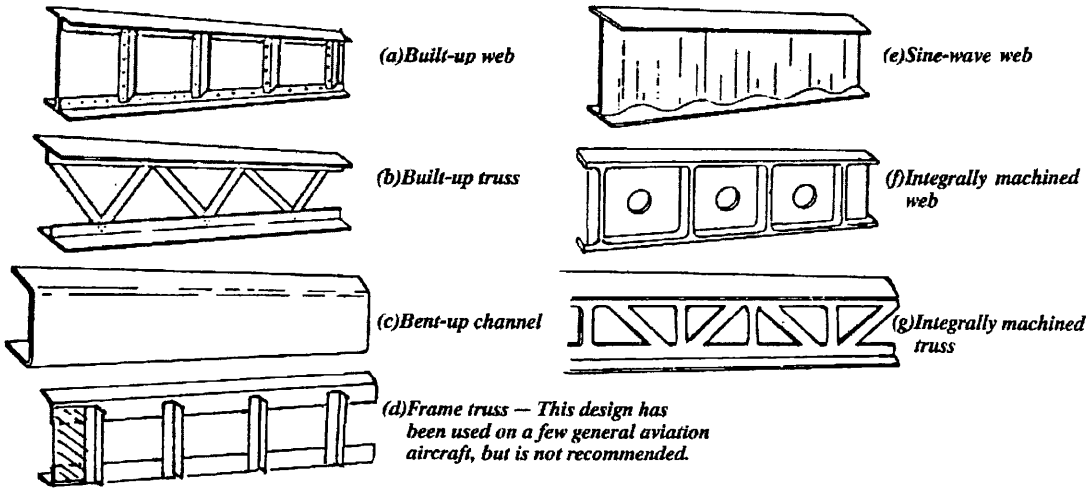

Figure 37 Schematic of Typical Metallic Spar Configurations [63]

In addition to web design the caps as previously mentioned can vary in their design configuration. Sloping spar caps are not uncommon due to the taper in both planform and box depth, an example of this is shown in figure 38. These sloping spar caps also have the advantage of relieving the beam web of considerable shear load [63].

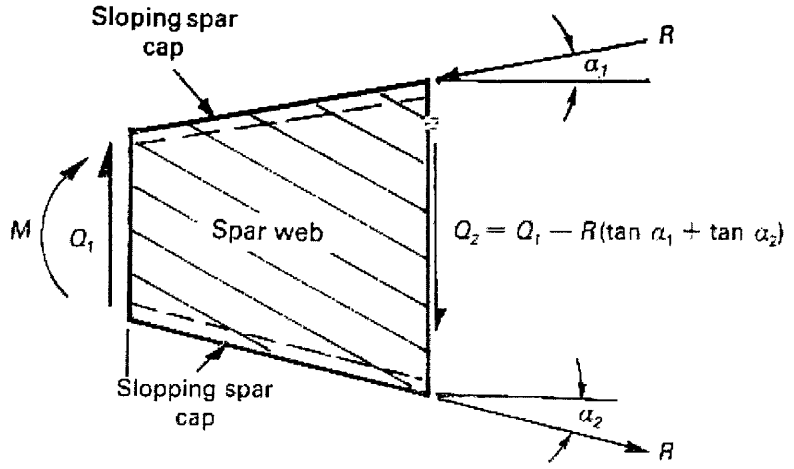

Figure 38 Schematic of Sloping Spars Which Enables the Relief of the Web Shear Load [63]

The two primary conditions which determine the overall efficiency of the spar are its construction cost and its efficiency as a load bearing member. The incomplete tension field beam is particularly adaptable to mass production. Semi tension type beams have better strength to weight ratios and are much stiffer than the truss type beam, with the truss type spar design also requiring a greater assembly time due to the larger number of parts. Truss type spars are unsuitable for standard Airbus configurations as they do not have the ability to withhold fuel. Figure 39 shows the behaviour of a spar web constructed in the semi-tension type design. The effect of the vertical component of web tension to compress the vertical stiffeners, bend the caps in the plane of the webs, introduce vertical shear loads on the web-to-cap rivets. The horizontal component of the web tension compresses both the beam caps, bends the stiffeners inwards, produces horizontal shear forces on the web-to-end stiffener rivets and on any vertical web splices that exist.

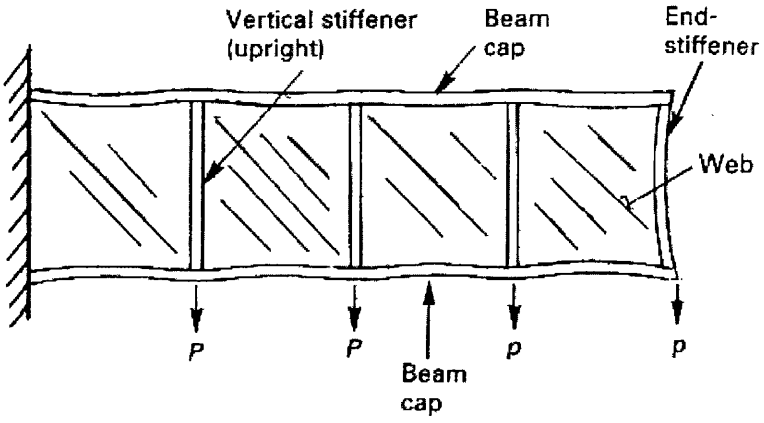

Figure 39 Schematic of Semi Tension Type Spar Behaviour [63]

3.7 Wingbox Ribs

The purpose of the rib within the wingbox is to resist the aerodynamic loads applied to it (discussed later in figure 45), thus maintaining the aerodynamic profile of the wing without any appreciable distortion. The rib is attached to the wingskin, typically through the use of mechanical fasteners, which then holds the contour of the wing to shape. At the same time the rib acts as a panel breaker limiting the length of the skin/stringers to an efficient column compressive strength (upper wing skin). Finally, the rib is also responsible for transmitting loads from the covers into the spars. The rib typically consists of caps (foot flange), stiffeners and webs, illustrated in figure 55 (discussed later). The rib may have to be designed with lightening holes within it. These serve the purpose of allowing people to access the wingbox bay by bay during assembly and for future maintenance; smaller holes may also be made to allow for fuel systems, which run throughout the wingbox structure. The loads exerted on the ribs will vary. Typically ribs design will vary where there is a high load input from flaps, ailerons, engine pylons and landing gear attachments. In addition to this some ribs have to act as bulkheads, where the wing is split into different fuel tanks, these ribs act as a boundary between tanks and also have to resist the loads that the fuel pressure and surge exerts on it [63].

Within the aircraft industry generally the use of shear web rib design is favoured as it has a number of advantages. The rib web acts as a fuel slosh inhibitor. Load concentrations are eliminated by gradual cross sectional change from the cap members into the shear web. The web provides continuous support for the wing cover panels for internal integral fuel tank pressures at the tip of the wingbox. Once sized the resultant rib web is usually capable of accommodating small changes in loading criteria or analysis, allowing the design to be modified in the future [63].

Trussed ribs on the other hand have none of the aforementioned advantages and can also have the disadvantage of being heavier, especially where the wingbox depth is large (i.e. inboard ribs approaching the lateral and centre wingbox root joint) as column lengths increase, compression become a problem. The advantage of the trussed rib is member end design for fixity and concentrated loads of truss members, particularly where they attach to tension members. They also have the added advantage over shear webs when large cut outs are required that do not leave room for a shear web, while at the same time having the disadvantage of being less convenient for attaching

fuel systems etc. without extensive use of brackets [63]. An example of a trussed structure rib is shown in figure 40 with an example of a shear web rib shown in figure 45.

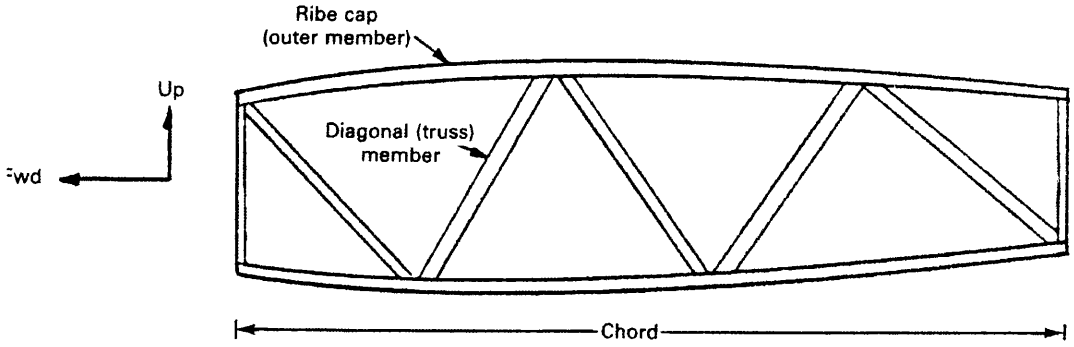

Figure 40 Schematic of a Truss Structure Rib [63]

Rib Spacing is usually defined early on in the design phase. The total weight of the ribs is generally considered to be a significant amount of the total wingbox structure; therefore it is important to consider them in the overall optimization of the structure. The relative weight of ribs covers and cover panels is shown in figure 41, presented for a Spanwise wing. It is advantageous to select larger rib spacing; for equal structure weight it leads to cost savings and less fatigue hazards. Wingbox spacing will increase with wingbox depth. For a typical wing which is tapered in plan form and depth, the optimal rib spacing would be variable with the maximum rib spacing at the inboard end of the wingbox. Practical considerations however will effect the ability to optimize the structure to this extent with alignment control, surface support structure, cover manhole size all being factors that have to be taken into account when carrying out optimisation [63].

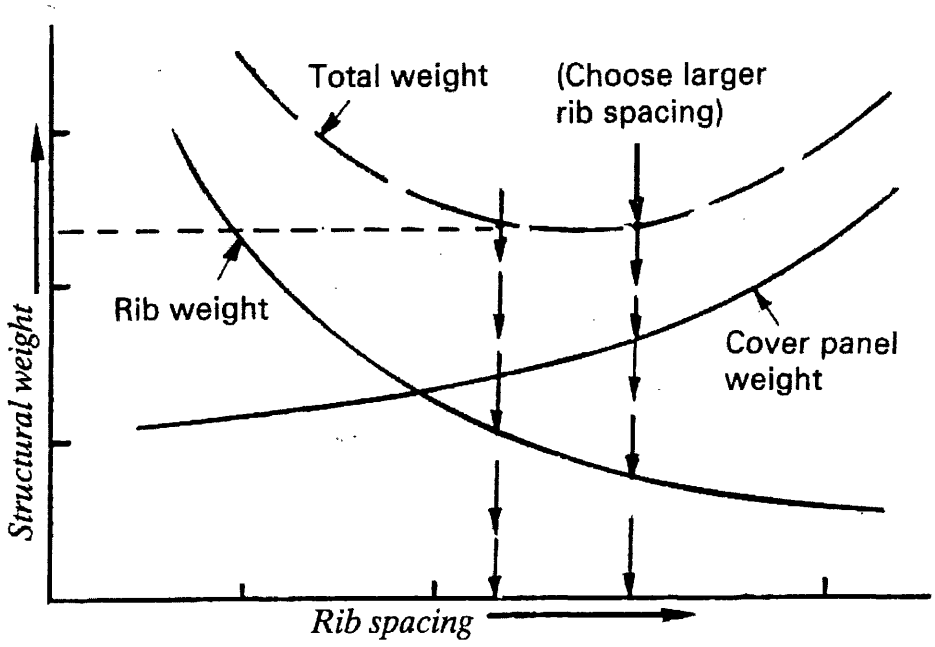

Figure 41 Determination of Rib Spacing by Structural Weight Comparison [63]

Wing rib arrangement outside of the wing root joint is critical for designing the compression structural stability especially for the wing's upper surface. The rib spacing here is considered as important as the root joint design. There are two basic rib arrangements shown in figure 42a & b. Figure 42 c shows a typical Airbus rib arrangement based on the layout of an A300 aircraft.

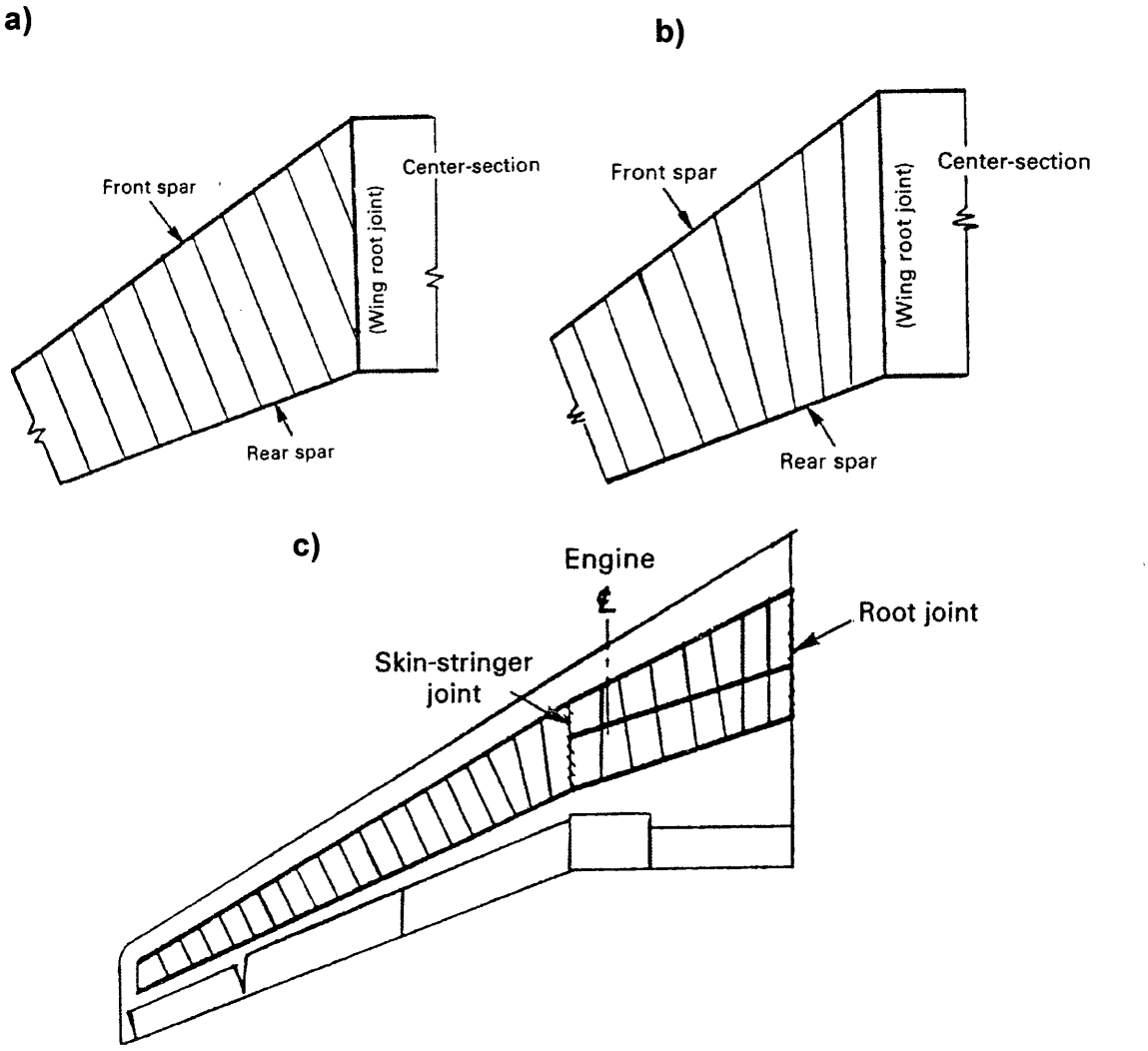

Figure 42a & b) Schematic of Basic Typical Transport Aircraft Rib Layout; c) Typical Airbus Rib Layout (A300)

3.8 Wingbox Covers

In high speed aircraft, the wing structure is usually made up of multiple spars which primarily are shear material carrying vertical shear. Very little bending material is contributed by the spars. The wing bending loads which cause compression on the upper surface of the wing are generally higher than those causing compression at the lower surface. This requires that the stiffening elements on the upper surface be more efficient and closer together than those on the lower surface. Torsional moments are primarily resisted by the skin and front and rear spars. The portion of the wing aft of the rear spar is usually over the greater portion of the chord for control surfaces which does not resist any of the torsional loads as shown in figure 43 [63].

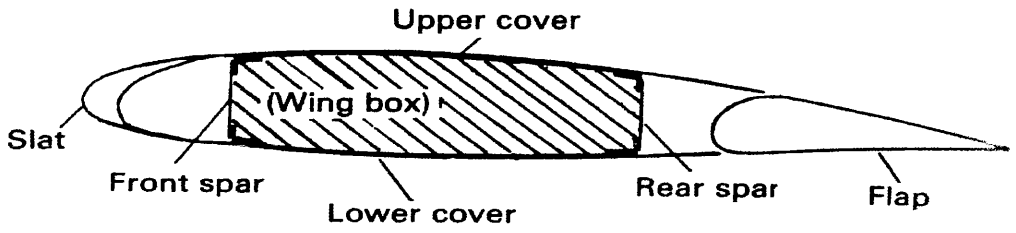

Figure 43 Typical Wing Torque Box Enclosed Area [63]

When designing wingbox skin panels it is important to consider failsafe. It is important that the Civil Aircraft Authorities requirements are met. With classic metallic design this often includes fatigue considerations and as such covers may be designed in several pieces to inhibit fatigue crack growth, as the joint acts as a 'tear stopper'. In addition to this the bolting patterns and shear strength are designed with sufficient strength to transfer a failed panels load into the adjacent panels. To achieve this structures are generally designed to carry 80% of limit load times 1.15 dynamic factor after a structural failure. Testing can also help establish safe structure life. As positive flight loads are always higher than for negative flight loads, the upper wing surface is usually critical for compression loads [63].

Airbus uses stringer stiffened panels, in which case the entire shear flow is carried by the skin. The stiffeners enhance the compressive loads which are attempting to cause the skin to buckle. It is good practice to avoid eccentricity when designing. Typical eccentricity occurs where stringers end and therefore stringers are typically ended at ribs where the shear load due to surface pressures can be resisted without over straining the skin. The stringer should also be tapered at the end to prevent a sharp change in section, which could overload the fasteners and cause failure. Typical wing skin stringer panel profiles are shown in figure 44 [63].

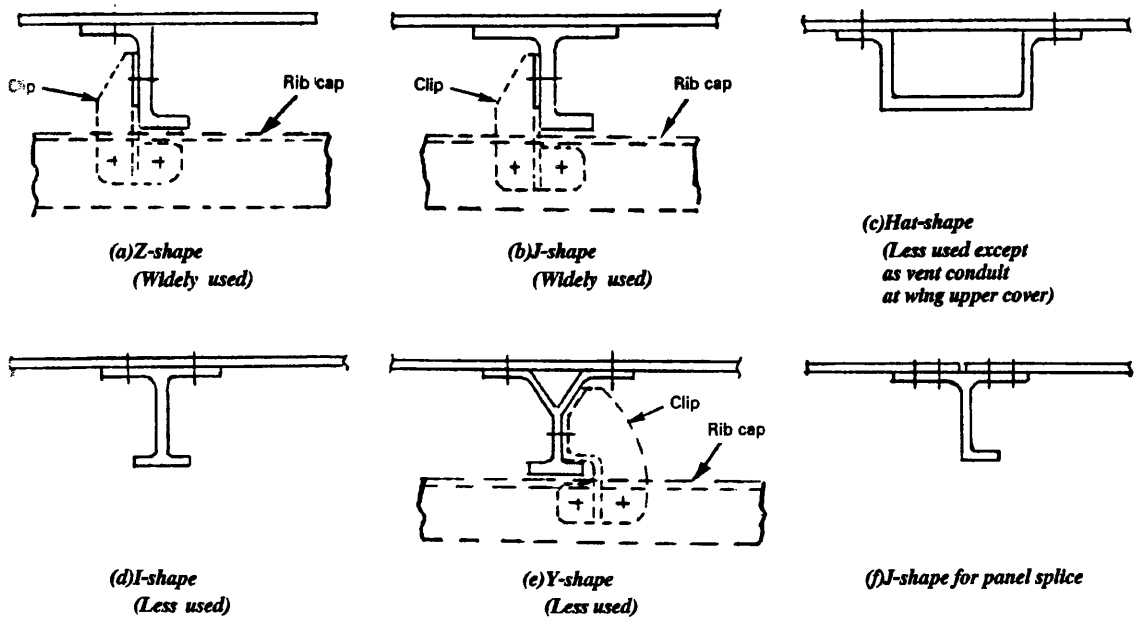

Figure 44 Typical Wing Skin Stringer Panels [63]

3.9 Composite Stress Analysis & Sizing Methods

3.9.1 Rib Loading

The main role of a rib is to maintain the shape and integrity of the Wingbox. The design of a rib requires several factors to be considered. Although the overall shape of the rib might be governed by the wing profile, the thicknesses and features of the rib require careful attention. A schematic of the typical loads acting on a rib is shown in figure 45 [64].

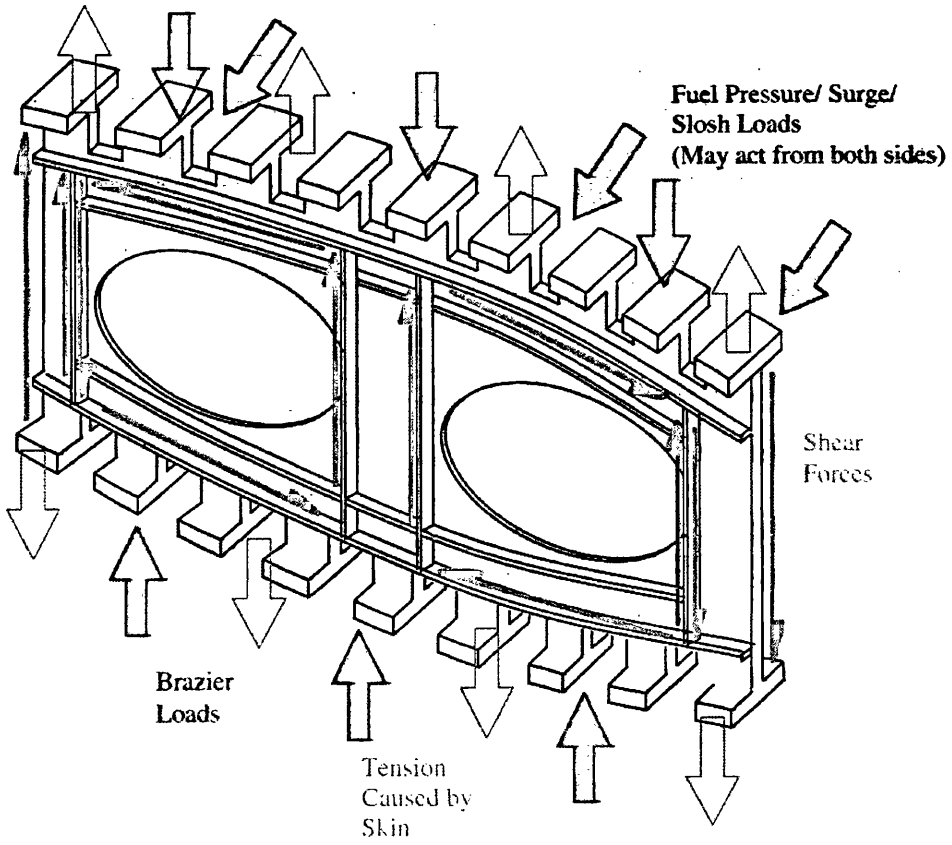

Figure 45 Schematic of a Wingbox Rib and Associated Loads [64]

One set of loads that ribs are subjected to are associated with the Fuel and air pressure. These are either caused by the fuel pressure putting a rib used as a tank wall in tension, or by fuel sloshing/surging during manoeuvres. The ribs transfer the pressure loads (fuel & air) from the wing covers into the spars [65] as shown in figure 46. The suction, caused by lift that is pulling the skins away from the Wingbox, places the rib feet into tension direct from the skin bolting and via the cleats used to support the top skin stringers. The load is then transferred through the rib and enters the spar in the form of shear [65].

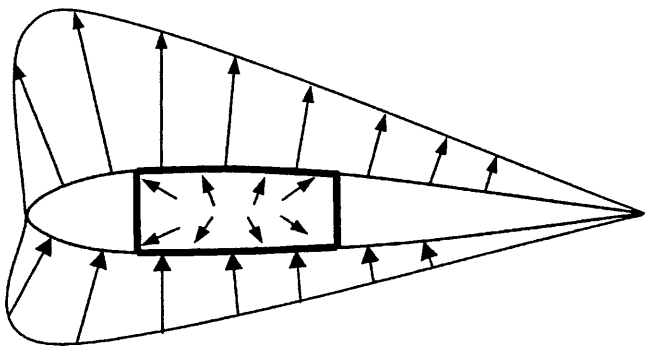

Figure 46 Schematic of Rib Loading Fuel/Air Pressure [65]

Shear Forces also occur in the flanges and webs of the rib due to the torque applied to the wing. The constant twisting puts considerable load into the part and this can be worsened if the rib is used to mount some additional structure/equipment. These shear loads are also transferred to the spars [64]. A schematic of this is shown in figure 47.

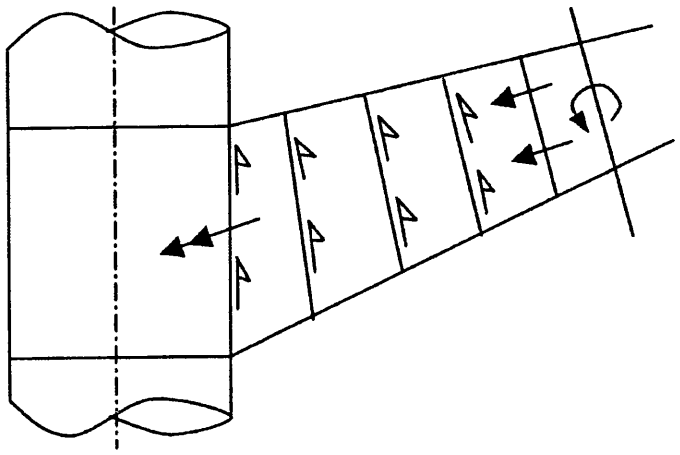

Figure 47 Rib Loading – Torsion Loading [65]

Another type of load that the rib is subjected to is called Brazier loading. This form of loading is a direct result of wing bending. Figure 48 illustrates how it works. When the wing bends then the top cover is placed in compression and the outboard end of the wing rises. The compressive load can therefore be split into its Horizontal and Vertical components. It is the vertical component of this load that acts inwards, towards the wingbox. On the lower surface the rising of the wing allows the tensile load the bottom covers transmit to be broken down into its component. It can be seen that the vertical component again acts in towards the wing box and as a result a crushing force is applied to the structure. This load is also distributed through the spar [64].

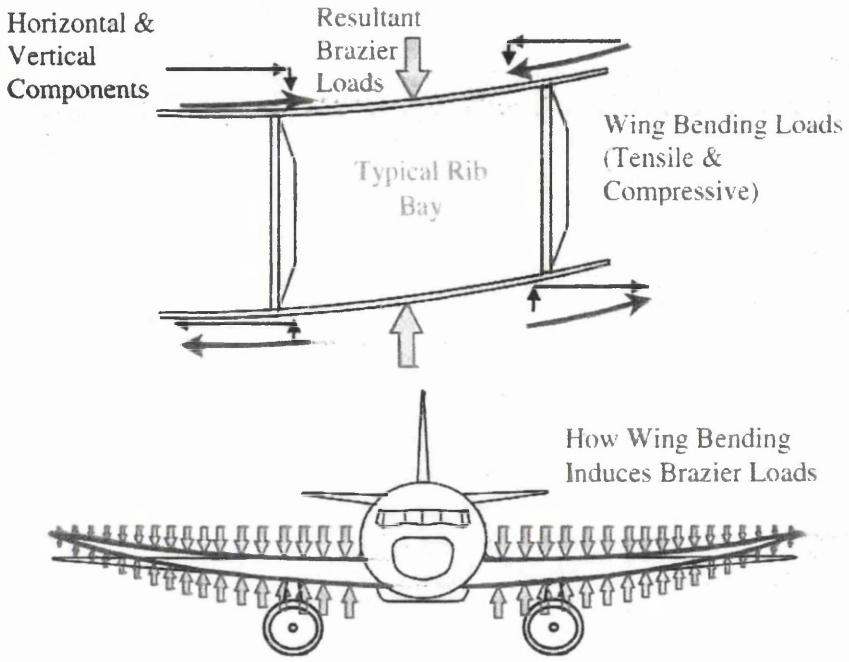

Figure 48 Brazier Loading Acting on the Wingbox [64]

The Wingbox acts as a fuel tank, which is split into sections. A rib can act as an internal tank boundary in which case it will have fuel pressures acting upon it. The rib must be able to react to lateral fuel loading as shown in figure 49.

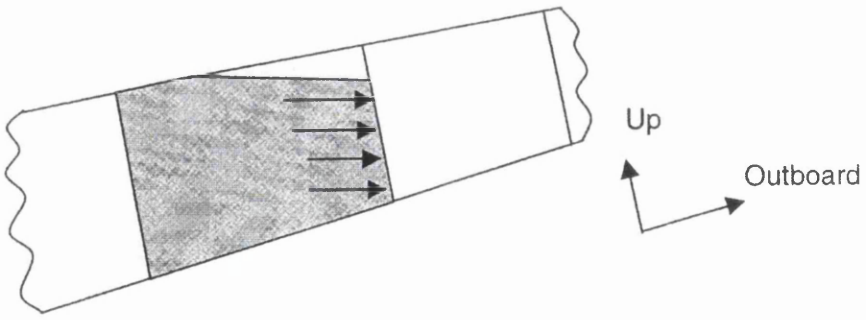

Figure 49 Rib Loading - Lateral Fuel Pressure [65]

3.9.2 Covers Loading

Wing-Covers is a term used to describe the skin and stiffener arrangement used on the wings. Because of their size and their load-carrying role they are generally very heavy and can account for around 40% of the weight of the wing. It is therefore very important to try and optimise the wing covers for maximum efficiency; one of the ways of doing this is to employ stringers. By dividing the mass of the covers between a skin panel and

a set of stiffeners it is possible to improve the panels effective resistance to bending. Figure 50 illustrates a typical top wing cover assembly; it is based around a skin panel which has a series of "J" section stringers attached to it.

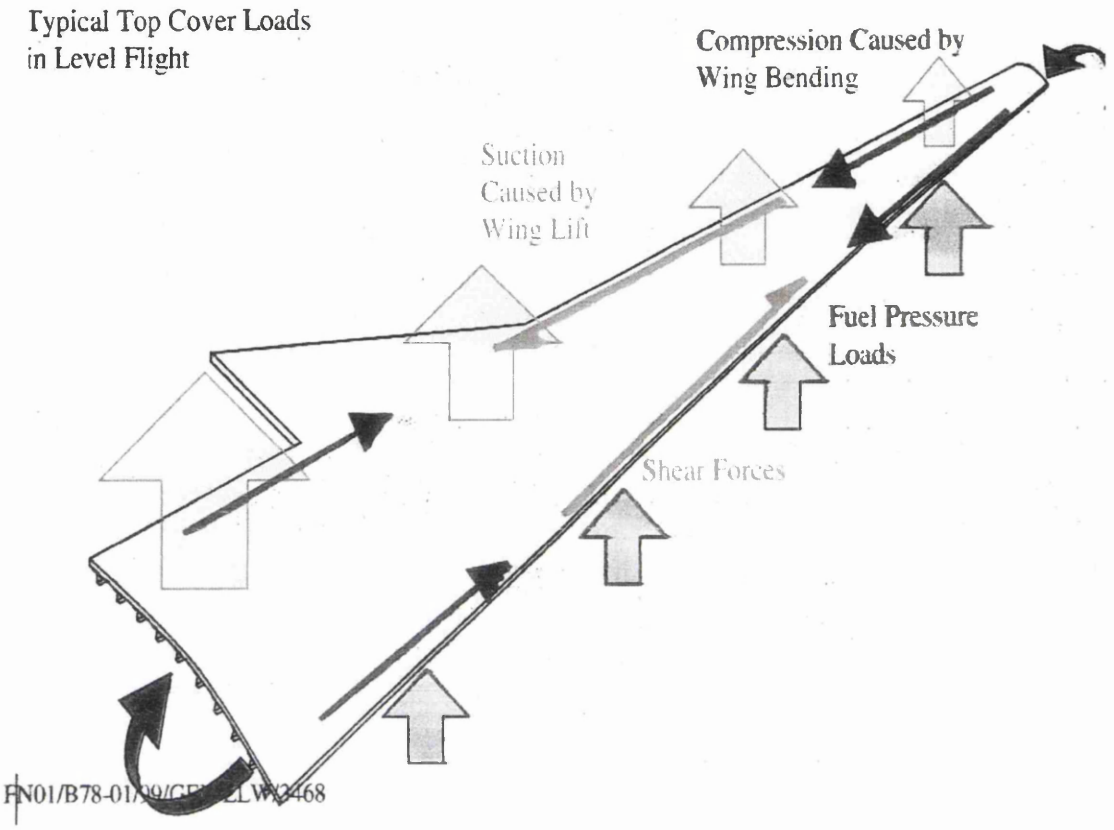

Figure 50 Typical Top Wing Cover Assembly & Associated Loading [64]

3.9.3 Spar Loading

The spar is a key element of the wingbox and is the main route of transferring load along the wing. The main purpose of a spar is to transmit shear forces but they also act as fuel tank walls and as such must be designed to cope with the high pressure associated both during normal flight, refuelling operations and during manoeuvre and crash cases. A schematic of the loading experienced by the spar is shown in figure 51. The weight of fuel in the wing of an aircraft similar in size to an A340 can be as high as 20 tons. When this is combined with a 9g crash requirement it can be seen that the loads involved are potentially very high. The spar caps do provide some additional material to transfer the bending moments but this is a relatively small amount and is an addition to its primary role of managing shear. The load applied from the skin acts in a similar way to that on the rib feet and is caused by wing lift. The rib loads appear in the

form of shear, as mentioned above, and are introduced at regular stages along the spar. This creates a whole series of shear webs along the spar. Spars are therefore mainly designed to cope with this shear and vertical flanges are positioned along the spar to reduce the size of the shear panels and also to allow the attachment of the ribs [64].

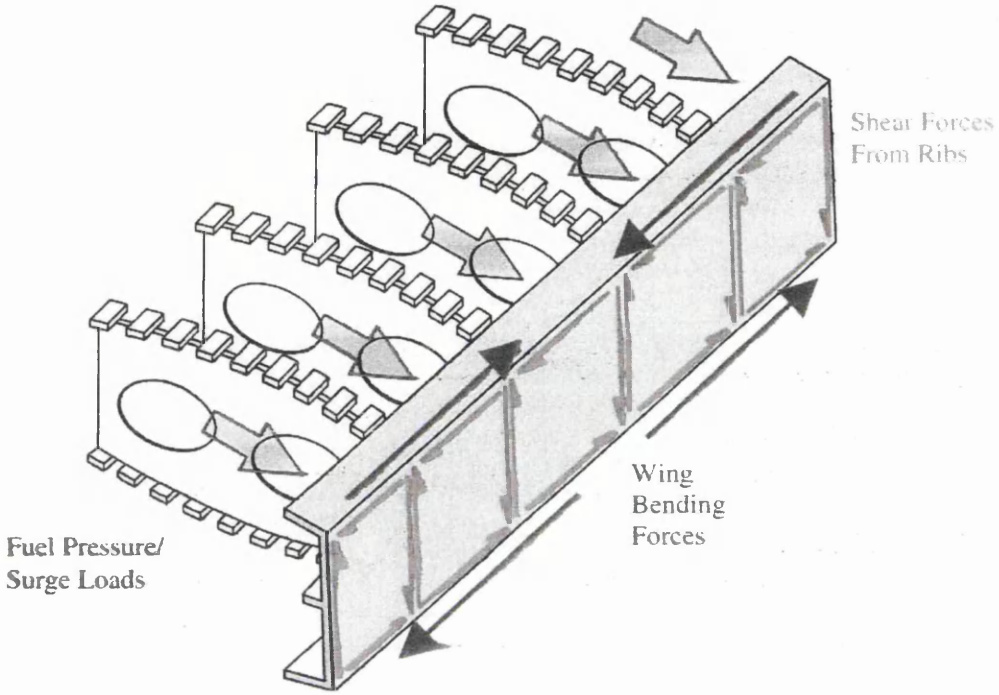

Figure 51 Schematic of Spar Section & Associated Loading [64]

3.9.4 Additional Wingbox Loading

There are other "local" loads applied to the wing, which cannot be considered exclusive to any one of the main components of the wing previously mentioned. Firstly there are the loads applied by the engine mounting points. The effect that the engine has on the overall wing has been mentioned previously in section 3.3, but it is important to consider how the enormous loads produced are distributed into the wingbox whilst maintaining the most aerodynamic shape possible. Figure 52 shows a typical arrangement.

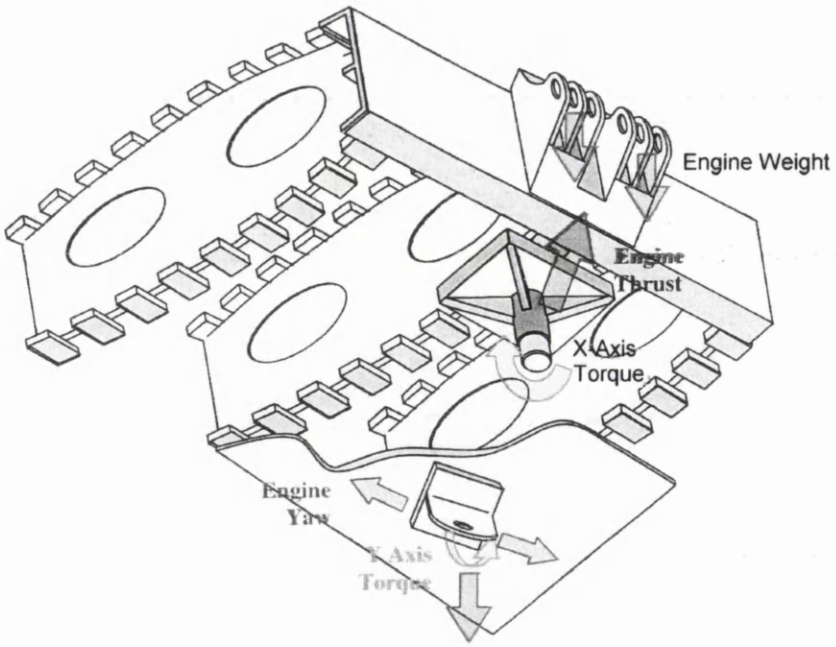

Figure 52 Typical Arrangements of Engine Attachments & Associated Loading [64]

The forward fitting attached to the front spar are manufactured as a pair for added fail-safe properties and supports the engine's weight. The link fitting additionally reacts against any engine "nodding". Everything has a natural frequency, this can be illustrated on an aircraft when it flies through turbulence, as the wingtip appears to flex up and down a few times before returning to its original position. When designing an aircraft it is desirable to ensure that the natural frequency of the wing structure is different to that of the engine installation to reduce the mass which is oscillating at the same speed. This is why the engine on an aircraft often appears loose during flight, and this movement is called nodding [64].

Mounted below and behind this, and connected to the bottom skin, is a thrust fitting, which transfers the thrust, produced by the engine into the wing through the spar and rib, and it is the key part of the engine installation. The other load that the thrust fitting is designed for is the torque produced during a fan damage condition. During a blade loss situation the fan becomes unbalanced and because of the speeds involved the engine may vibrate in its mountings [64].

The rear attachment point is mounted onto a thickened area of skin between two ribs (because ribs are oriented to the spar and not the direction of flight) and its main purpose is to resist any sideways movement and torque in the Y axis whilst also helping to support some of the engine weight [64].

The leading edge structure is all supported off the front spar and consists of a set of ribs, divided between track ribs (ribs close together to support the D-nose tracks, which allow the D-nose to move forward, therefore increasing lift) designed to support the moving parts of the leading edge and support ribs, either Intermediate or Hold-Downs, that are there to support the D-Nose. The load that the D-Nose is supporting is limited to its own weight and the suction effect around the front of the wing, and as such it is of relatively lightweight construction. These loads are transferred into the front spar as tension. Figure 53 shows the D-nose arrangement and associated loading [64].

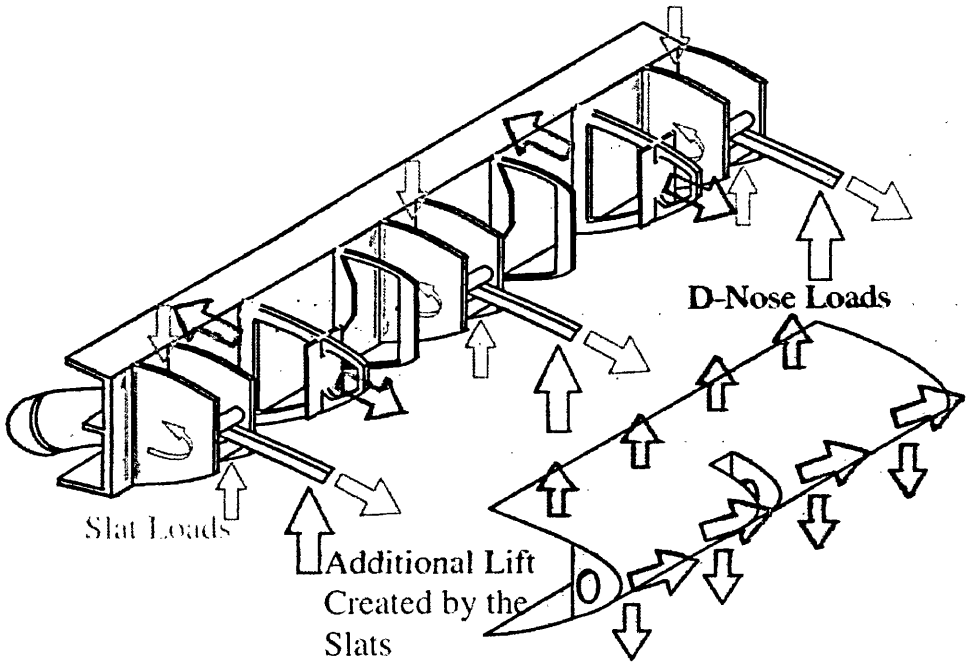

Figure 53 D Nose & Associated Leading Edge Loading [64]

The slats are supported by a series of slat tracks (16 per wing on A330-340) which are held in place on rollers connected to pairs of ribs. These loads are also transferred into the spar. The tracks also protrude through the spar and are covered by track cans to allow for fuel sealing in the tank and these too are supported off the spar [64].

Major portions of point loads applied to the wingbox arise from the trailing edge structure, the flaps and ailerons. Figure 54 shows the flap arrangements and associated loads. These are supported by the rear spar and specially reinforced ribs via the skin. While deployed, the flaps produce a large amount of additional lift and this lift needs to be transmitted as load by the structure into the wingbox. This is done via a series of flap beams. During operation the flaps exert a large upwards load on the beam which is transferred through two fittings, one in compression attached to the spar and a second usually connected through the skin to a rib and is usually in tension. This load is then transmitted through the structure as mentioned above [64].

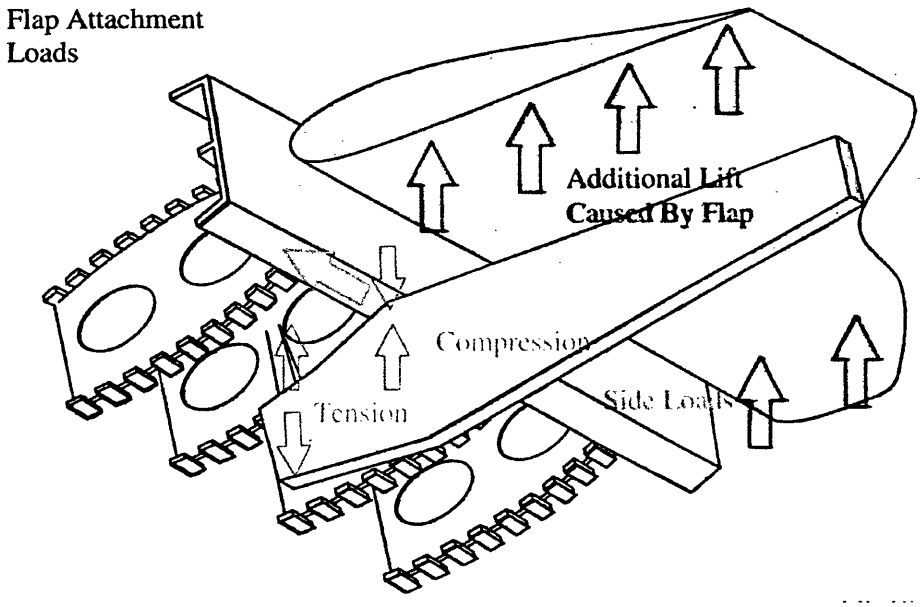

Figure 54 Flap Arrangements & Associated Loads [64]

3.10 Composite Structure Critical Stress Drivers

The critical stress drivers for composite components occur as a direct result of the aforementioned loading in section 3.3. Using Airbus experience based on the TANGO (Technology Application to the Near Term Business Goals & Objectives) project a number of key drivers have been identified. Note that these drivers allow for preliminary sizing of the Wingbox components but are not suitable for detailed component design and optimisation. These preliminary sizing methods are detailed in references [66,67,68]. In general these are taken from the Airbus Composite Stress Manual [65].

3.10.1 Ribs

For basic rib sizing consider a typical C-section composite rib, as shown in figure 55 that contains seven typically encountered features or elements. The rib can be broken down into key elements for analysis. Firstly we have the webs, represented by feature 1 and secondly webs with holes in them (feature 2), which although they have to resist the same stress will be analysed in different ways. Next there are the web stiffeners (feature 3), which help resist the Brazier loads and help optimise web design. Feature 4 is the rib post location, where the ribs are attached to the spars and therefore act as an interface for the transfer from the ribs to the spars. Feature 5 is the foot flange, which is the interface between the wing cover and rib. Being attached together through bolting/bonding the air/fuel loads are transmitted from the covers into the skin. Feature 6 is the foot radius which is critical to ensure the resulting bending moment from the fuel, air and Brazier loads can be successfully transmitted into the rib without failure. Finally there is the foot castellation (Feature 7), which have to be able to react the shear loading transmitted through the rib [65].

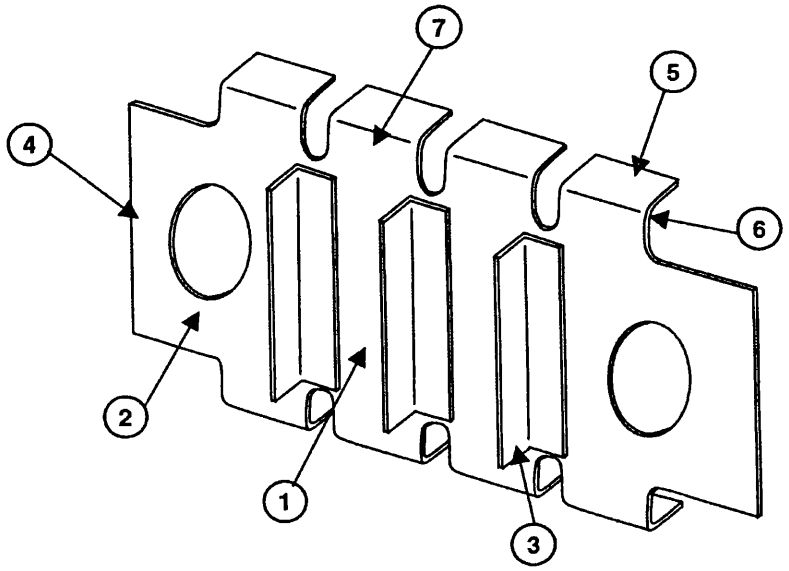

Figure 55 Typical Composite C-Section Rib Broken Down into Elements for Stress Analysis [65]

Each of the elements shown in figure 55 can be analysed using various mathematical stress analysis techniques. These are shown in the flow chart, figure 56, these analysis methods have been derived from Airbus experience, each one being detailed in reference [65]. It should be noted that these methods are in the process of being updated, improved and harmonized for Airbus UK, Airbus France, Airbus Germany and

Airbus Spain and therefore do not represent state of the art analysis methods in all cases.

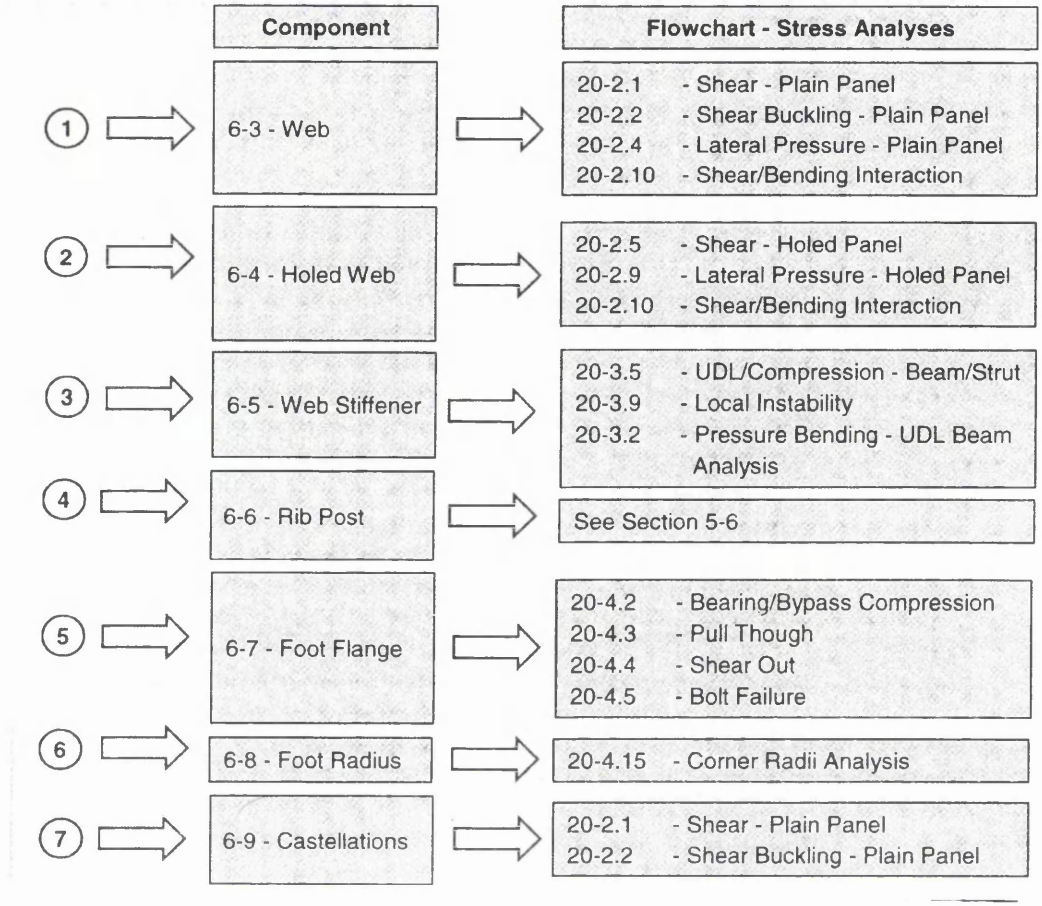

Figure 56 Typical Stress Analysis Methods for Each Element of a 'C' Section Rib [65]

As previously mentioned the loads on the ribs are in the form of Brazier loading, fuel pressure loading etc. Using TANGO data the key design drivers for the ribs can be identified [69]. These drivers are essentially web compression (as a result of Brazier loading) and shear buckling (as a result of induced shear in the Wingbox). This is followed by a through thickness, corner radius failure in the rib foot [66] as the rib feet and cleats fitted are usually critical under fuel/air pressure, as generated tension load causes bending at the rib feet and shear through the cleat flanges [65]. The design drivers are dependent on material properties and geometry as well as loading. The laminate lay-up can be tailored to produce the most light weight component capable of bearing the loads applied to the rib. The rib webs which are predominately loaded in shear require a high percentage of $\pm 45^{\circ}$ plies for optimum design, whereas the rib feet being bolted to the upper and lower covers may have a more quasi-isotropic lay-up for optimum design [65].

3.10.2 Shear Buckling

This calculation considers the forces acting on a composite web. All panels are considered to be of uniform thickness and plane design. This method is from the Airbus Composite Stress Manual [65]. It typically allows a designed web of known thickness to be checked to ensure it will not fail for a known shear load. It can however be rearranged to allow a web thickness to be derived as follows:

Starting with the equations for 'RF', known as the reserve factor shown in equation 101, this reserve factor allows safety to be built into components. An RF of 1 would mean the component would be capable of taking the load acting on it. Greater than 1 it is over designed for safety, lower than one means the component is not sufficiently designed to react the loads applied upon it. In this case the RF is a function of the allowable shear strength (f_{sal}, in MPa) over the applied shear stress (τ, in MPa).

$$RF = \frac{f_{sal}}{\tau} \qquad \textbf{(Equation 101)}$$

In calculating the 'RF' it is necessary to take into account the material strengths, in this case the shear strength of the material. This strength can allow again for conservatism where necessary to ensure confidence in the ability of the component to withstand the loading applied to it, taking into account material defects, potential damage etc. The allowable shear strength is a function of the laminate shear modulus (G_{xy}, in MPa) and laminate shear strain (γ_{xy}) shown in equation 102:

$$f_{sal} = G_{xy}\gamma_{xy} \qquad \textbf{(Equation 102)}$$

The applied shear load is derived from the shear flow in the web over the thickness of the web (t, in mm), shown in equation 103:

$$\tau = \frac{q}{t} \qquad \textbf{(Equation 103)}$$

By taking equation 101 and expanding it using equations 102 & 103 it is then possible to re-arrange it to calculate the web thickness providing equation 104:

$$t = \frac{qRF}{G_{xy}\gamma_{xy}} \qquad \textbf{(Equation 104)}$$

3.10.3 *Shear Buckling (Engineering Science Data Unit - ESDU)*

This calculation considers the forces acting on a composite web as a result of Brazier loading. All panels are considered to be of uniform thickness and plane design. This calculation is taken from ESDU analysis methods [70]

Starting with equation 105, the shear stress is calculated as a function of the coefficient of thickness 'k', the Youngs modulus of the material 'E' (MPa), the thickness 't' (mm) divided by the web width 'b'.

$$\sigma = kE\left(\frac{t}{b}\right)^2 \qquad \textbf{(Equation 105)}$$

However, the shear stress is also equal to the elastic shear at which the elastic web will buckle 'qbe' (N/mm) over the thickness of the web. This is shown in equation 106. It should be noted that this equation can be further modified to take into account plastic deformation in the panel. Plastic deformation in CFRP will not be considered in this case as any plastic deformation would be considered to be a failure.

$$\sigma = \frac{qbe}{t} \qquad \textbf{(Equation 106)}$$

By combining equations 105 & 106 and re-arranging for thickness gives equation 107. This also includes a substitution accounting for the Poisson's ratio of the material to be taken into account.

$$t = b\sqrt[3]{\frac{qbe \times \left(0.91/1-v^2\right)}{kE}} \qquad \textbf{(Equation 107)}$$

3.10.4 *Integral Rib Foot Flange*

With reference to figure 56 notation 5, the foot flange provides the interface a subsequent attachment point for the cover to the rib. This configuration is similar in design to a metallic design. This design does not lend itself to composites as the fibres are generally subject to bending perpendicular to the rest of the component. When

loading occurs this can cause cracking in the inner radius of the composite due to the through thickness strength of the laminate being relatively low to the tensile strength. Typically bolts are used to attach the foot flange to the wing skin. Figure 57, shows this typical arrangment. Here the typical loading element is typically fuel pressure pull off loading followed by brazier loading. It is assumed that the load acting on the flange is reacted along the centre line of the web of the rib. A moment is therefore created between the centre line of the bolt and the centre line of the web of the rib, named 'L'.

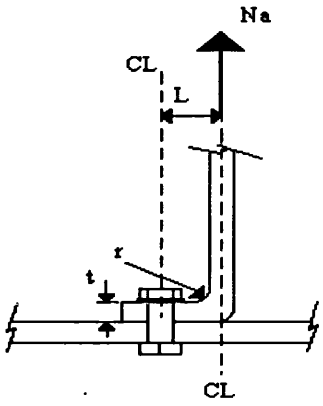

Figure 57 Typical Rib Foot Flange Bolted to Wing Skin

Typically a reserve factor (RF) factor can be calculated as shown in equation 108. The RF is a function of the allowable strength over the tensile strength in the through thickness dimension, '33'.

$$RF = \frac{f_{all}}{\sigma^{t}_{33}} \qquad \textbf{(Equation 108)}$$

The maximum tensile stress 'σ^{t}_{33}' (MPa) is a function of the moment arm multiplied by the applied load expressed as 'M' (N) divided by 2 times the thickness 't' (mm), multiplied by the radius 'r' (mm) plus half the web thickness. 'k' is a correction factor empirically derived to take into account bolting (a dimensionless factor). This is expressed in equation 109.

$$\sigma^{t}_{33} = k\left\{\frac{3M}{2t(r+t/2)}\right\} \qquad \textbf{(Equation 109)}$$

Substituting equation 109 into equation 108, it is possible to rearrange the resulting equation to provide a section thickness, 't' (mm), shown in equation 110:

$$t = -r \pm \sqrt{r^2 + \frac{3k\,M}{f_{all}/RF}} \qquad \textbf{(Equation 110)}$$

Equation 110 is known to be a very conservative method. This method is no longer in use by Airbus and a new method is under development, however to enable quick rough estimates to be produced, with a more realistic solution the equation can be modified. This simple modification is a reduction in length of the calculated moment arm 'L' and 'Na' the applied load per unit length. The moment arm as stated previously is assumed to act at the centre of the rib web, however to reduce conservatism it can be said that the moment arm acts from the centre of the fastening point to the outer face of the rib web. In this case half of the web thickness is subtracted from L, shown in equation 111:

$$M = Na \times \left(L - t/2\right) \qquad \textbf{(Equation 111)}$$

Equation 111 can be substituted into equation 110 and further rearranged to resolve the component thickness, as shown in equation 112:

$$t = \frac{-\left(4r\,\frac{f_{all}}{RF} + 3k\,Na\right) \pm \sqrt{\left(4r\,\frac{f_{all}}{RF} + 3k\,Na\right)^2 + 48\,\frac{f_{all}}{RF}\,k\,NaL}}{\frac{f_{all}}{RF}} \qquad \textbf{(Equation 112)}$$

4. AIMS

4.1 Introduction

As discussed in the literature review humidity and temperature have a profound effect on the strength of composite materials having a polymeric matrix, such as a thermoset or thermoplastic material. The strength of the fibres remains unaffected by the environment, which means the reduction in mechanical properties is confined to loading directions, which cause the load to be carried by the matrix and not the fibres. Typically tensile, shear and compressive strength are directly affected by exposure to hot and humid environments. Other factors which may be considered are bearing strength for bolted joints and damage tolerance. Unfortunately due to the constraints on time and budget these two later variables are not being fully considered in this work, with only limited investigations into performance being carried out.

Firstly, it is important to introduce the complementary work being carried out in support of this project. The specific aims and task of this project will be summarised at the end of this section. This project can be broken down into three constituent parts, with three additional smaller studies carried out in support (MRes projects). There is the materials-testing element. This involves testing materials at different levels of saturation. The second part is the Finite Element Modelling work. This focuses on utilising Fickian diffusion to predict moisture levels in composite structures. This modelling utilises the material strengths generated by the test programme to predict materials strengths for components. The third project (the subject of this thesis) practically applies the results and the developed model to evaluate potential weight savings of this new approach when predicting new material properties as a result of environment. The focus of this project moved away from full 3D FE and focused on a 1D diffusion model coupled with classical laminate theory, to predict laminate properties. This tool is known as ELAP 1D (Environmental Laminate Analysis Programme), which shall be discussed later. ELAP 1D was developed from the initial PhD modelling work by a Swansea University Research Assistant under the guidance of the author. This project then uses both the results of the testing element and the developed model to evaluate the potential weight savings of this new approach to predicting new material properties as a result of environment.

The author launched a collaborative project with EADS Innovation Works, Swansea University, Cytec and Airbus to provide the necessary resources combined with Welsh

Assembly government funding. This project was called EMOC (environmental modelling of composites) and the new modelling approach and attributes associated with this will be referred to as the EMOC modelling approach in this thesis.

Figure 58, shows the general approach of the FE, testing and application phases of the overall project. To the left hand side of the figure represents in the main the work being carried out by Swansea University via two supporting PhDs. In addition to these PhD a number of MRes projects have been commissioned by the author to explore specific areas to support the new approach. The 'Design & Stress Methods Section', directly influences the test and modelling elements in that it has defined the key material property drivers required for design by utilising Airbus Stress methods and their associated material properties. These stress methods come under the remit of this project. The modelling element utilised the basic mechanical property data derived from conditioned coupons to predict material strengths. The model is then used to predict the strength of a material and or components with a varying level of moisture through the thickness of the structure. Tests are then performed to validate the EMOC approach. The Box 'Stress, FE, CAD, Design Evaluation' represents the main proportion of this project. It directly drives and influences the ELAP 1D model, stress methods utilised and subsequent materials testing that is to be carried out. This project will utilise the ELAP 1D tool and test results to carry out evaluations on weight of components. This project is novel as this is the first time that such an approach has been adopted. In the past a conservative approach of assuming full saturation and high temperature (HOT/WET) was used. Alternatively the use of aggressive environmental knock-down factors (EKDF) applied to stress calculations was used.

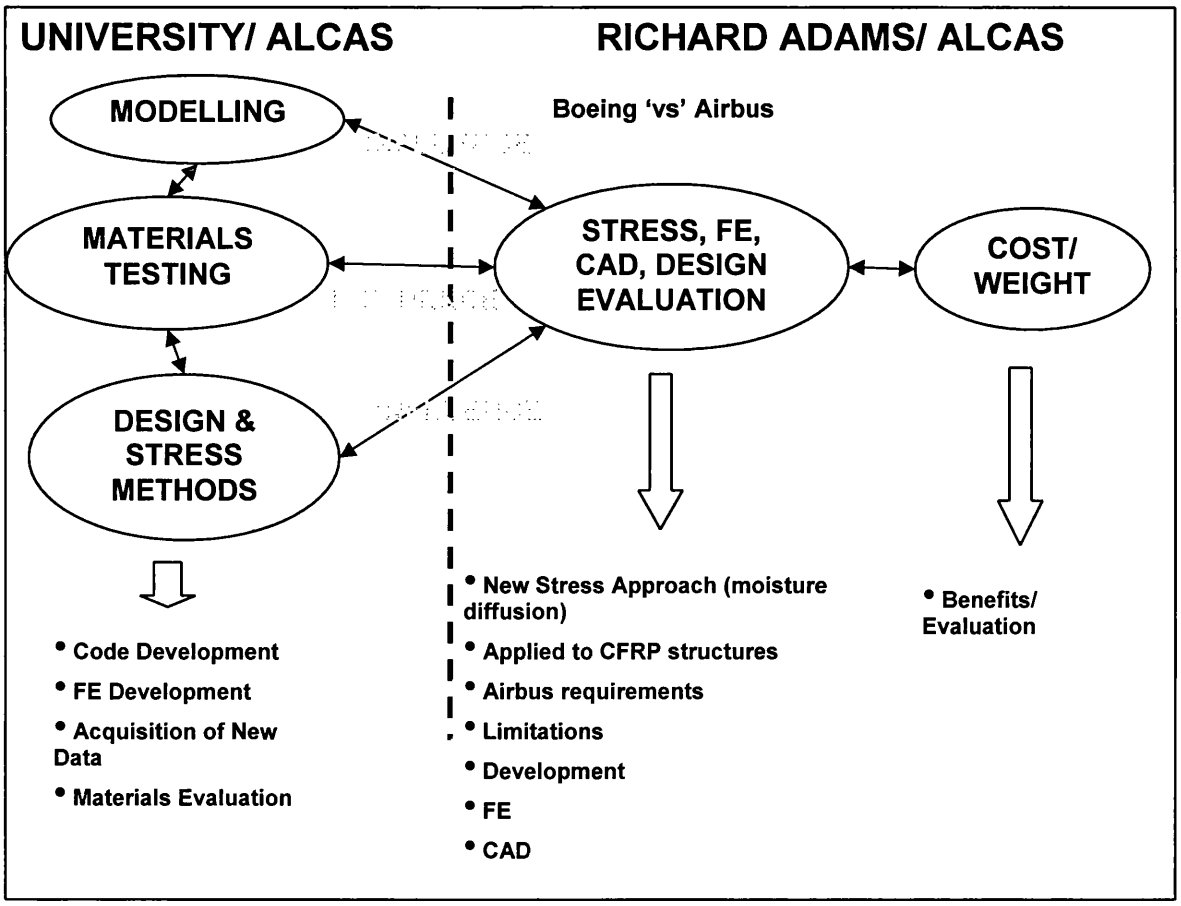

Figure 58 New Design Methodology for Composite Materials Exposed to Humid, High Temperature Environments

Finally, figure 58 shows the main aspects of each element of the project. Essentially the supporting work will provide new material design data and subsequent material evaluation in terms of failure modes and fracture mechanics for materials that are saturated to different levels from uniform saturation, to materials having a varying level of saturation through the thickness. The ability to model the material behaviour will be through the ELAP 1D model development. An evaluation of ALCAS ribs structure will then be carried out, where possible, using both the ELAP 1D tool and a sizing tool developed within this project. The resultant data will be evaluated for weight savings along with evaluation of the success and limitations of the other two PhD supporting projects. Further sizing studies of lugs have been carried to assess the weight saving potential of the project, which have been validated via lug case studies and associated testing.

Overall this work should help give Airbus a competitive edge over its main competitor Boeing. This work represents a leap forward in the analysis of Carbon Fibre structures,

through more detailed analysis. This should lead to the removal of unnecessary conservatism in the stress and design process, leading to a more efficient structure.

4.1.1 PhD Overview of FE Model (PR1)

The principal mechanism for the absorption of moisture in a graphite/epoxy laminate has been shown to be a diffusion-controlled process. Numerous diffusion models have been proposed over the years for modelling hygrothermal effects. The most frequently used model is the Fickian model, outlined in section 2.12 3 of the literature review.

The primary focus of this project at Swansea University is to model the diffusion of moisture into polymer matrix composites with varying temperatures and humidities using finite element techniques. Model predictions are compared with an existing in-house validated finite difference model [71].

A prototype 3D transient diffusion FE code has been developed during the first year of the commissioned project by PR1 at Swansea University. In order to examine the three dimensional capability of the model an average elemental concentration profile of a wing component was produced. Also at this stage, an experimentally-derived relationship between strength and moisture absorption has also been incorporated to demonstrate the capability of the FE code. Research will be carried out by incorporating a wide variety of measured property/moisture data (currently being carried out at Swansea University as part of the ALCAS research programme) into the model and interfacing it to existing commercial FE codes used in aerospace industry via Airbus Operations Ltd.

4.1.1.1 Transient Model

Transient conditions must be analysed in many physical situations, such is the case for moisture absorption in composite components. The governing diffusion equation for moisture absorption in three dimensions takes the form of equation 91.

The finite element discretisation process reduces the differential equation to a set of equilibrium type matrix equation (equation 113):

$$[k_c]\{C\}+[m_m]\left\{\frac{dc}{dt}\right\}=\{q\} \qquad \textbf{(Equation 113)}$$

where {C} are the nodal values of C and {q} represents additional source and sinks. This set of first order, ordinary differential equations can be solved by many methods, the simplest of which discretise the time derivative by finite differences.

It is assumed that the diffusion coefficient is only dependent on temperature and can be modelled with the Arrhenius law as shown in equation 83.

In addition to the coefficient of diffusion D, which characterises the rate of water absorption, a second parameter of practical interest is the equilibrium moisture content, M_m (noting that this terminology is similar to that used equation 82 with the method hear simply using different notation). This represents the maximum amount of absorbed moisture that a material can contain at moisture equilibrium for a given moisture exposure level, expressed as a percent of dry material mass, equation 82 (discussed in sections 2.12.6 and 2.12.7):

$$M_m = \frac{M_{sat} - M_{dry}}{M_{dry}} \times 100\% \qquad \textbf{(Equation 82)}$$

where M_{sat} is the mass at saturation (g) and M_{dry} the dry specimen mass (g).

M_m is not explicitly part of Fick's law but is used to determine boundary conditions. It is considered that locally, at the faces of the plate, the concentration is equal to the equilibrium moisture content. Thus it is assumed, at t = 0, the faces of the plate are instantaneously saturated with moisture.

In addition, the relative humidity influences the equilibrium moisture content. Its effect is modelled by the following empirical relationship in equation 92 (section: 2.12.7).

$$M_m = a(RH)^b \qquad \textbf{(Equation 92)}$$

where a and b are empirical constants and RH is the relative humidity (%).

4.1.1.2 Solution of First Order Time Dependent Problems

Using an element assembly method, $[k_c]$ becomes $[K_c]$, $[m_m]$ becomes $[M_m]$ and the basic equations can be written at two consecutive time steps "0" and "1" as shown in equation 114 & 115:

$$[K_c]\{C\}+[M_m]\left\{\frac{dC}{dt}\right\}_0=\{Q\}_0 \qquad \textbf{(Equation 114)}$$

$$[K_c]\{C\}+[M_m]\left\{\frac{dC}{dt}\right\}_1=\{Q\}_1 \qquad \textbf{(Equation 115)}$$

where [C] and {Q} represents the global counterparts of [c] and {q}.

A third equation advances the solution from 0 to 1 using a weighted average of the gradients at the beginning and the end of the time interval (equation 116):

$$\{C_1\}=\{C_0\}+\Delta t\left((1-\theta)\left\{\frac{dC}{dt}\right\}_0+\theta\left\{\frac{dC}{dt}\right\}_1\right) \qquad \textbf{(Equation 116)}$$

Elimination of $\{dC/dt\}_0$ and $\{dC/dt\}_1$ from equations (115) and (116) leads to the following recurrence equation shown in equation 117 between time steps "0" and "1"

$$([M_m]+\theta\Delta t[K_c])\{C\}_1=([M_m]-(1-\theta)\Delta t[K_c])\{C\}_0+\theta\Delta t\{Q\}_1+(1-\theta)\Delta t\{Q\}_0 \qquad \textbf{(Equation 117)}$$

This equation is only unconditionally stable" if $\theta \geq ½$.

4.1.1.3 Computer Model

The computer model uses 8 node linear hexahedral elements. Moisture concentration at the exposed surfaces is set to the equilibrium moisture content of the material. The interior nodes are set to zero and the total moisture content is calculated with time. Each element is given a material number which defines its material properties. Elements have six faces: north, south, east, west, fore and aft.

4.1.2 PhD Overview of Material Testing (PR2)

The main aim of this package of work is to define material properties at varying levels of saturation. These properties are then utilised by the FE model to carry out predictions of full scale components. By further testing it is then possible to validate the FE model for components having varying levels of saturation within them. Moisture

ingress has an affect on the strength of the resin but has little to no effect on the strength of the fibres. As a result the material mechanical properties are those that rely on the strength of the resin within the composite. There are many known resin dominated material strengths such as bearing, interlaminar shear, in plane shear and compression. To explore all mechanical properties that are affected by moisture represents an extensive test programme, requiring excessive resources and time to carry out. The author, in association with test specialists within the Airbus Composite Research team selected for the student a number of tests for initial exploration. Material choice was also a consideration and again this had to be limited to one material due to budget and time constraints.

A material was selected that has known Fickian behaviour and that has been extensively used by Airbus UK. This material is a Cytec pre-impregnated Material, utilising 977-2 resin system with HTS fibres. Material data was to be generated for the basic UD direction, utilising the material in a UD tape form. Evaluations on directed lay-ups were also to be made through a quasi-isotropic lay-up. In this case the coupons were manufactured using the material in a woven 5 Harness Satin form. This material is essentially an epoxy matrix, which requires autoclave cure at 180°C. The devised test matrix is shown in Tables 12-15 noting that this test matrix is not exhaustive. Before discussing the test matrix it is first important to understand the approach being adopted by the project.

4.1.2.1. The Approach

Firstly a diffusion coefficient is derived via the conditioning of coupons under constant temperature and humidity in an environmental chamber. This coefficient is derived by measuring moisture uptake over time. This gives a highly accurate moisture uptake rate for this particular batch of Unidirectional (UD) & woven material. Predictions of times to condition the coupons could then be made using the FD model produced by Swansea, which has been validated against the equivalent Airbus tool. Coupons were then conditioned to varying levels of saturation through the thickness. This was done by fixing the temperature and varying the humidity in the environmental chamber. Control in this way will allow a uniform level of moisture saturation through the thickness, as shown in figure 59. Each coupon can then be mechanically tested and strength and strain data obtained. This material data will then give a known material strength for a known level of saturation, which can then be utilised by the FE model.

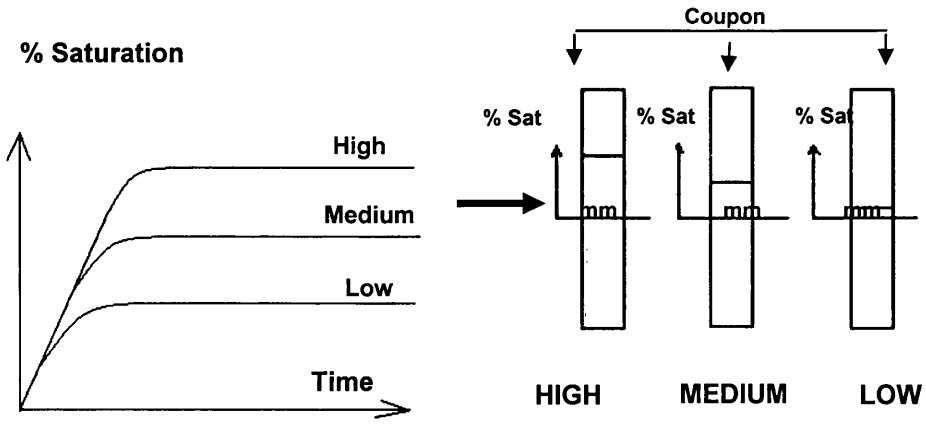

Figure 59 Different Saturation Levels Produced Give Uniform Moisture Levels Through The Thickness of the Coupon

Tests are then carried out for coupons that have a varying level of saturation through the thickness, a schematic of which is shown in figure 60. In tandem PR1 shall predict coupon strength for this varying saturation. If the test results match, then the model is to some extent validated. However for varying saturation levels it is possible that the failure mechanics could be complex. Although the main aim of this project is to supply and validate the developed model tool, it is equally important to characterise failure mechanics of the material and provide the necessary data to the model to allow the material behaviour to be accurately modelled. It should be noted that it is recognised that thick laminates will benefit most through this research through weight savings, as the components will see relatively low levels of saturation due to the time to saturation of the thick component. As a result when carrying out these varying moisture content tests it is important to leave the core of the coupon in a dry state to simulate a realistic condition, found in aircraft service.

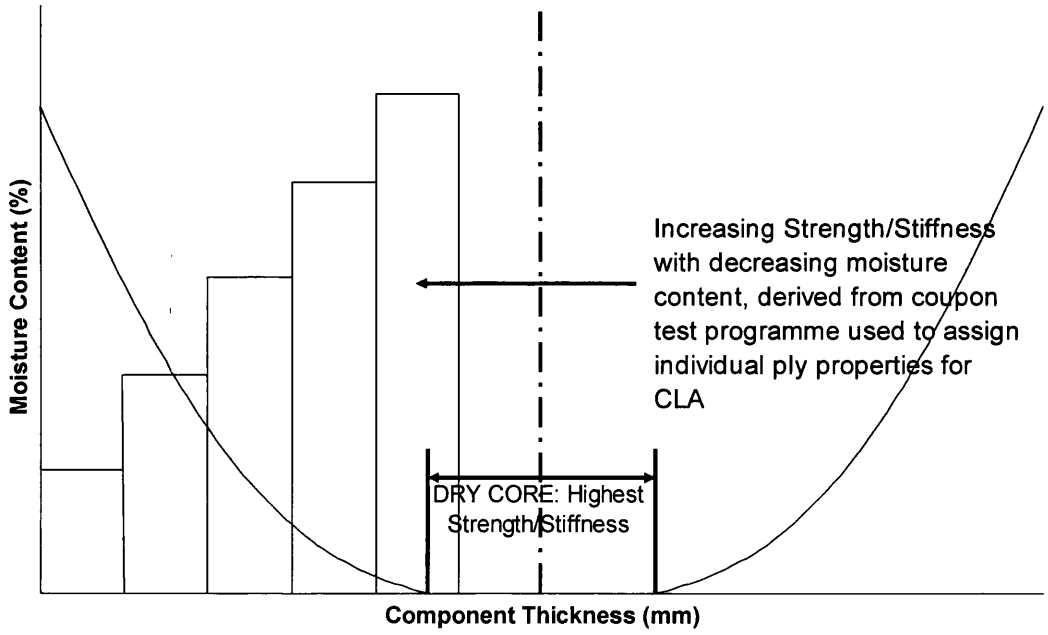

Figure 60 Showing Coupon with a Varying Level of Moisture through the Thickness and a Dry Core Potentially Operating at Full Strength

The test matrix as previously mentioned could potentially be very large. If one takes four different mechanical property tests and assumes that a minimum of 6 tests needs to be performed at each condition, for several conditions, multiplied by the number of different mechanical property tests to be formed it is quickly realised that the test matrix would become extensive. It was decided that resin dominated failure modes should be concentrated on because as moisture ingresses into the resin the strength and stiffness of the resin decreases. However, there may be some effect in reducing the tensile strength of the laminate. In order to ascertain any effect on tensile strength the tensile property of the materials was to be tested. Material tensile strength perpendicular to the fibre direction will be driven by the strength of the resin and thus would be tested more extensively. Compression, in-plane and interlaminar shear were also highlighted as valuable mechanical properties. All tests were carried out using Airbus Industrie Test Methods (AITMs). As previously mentioned the initial material properties defined were to be for unidirectional laminates, summarised in table 12 for uniform levels of saturation through the thickness of 0,25,50,75 & 100% (of total saturation).

Table 12 Unidirectional Material Tests at Different Levels of Uniform Saturation through the Thickness of the Coupons

%Saturation	Tension		Compression		In-Plane Shear (+-45)	Interlaminar Shear (3 Point Bend Test)
	0	90	0	90		
0	6	6	6	6	6	6
25	-	6	-	6	6	6
50	6	6	6	6	6	6
75	-	6	-	6	6	6
100	6	6	6	6	6	6
SUB Totals	18	30	18	30	30	30
					Total =	156

Once the initial material properties are defined it is necessary to understand what happens with regard to failure strength and stiffness of components having a varying level of saturation through the thickness, as shown in figure 60. Again this was to be carried out for UD material. To represent thick components a dry coupon core was to be maintained. This dry core was proposed to be 33% and 66% of the total coupon thickness. Again the number of different moisture distributions had to be limited to keep the test programme realistic (c.f. table 13). When conducting tests detailed failure characterisation was to be conducted, to monitor fracture mechanics, specifically noting any deviation from a conventional failure.

Table 13 Unidirectional Tests Performed With Varying Saturation Levels Maintaining a Dry Core of 33 & 66% Respectively

% Dry Material	Tension		Compression		In-Plane Shear	Interlaminar Shear
	0	90	0	90		
33	6	6	6	6	6	6
66	6	6	6	6	6	6
SUB Totals	12	12	12	12	12	12
					Total =	72

The previous test matrices were focused on unidirectional material properties. Typical laminate analysis methods enable 'Stress' to calculate directed laminate strengths. However to ensure these typical procedures are valid, tests were to be conducted for a laminate having a directed lay-up. The chosen lay-up was to be quasi-isotropic, as this ensures applicability to cover generic lay-ups. The material was changed from a UD tape to a five harness satin (a mistake, discussed later). The initial test matrix is shown in table 14 and essentially repeats the UD testing for different uniform levels of

saturation through the thickness of the coupons to be tested. Saturation levels tested in this case were different conditions 0, 50 and 100%.

Table 14 Quasi-isotropic Material Tests at Different Levels of Uniform Saturation through the Thickness of the Coupons

%Saturation	Tension		Compression		In-Plane Shear	Interlaminar Shear
	0		0			
0	6	-	6	-	6	0
50	6	-	6	-	6	0
100	6	-	6	-	6	0
SUB Totals	18	0	18	0	18	0
					Total	54

Finally, the test matrix shown in table 13 was repeated for the quasi-isotropic material again focusing on strengths, stiffness and fracture mechanics. These tests are summarised in table 15. For both the UD & quasi-isotropic material tests carried out here, the results were used to validate predictions created by the model being developed in tandem with this materials testing project.

Table 15 Quasi-isotropic Tests Performed With Varying Saturation Levels Maintaining a Dry Core of 33 & 66% Respectively

% Dry Material	Tension		Compression		In-Plane Shear	Interlaminar Shear
	0		0			
33	6	-	6	-	6	0
66	6	-	6	-	6	0
SUB Totals	12	0	12	0	12	0
					Total	36

Three supporting MRes projects were commissioned by the author to perform specific detailed experimentation in addition to PR1 & PR2.

4.1.3 Supporting MRes 1 – Residual Moisture

The aim of this study was to determine how much moisture was trapped in the material after conditioning to saturation, followed by drying until no significant loss of moisture was observed. As non-Fickian diffusion is understood to take place, it was necessary to attempt to quantify the significance of this mechanism. In this case in-plane shear and

90° tension were chosen to quantify the affects. The test matrix created by the author is shown in table 16. All tests were carried out at room temperature.

Table 16 Showing Test Matrix to Investigate Residual Moisture Effects on Mechanical Performance

Residual Moisture Tests						
Test Type	Conditioning Temp (°C)	Conditioning %RH	Drying Cycle 90°C	Material type	Specimens/ condition	Total Specimens
In-Plane shear	-	-	90	977-2	6	12
	70	85	90	977-2	6	
90 Tension	-	-	90	977-2	6	12
	70	85	90	977-2	6	

4.1.4 Supporting MRes 2 – Diffusion Coefficient Studies

The purpose of this MRes project was to explore and determine the diffusion coefficients of the 977-2 material. The standard test method approach for determining moisture uptake via test is to use traveller specimens of the same material that is to be mechanically tested. However this typically provides a diffusion coefficient through the thickness of the material on the basis that the edges of the specimens are relatively small and insignificant. The overall aspiration on the EMOC project was to produce a full 3D model and therefore for accuracy would require a diffusion coefficient in all planes of the material. Furthermore the purpose of this study was look at how different lay-ups would affect the diffusion coefficient with the overall goal of ensuring that a realistic diffusion coefficient could be determined for modelling of components for each material.

Figure 61 shows how the diffusion coefficients in the 'x', 'y' & 'z' directions were determined. Face three is the standard diffusion value used for analysis as it represents the largest area of material exposed to the environment. Face 1 & 2 represent fibre ends and sides. It should be noted that due to the scope of the project different lay-ups were not specifically studied. The method for tracking moisture absorption was determined using [9]. To maintain a similar area of material to the standard, which therefore limits the influence of diffusion along the less significant end faces, each coupon produced attempted to replicate the same surface area as [9]. A laminate was manufactured to a thickness of 30mm, which meant that that to maintain a similar surface area the coupons where relatively long in length.

In addition to the diffusion of moisture into the composite a comparison was also made to pure neat resin to compare the diffusion coefficients, where the intention was to compare the difference in the rate of uptake, but also to link maximum moisture content in the neat resin to the maximum moisture content in the CFRP samples, taking into account fibre volume fraction. If successful and although outside of the scope of the MRes students work, the maximum moisture values of the neat resin could theoretically be used as a reference to determine the maximum moisture content of any laminate of a specific fibre volume fraction.

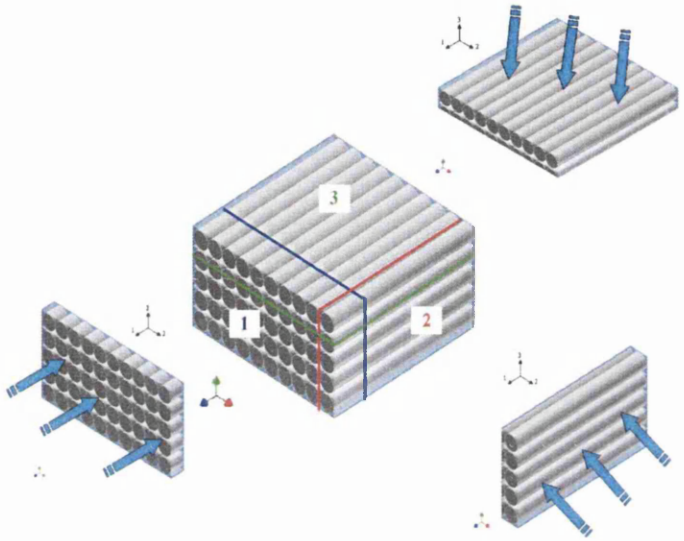

Figure 61 Showing Diffusion Coefficient Determinations across Different Material Plans of 977-2

4.1.5 Supporting MRes 3 – Single & Double Lap Bearing Strength

Airbus has a specifically developed a tool to analyse composite bolted joint performance. This tool determines the interaction between bearing strength and bearing by-pass strength. Bearing by-pass is where the bearing load from an adjacent fastener in a row of fasteners in a given loading direction transmitted to its nearest neighbour in the direction of load in addition to the bearing load exerted on it. This tool is empirically driven although the calculations methods are typically straightforward. To determine bolted joint performance the method described in [18] was used. For the Airbus bolted joint method a wide range of joint configurations is typically tested, having variations in fastener size and thickness of the constituent composite parts, further complicated by the need to test both double and single lap shear joints. Due to such an extensive test campaign requirement, it was felt by the author that it may not be

practical to use the EMOC methodology to assess bolted joint performance, especially within the scope of this project.

The author did however believe that as bearing performance is based on the performance of the resin, where failure is typically by locally crushing around the bearing area of the hole, the principle of not using HOT/WET properties would still be applicable. However this is complicated with single lap shear as the bearing failure is typically surface initiated and therefore the failure is within the fully saturated area of the material. Sceptics may therefore argue that it would not be appropriate to use anything other than HOT/WET properties in this case. However it could be hypothesised that although the outer material was saturated its loss in stiffness would lead to a greater load distribution in the stiffer unsaturated plies and therefore it may have been possible to see some advantage in a single lap shear joint. As the load distribution is relatively more uniform in a double lap joint the principles of EMOC could have been easier to justify. The test matrix shown in table 17 shows the range of single and double lap tests commissioned by the author to provide data to assess the applicability of EMOC principles to bolted joints.

The single lap tests utilised a ¼" fastener and were countersunk, with the double lap tests being of the same fastener diameter using a pan head fastener. In both instances the laminate thickness was 4mm. This was considered by the author and colleagues who had generated bolted joint data for the A350 aircraft to be the best choice in terms of representing joint performance in such a limited test campaign. These tests being the thinnest also therefore reduced the conditioning time. The use of a countersink fastener for single lap shear purposes typically provides the lowest bearing strength.

Table 17 Single Lap Bearing (SLB) and Double Lap Bearing (DLB) Test Matrix to Study the Effects of Moisture

Test Type	Conditioning		Test Temperature (°C)	Lay-up	Material	No. Specimens/ Condition	Specimens/Test Type
	Temp (°C)	%RH					
DLB	N/A	0	20	QI	M21 T800	6	72
			60	QI	M21 T800	6	
			90	QI	M21 T800	6	
	70	45	20	QI	M21 T800	6	
			60	QI	M21 T800	6	
			90	QI	M21 T800	6	
	70	65	20	QI	M21 T800	6	
			60	QI	M21 T800	6	
			90	QI	M21 T800	6	
	70	85	20	QI	M21 T800	6	
			60	QI	M21 T800	6	
			90	QI	M21 T800	6	
SLB	N/A	0	20	QI	M21 T800	6	72
			60	QI	M21 T800	6	
			90	QI	M21 T800	6	
	70	45	20	QI	M21 T800	6	
			60	QI	M21 T800	6	
			90	QI	M21 T800	6	
	70	65	20	QI	M21 T800	6	
			60	QI	M21 T800	6	
			90	QI	M21 T800	6	
	70	85	20	QI	M21 T800	6	
			60	QI	M21 T800	6	
			90	QI	M21 T800	6	

4.2 This Projects Specific Tasks

The primary task of the current project is to utilise the mechanical test data and ELAP 1D model being created in the complementary work to quantify weight savings through the use of less conservative material properties for the stress calculation of wingbox components. In order to calculate mass effects a sizing tool will be developed for the ALCAS wingbox ribs, within Microsoft Excel utilising the equations given in section 3.10. This tool will carry out simplistic mass calculations based on 'C' & 'I' section design. Data provided from the mechanical testing programme can then be integrated directly into the sizing tool to determine weight savings where applicable.

In addition to the direct use of the mechanical data in the sizing tool, the developed ELAP model will be utilised to predict the material properties in a component. Environmental conditions will be defined within the ELAP tool (temperature & humidity), along with an exposure timescale that will enable an accurate prediction of moisture levels to be ascertained within the structure. The ELAP tool will then define the material properties throughout the structure. The results from the ELAP tool will then be fed

back into the Microsoft Excel rib sizing tool, where a study can be carried out to determine the effect on the structure can be made. It will be possible to use the ELAP tool to predict the material properties of a specific region of a component. Hand calculations and the stress sizing tool will then be used to determine any weight savings that occur.

Once these first two tasks are complete a comparison and evaluation will be made to determine the accuracy and limitation of the calculation methods. Then an investigation will be carried out into the use of different materials (different polymer matrices & fibre types) by the model, along with a rationalisation of the mechanical testing programme used in this research for validation of new materials.

A preliminary investigation will be carried out to assess the thermal effects on the materials mechanical strength. This will be via mechanical testing and will be the first step towards modelling combined thermal and moisture effects in the structure, which will be beyond the scope of this research project.

Once all tasks have been completed a plan of future work will be created based on the findings of this research project to further enhance the modelling capability for evaluating composite materials exposed to different atmospheric environments.

A summary of the task is as follows:

4.2.1 Task Summary

- Create a simplistic sizing tool for weight evaluation of ribs.
- Evaluate supporting PhD and MRes test programmes, define enhancements and create new CAT 2 test programme (known as the EMOC test campaign).
- Carry out a preliminary investigation on thermal effects on material strength and adapt EMOC test campaign based on findings.
- Quantify differences between 977-2 & M21 resin systems in terms of moisture uptake and in-plane shear properties.
- Use mechanical test data, developed ELAP 1D tool, in association with sizing tool to determine where possible component mass and subsequent weight savings.

- Carry out a component case study, using mechanical property data, component testing and the developed modelling tool.
- Evaluate the success of the modelling approach via the case study and recommend improvements where possible.
- Quantify lug weight savings potential using the ELAP 1D tool.
- Evaluate & Analyse ELAP 1D model for accuracy, pitfalls and carry out a comparison between the ELAP 1D tool and rib sizing tool data (using the mechanical test data).
- Propose future work to improve modelling capability.

5. EXPERIMENTAL PROCEDURES

5.1 Ribs Sizing Tool

The ALCAS rib sizing tool has been developed by the author. This has been utilised to provide initial sizing estimates and subsequent masses for the rib package of ALCAS. The tool focuses on what are considered to be critical design drivers for state-of-the art composite wingbox design within Airbus. The sizing methods are summarised in section 3.9. The tool is Microsoft Excel based, which gives the ability to carry out rapid analysis of a full rib set within an airliner wing. This tool will be utilised to provide initial quantification of potential weight savings between room temperature/dry and hot/wet material properties. As material property results are generated from the complimentary work supporting this project, the tool will be used to approximate the impact on weight of the components. Generally speaking, as time to condition material is thickness dependent the author has chosen to focus on Rib numbers 2-12 for this analysis, as these inboard ribs have thicker section. The manufactured ALCAS test article wingbox will also represent these 12 ribs and therefore makes this study comparable to data produced by the ALCAS rib partners.

The tool does however have its limitations. The tool uses loads that are worst case and does not take into account local loading conditions, only global loading conditions. The tool does not take into account wing curvature and uses an average rib height for calculations. Finally the mass estimates are based on crude geometric calculations. None of these limitations is expected to hinder the project as it is not the aim of the project to carry out detailed and accurate component sizing; the aim of the project is to evaluate the difference of the new sizing approach.

5.1.1 Tool Overview & Architecture

The tool has been designed to be user-friendly and quick to use. It requires geometry, loading, material properties and some constants to be entered prior to analysis. An overview of the general tool architecture is given in figure 62.

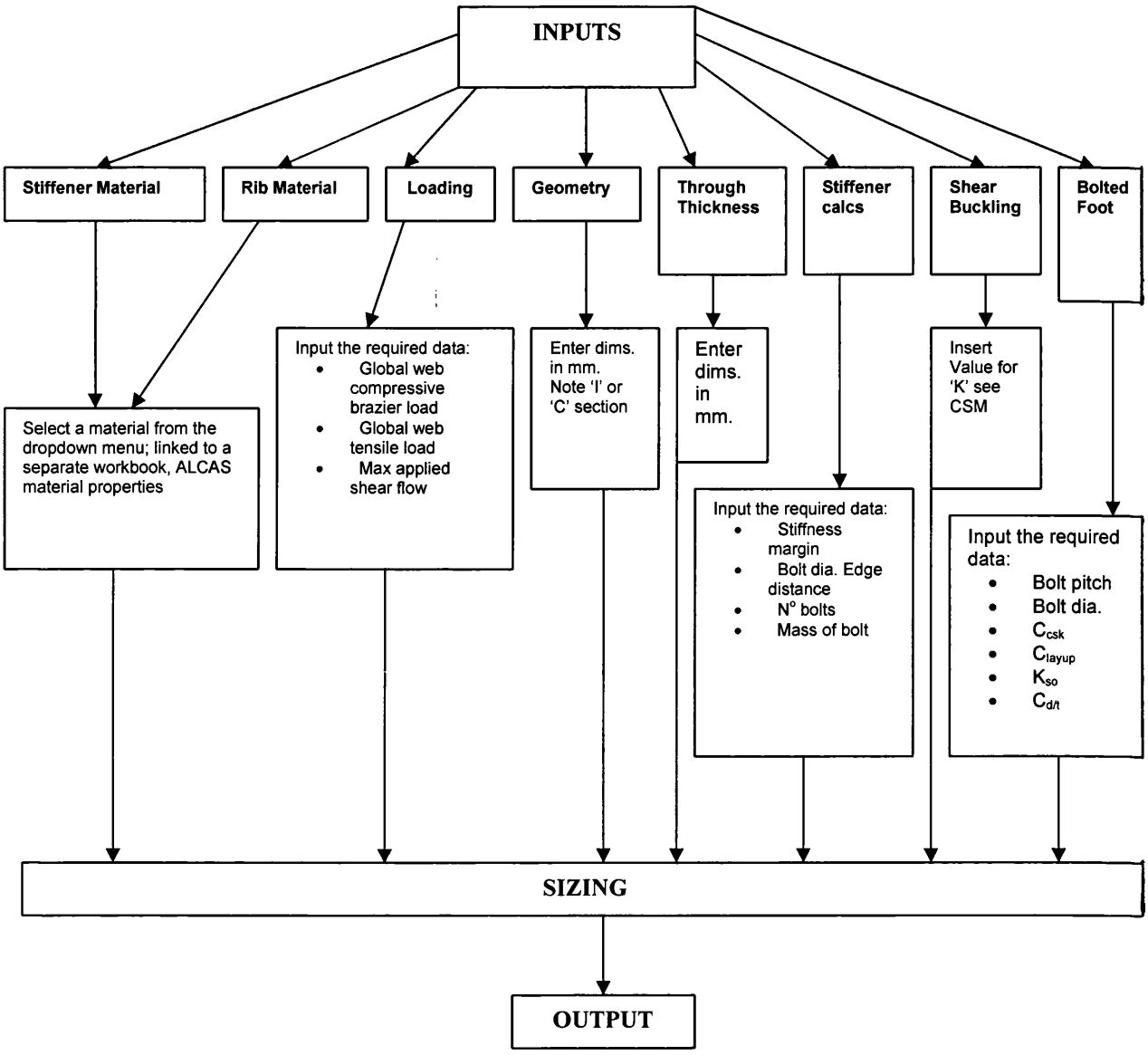

Figure 62 Flow Process of Ribs Sizing Tool

5.1.2 Variables

Figure 63, shows the start point for running the sizing tool. All sections are required to be entered to carry out rib sizing. The variables do not have to be entered in any order and may be changed at any time to perform optimisation. Material properties are defined for the rib and the rib stiffeners separately. This is because the stiffeners can be considered to be a part in their own right which form part of the rib assembly (see figure 55). Loading and Geometry is stored on a separate work sheet. The loads are taken from the Global Finite Element Model (GFEM), produced by the ALCAS stress team. The 'loads tab' takes the user to the loads required for the calculations, these have been manipulated to allow the calculations to be made.

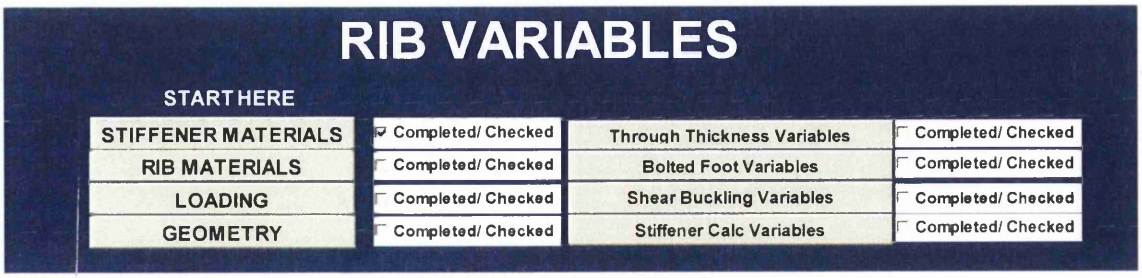

Figure 63 Screenshot of ALCAS Rib Sizing Tool Variable Start Point

Firstly, the material properties need to be defined. The material properties required are based on the sizing tool methods, highlighted in section 3.9, composite material properties are dependent on lay-up of the laminate. The tool allows the lay-up to be specified and subsequent material properties to be derived. This works on a principle of percentage of fibres present in each direction, as used in classical laminate analysis. For both the stiffener and rib properties the format for material selection is the same. An example of the material property input table is shown in figure 64. Materials properties form part of another worksheet. A range of materials are available and the material data will be updated by the complimentary project to allow evaluation. The atmospheric conditions i.e. room temperature/dry, HOT/WET etc, can be selected for each material. For the rib sizing tool most material properties are affected with conditioning to hot/wet because the design drivers are dependent on resin dominated properties. It should be noted at this stage that bearing strength data is not being generated by the complimentary work and the effect of reductions in bearing strength will not be evaluated using this tool.

MATERIALS SELECTOR

BACK

RIB MATERIAL PROPERTIES

Rib No	Material	Atmospheric Conditions	LAY-UP 0° (%)	LAY-UP 45° (%)	LAY-UP 90° (%)	E_x^1 (N/mm²) Comp	Laminate Shear Modulus G_{12} (N/mm²)	Laminate Allowable Shear Strength F_{s6}	Bearing Strength f_{bu}	F_{tu}^1 $(0.7*f_{22}^1$ MPa	ρ (kg/m³)
1	NCF-100	RT/dry	10.00	80.00	10.00	23240.80	25414.00	203.31	670	#DIV/0!	1580
2	Intermeadiate Modulus Fibre Pre-Pregs-	RT/dry	10.00	80.00	10.00	26373.33	30782.67	246.26	670	37.3333	1560
3	Intermeadiate Modulus Fibre Pre-Pregs-	RT/dry	10.00	80.00	10.00	26373.33	30782.67	246.26	670	37.3333	1560
4	High tensile Fibre Pre-Pregs-200	RT/dry	10.00	80.00	10.00	24094.76	26251.35	210.01	670	50.8667	1650
5	High tensile Fibre Pre-Pregs-100	RT/dry	10.00	80.00	10.00	24113.71	26282.86	210.26	670	49.7	1650

Figure 64 Screenshot of Material Property Table

Rib loading is now required as shown in figure 65. First the global web compressive brazier load is required. This load is generated from the GFEM. However, if more detailed loading information was to become available this could be fed into the model. For the purpose of understanding the effects of environment on the strength and subsequent component sizing the loads used will be up to date at the time of analysis and will not be updated in order to ensure consistent comparison of material property effects. It should be noted that as material is subjected to moisture and temperature the stiffness of the material is reduced. This would mean that the load distribution in the structure would change, however these effects are beyond the scope of this project. The global web compressive Brazier load (compressive load), is required for the stiffener analysis. The load in this case is assumed to be carried equally between all of the stiffeners in the structure. Typically a stiffener is found at each stringer cut out, with the number of stringers being defined by the stringer pitch and rib cord. This is also true for the global web tensile load (fuel pressure pull off load), dividing the load by the number of available stiffeners in the rib. Global web tensile loading is provided again from the GFEM. The shear flow used for calculating rib web thickness is again provided by the GFEM.

BACK	LOADING					
Rib No.	Global Web Compressive Brazier Load (N)	P_{comp} per stiffener (N)	Global Web Tensile Load (N)	$P_{tensile}$ per stiffener (N)	Pull-Off Load Na (N/mm)	Max Applied Shear Flow 'q' in web (N/mm)
1	5265.00	5265	1487992.0	82666.2	444.6	2242.76
2	4633.00	4633	2288583.6	134622.6	720.1	1781.95
3	4500.00	4500	823481.2	54898.7	314.1	760.45
4	5823.00	5823	1828412.7	130600.9	744.5	626.52
5	8584.00	8584	1894001.7	145692.4	819.5	221.325
6	11250.00	11250	1547878.1	128989.8	712.5	238.35
7	12951.00	12951	1426949.4	118912.5	701.0	187.275
8	13900.00	13900	1462833.6	132984.9	774.6	111.23

Figure 65 Screenshot of Rib Loading for Sizing Calculations

The next input that needs defining for the analysis is the geometry. The sizing tool assumes a baseline of two basic rib configurations, the simple C-section and the I-section designs. A schematic of these two rib designs is shown in figure 66. The wingbox geometry is fixed at the concept stage and therefore the rib chord and rib height is fixed, which are the two main geometric properties required by the rib sizing tool. The rib sizing tool does not account for curvature of the wing skins, which will produce variation in rib height. For the purpose of the ribs sizing either a maximum,

minimum or mean rib height can be used for analysis, either of which is suitable but should be fixed for consistency.

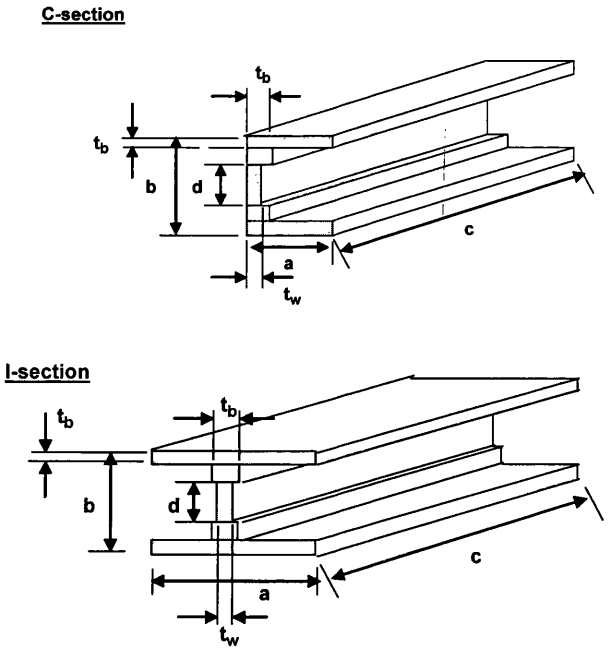

Figure 66 Schematics of Basic Rib Designs Used by the Sizing Tool

The rib chord 'c' and the rib height 'b' are defined as stated previously. The top and bottom flange length 'a' is defined by bolting requirements. For bolted joints a general design rule is applied. This is defined in terms of bolt edge distance 'D', which is defined by the bolt diameter. 1D would therefore be one times the diameter of the bolt, with the distance being defined from the bolt centre to the outer face of the component. Typically 2D is specified for metallic materials and a conservative 3D for composite materials. At this edge distance the only relevant failure mode is bearing, lower edge distances could result in varied failure modes known as shear out, bursting, net section failure etc. In summary as the bolt edge distance is driven by the bolt diameter the bolt size drives the flange width, with the bolt being sized to accept the loads applied to it. Once the flange width has been calculated, 'd' can be defined. Usually flange thickness is greater than web thickness at 'd' and it would therefore be necessary to ramp down to the lower thickness. This model does not take into account ramping effects which can vary from 1:10 or even >1:20, which are important from both stress concentration and manufacturing perspectives. For simplicity 'd' is therefore assumed to be:

$b-(2*a)=d$ For a C-section rib **(Equation 118)**

or

$$b-(2*\frac{a}{2})=d$$ For an I-Section rib **(Equation 119)**

Now the reference geometry has been defined the thickness of the web 't_w' and the thickness of the flange 't_b' can be defined using the appropriate stress methods.

The variables for each stress method now need defining within the tool. However this will be described along with a worked example of the calculation methods in section 5.1.4. Once the calculation variables are entered the sizing can be completed. As the tool is in Excel the calculations for the foot flange and rib web are sized automatically, however the stiffeners vary in that they require the use of a macro (a subroutine written in visual basic for Microsoft Excel). The macro manipulates geometry within the stiffener to optimise the thickness to reach a reserve factor (RF) of one. This macro is called a 'Goal Seek', an example of which follows:

```
---------------------------------------------------------------------------------------
Sub find_hw_C_sectionALCAS()
'
' find_hw_C_sectionALCAS Macro
' Macro recorded 16/09/2004 by RAdams1
'
Sheets("ribs calcs").Select
  Range("AJ49").GoalSeek Goal:=1, ChangingCell:=Range("Aa49")
   Range("Aj50").GoalSeek Goal:=1, ChangingCell:=Range("Aa50")
   Range("AJ51").GoalSeek Goal:=1, ChangingCell:=Range("Aa51") etc…
   ---------------------------------------------------------------------------
```

In the case shown the Range, defined as cell 'AJ', is equal to Ixx/Iu to achieve 1, by changing cell 'Aa', which is the web height 'hw' of the stiffener. Each line of code shown represents a different rib.

There can be many different stiffener geometries but the sizing tool focuses on the most simplistic case know as a 'T' Shape stiffener. Other stiffener designs can be more efficient, such as the integral stiffener, but a simplistic 'T'-shape design is considered to be a good baseline for reference during structural optimisation. A schematic of the 'T'-Shaped stiffener is shown in figure 67. As with the foot flange in the rib calculations the stiffener foot is sized by bolt edge distance requirements in exactly the same way. The

height of the web 'hw' and the thickness of the stiffener 'tf' are then calculated via the relevant sizing methods.

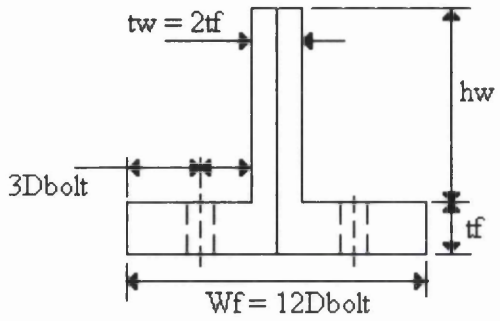

Figure 67 Schematic of 'T' Stiffener & Associated Geometry

5.1.3 Sizing Tool Outputs

The sizing tool output sheet can now be viewed to review component thicknesses and subsequent mass calculations based on the geometry previously described within this section. Figure 68 shows the sizing outputs for the foot flange calculations and the web sizing calculations. For the foot flange sizing to produce calculations thicknesses, 't_a' and 't_b', these can be referenced to calculations provided in section 3.10.1, in this instance thickness t_b is assumed to be the most realistic and less conservative. Web sizing is for stiffened and un-stiffened webs. Stiffened is the most efficient structure and produces the thinnest web thicknesses (note in figure 68 all thickness units are in mm). Shear of a plain panel is calculated based on shear loading in the rib, while the buckling calculation is driven by compressive (brazier loads), the highest thickness from these two calculations is considered to be the design driver and is dependent on the load case used. Note in figure 68 rib one is not show as this is a joint interface with the centre wingbox.

	FOOT FLANGE SIZING						WEB SIZING		
	Through Thickness Corner Radius CSM 20.4-15						Shear Plain Panel	ESDU 71005 Shear Buckling	
		C-SECTION		I-SECTION				UN-STIFFENED	STIFFENED
Rib No	Krt applied	Flange Thickness t_a	Flange Thickness t_b	t_a	t_b	Rib No	WEB Thickness t_w	WEB Thickness t_w	WEB Thickness t_w
2	1.30	27.41	19.25	14.90	12.00	2	8.47	17.14	6.78
3	1.30	18.67	14.25	9.72	8.29	3	3.62	12.21	4.93
4	1.30	26.04	18.01	14.07	11.24	4	2.98	10.32	4.65
5	1.30	27.23	18.26	14.79	11.58	5	1.05	6.57	3.32
6	1.30	24.09	16.48	12.91	10.25	6	1.13	6.11	3.46

Figure 68 Screenshot of Rib Foot Flange & Web Result Thicknesses

Figure 69 (again negating rib one as in figure 68) shows the stiffener resultants. The web height 'hw' is shown and the resultant mass of the stiffener. The resultant mass is calculated based on the geometry given in figure 67, but also includes the bolting requirements, taking into account standard bolt masses, which can be manually entered as a variable to represent an accurate selection of bolt in terms of size and material.

T' STIFFENER SIZING			
Stiffener Final Properties			
h_w	Stiffener Mass (kg)	Mass of Nuts and Bolts (kg)	Total Mass of Stiffener Assembly (kg)
116.22	22.251	0.138	22.389
64.90	8.052	0.122	8.174
48.98	5.157	0.114	5.271
26.23	2.758	0.106	2.863
21.65	1.944	0.097	2.042

Figure 69 Screenshot Showing T-Stiffener Outputs & Subsequent Masses

Based on the sizing data the rib mass can now be summarised based on geometry given in figures 66, 67 and 68 taking into account the density of the material that has been selected. The calculations include 4 rib configurations based on I & C rib designs, with and without the inclusion of stiffeners. A summary of these mass calculations are shown in figure 70 (negating rib one as in figure 68 and 69).

RIB CONFIGURATION MASS COMPARISON			
C Section Total Mass (kg)	C-Section Stiffened Total Mass (kg)	I-Section Total Mass (kg)	I-Section Stiffened Total Mass (kg)
172.40	201.63	146.46	175.69
126.11	169.53	106.71	150.13
66.23	60.82	53.92	48.51
50.89	46.77	42.39	38.26
30.46	27.82	25.09	22.45
19.77	18.08	16.64	14.95

Figure 70 Screenshot of Summary of Masses for Each Rib Design

The thicknesses produced via the sizing calculations can be manipulated into standard Airbus FE models. This will provide an initial set of thicknesses to be used for distribution of loads throughout the wingbox. Once the loads have been updated the sizing tool can then be used for a second iteration to improve the sizing results via refinement of the loads. This change in loading is material dependent. Stiffness varies depending on the material selection for each rib and as section thickness increases the stiffness of the component increases therefore causing a redistribution of the loads.

5.1.4 Calculation Methods Worked Examples

The following section provides a set of worked examples for each calculation method used to size the rib and stiffener thicknesses.

5.1.4.1 Foot Flange Sizing

A schematic of the foot flange sizing process is shown in figure 71. Geometry and loads for the sizing have been covered in section 5.1.2. However there are some variables that still need defining, which are specific to the calculation methods. Firstly there is bolting requirements. A bolt size should be chosen for each rib flange to skin attachment. Bolting requirements are generally driven by the loading that they have to bear between the skin and the rib through shear and tension. The size of the bolt is determined by the number of fasteners used in attachment of the cover to rib, with the global load being distributed amongst them. The rib sizing tool is not designed to size the bolts specifically but the calculations are relatively simplistic, with bolt size and material being varied to ensure the loads can be carried by the fasteners in the loading cases defined. In terms of foot flange sizing, assuming a constant load, the smallest bolt size will provide the smallest moment arm 'L' and therefore the lowest thickness.

Bolt edge distance then needs to be defined, bearing in mind the standard philosophy for composite and metallic structures. Finally the inner radius 'r' of the flange needs to be defined. Generally speaking a tight radius is preferable as it again limits the moment arm 'L', as Airbus can produce a radius of 5mm this has been set for every rib. A tighter radius tends to be hard to achieve due to manufacturing constraints.

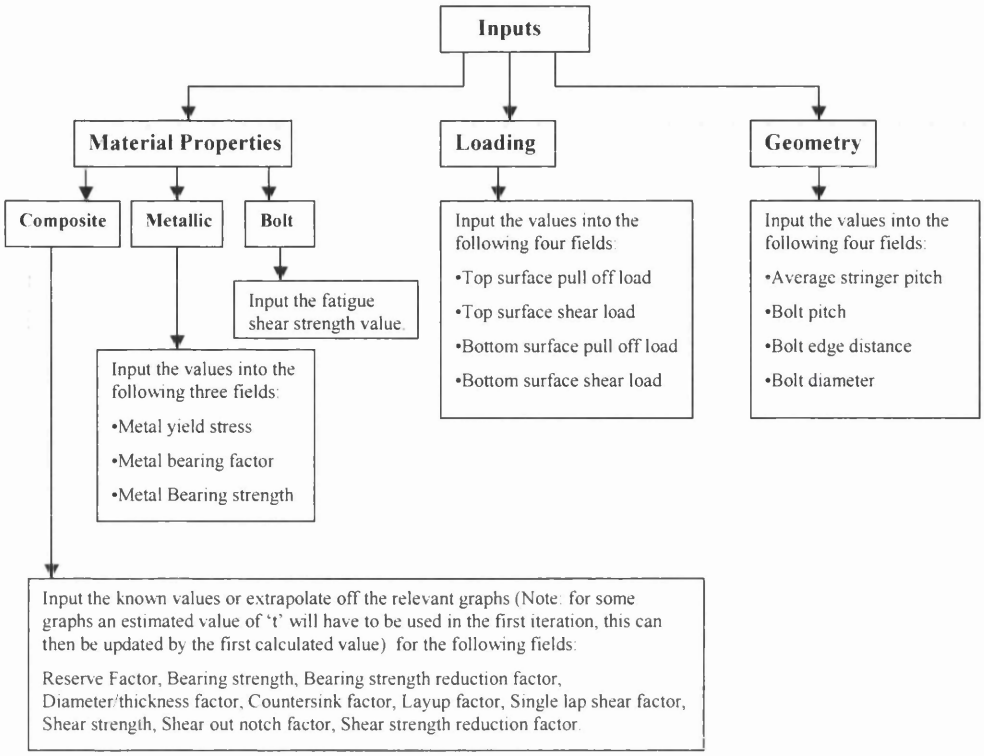

Figure 71 Schematic of Foot Flange Sizing Process

The additional inputs required for the foot flange calculations are shown in figure 71. The moment arm 'L' is then calculated from the centre of the fastener to the centre of the flange as shown in figure 72.

Bolt Edge D	Bolt Dia. (mm)	Rib No.	L (mm)	r (mm)
2	12	1	24	10
2	11.5	2	23	10
2	11	3	22	10
2	10.5	4	21	10

Figure 72 Screenshot Table of Inputs for Foot Flange Calculations

To show a worked example of the ribs sizing tool the initial values for material, geometry etc, will be used for rib one. This provides the following inputs for the calculations:

RF	(Reserve Factor)	=	1
f_{all}^{t}	(Allowable Tensile Strength)	=	49.7 MPa
L	(Moment Arm)	=	24mm
r	(radius)	=	10mm

k	(Thickness Compensation Factor)	=	1.3
Na	(Applied Tensile stress)	=	444.6 N/mm

112 is used to calculate the thickness discussed in section 3.10.4, 't'.

$$t = \frac{-\left(4r\frac{f_{all}{}^{t}}{RF} + 3k\ Na\right) \pm \sqrt{\left(4r\frac{f_{all}{}^{t}}{RF} + 3k\ Na\right)^2 + 48\frac{f_{all}}{RF}k\ NaL}}{\frac{f_{all}{}^{t}}{RF}} \qquad \textbf{(Equation 112)}$$

This gives for a C-Section Spar:

$$t = \frac{-\left(4*10\frac{49.7}{1} + 3*1.3\ *444.6\right) \pm \sqrt{\left(4*10\frac{49.7}{1} + 3*1.3\ *444.6\right)^2 + 48\frac{49.7}{1}*1.3\ 444.6*24}}{\frac{49.7}{1}}$$

t =14.9mm

5.1.4.2 Web Sizing

For composite web sizing all variables have been covered by section 5.1.2. The web is driven by Shear Buckling. The equations required are provided in the literature review corresponding to equation 104, 107 respectively. The following example again utilises Rib 2. The variables required are as follows:

For Shear Plain Panel Buckling:

q	(Max Applied Shear Flow)	=	1781.95 (N/mm)
RF	(Reserve Factor)	=	1
G_{xy}	(Laminate Shear Modulus)	=	26282.86 (N/mm^2)
γ_{xy}	(Shear Strain)	=	0.0008

For Shear Buckling (ESDU):

qbe	(Elastic Shear at which plate will Buckle)	=	1781.95 (N/mm)
b	(Web Width)	=	798.9 (mm)
K	(Young Modulus)	=	8.6 (N/mm^2)
E	(Shear Modulus)	=	26282.26 (N/mm^2)

A worked example for the first method, equation 104 (see section 3.10.2), is as follows:

$$t = \frac{qRF}{G_{xy}\gamma_{xy}}$$ **(Equation 104)**

Gives:

$$t = \frac{1781.95 * 1}{26282.86 * 0.0008} = 84.7mm$$

5.1.4.3 Stiffener Sizing

Stiffeners are sized using Brazier loads. In all cases in the sizing tool it is assumed that the stiffeners bear all of the Brazier loading and that no load is carried by the rib webs. This is of course an untrue statement, as load will be transferred to the webs as well as the stiffener. This approach can therefore be said to be conservative as the stiffeners, assumed to carry the entire load will be slightly over-engineered. Again for the purpose of this project it is not necessary to produce accurate sizing data, but to simply quantify the effects of mechanical property degradation brought about by the in-service environment.

As previously described, stiffeners have their own material property inputs. The lay-up in the stiffeners can be optimised in a similar way to the ribs. The stiffeners are driven by the tension and compression properties of the material as well as material modulus. The calculations considered to be the most critical design drivers are considered to be 'Effective Panel Breaker Analysis', 'Column Stability', 'Compressive Strength Analysis' and 'Tension Strength Analysis'. The EMOC project failed to generate compressive modulus for both 0° & 90° orientations, with only 90° strength being generated. Therefore the stiffener material properties shall be fixed and unchanged and hence the calculation methods have not been described in detail.

5.1.5 Rib Sizing Tool Iterations

The ribs sizing tool is used here to determine the difference on a component design between HOT/WET and RT/DRY material properties. This quantifies the weight penalty brought about by the use of HOT/WET material properties. Material properties used by

the sizing tool are from the Airbus material library. The Key Properties used in both of these cases are summarised in table 18. 'Ex' (Laminate Compressive Stiffness) & 'Gxy' (Laminate Shear modulus) values are calculated by the sizing tool from the basic lamina properties for the chosen material using the Hart-Smith 10% rule for calculating properties based on percentage fibres in each direction. The shear strain allowable is the shear stiffness of the material multiplied by a strain limit, in this case 4500με, which allows for damage tolerance. The lay-up for these shear webs is 10/80/10 where a high proportion of ±45° plies has been utilised to resist shear best, which is the dominate loading mode that the rib experiences.

Table 18 Properties Used for Rib sizing Calculations from Existing Airbus Data

Material Property	RT/DRY	HOT/WET
-Ex (N/mm^2)	24113.7	23929.6
Gxy (N/mm^2)	26282.8	25393
F_{22T} (MPa)	49.7	18.2
Density (kg/m^3)	1650	1650
Shear Strain limit (με)	4500	4500
Shear Strength Alowable (MPa)	118.27	114.27
Laminate Lay-up	10/80/10	10/80/10

A table showing the rib loads is shown in Appendix A table A.1, with a schematic of how these loads act on the rib shown in figure 45.

Using the EMOC modelling tool ELAP with the Rib Sizing Tool was considered, however it soon became apparent that the rib sizing tool and the EMOC principles would not be compatible for a number of reasons. Firstly, much of each rib is made up of a relatively thin shear web (typically less than 6mm) and it would therefore be difficult to quantify significant weight savings. Secondly the corner radius calculation for the foot flange is governed by the through-thickness strength of the laminate, denoted by F_{22t} in the ribs sizing tool. This is the 90° Tensile strength property of a ply and unless it is possible to predict the exact point through the thickness that the flange typically fails it would not be possible to look at the knock-down on this property at that point. Furthermore significant work would be required to marry the EMOC tool to the rib sizing tool, because it would be necessary to construct an exact lay-up for a given thickness, adjust for temperature and moisture absorption and then re-run the model until a final solution was converged on. Without extensive development of the tools it is not possible to do this. The applicability to ribs is therefore limited to the heavily loaded ribs, where only a small weight saving may be realised. It was therefore decided not to

continue developing this tool to offer weight savings within this programme of work. Despite this, the new modelling approach may still be assessed using more appropriate design scenarios.

5.2 Assessment of Benefits

Two component case studies were chosen to validate the new modelling approach, allow the further development of the model and evaluation of the theory used to validate component strengths. The two components chosen were a lug and an L-section. These components were to be manufactured both in two different sizes, and in the two different materials studied in this project. The geometry and size of both components had been tested by Airbus before for un-conditioned specimens, with the previous purpose of stress method development.

The lug was selected because it would typically represent a thick composite component found within the wingbox (12mm or greater), where uses include landing gear and pylon attachment structure. The high load inputs transmitted at these attachments results in a thick structure. As previously stated, these thick structures are then designed using HOT/WET properties.

The L-sections represent typical bolted joint design for both Wingbox Ribs & Spars. The stress method used to calculate these in the ribs sizing tool is discussed in section 3.10. Providing some actual tests data allows accurate sizing of a Rib flange to help assess weight savings for a realistic aircraft structure.

5.2.1 Stress Method Approach

The stress method approach being described here is to be utilised by the EMOC ELAP (Environmental Laminate Analysis Programme) modelling tool, which has been coded by a Swansea University Research Assistant (Dr Robert Walden-Bevan), under the instruction of the author.

The stress method approaches have all been conceived by the author. The approach for assessing the components is based on ascertaining the basic mechanical properties of the laminate from basic UD properties. These properties originate from the EMOC test programme discussed in section 5.7. At this point there are two ways

to proceed, one using simplistic plate theory, where simple analytical methods can be used to evaluate the components performance, or secondly the full 3D Finite Element solution. The work described here is using the more simplistic approach, integrated with the developed ELAP model to accurately model moisture levels within the structure, assignment of realistic mechanical properties based on this environmental history and the use of classical laminate theory (section 2.1.8). The second approach is the ultimate goal and is set to continue past this project. In this case moisture gradients and mechanical properties are completely modelled in 3D. A full orthotropic mechanical FE model is used to predict the failure of components. Further research is required to validate the methods used in running the failure model, which again utilises the theory discussed in section 2.11.2. The procedures stated here are also to be applied to the Rib sizing tool described in section 5.1.

The method can be broken down into a number of simple steps:

- Generation of Mechanical Property (basic UD lamina properties) in the HOT/WET condition to ascertain starting thickness.
- Definition of Lay-up & derivation of laminate properties from classical laminate theory.
- Pre-sizing to determine thickness requirements.
- Environmental Model (1D simulation), run to determine through thickness moisture distribution.
- Mechanical properties assigned to each ply through the thickness dependent on moisture level (not for a fixed operating temperature).
- Classical laminate theory used to derive new mechanical properties (ultimate strengths used in this procedure).
- Post simulation sizing to determine new component thickness.
- Iterate until solution convergence to within 1 ply.

It should be noted for aircraft design it is necessary to be conservative and it would therefore normally be standard practice to use the first ply failure strengths, instead of ultimate laminate failure strengths. However, in this instance ultimate failure strength is deliberately chosen to attempt to get a good correlation to actual tests.

Using the methodology described, the ELAP modelling tool firstly predicts moisture distribution for a predefined laminate thickness, based on the 'Wet Aging Tool'

principles described in section 2.12.6. It then assigns ply-by-ply lamina material properties from the EMOC database and then uses laminate theory to derive laminate properties. These properties can then be used to carry out structural sizing, which can then be re-run through the model with the new thickness to ensure that a thickness can be converged on for a component. The ELAP modelling tool is a 1D simulation for the prediction of laminate properties, with a 3D FE version of the tool in development, which is not available within the timescales of this project.

5.2.1.1 Lug Analysis Case Study

Lug geometry was defined from existing Airbus stress development data for lugs [75,76]. The work carried out in the references highlighted inaccuracies with the stress calculations for shear-out and net section failure modes. The reports offered a test factor to account for the inaccuracies in the calculation methods. If the lug fails in net section the material around the outer edge of the lug is too thick. Net section is dependent on the tensile properties of the materials, which from the supporting work do not change as moisture ingresses into the structure. If the material around the edge of the lug is optimised the critical design driver becomes shear-out failure. Shear out failure is directly related to the in-plane shear performance of the material, which is directly affected by moisture ingress into the structure. The previous lug test geometry is shown in figure 73.

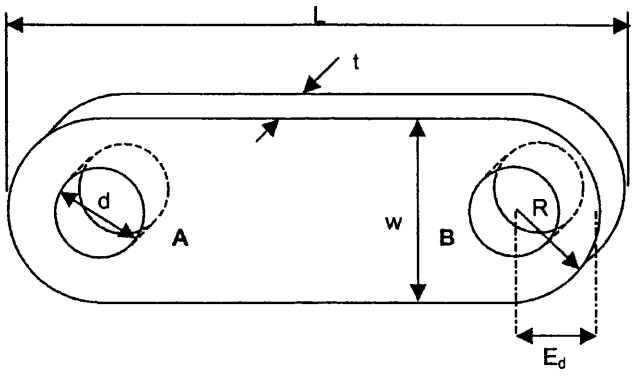

Figure 73 Airbus Lug Tests Previous Work [75]

Taking into account the previous discussion points the author decided to modify the lug geometry to ensure the probability of a predictable shear-out failure. For the previous lug tests a width (w) of twice the hole diameter was used. Although a shear-out failure was initially predicted a net-section failure was evident during the test. To prevent this the author changed the width to three times the hole diameter, to ensure a larger area

to distribute the tensile load applied to the lug and thus reduce the stress concentration, associated with this failure mode. The new lug geometry is shown in figure 74.

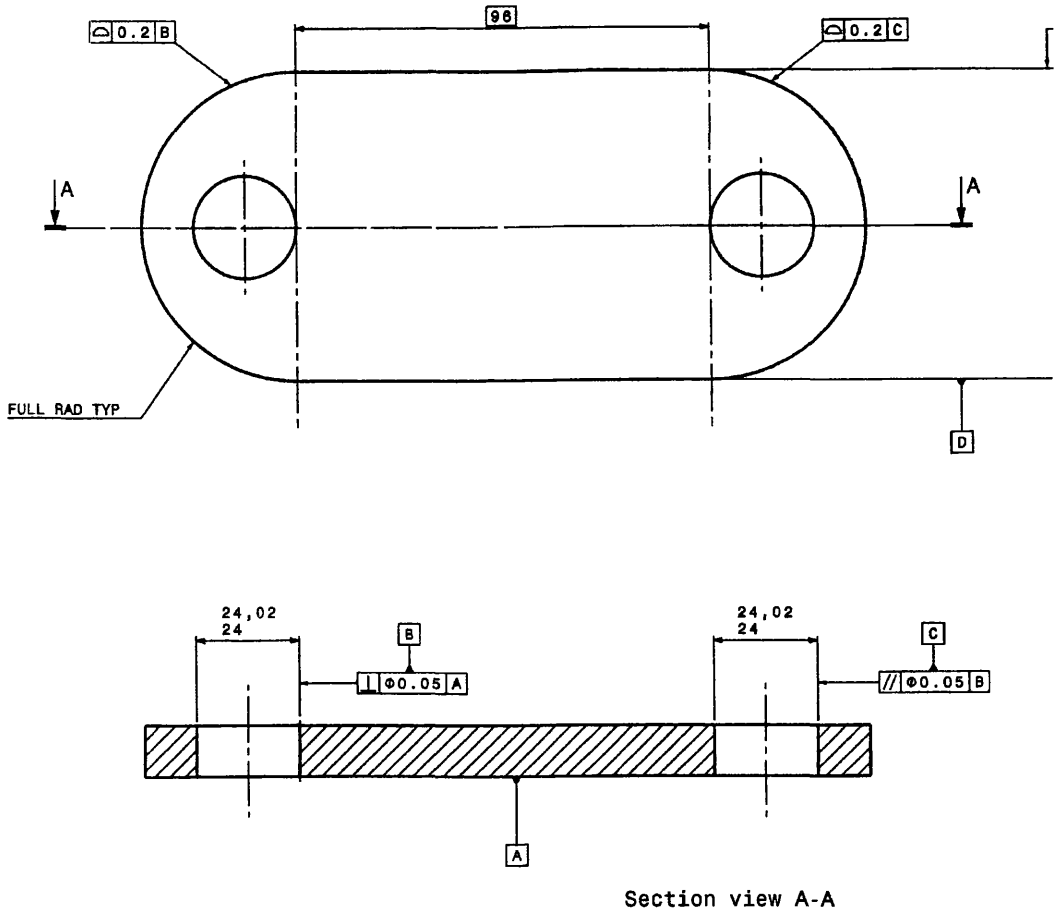

Figure 74 Modified Lug Test Coupon Geometry to Ensure Predicted Shear-Out Failure

Two thicknesses were chosen for investigation, 12mm & 26mm, both of which had been previously tested. Two materials would be used for the test, M21/T800 & 977-2 /HTS. The purpose of two different materials is to allow the model to be validated for different resin systems and different fibre types. For the purpose of this project only the 977-2 material will be considered because the basic mechanical properties required for stress calculations were not available for the M21 material. In line with the previous test programme the laminate was quasi-isotropic in the in-plane direction, where in plane is the loading direction applied to the lugs. As can be seen from the figures both lug designs feature a double lug. Stress in, is equal to stress out and therefore the lug end

that fails cannot be ascertained without detailed measurements of lug geometry and the knowledge of any impurities/defects within the material.

A schematic of the basic test arrangement is shown in figure 75.

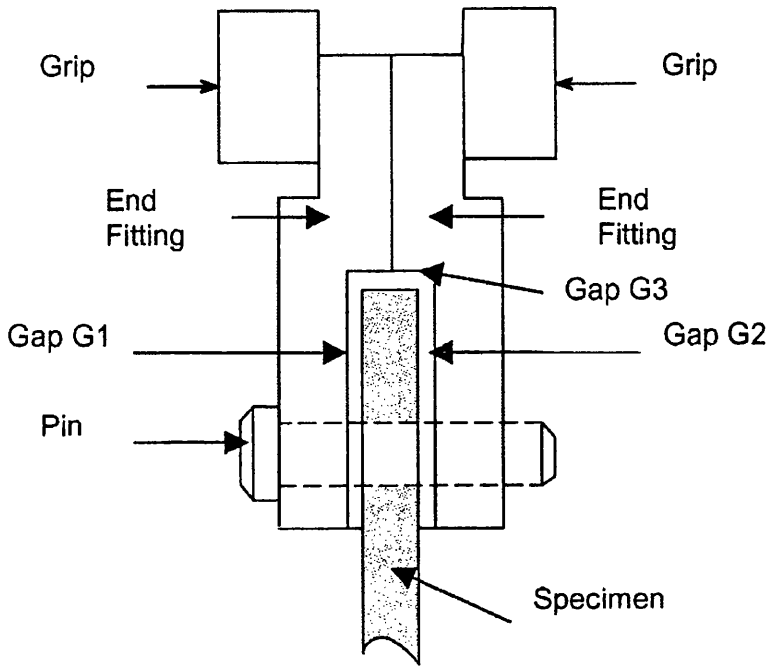

Figure 75 General Arrangement of Lug Test Rig

5.2.1.2 Lug Test Matrix & Procedure

Table 19, provides a summary of the lugs that were proposed by the author for testing. Due to budget constraints it was decided that only 1 batch of the thicker 26mm lug would be tested. In all instances a batch of 6 of each test condition were proposed to provide confidence in the results and where possible the small sample size could be then used to calculate B-values. The aim was for both dry samples and conditioned samples to quantify the strength reduction and allow comparison to be made to the modelling approach. All specimens followed the procedure for environmental control, as stated in section 5.5. The lugs that were to be tested in the dry state were stored in a dessicator, however to ensure that they were in a completely dry state the lugs were dried in an oven prior to testing. Due to the weight of the lugs it was not possible to monitor any weight loss, due to the accuracy of the available balances. Conditioned coupons were placed in the humidity chamber for 1000 hours at 70°C 85% RH. A 1%

tolerance was placed on the conditioning time, which allowed a test window of 10 hours. Note notation for lay-up indicated quasi-isotropic [0°/±45°/90°].

Table 19 Summary of Lug Specimens & Test Parameters

Lug Thickness (mm)	Condition		Time Conditioning (Hours)	Test Temperature (°C)	Material	Lay-Up	No. Coupons Tested	Total Tested
	Temperature (°C)	Humidity (%RH)						
12mm	70	0	Until Dry	20	977-2 HTS	25/50/25	6	24
12mm				90	977-2 HTS	25/50/25	6	
12mm	70	85	1000	20	977-2 HTS	25/50/25	6	
12mm				90	977-2 HTS	25/50/25	6	
26mm	70	85	1000	90	977-2 HTS	25/50/25	6	6

Displacement transducers (LVDTs) were requested; however the operating temperature of 90°C was outside the limit of the LVDTs available and for these tests load frame cross head displacement was used to measure displacement during testing. A calibrated load cell was used for all tests. One specimen of each batch was strain gauged to record localised strains around the hole at different points relative to the respective failure modes of shear out and net section failure. A schematic of the strain gauge locations on each coupon is shown in figure 76. A total of 8 uniaxial gauges and 4 rosette gauges were required per gauged lug.

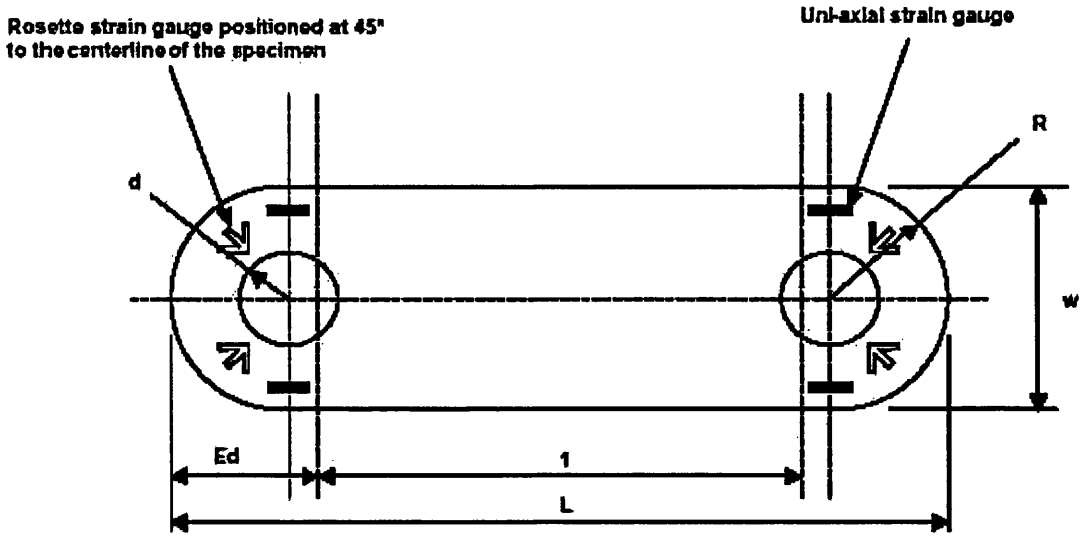

Figure 76 Schematic of Lug strain Gauge Locations

To achieve a test temperature of 90°C, it was necessary to fabricate an environmental heater box. This box was made from plywood and lagged with a readily available foam material to provide adequate insulation. The inside of the box was lined with two layers of vacuum bag breather material, which could withstand temperatures up to 200°C. On

top of the vacuum bag breather was placed a coating of tin foil to aid heat reflection, followed by a layer of plastic bag film to hold all of the materials in place. An inlet and an exhaust port were incorporated into the box design to allow thermal control equipment to circulate the air within the environmental box, which would heat up and maintain the required test temperature of 90°C. On testing the box it was found that a third port was necessary for a controllable temperature heat gun. This supplemental heat was required because of the large test fixture mass. Without the heat gun it would have taken a large amount of time to reach the desired test temperature that would have led to significant drying of the test piece. To aid with rapid heat up coupons were left in the chamber or drying oven until the very last minute to retain their heat as much as possible, thereby reducing the time required to reach the test temperature. This allowed even the 26mm lug to reach test temperature within 15 minutes of being loaded into the test rig. The general arrangement of the lug test, with environmental box around the specimen and test frame is shown in figure 77.

Figure 77 Showing General Test Arrangement of Lug Test, Note Heater Gun Port

The overall test sequence for the testing of the lugs was as follows:

- Specimen measurements and weights were determined before conditioning/ drying.

- Specimens were conditioned for 1000 hours, with specimen introduction into the environmental chamber being staggered accordingly to ensure consistency with conditioning to within 1% of the overall conditioning time.
- Second measurement of lug weight prior to testing.
- Where applicable gauging of specimens was carried out, allowing a maximum of 1 hour to apply gauges, once the 1000 hour conditioning had been completed. Once gauged, specimens were placed back in the environmental chamber until the point at which the test was to commence to ensure as close to 90°C was maintained and to aid with heat up time in the heater box on the test rig.
- Specimens were loaded directly from environmental chamber/drying oven into the test fixture and where applicable gauge wires attached to logging hardware using quick release connectors.
- A thermocouple was attached to the specimen surface and insulated from any direct heat source, with another thermocouple being used by the equipment to monitor air temperature.
- Once the thermocouple monitoring the lug reached 90°C, load introduction was started. In reality it was found that with all 90°C lug tests it was only possibly to maintain temperature to within ±5° of 90°C.
- Specimens were loaded until a significant drop in load was exhibited on the real time load displacement plot, being generated by the logging software. Loading was continued until no further increase in load after first failure was exhibited by the specimen.

5.2.1.3 Initial Lug Predictions Using a Manual Analytical Approach

Using the method described in section 5.2.1 it was necessary to predict that in principle the EMOC modelling approach would be successful, before the full modelling tool was available. The approach discussed here is time intensive and has essentially been carried out by hand.

To define the predicted requirements for the test it was necessary to derive an approximate load required to break the specimen, this in turn defining the load frame capacity required to fail the specimen. Initial predictions were carried out using the strongest mechanical properties, which would represent a lug in a dry state, tested at room temperature. This would then provide a baseline for future predictions using the

new stress method approach defined in 5.3.1. Along with this prediction of load, it was also necessary to check the failure modes and as described in 5.2.1.1 to ensure a consistent failure mechanism. This shall be called STEP 1.

Once the maximum load was predicted, a second iteration was required to define the weakest condition, namely HOT/WET tested at room temperature (STEP 2). In both the RT/DRY (STEP 1) & HOT/WET conditions, uniform through thickness properties are assumed. The use of laminate theory therefore defines the material properties. These two iterations provide the upper and lower load limits of the lug, i.e. the weakest and strongest point. A third step (STEP 3) is then carried out where the material properties are substituted from the supporting PhD with Airbus existing properties, which also take into account testing at elevated temperature (90°C).

STEP 4 then applies EMOC properties, which are generated from the same batch of material as the actual lugs to be tested.

The fifth iteration is to apply the new stress approach (STEP 5/6). Step 5 is a more conservative approximation assuming a B-basis knock down on strength of 0.8 and step 6 assumes no knock down on material properties. The sensitivity and accuracy of this stress approach will rely on the accurate derivation of mechanical properties for that laminate. Using the ELAP 1D tool, it is possible to discretise the material through the thickness at a ply level, therefore deriving material properties for each ply, before running classical laminate theory to ascertain the mechanical properties of the laminate. The thin lug has 48 plies (equating to 12.192mm theoretical thickness, using a cure ply thickness of 0.254) through the thickness and by hand it would take many iterations to define the properties for laminate theory to be used. It was therefore decided to run two iterations discretising the through thickness properties of the plies into 3 and 5 discrete elements through the thickness respectively.

Before STEPS 5 & 6 could be run, it is necessary to derive a through thickness moisture distribution. In this case the Airbus 'Wet Aging' Software was used (see section 2.12.6), to show a 1D through thickness moisture distribution. The conditioning cycle used was 1000 hours at 70°C 85%RH, which is considered to be the same as an aircraft lifecycle (25 years at 20°C 85% RH). An example of the resultant output for the 12mm lug is shown in figure 78.

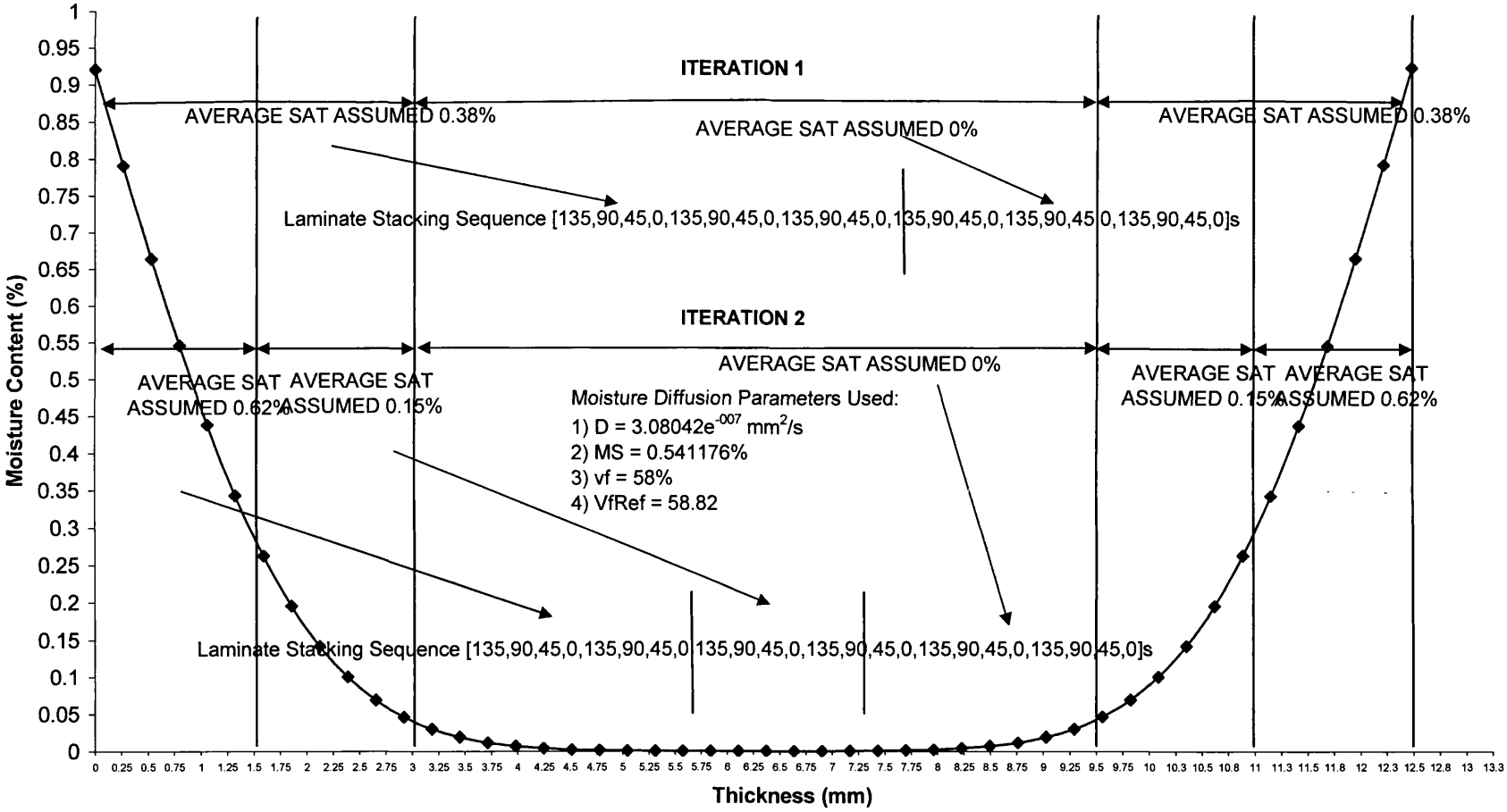

Figure 78 12mm Through-thickness Moisture Distribution

The graph shows the values used to derive the moisture content when running the Wet Ageing software. For both iterations the laminate stacking sequence is the same. On both iterations the average saturation for each discrete element through the thickness has been calculated and is shown on the graph.

Once the through thickness mechanical properties have been assigned for each ply, the properties can be put into classical laminate theory. In this instance LAP (laminate analysis programme) was used for all laminate property calculations, the tool being based on theory described in section 2.11.2. In this case the max stress failure criterion was used, because the default Airbus method, which is Hoffman, is insensitive to changes in shear properties. Further iterations were added to assess the sizing methods sensitivity to changes in stiffness, which confirmed the methods were insensitive to changes in the stiffness properties of the material, degraded by moisture content.

A further two steps (STEP 7 & 8) were then carried out, one assuming the B-basis knock down and the other without, to predict room temperature mechanical properties using EMOC data. Step 9 was then carried out using an FE approach to model the lug failure, followed by a final iteration, where the diffusion values were used from EMOC data. A summary of all iterations is shown in table 20, for each step a number of iterations were carried out:

Table 20 Pre-Test Predictions of Lug Performance for Each Step

STEP 1 Room Temp Test Using Dry Material	Basic Calculations Assuming Kso of 1, Stiffness derived from B-basis
	Modified Using Jo Ryan's Stiffness -negligible change
	Kso modified to 2 & 0.8 B-basis value applied to shear strength
	Reduced load to achieve RF of 1
	Width increased from 2D to 3D to prevent Net Section
	Modified from test to reduce RF for net section to confirm shear out failure
STEP 2 Room Temp Test Using Fully Saturated Material (Jo Ryan's supporting thesis)	Basic Calculations Kso of 1 stiffness from B-basis
	Modifies Using Jo Ryan's Stiffness -negligible change
	Kso modified to 2 0.8 B-basis added to shear strength
	Reduced load to achieve RF of 1
	Modified Load to achieve RF of 1
	2D pitch changed to 3D to prevent net section
	Modified from test to reduce RF for net section to confirm shear out failure
STEP 3 HOT/WET Wet Material Tested at 90C/ Saturated (Airbus Design Data, to be replaced with EMOC data)	All properties re-defined
	Kso modified to 2 0.8 B-basis added to shear strength
	Reduced load to achieve RF of 1 for net section
	Modified Load to achieve RF of 1 for shear out
	2D pitch changed to 3D to prevent net section
	Modified from test to reduce RF for net section to confirm shear out failure
STEP 4 HOT/WET Wet Material Tested at 90C/ Saturated, EMOC Mechanical Property Data	HOT/WET 95%RH 90C Using EMOC Data with no test factor applied.
	HOT/WET 95%RH 90C Using EMOC Data with test factor reducing net section RF
STEP 5 HOT/WET Modelling Approach	**With** 0.8 B-Basis Knock Down Using MAX STRAIN CRITERION AND EMOC DATA
STEP 6 HOT/WET Modelling Approach	**Without** 0.8 B-Basis Knock Down Using MAX STRAIN CRITERION AND EMOC DATA
STEP 7 RT DRY	
STEP 8 RT DRY	AS ABOVE BUT ASSUMING B-basis value of 0.8
STEP 9 FE	FE Model: increasing load until elements fail 88.1KN is Net Section Failure
STEP 10 New Moisture Profile from EMOC Diffusion Data & EMOC Mechanical Properties	Latest Iteration Using Swansea Produced Through Thickness curve

The sizing, as previously mentioned, was for shear-out and net-section failures, and however due to the change in geometry a check on the bearing capability was made on the lug to ensure that the bearing strength of the material was not exceeded. This was necessary as to date there is no bearing strength data available from the complimentary work. Should bearing data become available and prove to be sensitive to moisture distribution it would be possible to carry out an accurate bearing analysis in the same way. The calculation methods used are defined by [65,76,77].

5.2.1.4 Shear-Out Analysis

For shear out analysis the shear strength of the material is first required 'fs', which is derived from laminate theory, using the 'max stress' failure criteria discussed earlier in this section. This shear strength is equivalent to 'Gxy', in classical laminate theory notation (MPa). In current practice there is an environmental knock down factor used, known as 'C_{ssr}', which accounts for moisture, assuming full saturation. Furthermore there is also a shear out notch factor, 'K_{so}' which is related to the percentage of ±45-degree plies in the laminate. Both of these factors are based on carpet plots, derived from extensive test data, noting that this test data is not generated from the same material as this project, although it does come from the same Airbus specification and therefore can be considered applicable. The required geometry is shown in figure 79, essentially the hole diameter 'd' (mm), thickness 't' (mm) and the edge distance 'e'' (mm) is required.

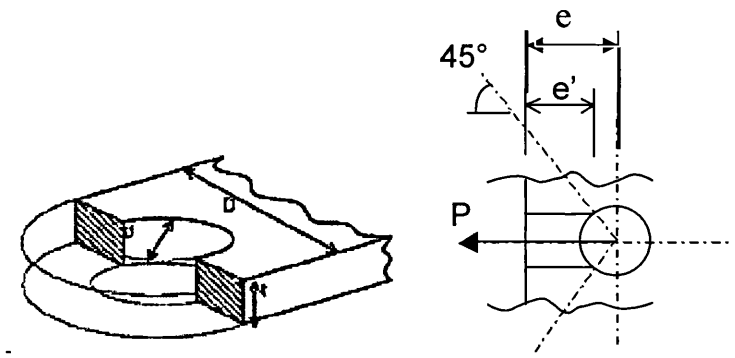

Figure 79: Geometry for Shear-Out Calculations [76]

Firstly it is necessary to calculate the effective edge distance 'e'' because the calculation method assume that the load acts at 45° off axis of the load around the hole, as shown in figure 79. e' is determined by equation 120:

$$e' = e - (d/2)\cos\left(45\frac{\pi}{180}\right) \qquad \textbf{(Equation 120)}$$

Once 'e'' has been determined the area by which the load is applied can be calculated known as 'A_s', given by equation 121:

$$A_s = 2 \cdot e' \cdot t \qquad \textbf{(Equation 121)}$$

The applied shear stress, 'τ' (MPa) can then be calculated, for an applied load (kN), as shown in equation 122. Furthermore it is necessary to calculate an allowable for the shear strength. The allowable shear strength is ascertained from the shear strength of the material, taking into account the notch and shear strength reduction factors, previously determined. This provides the allowable strength 'f_{sal}' (MPa) shown by equation 123:

$$\tau = \frac{P}{A_s} \qquad \textbf{(Equation 122)}$$

$$f_{sal} = \frac{f_s \cdot C_{ssr}}{K_{so}} \qquad \textbf{(Equation 123)}$$

Finally the shear out reserve factor, 'RF' for a given load can be calculated using equation 124:

$$RF = \frac{f_{sal}}{\tau} \leq 1.0 \qquad \textbf{(Equation 124)}$$

In this instance we are not evaluating the load carrying capability of a material for a known load, we are attempting to assess the load carrying of a material of fixed geometry and varying mechanical properties. The criteria to determine failure is firstly to change the material properties to the desired value based on the laminate theory results and then change the load accordingly until an RF of 1 is achieved.

5.2.1.5 Net Section Failure

The key geometric properties with this failure mode are illustrated in figure 79 and are the width of the lug 'D' (mm), the thickness of the lug 't' (mm) and the diameter of the hole 'd' (mm). In this instance the laminate tensile strength from lap is required 'Nx' (MPa), which shall be known as 'f_{tb}', which is typically a B-basis value or in the absence of B-basis data a factor of the full strength from laminate theory times 0.8. As there is a hole in the laminate it is necessary to determine from carpet plots [78] a stress

concentration factor, 'k_{tlh}', which is based on D/d and the number of 0° plies in the laminate. A further strength reduction factor is required accounting for the degradation of mechanical performance due to moisture, which in this case shall be set to 1 (as it is not required using the new approach). Firstly, the net section stress is calculated, using equation 125, where P is load (kN):

$$\sigma_{ns} = \frac{P}{(D-d)\cdot t} \qquad \textbf{(Equation 125)}$$

To calculate the allowable strength it is necessary to determine the theoretical notch factor, which takes into account that laminate stiffness in 'E_{xx}', 'G_{xy}' & 'E_{yy}' directions (GPa). The Poisson's ratio relative to the 'x' & 'y' direction is also required known as 'ν_{xy}'. The theoretical notch-factor is given from equation 126:

$$K_{E1} = 1 + \sqrt{2\cdot\left(\sqrt{\frac{E_x}{E_y}} - \upsilon_{xy}\right) + \frac{E_x}{G_{xy}}} \qquad \textbf{(Equation 126)}$$

This derived notch-factor can then be combined with the stress correction factor the applied stress and the hole-size correction factor, 'C_{hs}' to give the allowable stress as shown in equation 127:

$$\sigma_{\max 1} = C_{hs}\cdot\frac{K_{tlh}\cdot K_{E1}\cdot\sigma_{ns}}{K_{E1}} \qquad \textbf{(Equation 127)}$$

The reserve factor can now be calculated using equation 128:

$$RF_{ns} = \frac{f_{th}}{\sigma_{\max 1}} \qquad \textbf{(Equation 128)}$$

5.2.1.6 Bearing RF Check

The bearing strength of the material is directly defined from section 2.9.4 and in this instance the value was taken from bearing tests calculated by a supporting MRes

project [74] and shall be assumed for all calculations to be 737MPa, which shall be known as 'f_{bru}'. Induced bearing strength can be calculated by equation 129:

$$\sigma_{br} = \frac{P}{D \cdot t} \qquad \textbf{(Equation 129)}$$

Where 'P' is applied load (kN), 'D' is the hole diameter (mm) and 't' the thickness (mm). As with the other two calculation methods there a number of applied correction factors, to take into account. The Bearing strength reduction factor 'C_{bsr}' is related to the presence of moisture and shall therefore be set to 1. The diameter/thickness factor 'C_{dt}' equates to 2 for both the 26mm and 12mm thick lugs. The countersink correction factor 'C_{csk}' is set to 1 as there is no countersink fastener in use. The Lay-up factor 'C_{layup}' is based on the percentage of ±45° plies in the laminate, which for this quasi-isotropic laminate equates to 1. Finally there is the single lap shear factor, 'C_{sls}', which has been set to 1, as the lugs represent a double lap shear joint. These factors are brought together to determine and allowable bearing strength, as shown in equation 130:

$$f_{bral} = f_{bru} \cdot C_{bsr} \cdot C_{dt} \cdot C_{csk} \cdot C_{layup} \cdot C_{SLS} \qquad \textbf{(Equation 130)}$$

Finally the bearing reserve factor can be calculated by equation 131:

$$RF = \frac{f_{bral}}{\sigma_{br}} \qquad \textbf{(Equation 131)}$$

The bearing calculation here was simply a check that was performed before fixing the geometry of both lugs and in terms of changes in properties the bearing strength was significantly higher than the other two failure modes (≥2).

An iteration (STEP 9) was carried out using FE to predict the lug performance. Altair Hyperworks was the software package used. The model created was an elastic linear model, using shell elements. Material properties were derived from LAP as with the previous iteration for both room temperature and dry mechanical properties. 2D shell

models are typically used for analysis of aero structures in composites. It should be noted that for the purpose of this analysis the material properties entered into the 2D shell model, would not account for individual ply performance during loading. Furthermore the 2D modelling approach does not account for the inter-laminar performance of the material. Finally, it is not possible to predict the ultimate failure of the lug using this method, as the use of a single material property does not allow progressive failure to be modelled.

The lug geometry was imported from Catia V5. The geometry was then split so that only one side of the lug would be modelled. When splitting the geometry care was taken to ensure that the lug hole was significantly away from the cut geometry to ensure that there were no significant edge effects, which may have become significant during loading. The load is then applied via an RBE 3 element. This element is a multi-noded element with one dependent node and a variable number of independent nodes. Each node contains a coefficient (weighting factor) and a set of user-defined degrees of freedom. In this instance the model is constrained for translation in x, y and z directions but allowed to rotate, thereby replicating reality by not allowing linear movement and thus tracking load into the elements at the point of introduction. Once the model was set up, the load was increased until elements begin to failure around the load introduction points. Failure was considered to be at a point where the stress exceeded the allowable stress derived from the LAP calculations. Although the ultimate failure strengths were assumed, when modelling in FE, this 2D simple model is not a progressive failure model and thus unable to simulate ultimate strength.

A screen shot of the constrained lug, with applied loading is shown in figure 80.

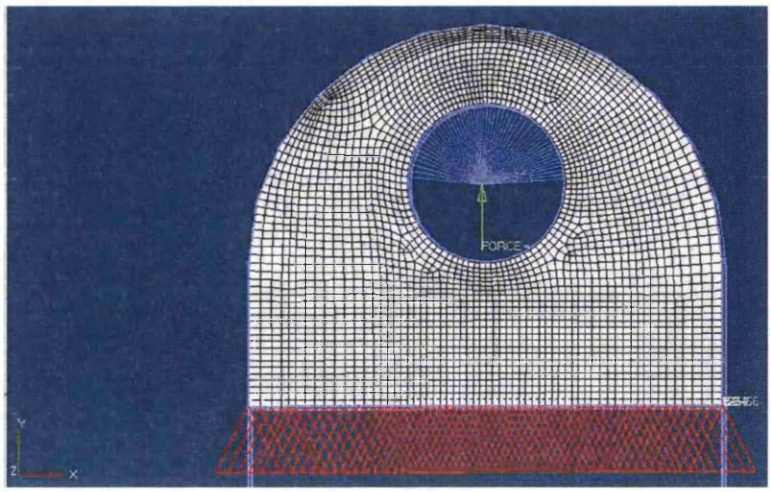

Figure 80 Showing the Lug FE Model: Constraints are shown at the bottom of the figure with the load introduction via a node at the centre of the hole

A final Iteration was carried out in line with STEPS 7 and 8 using a new moisture profile (see results section), which used moisture parameters from Swansea University.

5.3 ELAP 1D Model Validation against Laminate Analysis Programme (LAP)

The ELAP model is based on the principles defined in 4.3 and the creation of a new analysis is relatively simple. As with lamina failure criterion, a variety of laminate failure analysis methods have been proposed. Following is a brief description of each methodology:

5.3.1 Ply-by-ply Discount Method

This is a common method for laminate failure analysis. The laminate is treated as a homogeneous material and is analyzed with a lamina failure criterion at a mechanistic level. Laminated plate theory is used to initially calculate the state of stress and strain in each ply given the global loading situation and the material's elastic and strength properties. A lamina failure criterion is then used to determine the particular ply which will fail first and the mode of that failure. A stiffness reduction model is used to reduce the stiffness of the laminate, due to that individual ply failure. The laminate with reduced stiffness is again analysed for stresses and strains. Lamina failure criterion predicts the next ply failure and laminate stiffness is accordingly reduced again. This cycle continues until ultimate laminate failure is reached.

There have been a number of definitions proposed on how to determine ultimate laminate failure. One common way is to assume ultimate laminate failure when fibre breakage occurs in any ply. Another way is to check if excessive strains occur (i.e., a singular laminate stiffness matrix). Matrix-dominated laminates such as $[\pm 45]_s$ may fail without fibre breakage. Others have suggested a "last ply" definition in which the laminate is considered failed if every ply has been damaged. For this comparison, the laminate is loaded until fibre breakage occurs in any ply, unless the reduced stiffness matrix is singular which denotes a matrix dominated ultimate failure.

5.3.2 Sudden Failure Method

In highly fibre-dominated composite laminates, the laminate stiffness reduction due to progressive matrix failures insignificantly affects the laminate ultimate strength. This suggests that in such laminates, the progressive stiffness reduction seen in the previous method may be unnecessary, and laminate failure may be taken to coincide with the fibre failure of the load-carrying ply (the ply with fibres oriented closest to the loading direction). To perform this analysis, a lamina failure criterion is chosen and the

failure load is determined by calculating the load required for fibre failure in the dominant lamina. No stiffness reductions are included in the process. The laminate strength predicted by the Sudden Failure method is usually higher than by the Ply-by-Ply Discount method.

5.3.3 Stiffness Reduction

After an individual ply within the laminate has failed, there are two methods that can be utilised to 'discount' the failed ply and reduce the laminate stiffness accordingly. The first method is known as the 'Parallel Spring Model' and the 'Incremental Stiffness Reduction Model'.

Firstly, considering the 'Parallel Spring Model', each lamina is modelled with a pair of springs representing the fibre (longitudinal) and matrix (shear and transverse) deformation modes. The entire laminate is modelled by grouping together a number of parallel lamina spring sets as shown in figure 81. When fibre breakage occurs, the longitudinal modulus is reduced. When matrix cracking occurs, the shear and transverse moduli are reduced. The value to which the moduli are reduced is arbitrary.

This model is also capable of differentiating between types of matrix failure if desired; i.e., the transverse and shear moduli can be reduced separately depending on the specific type of matrix failure mode. The model which reduces E_1 for fibre failure and E_2 and G_{12} for either transverse or shear matrix failure is denoted the 'PSM'. The model which reduces E_1 for fibre failure, E_2 for transverse matrix failure, and E_2 and G_{12} for shear matrix failure is denoted the 'PSMs'. The idea behind the 'PSMs' is that a transverse matrix failure does not necessarily inhibit the ability of the lamina to carry loading in the shear direction. Creating these two different reduction models has little micromechanical basis, and is done mainly for curve fitting purposes.

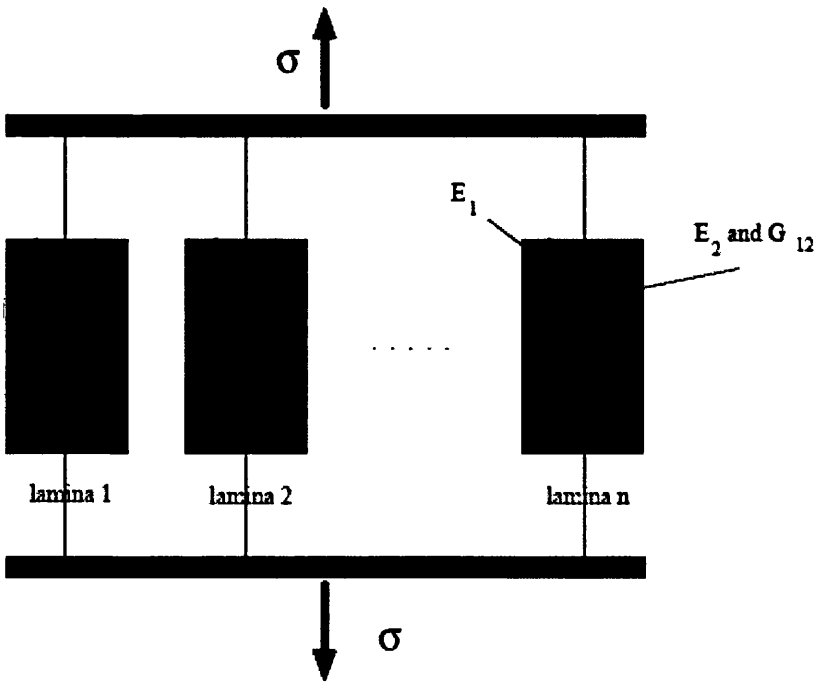

Figure 81 Schematic of Parallel Stiffness Model

For most fibre-dominated composites, setting the stiffness constants directly to zero after the corresponding mode of failure is simple and unambiguous. The use of such reduction can be justified by regarding the laminate analysis to be at the in-plane (x, y) location where all ply failures would occur. Consider a 90° lamina (within a laminate) containing a number of transverse matrix cracks, as shown in figure 82. The 90° ply still retains some stiffness in the loading direction (E_2 direction locally). However, the assumption is made that ensuing 0° fibre failure will occur at the weakest point. This point is where matrix cracking has occurred in the 90° plies, or where locally $E_2 = 0$. Thus, it is acceptable to reduce E_2 directly to zero after transverse matrix cracking for an ultimate strength analysis. This is the approach used in ELAP. Since matrix cracks are discrete, between two cracks a failed lamina would still contribute fully to the laminate stiffness. It is obvious that such drastic lamina stiffness reduction, if assumed to be true over the whole laminate, would greatly overestimate the ultimate strains of the laminate. In fibre-dominated laminates, the effect of matrix cracks on the overall laminate stiffness is usually very small. It is reasonable to estimate the laminate ultimate strains by using the virgin laminate stress-strain relations and the laminate failure stresses obtained from the laminate failure analysis.

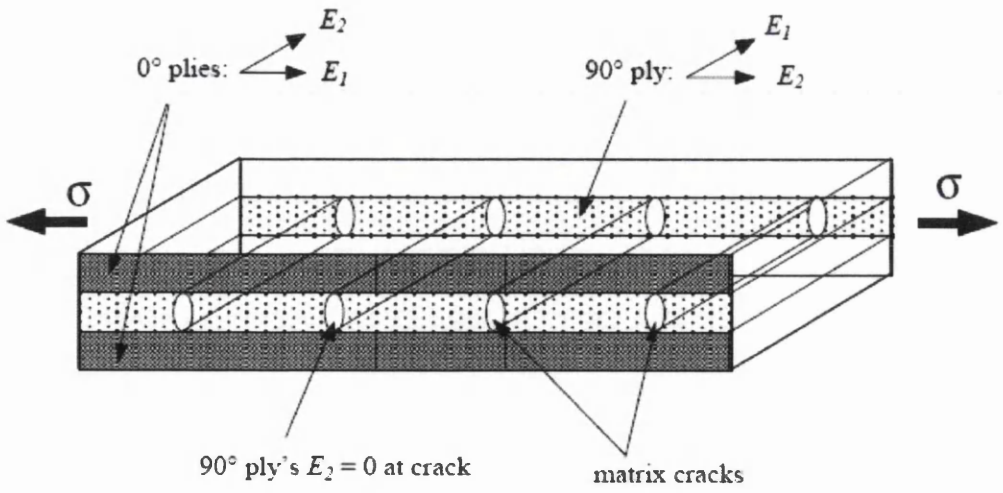

Figure 82 Schematic of the Parallel Stiffness Model in a Composite

It should be noted that although not discussed in this thesis the ELAP tool is being developed to capture additional failure criteria, which will meet Airbus requirements in the future. To have confidence in the ELAP model it is necessary to check the predictions it makes of the laminate properties against a tried and tested tool used by Airbus, which in this case is LAP. Three test cases were derived to carry out direct comparisons for all failure criteria common to each tool. A brief overview of the functionality of the ELAP tool is first considered. The first step is to select the appropriate material from the tool database. The materials in this database have been generated as part of the EMOC test programme; this is shown in figure 83.

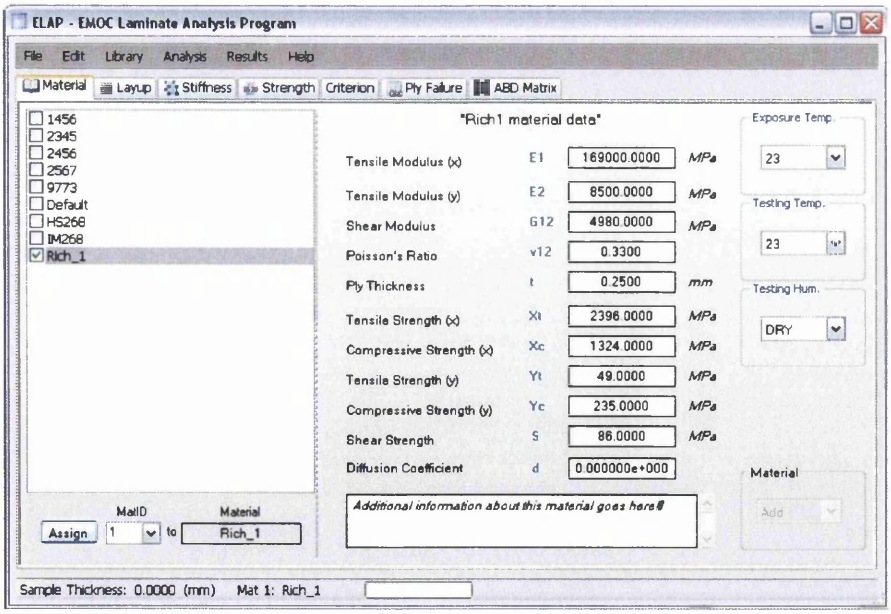

Figure 83 Selecting Material Properties in ELAP

The next step is to define the lay-up of the laminate being analysed as shown in figure 84. At this point the diffusion coefficient and maximum moisture content is defined by selecting the moisture degradation button. Once the parameters are entered the model updates each ply with a moisture values based on the defined time period.

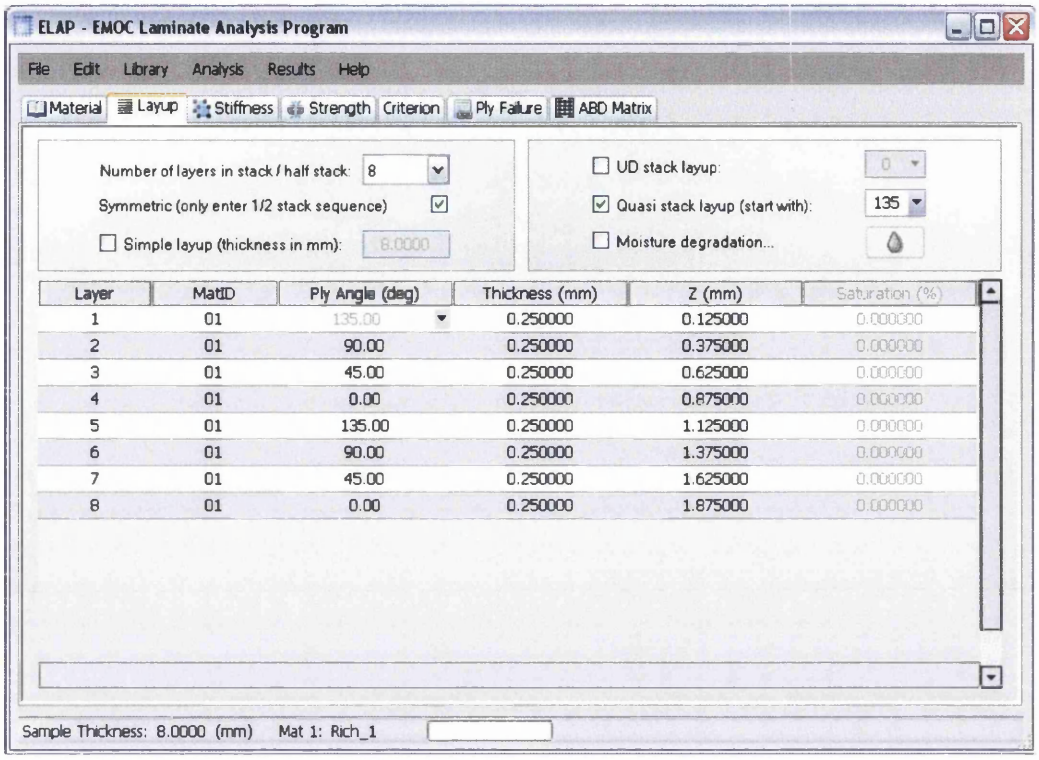

Figure 84 Defining the Laminate Lay-up in ELAP

Next, we define the loading conditions and select the failure criterion we want to use, as shown in figure 85. Note that for the purposes of the lug case study and all analysis methods within the rib sizing tool, the max stress failure criteria shall be used, as this is sensitive to changes in shear properties.

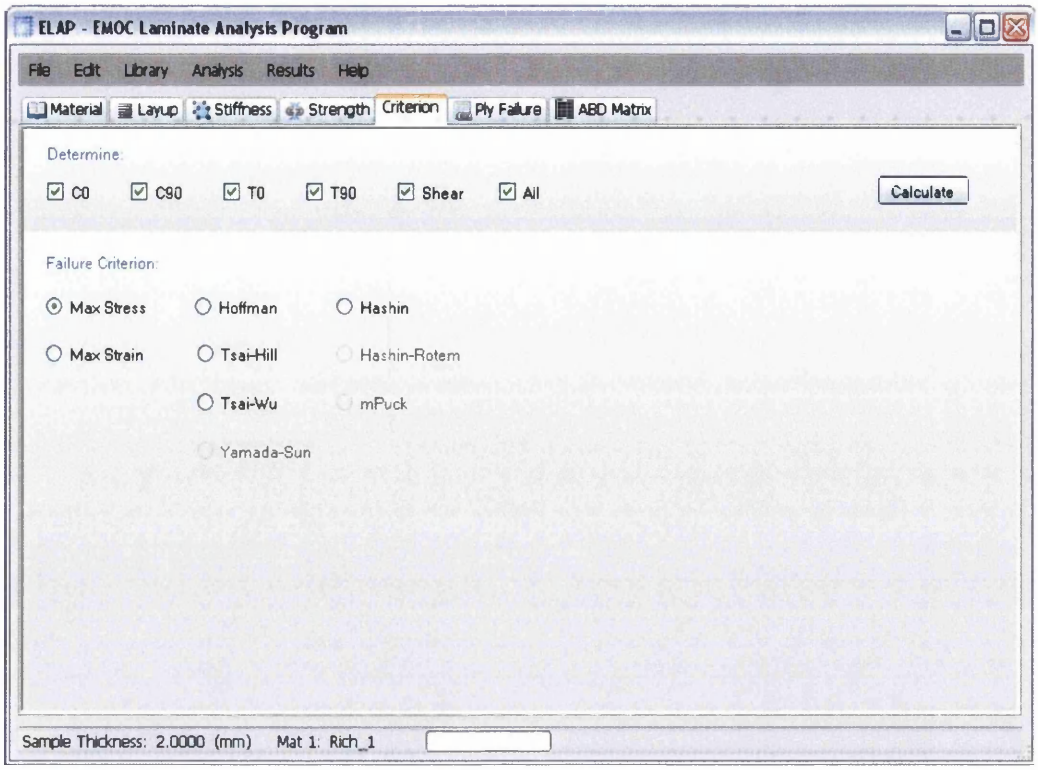

Figure 85 Defining Loading Conditions & Criteria in ELAP

An example of the ELAP output is shown in figure 86. The stiffness properties are generated from the inverse 'ABD' matrix for plain loading in the 'x' and 'y' directions as well as the shear stiffness relative to these two axes, where 'x' is relative to the 0^{o} fibre direction. Each of the strength properties is then provided, where first ply failure can be identified by the ply having the lowest strength and the ultimate failure derived by the plies with the maximum strength values.

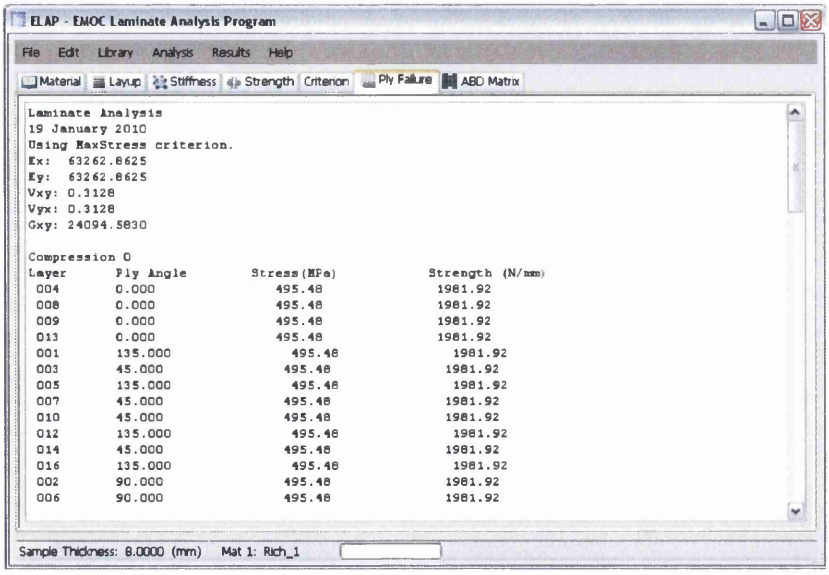

Figure 86 Results Output from ELAP

Three test cases were compared for the initial validation of the ELAP model. For all cases, the same material properties (table 21) were used. The ELAP software employs a ply-by-ply discount method using the parallel spring model (PSM, above) for stiffness reduction. The 'knockdown' multiplier (an arbitrary figure) in the PSM routine was 10^{-5}. It is not known the value LAP uses. Three symmetrical cases were compared, layups of which are shown in table 22. All cases were tested assuming the laminate in a dry condition. The value of the interaction factor for use with the Tsai-Wu criterion was set to zero.

Table 21 Material Properties Used for the Test Cases

	Value	Units
E_{11}	169000	MPa
E_{22}	8500	MPa
G_{12}	4980	MPa
γ_{12}	0.33	
S_{11T}	2396	MPa
S_{11C}	1324	MPa
S_{22T}	49	MPa
S_{22C}	235	MPa
S_{12}	86	MPa
t	0.25	mm

Table 22 Showing Symmetric Lay-up Stacking Sequence for Each Case

Case 1	Case 2	Case 3
-45	0	-45
90	45	0
45	-45	0
0	90	45
-45	0	90
90	45	- - - - - - symmetry - - - - - -
45	- - - - - - symmetry - - - - - -	
0		
- - - - - - symmetry - - - - - -		

5.4 Initial Quantification of Thermal Affects Combined with Moisture Ingress Effects on Strength

This project and associated work have focused on the effects moisture has on the strength of CFRP material. However as previously discussed, Airbus designs their components using what is known as HOT/WET material properties. These are known as the worst operating conditions a component is likely to see during its service life in terms of both moisture absorption and operating temperature. In reality the research conducted here and the complimentary work, does not provide a complete design tool/package that could be used by Airbus in the future. The thermal affects on material strength need to be taken into account. These effects are being quantified by the author via a project called EMOC (Environmental Modelling of Composites), which will build on this research to incorporate thermal effects.

However the author believes that this project would not represent a true study of potential weight savings without taking into account the thermal effects on composite strength. Based on preliminary findings within the complimentary testing research, it was evident that shear strength appeared to have a high sensitivity to moisture ingress in terms of the strength of a component. Therefore this mechanical property was selected to help define combined moisture/thermal effects on component strength.

As before the worst case condition has to be taken into account when designing any civil aircraft. In the case of carbon fibre materials, reinforced by either a thermoset or thermoplastic polymer matrices, high operating temperatures have the greatest effect on the strength and stiffness of a component i.e. the higher the temperature the weaker the material. The operating limits of a specific matrix will be determined by is glass transition temperature 'Tg', where the material will lose its structural integrity. It is still important however, to understand the materials behaviour at different levels of saturation and temperature. The complementary model being developed can then be modified to take into account the temperature of the operating environment, subsequent temperature of the component being modelled and therefore the strength of the component as a function of both moisture ingress and temperature. The following test matrix shown in table 23 provides the test matrix defined by the author to provide an initial evaluation of the thermal effects on material strength.

Table 23 Test Matrix for In-Plane Shear Tests Conditioned at 85%RH 70°C & in the As-received Test Condition

Coupon Number	Environmental Chamber Condition	Test Temperature (°C)
A1	70°C/ 85%RH	23
A2	70°C/ 85%RH	23
A3	70°C/ 85%RH	23
A4	70°C/ 85%RH	23
A5	70°C/ 85%RH	23
A6	70°C/ 85%RH	60
A7	70°C/ 85%RH	60
A8	70°C/ 85%RH	60
A9	70°C/ 85%RH	60
A10	70°C/ 85%RH	60
A12	70°C/ 85%RH	90
A13	70°C/ 85%RH	90
A14	70°C/ 85%RH	90
A15	70°C/ 85%RH	90
B2	No Conditioning	23
A24	No Conditioning	23
B1	No Conditioning	23
A19	No Conditioning	23
A20	No Conditioning	23
A17	No Conditioning	60
A21	No Conditioning	60
A22	No Conditioning	60
A23	No Conditioning	60
A18	No Conditioning	90
B4	No Conditioning	90
B5	No Conditioning	90
B6	No Conditioning	90
B7	No Conditioning	90

Firstly, it is important to understand the thermal effects on the material without the presence of moisture in the structure and therefore dry coupons were tested at the three temperatures. The chosen temperatures where set at 40° intervals to try to understand material properties over a range of temperatures.

Coupons A1-A15 (noting coupon 11 was scrapped due to quality) were placed in a conditioning chamber and the moisture uptake levels monitored on a weekly basis until saturation was reached, i.e. the coupons reach equilibrium with the surrounding environment. These coupons where then tested at the three different temperature levels. This allowed the effect of temperature on material strength to be evaluated and also the combined effect of temperature and moisture ingress to be quantified.

Unfortunately this test matrix did not allow the effects of different moisture levels combined with different temperatures to be evaluated; however comparisons to existing Airbus data could still be made. It was also possible to carry out a comparison to the moisture uptake rates and subsequent diffusion coefficient between the material being used here (M21/T700) and the material being used in the PR2 (977-2/HTS), while also comparing uptake rates to existing Airbus data for M21 resin.

To simplify the test programme and reduce cost no drying was undertaken for any of the coupons prior to testing. This meant that there was inevitably some moisture present within each of the coupons, however this was assumed to be negligible because the environmental conditions the coupons were stored in will not have permitted significant levels of moisture to be absorbed. It should also be noted that when considering the conditioned tests there will also be an error in the presented percentage moisture uptake levels as zero moisture is assumed prior to conditioning. To quantify the levels of moisture in the coupons and allow corrections of moisture levels to be accounted for spare coupons (both conditioned and as-received), were dried in a drying chamber where weight reductions were recorded periodically to determine the actual coupon dry weights.

The selected test method was the ±45 Shear Test [14] previously discussed. This test method appeared from preliminary tests to be most sensitive to the uptake of moisture. The coupon material differed from the complimentary work (which was based on Cytec material 977-2/HTS) instead utilising a different resin system and fibre type, M21/T700. Having a different resin system this material has a different rate of moisture uptake. These materials and their differences will be discussed further in section 6. Coupons were saturated with moisture to the required level for each test by controlling the temperature and humidity of the conditioning chamber in accordance with [9]. Once conditioned, coupons were removed from the chamber. Strain gauges were fitted to the coupons after conditioning and tested within 30 minutes of removal from the chamber. The time between chamber removal and testing was kept to a minimum to ensure the coupons do not begin to dry out to such an extent that the mechanical properties could have been significantly affected (typically coupons were tested within 30 minutes of being removed from the chamber. Further details of the tests can be found in Appendix A, section A.1.

5.5 Control of Material Prior to Environmental Conditioning & Testing

When performing tests on specimens or components that require exposure to environmental conditions other than ambient, there are many opportunities for inaccuracy to be introduced during the manufacturing and handling processes. These inaccuracies were highlighted during the initial test programme discussed in section 4.1.2 and the tests described in section 5.4. The above testing also showed how the combined effect of temperature and moisture level has a more profound affect on the mechanical properties than moisture alone. As the EMOC project continued, the author commissioned a full suite of elevated temperature properties on the original 977-2 resin system, which is to be further complemented by an ongoing test programme to explore M21/T800 material.

The control of material was initially very poor with coupons being left in the office environment prior to conditioning (up to 18 months), in the case of the testing carried out in 4.1.2. Further to this the use of end tab material, made from Tufnol 10G/40, further added to an error in the recorded moisture content in the coupons. From an aircraft certification perspective the previous testing methods would not be acceptable and as a result a procedure was created to allow strict control of material for future testing. This future test work would conform to fully traceable documentation suitable for Audit and will provide highly accurate material property data for use by the developed model. Furthermore any uncontrolled moisture ingress leads to specimens requiring oven drying prior to test, typically increasing timescales and cost to test programmes.

All specimens or components to be used for tests involving environmental conditioning should begin the process in a dry state. Time spent by the specimens in ambient conditions will inevitably lead to ingress of moisture into the specimen. Although this process is slow at room temperature, moisture ingress is measured as a percentage increase in weight and therefore if the specimen has undergone any 'pre-conditioning' their weight will accordingly increase and all following results will be affected. This was clearly shown in the supporting PhD work, which led to further coupons being manufactured for the student to help rectify the errors inherent in all measured moisture concentrations. Details of material control can be found in Appendix A section A.2.

5.5.1 Procedure

All test work and associated results with exception of the supporting PhD and testing discussed in 5.4 have been subjected to this procedure defined by the author. The aim is to limit exposure to the ambient environment prior to testing to a minimum, therefore limiting any 'pre-conditioning' that may occur as a result. A flow chart outlining the process is presented in figure 87. When recording temperature and humidity the following tolerances are considered acceptable, temperature: +/-2°C, relative humidity: 1%RH. These tolerances have been defined by the author to be as stringent as possible, however they are realistic in terms of what is achievable by engineers carrying out the tests. A more detailed description of each of the control procedures can be found in Appendix A section A.2.

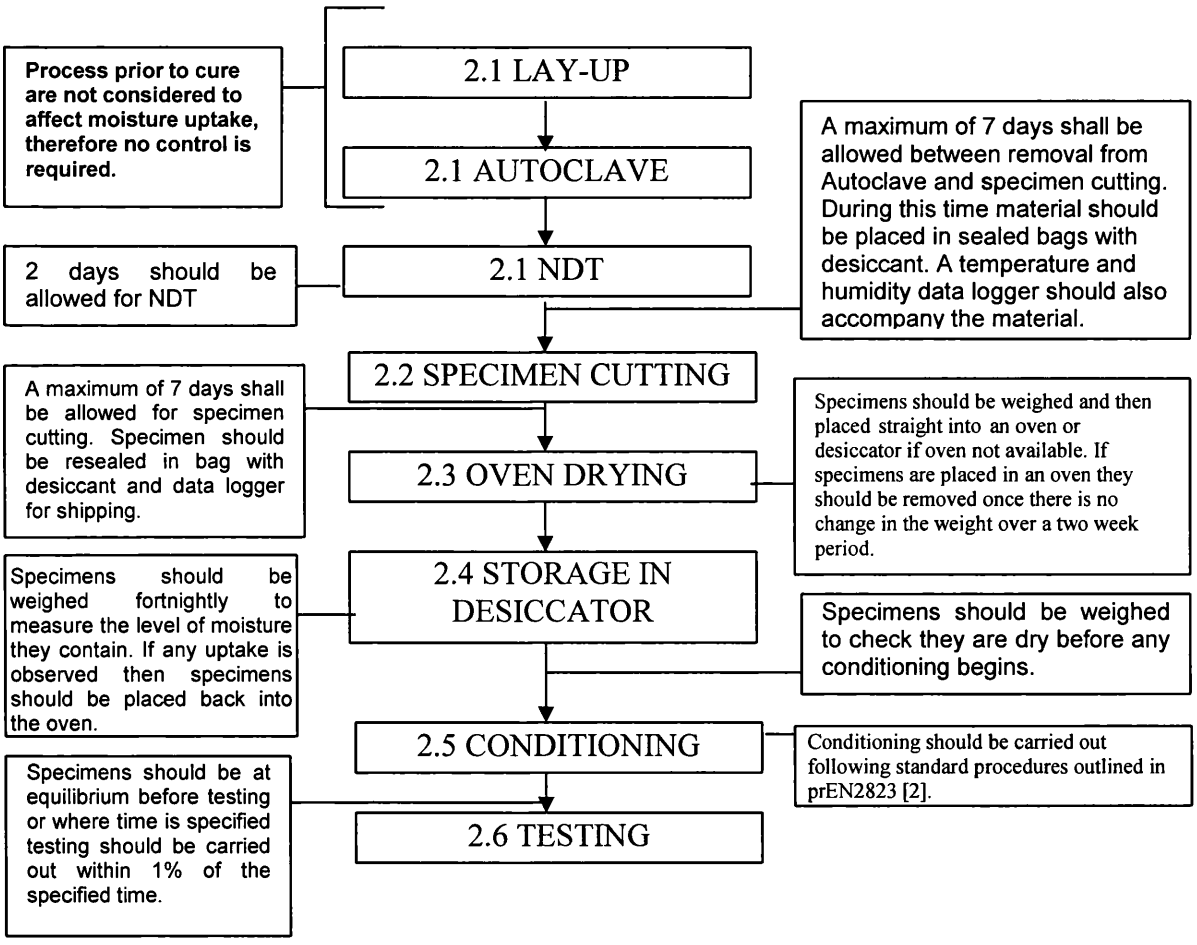

Figure 87 Flow chart outlining the specimen handling procedure

5.6 Replacement of End Tabs Using Double Sided Abrasive

As discussed in section 5.5, end tabs directly affect the monitored levels of moisture that diffuses into composite coupons. Furthermore the rate of uptake is affected as the end tab material has different physical properties, which result in a different rate of moisture uptake. This problem is further compounded because in many cases the total mass of the end tab material exceeds that of the composite material being tested. This section specifically explores the removal of the end tab material used in the construction of the coupons that are to undergo environmental conditioning. The end tabs are applied to the coupons only when conditioning has been completed and the coupons are to be fitted to the test frame for testing.

Bonding the end tabs to the specimen post conditioning is also not acceptable as the time taken is restrictive especially where large numbers of specimens are involved. The result of this is that long periods of time will be spent between removal of the specimen from the conditioning chamber and the completion of the test. This excessive time spent at ambient conditions can alter the moisture level in the specimen and therefore the result of the test.

With this in mind a simple tensile test was performed to assess the effectiveness of using a double-sided abrasive. The abrasive was used to provide friction between end tab and specimen to prevent slippage. Such tests would also allow a suitable grip pressure to be derived for use in future coupon tests. The details of this can be found in Appendix A section A.3, with the main conclusions of this work as follows:

Using a double-sided abrasive such as dry wall sanding screen to replace bonding for end tabs in tensile testing is acceptable.

- It is important to use end tab dimensions that allow a suitable grip pressure to be used that prevents slippage without resulting in crushing of the specimen. 60mm is recommended as a starting point for standard tensile tests.

5.7 New EMOC Test Campaign

Lesson learned from the supporting PhD showed that with end tabs and poor specimen control it was not possible to track the moisture levels accurately within the samples as first envisaged. Furthermore no traveller coupons were utilised to allow this to be corrected for. For aircraft structural design it is necessary to operate at temperatures

above ambient, which the original test programme did investigate. The combination of moisture and temperature has a more profound affect on mechanical performance.

The author therefore commissioned a further test campaign for the 977-2 material, using Swansea University resources. This test campaign takes into account much of the learning derived from the original test programmes, such as the control of material and the removal of end tabs on the specimens as previously described. Test methods used to generate this data come from references [11,13,14]. The test matrix is shown in table 24.

Table 24 New EMOC Material Test Campaign

EMOC TEST MATRIX							
test type	Condition Temp (C)	%RH	Test temp (C)	Material type	UD/QI	No. Specimens	Total Per Test
In-Plane Shear	70	dry	20	977-2	UD	6	54
			60	977-2	UD	6	
			90	977-2	UD	6	
	70	60	20	977-2	UD	6	
			60	977-2	UD	6	
			90	977-2	UD	6	
	70	85	20	977-2	UD	6	
			60	977-2	UD	6	
			90	977-2	UD	6	
90 Tension	70	dry	20	977-2	UD	6	54
			60	977-2	UD	6	
			90	977-2	UD	6	
	70	60	20	977-2	UD	6	
			60	977-2	UD	6	
			90	977-2	UD	6	
	70	85	20	977-2	UD	6	
			60	977-2	UD	6	
			90	977-2	UD	6	
90 Compression	70	dry	20	977-2	UD	6	54
			60	977-2	UD	6	
			90	977-2	UD	6	
	70	60	20	977-2	UD	6	
			60	977-2	UD	6	
			90	977-2	UD	6	
	70	85	20	977-2	UD	6	
			60	977-2	UD	6	
			90	977-2	UD	6	

5.8 Lug Case Studies Using ELAP 1D

The ELAP 1D has been programmed to use the mechanical properties generated by the EMOC test programme previously described. The aim was to use the ELAP tool to predict the mechanical properties of two different size lugs after they had been exposed to an aircraft life cycle, as previously described in the lug case study section. Therefore the conditioning parameter used to determine the moisture distribution was

1000hrs at 70°C 85% Relative Humidity. The maximum moisture content was derived from the quasi-isotropic material diffusion values, which is the same lay-up as both lugs. This value equated to $3.519X10^{-7}$ mm^2/s, with a maximum recorded moisture content of 0.82%, where the reference material had a fibre volume fraction of 58%.

Both lugs being modelled were tested at 90°C so the following material properties (132-136) were used by the model to assign mechanical properties based on moisture content (x):

- 90° Compression Strength = -77.605x + 209.66 (MPa) **(Equation 132)**
- In-plane Shear Strength = -10.744x + 86.58 (MPa) **(Equation 133)**
- 90° Tension Strength = -22.865x + 47.38 (MPa) **(Equation 134)**
- 90° Tensile Modulus = -2.0465x + 9.81 (GPa) **(Equation 135)**
- In-plane Shear Modulus = -0.995x + 4.20 (GPa) **(Equation 136)**

Once the ELAP model had provided the laminate properties the calculation previously described were used to predict the mechanical performance of the lugs.

5.9 Lug Weight Saving Identification

The rib sizing tool, which was originally envisaged to identify weight savings using the EMOC approach, proved to be inappropriate as discussed in section 5.1.5. In an attempt to identify a quantifiable weight saving was decided that the most appropriate course of action would be to assess the lugs, where the equations would be re-arranged to predict a thickness for a given load. This also had the advantage of being able to provide validated results against the lug test campaign. Two lugs were selected, the first was a lug that would experience a typical landing gear load, determined to be ~1.5MN, similar to a landing gear side stay fitting. A typical side stay fitting has a twin CFRP lug to react the load as a double lap shear joint, where a metallic landing gear component would be attached via a large pin. Therefore this 1.5MN load was assumed to be reacted equally by both lugs, therefore equating to a load of 750kN. The second lug selected was to deal with a load of ~50kN (which from initial sizing results in a lug of ~6mm). This was done to assess whether or not a weight saving is possible on a thin component of less than 8mm thick.

To ensure consistency with previous tests and analytical methods the same rules for lug geometry were adhered to with regard to the ratio of the hole diameter to the lug width. Furthermore the calculation methods used the same factors as before, along with the same philosophy for deriving laminate properties using ultimate strength instead of first ply failure strength. The assumed operating temperature was set at 90°C.

The ELAP tool was used to predict the properties of the lug in each case. The first step was to determine a starting thickness for the lug based on HOT/WET mechanical properties, taken from the EMOC database. As with the other lugs, a quasi-isotopic lay-up was to be assumed, with the ELAP model employing the Max Stress failure criteria to determine the laminate properties at full saturation. These derived laminate properties were then used in the lug calculations to produce a thickness.

Once the HOT/WET thickness was derived for each lug, the thickness was divided by the individual ply thickness (0.254mm) to determine the number of plies. This was then programmed-in to the ELAP tool, adjusting the number of plies by ±1 ply to ensure a symmetric lay-up. The ELAP model was then used to produce a moisture profile after an aircraft life-cycle, as before simulated by 1000hours conditioning at 70°C/85%RH. The ELAP programme then used the equations in section 5.8 (equation 132-136) to assign individual ply properties. The laminate theory simulation was then run to determine the stiffness and strength properties, required to carry out the lug sizing. Using these properties a thickness reduction was defined. The next step was then to determine the number of plies in the newly derived thickness and repeat the process until no significant change in thickness was observed.

A reduction in thickness will result in an overall higher level of saturation, which could result in the thickness of the component leading to an optimistic prediction. The second iteration may then result in an over estimation of the required thickness, with each iteration resulting in convergence of the optimal solution. The plan was to continue iterating until a thickness change to within 1 ply was observed, at which point it would not be practical to optimise the lay-up any further without resulting in an asymmetric lay-up.

Once the determination of thickness was complete the next step was to quantify a weight saving for each lug. To do this a simplified mass was derived for each lug where the length '*l*' (mm) of the lug was multiplied by the width 'w' (mm), multiplied by the

thickness 't' (mm) to provide a volume. The hole was then subtracted from this volume, where 'd' is the hole diameter (mm) illustrated by equation 137:

$$Vol_{lug} = (l * w * t) - \left(\frac{\pi d^2}{4} * t \right)$$ **(Equation 137)**

Where 't' is the lug thickness (mm) and 'd' the diameter of the lug (mm).

6. RESULTS

6.1 Ribs Sizing Tool Results

Firstly when considering the different ribs designs considered by the sizing tool, which were stiffened and un-stiffened 'C' & 'I' section designs it is clear from figure 88 that the stiffened I-beam design is the most efficient. However from ribs 15 onwards there appears to be very little difference in weight, which would mean for a more lightly loaded rib design it would probably be cheaper to manufacture a more simple C-section rib design. The specific results from the rib sizing tool can be found in Appendix A tables A.2-A.3 for both the RT/DRY and HOT/WET material property calculations.

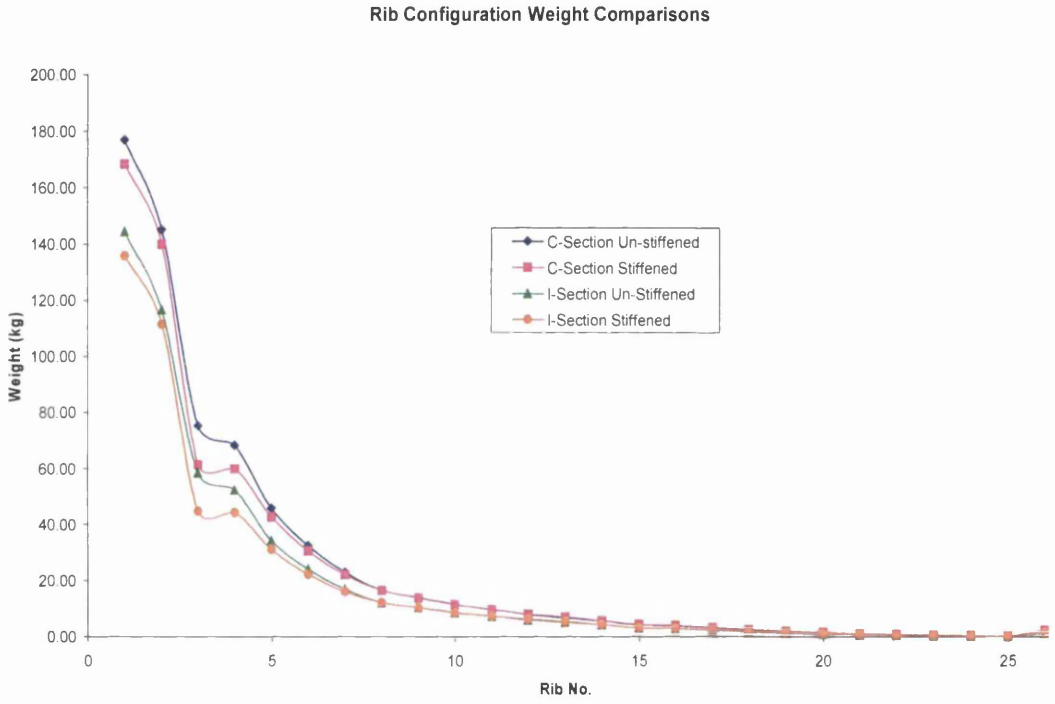

Figure 88 Rib Design Weight Comparison Based on the ALCAS Wingbox Loads, as generated by the Rib Sizing Tool

The difference by rib in weight between HOT/WET & RT/DRY properties is illustrated in figure 89. Clearly the biggest weight opportunity lie in the higher loaded inner wingbox ribs, having thicker section and therefore are less likely to be fully saturated. The weight across ribs 3, 4 & 5 is similar due the increased loads brought about by the engine pylon, increasing the shear flows in these ribs, as would be expected.

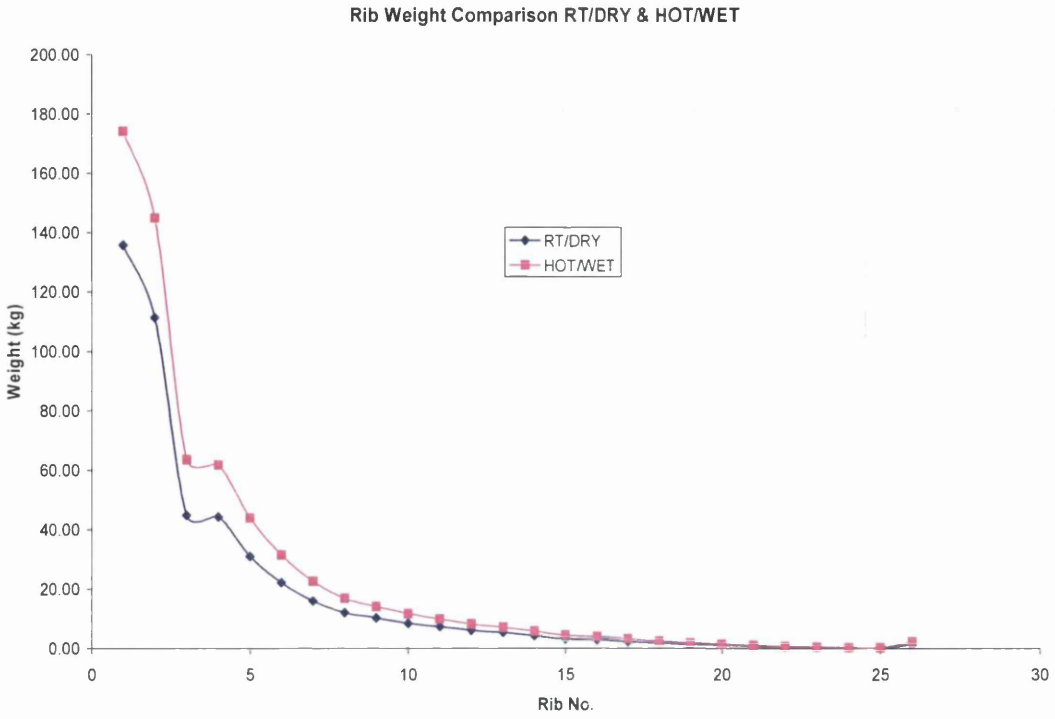

Figure 89 RT/DRY Property Comparison to HOT/WET in terms of Individual Rib Weight

Table 25 summarises the weight increase by rib design, brought about by using HOT/WET properties. This has resulted in a weight increase in this instance of 26% for the most efficient rib design. It was this basic viewpoint, which inspired the EMOC programme hoping to capitalise on this large weight penalty, however it was realised at the time many of these ribs would have sections of much less than 6mm, making it hard to capitalise on the EMOC approach.

Table 25 Showing Summary of Wingbox Rib Mass by Design and Increase In Weight by Using HOT/WET material Properties

	RIB CONFIGURATION MASS COMPARISON			
	C Section Total Mass (Kg)	C-Section Stiffened Total Mass (Kg)	I-Section Total Mass (Kg)	I-Section Stiffened Total Mass Kg)
RT/DRY	484.84	452.65	374.38	342.19
HOT/WET	615.41	584.00	498.35	466.94
Percentage Increase	21.22	22.49	24.88	26.72

6.2 Thermal Effects Combined with Moisture Ingress Effects on Strength

This section presents the results of the test programme detailed in section 5.3. Before mechanical property data could be generated the coupons required conditioning in line with reference [9]. In summary the coupons were weighed before conditioning. Coupons could be considered to be in the 'as received' condition. This term typically refers to coupons, which have not been kept in a controlled environment during the period from completion of manufacture to their use in this test programme. This period of time was approximately four months. The coupons were stored in an office environment, which typically had a humidity of ~50-60%RH and a temperature of around 23°C. In all cases, standard deviations have been calculated, although it should be stated that the number of coupons tested in each case results in a small population, which is not ideal for statistical analysis. The standard procedures state the testing of coupons can only occur, once no measurable increase in moisture content is shown over a two week period. Figure 90 shows the mean moisture content of the coupons over the conditioning period.

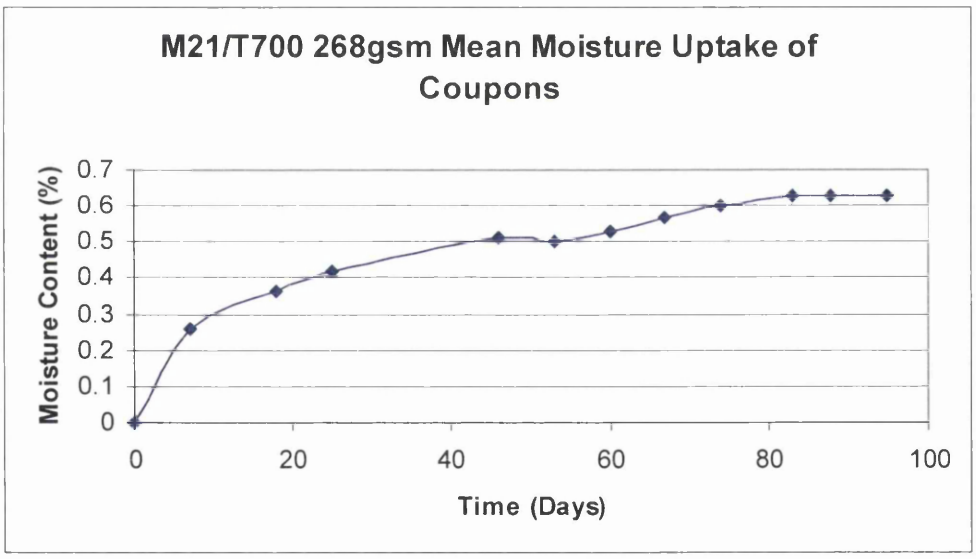

Figure 90 Mean Moisture Uptake of M21/T700 Coupons, Conditioned at 70°C 85%RH

In Appendix A table A.4 shows the moisture contents for each coupon. The results are presented in coupon weights, which are then converted into the percentage increase. The results of the uptake rates can be considered consistent, having a standard deviation of 0.03g. The average coupon overall weight increase, as shown in figure 90

was 0.655g. During conditioning a number of events occurred, which have affected the uptake rates shown in figure 90. The TINYTAG data loggers that were employed to measure the temperature and humidity, independently of the testing equipment, failed to operate correctly. In addition the Airbus logging software has not captured the environmental history. There were essentially two events that occurred. There was an equipment failure with the humidity chamber in that the distilled water used to maintain the humidity ran out. This resulted in reduced chamber humidity. Fortunately the chamber appears to have retained some humidity and therefore did not cause any drying out of the coupons, simply a reduced uptake rate. The second incident was where coupons were removed from the chamber for a period of 48 hours. This was due to the chambers being calibrated by Airbus.

As the coupons were in the as-received state, it was necessary to determine the amount of residual moisture they had absorbed, as a result of sitting in the office Environment. Coupons A18 & A21 were selected for drying. The results of are summarised in figure 91.

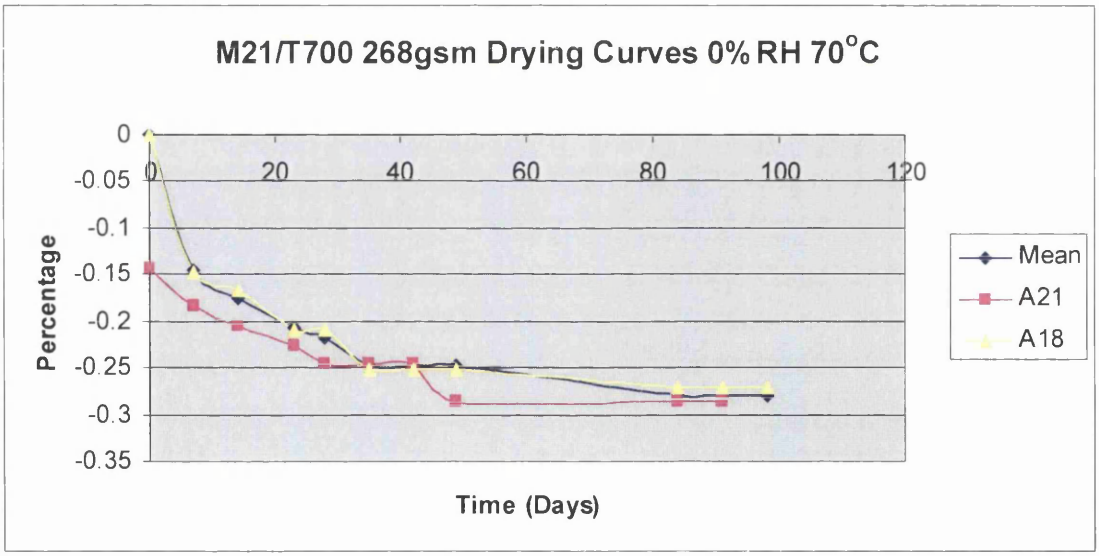

Figure 91 Showing Drying of In-Plane shear Coupons for M21/T700 Material

A full list of the results can be seen in Appendix A tables A.4 & A.5. It can clearly been seen that there was a significant amount of moisture present in the coupons. The average of this is 0.28%. It is therefore necessary to adjust the results in figure 90, as these results assume initial moisture content of zero, which is incorrect. The corrected curves use the average of the two coupons, which were dried. The corrected results are presented in figure 92. All values generated for the correct moisture curves shown

in figure 92 are shown in Appendix A, table A.5. Finally it should be noted that all weights and conditioning curves observed are inclusive of end tab materials. Furthermore, it is known that that different resin systems absorb different quantities of moisture, which will be the case for the end tab material used. After some investigation it was possible to determine that the end tab material, manufactured from Tufnol 10G/40, which has an epoxy resin system only absorbs 0.5% of its weight in moisture even when tested in a 100% humidity [79].

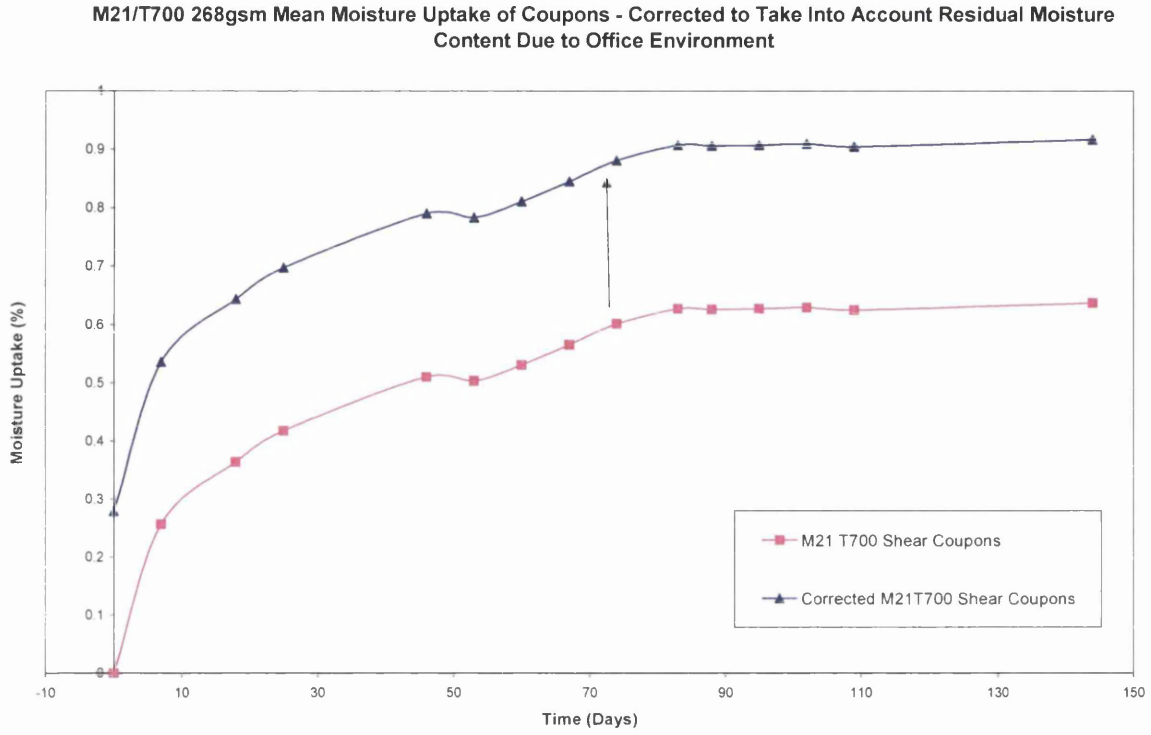

Figure 92 Showing Original and Corrected Moisture Uptake Values for M21/T700 Material

The average maximum moisture content is 0.91%. Taking this average it is possible to plot the average shear strength of the coupons for elevated temperatures. Included is the control, consisting of dry coupons, which have then been tested at the same temperatures. Figure 93 shows these averages. In a similar way the modulus has been plotted, shown in figure 94. The individual coupon test results can be seen in tables A.6-A.11 with the results plotted in figures A.3 to A.4 in Appendix A.

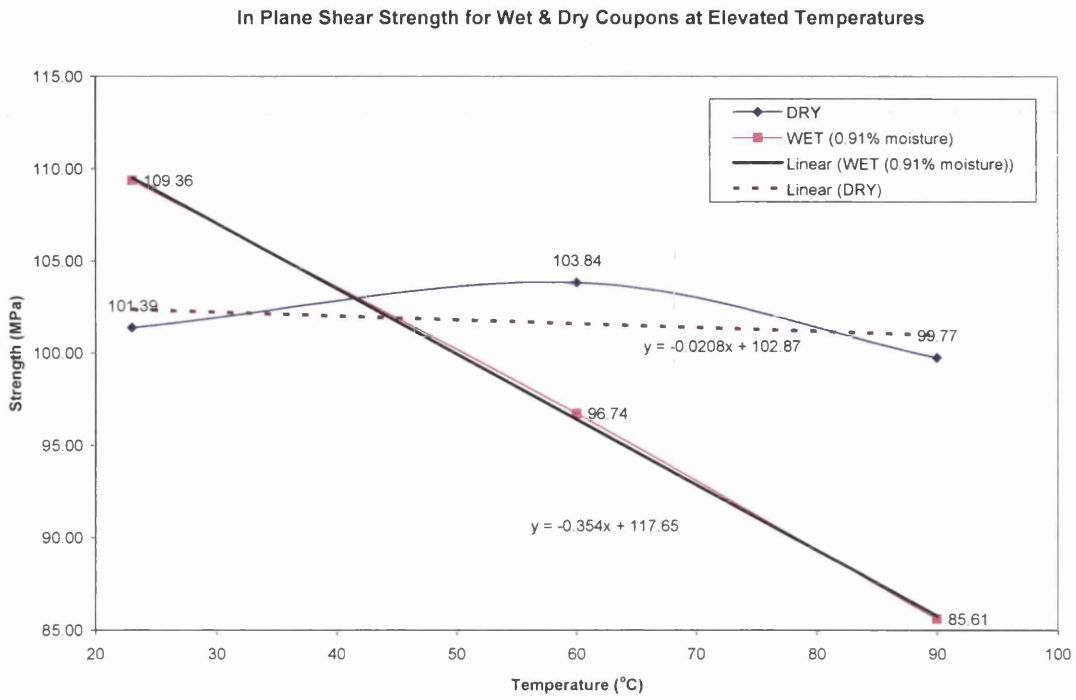

Figure 93 In-Plane Shear Strength of M21/T700 Material for Wet & Dry Samples Tested at Different Temperatures, with Linear Approximations Shown Against Plotted Trend lines

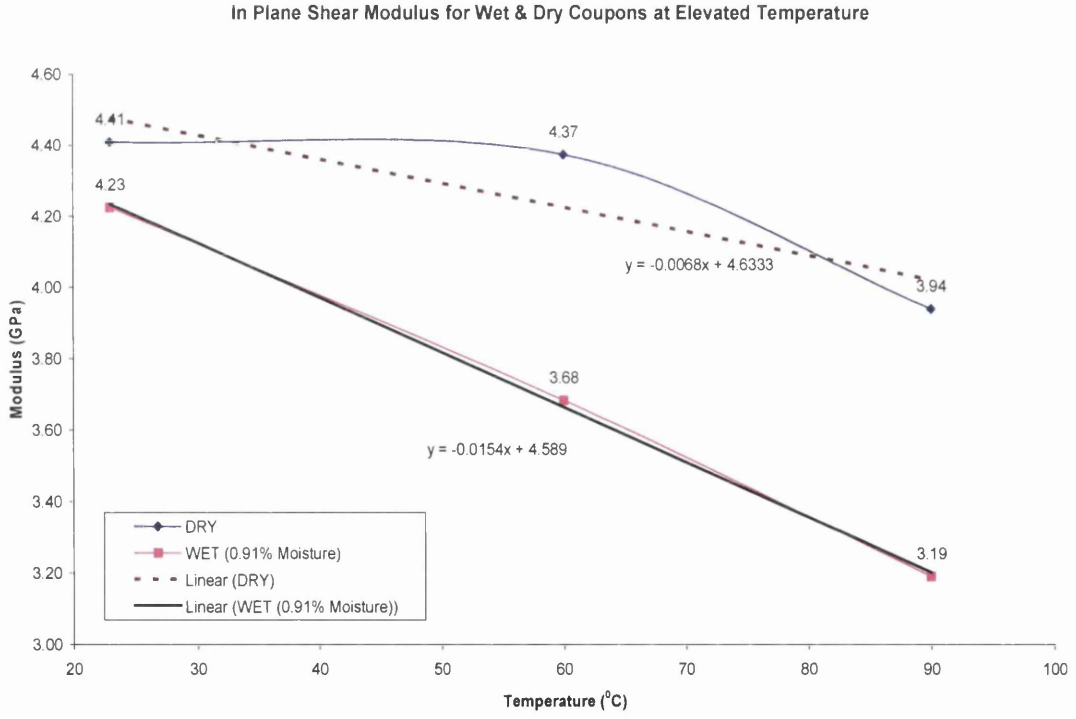

Figure 94 In-Plane Shear Modulus of M21/T700 Material for Wet & Dry Samples Tested at Different Temperatures, with Linear Approximations Shown Against Plotted Trend lines

For figures 93 and 94, linear trend lines have been added. This would appear to be more applicable to the 'wet' coupons than the dry coupons. It is emphasised that the amount of data points limits the accuracy of the results and it is not clear if the non-linear behaviour is as a result of scatter and therefore error in the results, or whether there is a mechanical effect induced by temperature to relieve internal stresses. This linear relationship can be added into the ribs sizing tool for evaluation of component weight as a result of degraded mechanical properties.

In addition to assessing the strength of the material a study of the fracture surfaces was conducted. This was necessary to ensure that there was no difference between the fracture surface between conditioned and unconditioned specimens being tested at both room temperature and elevated temperatures. Specimens B6, B7, & A12 were chosen for study.

6.3 Lug Case Study Preliminary Sizing Results

The results of the initial lug sizing, using a manual approach, described in section 5.2.1 are shown in table 28 (at the end of this section). In all cases the strengths were derived from classical laminate theory using LAP and in all cases ultimate failure strength was taken. When designing aircraft structure, typically the first ply failure strength would be utilised to ensure conservatism, however in this instance the aim was to accurately predict the performance of the lugs being tested. It can be seen in table 28 in some instances the use of a test factor for net-section. This factor was derived from [76], where it was found that the net section failure mode was non-conservative. However after closer inspection, a mistake was identified with this report in the net-section calculation, which means that in all iterations the test factor actually makes the failure mode more conservative i.e. it reduces the RF.

Step 1 was carried out simultaneously to step 2. Step 1 explores the dry 12mm lug, tested at room temperature, with step 2 exploring a fully saturated lug, again tested at room temperature. From this it can be seen that the room temperature dry coupon fails in net section with a coupon width of 48mm and fails in shear out in step 2 in the presence of moisture.

The first iteration used stiffness derived from Airbus B-basis data. The strength properties for tension and shear where taken from the supporting PhD conducted by PR2. Bearing data did not become available throughout the project so the bearing

strength used in all calculation has been fixed, with the strength taken from Airbus B-basis data. It should be noted at this point that bearing strength is a predominately resin dominated property and will also be affected by moisture ingress and operating temperature, however it is assumed that the effect on mechanical performance will be in line with the reduction in tension and shear strength of the laminate. Iteration 2 changes the stiffness properties from the Airbus B-values to the stiffness values derived from the supporting research. As only the net section calculation utilises stiffness there is very little effect on the predictions and the changes to RF are insignificant, indicating that the failure loads are insensitive to changes in stiffness. Iteration 3 changes the notch factor K_{so} to 2, which typically makes the calculation more conservative, while at the same time applying a B-basis knock down factor on the shear strength of 0.8. This resulted in a significant drop in the shear out reserve factor. Iteration 4 then reduces the load slightly until an RF of 1 is achieved. At this point sizing is complete and it can clearly be seen that net-section is the failure mode.

As previously mentioned when the material is saturated the failure mode changes from net section to shear out. To avoid the complexity of failure mode interaction during testing, it was decided to modify the lug geometry to ensure that the shear out failure would always be the predominant failure mode. Therefore the width of the specimen was increased, which lowers the net section stress for the same amount of load and hence increases the RF for the net section failure mode. This modification to the geometry was then repeated for step 2.

Step 3, uses Airbus B-basis mechanical properties and assumes full saturation and an operating temperature of 90°C. PR2 properties were no longer applicable, as the supporting thesis did not explore temperature. Although the tests had been planned to explore both moisture and temperature, this information was not available before testing was due to begin and therefore the existing Airbus properties had to be used. Six iterations were carried out in a similar manner to the previous 2 steps. Iteration 6 can be considered to be the one for comparison purposes.

Step 4, was created once the mechanical property data became available for different temperatures and humidities and corresponds to the same batch of material as the lugs. Again saturation is assumed but only 2 iterations are carried out, one with the shear out test factor and one without the shear out test factor.

6.3.1 Steps 1-4 Comparisons

In summary at the end of the first 4 steps, it is possible to predict the room temperature dry performance of the lugs, which equates to 100kN. Although the fully saturated data cannot be used to predict the conditioned lug strength, as the lug was not fully saturated, it can be seen that the Airbus B-values are significantly lower when using the mean data taken from the supporting research with failure load predicted to be 52.3kN and 83.2kN respectively, noting that this difference should be due to the different temperature between the two data sets of ~70°C. When comparing step 3 to step 4 it can be seen that the EMOC properties generated, result in a failure load of 78.6kN for saturated material, tested at 90°C, compared to the Airbus B-values of 52.3kN. A summary of these predicted failure loads is shown in table 26:

Table 26 Step Failure Load Comparison

STEP	Properties	Failure Load (kN)
1	RT/DRY	100kN
2	RT/WET	83.2kN
3	HOT/WET (Airbus)	52.3kN
4	HOT/WET (EMOC)	78.6kN

6.3.2 Lug Predictions Steps 5-10 Results

Step 5 & 6 is the first attempt at using the stress method approach defined in 5.3.1. Figure 78 shows the through thickness moisture distribution with the assumptions made for both iterations one and two. Note that the diffusion parameters used are from the Airbus database, which do not represent this exact batch of material, fibre volume fraction etc, which will inevitably mean an error in the moisture profile used. The mechanical properties for in plane shear, 90° Tension & Compression were taken from the EMOC generated data, shown in figures 107-111. Using the moisture content for each discrete section through the thickness, the material properties were determined by direct read off from this data. Iteration 2 can be considered to be a more detailed approximation. The difference between steps 5 & 6 is that step 5 assumes a B-basis knock down factor on material properties of 0.8. Step 7 & 8 use EMOC data to predict the room temperature, dry state, again with and without a B-basis knock down factor.

Step 9 is the results from FE, using the same mechanical properties as step 6 iteration 2. In this instance the failure load predicted is small compared to the equivalent hand calculated method and failure was assumed to have occurred, once elements began to exceed the maximum stress pre-determined by laminate analysis. As all of the other prediction methods have been based on the ultimate laminate strength and not the 1st ply failure strength, it is not accurate to make a direct comparison to the FE Model in this case.

Figure 95 & 96 shows the stress results for shear and tension loading. The load on the model was progressively increased until elements started to exceed the shear strength of the bulk laminate properties. At this point failure was assumed to have occurred at a load of 97kN (summarised later when comparing analysis steps in table 27), where theoretically the shear strength of the material has been slightly exceeded by 5MPa.

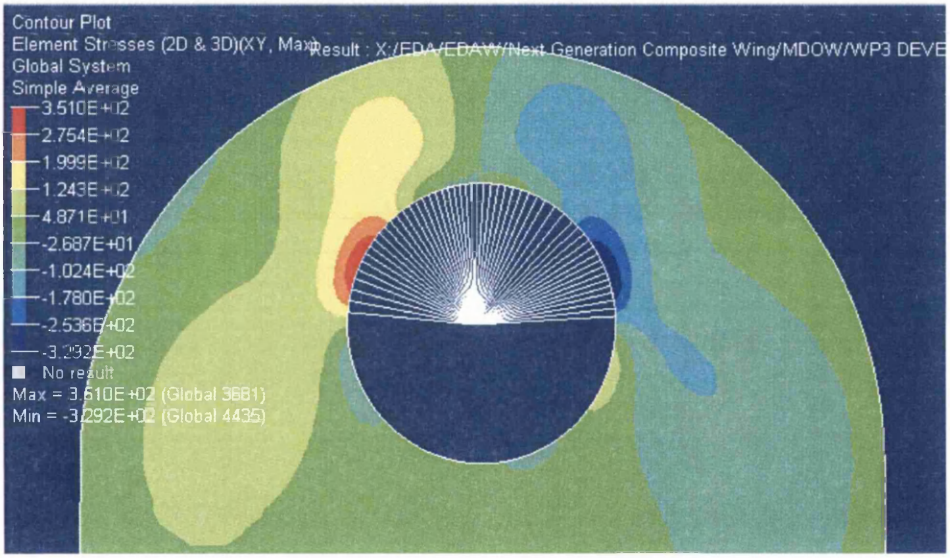

Figure 95 Showing XY (Shear) Stress for the 12mm lug with Load at 87kN Achieving Shear Strength of 351MPa

At the point where elements failed in shear, the tensile loads were checked and again it can be seen that the lug has failed at 87kN by 1MPa. Therefore this should be a secondary failure. It should be noted that as laminate properties have been used for every element, there is a risk that the local failed elements have different properties locally to the bulk material and therefore this adds risk for both tension and shear cases.

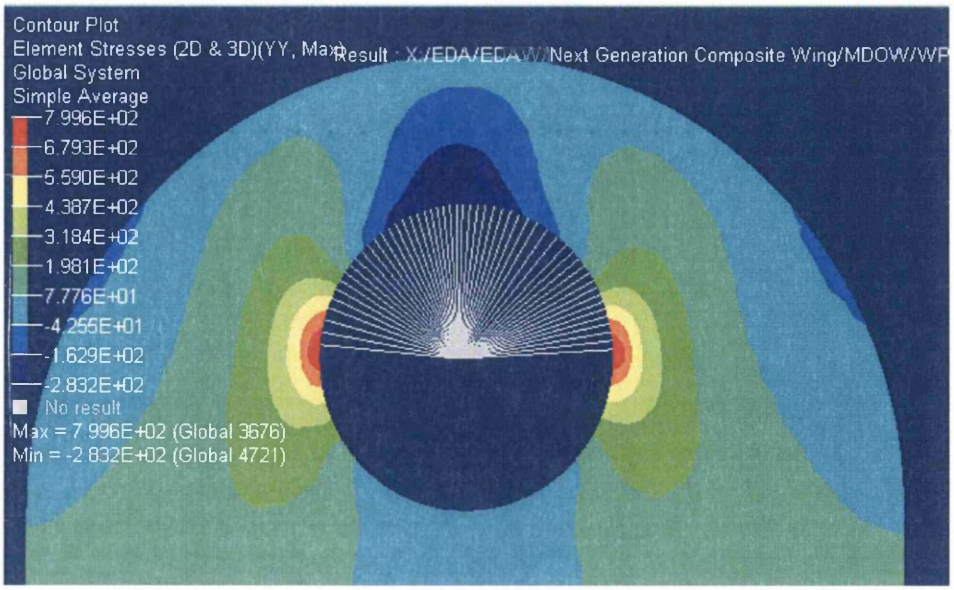

Figure 96 Showing XX (Tensile) Stress for the 12mm lug with Load at 87kN Achieving Tensile Strength of 351MPa

The FE analysis was repeated for the large lug and showed the same outcome as that depicted for the 12mm lug. The contour plots for the 26mm lug can be found in Appendix A, figures A.5-A.6.

The final step, step 10 modified the diffusion parameters and utilised a new through thickness moisture distribution, based on actual EMOC moisture uptake, as shown in figure 97. This provided a slightly more accurate moisture distribution than the Airbus data, as it was specific to the batch of material being tested. Furthermore in this instance the lug was discretised into 6 sections, each with an average moisture distribution through the thickness, further increasing the fidelity of the model. However there is a large discrepancy with regard to maximum moisture content as in this instance the maximum moisture content derived by the supporting PhD test programme indicated much lower moisture content than the new EMOC material data generated. This maximum moisture level is known to be inaccurate because there were major flaws in the way the moisture was calculated, brought about by poor atmospheric control of specimens and secondly, the use of Tufnol end tabs having a greater overall mass than the carbon fibre. These end tabs absorbed a different amount of moisture and therefore it was impossible to determine with any degree of accuracy the amount of actual moisture in the carbon, which has led to a significantly lower moisture level than would typically be observed. This also has an effect on the diffusion coefficient derived from update over time, which in this case for the diffusion coefficient for the combination of the carbon epoxy and Tufnol material.

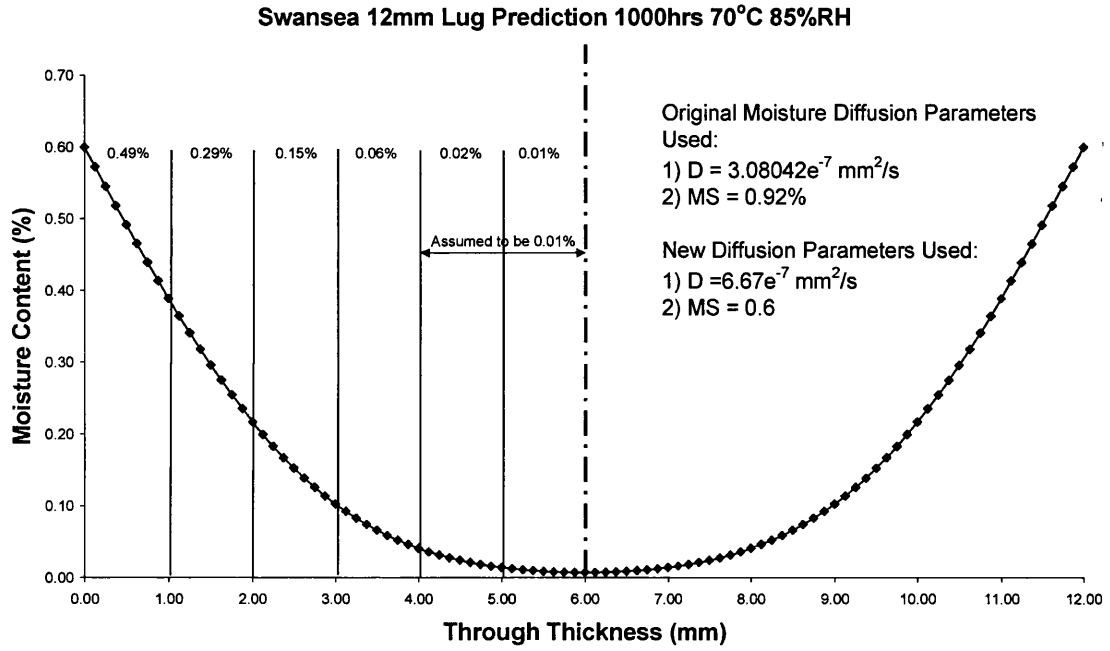

Figure 97 EMOC Through-thickness Prediction of Moisture Distribution for 12mm thick Lug Exposed to 70°C 85%RH for 1000 Hours

6.3.3 Comparisons of Steps 5-10

A summary of the failure load predicted for steps 5-10 is shown in table 27. The key values of interest are steps 6, 7 and 10. Firstly comparing step 6 & 7 it appears that there is only a negligible drop in load carrying performance between the conditioned samples and the ones exposed to 1000 hours conditioning. Furthermore when comparing this to the higher fidelity step (10), it can be seen that the load level drops slightly, which can be attributed to a more accurate through thickness moisture distribution and therefore a more accurate definition of individual ply properties as a function of moisture.

Table 27 Summary of Failure load Predictions Produced by Steps 5-10

STEP	Properties	Failure Load
5	Modelling Approach 0.8 B-basis Factor	91.4kN
6	Modelling Approach	114.4kN
7	EMOC RT/DRY	116.5kN
8	EMOC RT/DRY 0.8 B-Basis Factor	93.1kN
9	FE Modelling Approach	87kN
10	Modelling Approach New Moisture Profile	109kN

Table 28 Summary of all Failure Load Predictions for the 12mm 977-2 Lugs

12mm Thick Lug with 24mm Hole - Summary Table for Shear Out/ Net Section Calcs for EMOC														
STEP Iteration Details	Iteration	Strength (LAP)			Stiffness (LAP)			Geometry		Factors		Load (kN)	Reserve Factors	
		Tensile (MPa)	Bearing (MPa)	Shear (MPa)	Ex (GPa)	Ey (GPa)	Gxy (GPa)	Width (mm)	Thick-ness (mm)	KSO (shear out notch factor)	TEST FACTOR (net section)		RF Net Section	RF Shear Out
STEP 1 Room Temp Test Using Dry Material	1	801	737	379	63.2	63.2	24.09	48	12	1	0	96.5	0.99	2.594
	2	801	737	379	55.1	55.1	20.93	48	12	1	0	96.5	0.99	2.594
	3	801	737	303	55.1	55.1	20.93	48	12	2	0	96.5	0.99	1.037
	4	801	737	303	55.1	55.1	20.93	48	12	2	0	95.5	1	1.048
	5	801	737	303	55.1	55.1	20.93	72	12	2	0	95.5	2	1.048
	6	801	737	303	55.1	55.1	20.93	72	12	2	0.763	100	1.526	1.002
STEP 2 Room Temp Test Using Fully Saturated Material (Jo Ryan's supporting thesis)	1	801	737	315	63.2	63.2	24.09	48	12	1	0	96.5	0.991	2.156
	2	801	737	315	54.29	54.29	20.64	48	12	1	0	96.5	0.991	2.156
	3	801	737	252	54.29	54.29	20.64	48	12	2	0	96.5	0.991	0.82
	4	801	737	252	54.29	54.29	20.64	48	12	2	0	95.5	1	0.82
	5	801	737	252	54.29	54.29	20.64	48	12	2	0	83.2	1.149	1
	6	801	737	252	54.29	54.29	20.64	72	12	2	0	83.2	2.298	1
	7	801	737	252	54.29	54.29	20.64	72	12	2	0.763	83.2	1.754	1.002
STEP 3 HOT/WET Wet Material Tested at 90C/ Saturated (Airbus Design Data, to be replaced with EMOC data)	1	743	737	198	51.2	51.2	19.38	48	12	1	0	96.5	0.919	1.355
	2	743	737	158.4	51.2	51.2	19.38	48	12	2	0	96.5	0.991	0.542
	3	743	737	158.4	51.2	51.2	19.38	48	12	2	0	88.7	1	0.82
	4	743	737	158.4	51.2	51.2	19.38	48	12	2	0	52.3	1.696	1
	5	743	737	158.4	51.2	51.2	19.38	72	12	2	0	52.3	3.391	1
	6	743	737	158.4	51.2	51.2	19.38	72	12	2	0.763	52.3	2.588	1
STEP 4 HOT/WET Wet Material Tested at 90C/ Saturated, EMOC Mechanical Property Data	1	744	737	229.7	50.8	50.8	19.15	72	12	2	0	75.9	2.34	1
	2	798	737	238	54.9	63.5	24.3	72	12	2	0.763	78.6	1.849	1
STEP 5 HOT/WET Modelling Approach	1	616.64	737	232.96	47.76	47.84	17.52	72	12	2	0.763	76.9	1.461	1
	2	638	737	276.8	50.16	50.16	18.96	72	12	2	0.763	91.4	1.271	1
STEP 6 HOT/WET Modelling Approach	1	770.8	737	291.2	59.7	59.8	21.9	72	12	2	0.763	96.1	1.461	1
	2	798	737	346	62.7	62.7	23.7	72	12	2	0.763	114.4	1.271	1
STEP 7 RT DRY	1	798	737	353.96	63	63	23.8	72	12	2	0.763	116.5	1.248	1
STEP 8 RT DRY	1	638	737	282	50.4	50.4	19.1	72	12	2	0.763	93.1	1.248	1
STEP 9 FE	1	798		346	62.7	62.7	23.7	72	12	2		87	1.02	1
STEP 10 New Moisture Profile from EMOC Diffusion Data & EMOC Mechanical Properties	1	798	737	330	62.7	62.7	23.7	72	12	2	0.763	109	1.328	1

6.3.4 26mm Thick Lug Prediction

For comparison purposes only one batch of the 26mm lugs was tested. Tests as previously mentioned were in the conditioned state, having been exposed to 1000hours conditioning at 70°C 85% RH, equivalent to an aircraft life. Therefore one step containing two iterations was carried out with and without an assumed B-basis knock

down factor of 0.8, to predict the strength of the lug in this instance. The EMOC moisture profile shown previously in figure 78 was used again in the absence of the fully working EMOC tool being available. This was considered acceptable because the core could be considered to be in the dry state and therefore the additional of material would merely constitute an increased dry core. The moisture profile shown in figure 98 was therefore used to determine ply properties through the thickness, using classical laminate theory to produce the strength values, again using the max stress failure criterion. Again the maximum moisture content is known to be in error for the purposes previously discussed, with the EMOC test data indicating a moisture content of ~1% for a 60% fibre volume fraction component at saturation (85% RH).

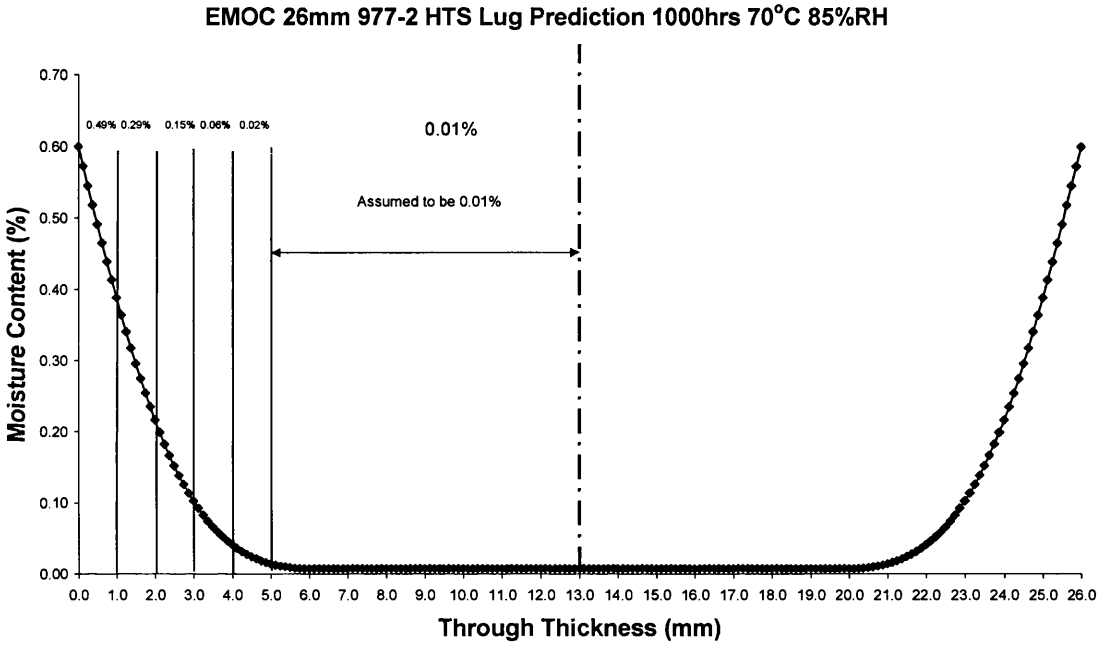

Figure 98 Moisture Profile for 977-2 HTS Material after 1000 Hours Conditioning With Discretised Sections with Assumed Moisture Contents Shown

Using figure 98 the ply properties can be determined as a function of moisture content in each ply. As with the small lugs two iterations were performed, one using a B-basis knock down factor and the other without a B-basis knock down factor. The results are presented in table 29:

Table 29 26mm Thick Lug Mechanical Properties and Load Predictions Derived from Moisture Distribution in Figure 96

STEP Iteration Details	Iteration	Strength (LAP)			Stiffness (LAP)			Poissons Ratio Vxy	Geometry				KSO (shear out notch factor)	Load (kN)	RF Shear Out
		Tensile (MPa)	Bearing (MPa)	Shear (MPa)	Ex (GPa)	Ey (GPa)	Gxy (GPa)		Edge Distance (mm)	Width (mm)	Thick-ness (mm)	Hole Diameter (mm)			
WET/90C	1	798	737	338	62.62	62.62	23.68	0.32	1D	156	26	52	2	523.6	1.000
WET/90C with 0.8 B-Basis	2	798	737	338	62.62	62.62	23.68	0.32	1D	156	26	52	2	418.88	1.000

6.4 Lug Test Results

A results summary of the 12mm thick lug tests can be seen in table 30. All load displacement data for each lug (12mm and 26mm) can be found in Appendix A, figures A.16-A.20. There appears to be good correlation between all tests, with little scatter between results and no noticeable outliers. A B-basis strength was generated for each batch as a comparison against the mean data and in all cases except the batch 1000hrs Wet/ tested at 90°C the Weibull B-basis method could be applied. The exception was applicable to the normal distribution method. This difference is attributable to a smaller batch size. The lug was considered failed when a significant drop in load was observed during test (≥1kN). Individual failure loads for both conditioned and dry samples at each test temperature can be found in Appendix A, figure A.21.

Table 30 12mm Thick Lug Test Results for Dry & Conditioned (70°C/85%RH for 1000 hours) Tested at 20°C & 90°C

977-2 12mm Thick Lug Results							
Specimen No.	Condition	Test Temperature (°c)	Failure Load (kN)	Displacement At Failure (mm)	Average Load (kN)	Average Displacement (mm)	B-Basis Load (kN)
9222-21	Dry	20	106.29	1.64	108.42	1.65	95.01
9222-14	Dry	20	111.2	1.705			
9222-6	Dry	20	110.01	1.68			
9222-20	Dry	20	109.89	1.61			
9222-2	Dry	20	104.73	1.6			
9222-15	Dry	90	109.91	1.65	111.44	1.70	99.89
9222-27	Dry	90	114.01	1.77			
9222-19	Dry	90	112.65	1.65			
9222-10	Dry	90	111.1	1.81			
9222-28	Dry	90	109.53	1.64			
9222-22	1000hrs Wet	20	107	1.65	103.56	1.55	88.52
9222-08	1000hrs Wet	20	99.8	1.45			
9222-03	1000hrs Wet	20	105	1.53			
9222-26	1000hrs Wet	20	102	1.57			
9222-05	1000hrs Wet	20	104	1.54			
9222-7	1000hrs Wet	90	109.57	1.68	107.47	1.71	101.59
9222-17	1000hrs Wet	90	106.95	1.75			
9222-13	1000hrs Wet	90	106.74	1.69			
9222-23	1000hrs Wet	90	106.6	-			

When examining the failed specimens a clear shear failure could be seen and appeared to correlate to the ply position through the matrix. Figure 99 shows an example of a lug where the outer set of plies have been removed to reveal the failed surface. At this point a 135° ply and 90° ply can be clearly seen. The 0° fibres are clearly intact in all cases, until final failure. One of the 0° plies has been exposed and can be clearly seen in the figure. These failures occur at relatively equal intervals, through the thickness of the sample as seen in figure 99.

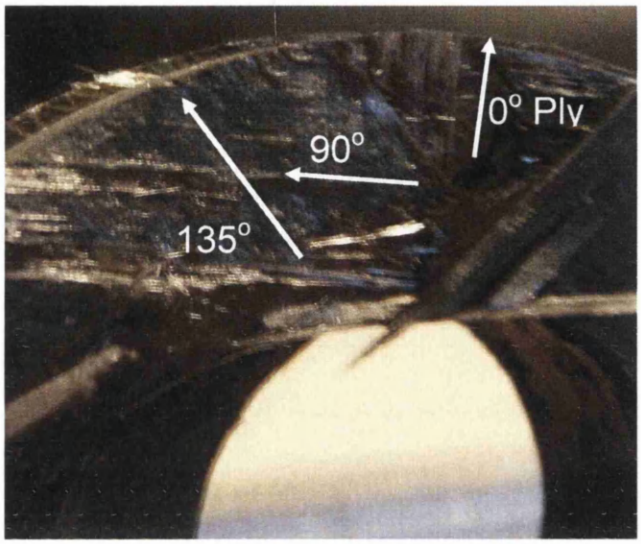

Figure 99 Failure Surface of a Lug Loaded to Ultimate Failure Point

When looking at the top surface of the lug, shown in figure 100, it can be seen that multiple ply failures have occurred once the lug has reached ultimate strength. This fracture surface did however vary across samples, as shown in figure 101.

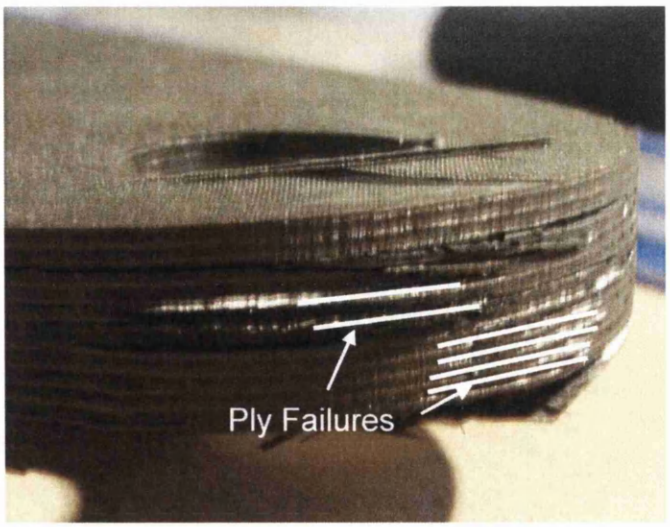

Figure 100 Showing 12mm Specimen Showing Typically Characteristic end after Ultimate Failure

Figure 101 shows typical failure acting at 45° to the 0° fibre direction. On further inspection, what appear to be a net-section style failure mode has occurred. This is likely to be as a result of dimensional inaccuracies in the coupon, which has lead to uneven loading. The shear failure has occurred on the right hand side of the lug and once failed has acted as a lever causing a secondary failure, above the ultimate strength of the lug, which has caused a secondary net-section failure.

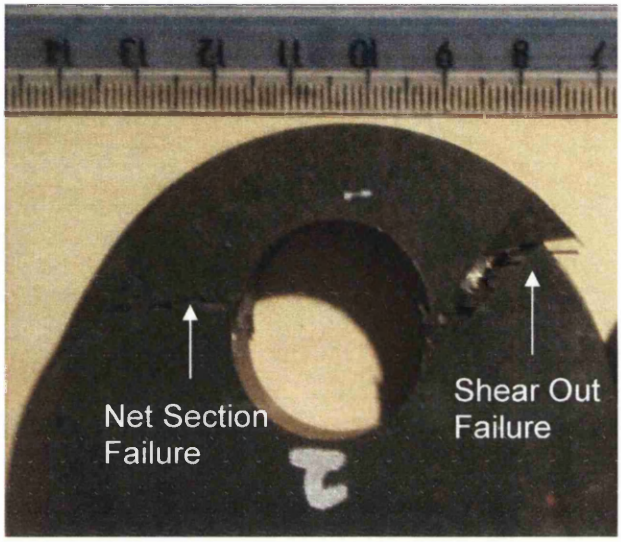

Figure 101 Showing Initial Shear-Out Failure, Followed by a Net-section Failure

From the data in table 30, the results can be plotted to show degradation in performance, brought about by the presence of moisture after 1000hrs conditioning. It can be clearly seen that for both wet and dry material, an increase in performance can be seen that appears to be as a result of temperature. This increase in strength equates to a 2.78% increase in strength for dry tests and 3.63% increase between the wet tests. Comparing the room temperature tested lugs it can be seen that there is a 4.5% drop in load carrying performance brought about by the presence of moisture. When carrying out the same comparison at 90°C a 3.5% reduction in strength is observed. The B-values are displayed and show a 12.4% reduction in dry/20°C test, 10.4% reduction in dry/90°C tests, 14.5% reduction in conditioned/20°C tests and only a 5.5% reduction in conditioned/90°C tests. Overall a significantly lower reduction in strength is seen than would typically be expected and means the application of a 0.8 reduction factor on the lug predictions for B-basis was too conservative (figure 102).

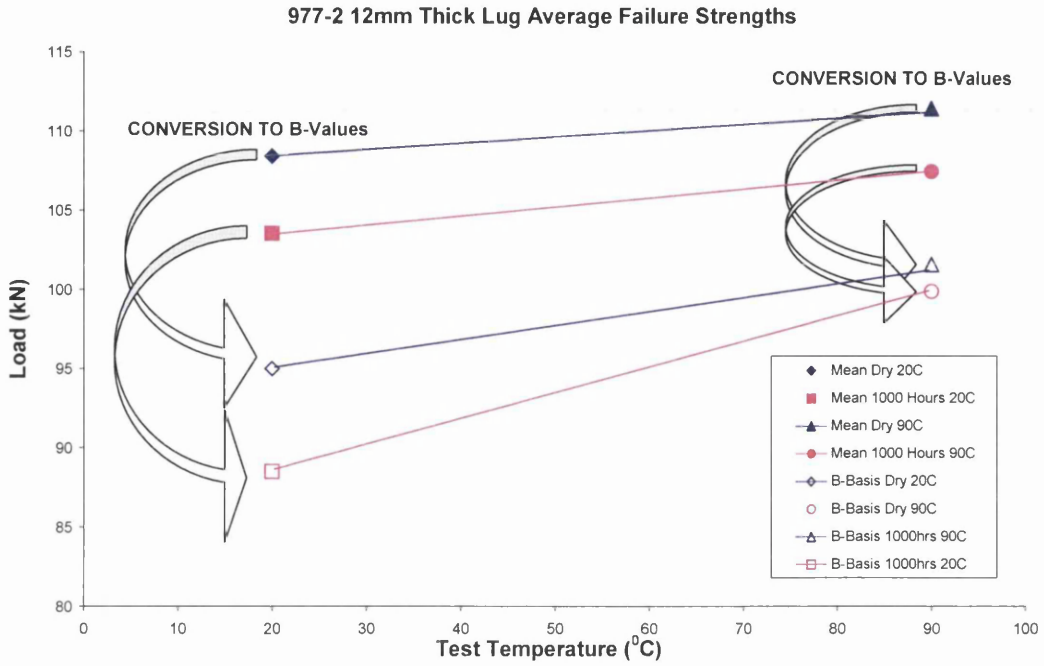

Figure 102 Showing Maximum Load at failure for Dry & Conditioned Lugs, with B-Values also Shown

To help account for the improvement in load carrying capability between tests conducted at 20°C and 90°C the shear strength data for both M21 and 977-2 materials is shown in figure 103. It is clear that the M21/T800 material has superior shear strength performance to the 977-2 material. When focusing on the 977-2 material it can be clearly seen that the basic shear test exhibits good agreement with the lug tests. This not only helps validate the improvement in strength seen, but also helps reinforce that the failure mode being seen is a shear failure, as predicted, when designing the coupon geometry and making strength predictions.

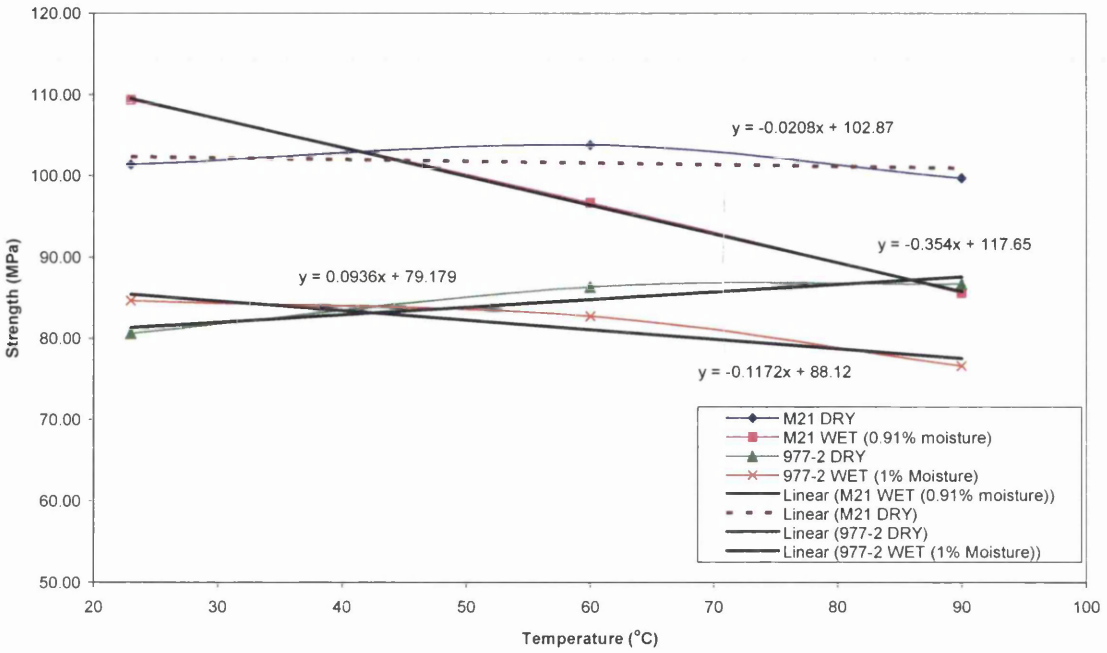

Figure 103 Showing In-plane Shear Strength Comparisons for 977-2 HTS & M21 T800 Materials in both Dry and Fully Conditioned states as Temperature is increased

Table 31 shows the results for the 26mm lug test carried out in the conditioned state and tested at 90°C. Results appear to be in good agreement with B-values, using the Weibull method resulting in a reduction in strength of 5.4% compared to the mean value.

Table 31 26mm Thick Lug Tests Results Conditioned for 1000 hours at 70°C/85%RH and Tested at 90°C

977-2 26mm Thick Lug Results									
Specimen No.	Condition	Temperature (°c)	Load (kN)	Theorectical Net Section Stress (MPa)	Theorectical Shear Out Stress (MPa)	Displacement (mm)	Average Load (kN)	Average Displacement (mm)	B-Basis Load (kN)
9227_01	1000hrs Wet	90	517.54	191.40	723.44	3.82	510.57	3.74	482.85
9227_04	1000hrs Wet	90	500.96	185.27	700.26	3.64			
9227_05	1000hrs Wet	90	513.95	190.07	718.42	3.76			
9227_06	1000hrs Wet	90	509.83	188.55	712.66	3.75			
9227_07	1000hrs Wet	90	503.95	186.37	704.44	3.65			
9227_08	1000hrs Wet	90	514.93	190.43	719.79	3.78			

Typical failures can be seen in figures 104a & 104b, which correlate well to the 12mm lug tests, showing similar fracture surfaces. Again failure occurred typically at 45^0 to the 0^o ply and loading direction.

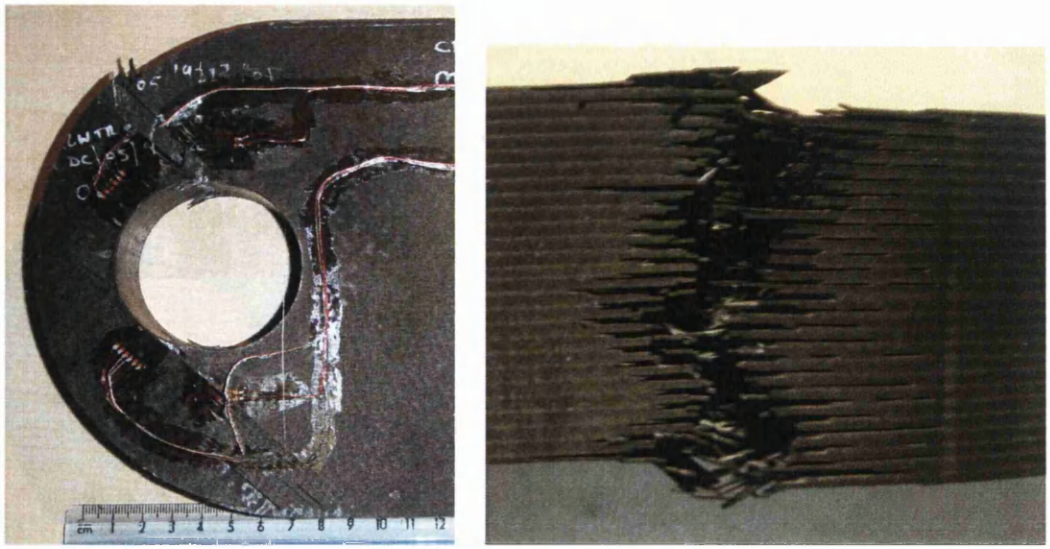

Figure 104 a) Large Lug Failure at 45° to Loading Direction b) the Fracture Surface on the end of the Same Lug

6.5 Comparison of Pre-test Sizing to Test Results

Figure 105 shows an overall summary of the pre-sizing predictions and actual test results. The test data presented is mean data. Firstly it can clearly be seen that the modelling approach predicts a slightly higher reduction in strength between the dry samples, tested at room temperature and wet samples tested at 90°C. Using the original moisture distribution curve derived from Airbus data it can be seen that the model over estimates the performance of the lug, which is also the case for the RT/DRY case, predicted using EMOC data. When an assumed B-basis factor is used (0.8% of original strength), both data points become conservative. Using the modified EMOC moisture profile it can be seen that the result is much closer to predicting the actual mean strength derived from test. It should be noted though that the maximum moisture content in this case, as previously discussed, is unlikely to be accurate.

For reference a calculation was performed assuming HOT/WET material properties, derived from the EMOC database. In this case the material is assumed to be fully saturated through the thickness. Clearly this is extremely conservative compared to the actual results, showing a prediction of -26% of the actual test result.

Overall it appears that the modelling approach is predicting similar behaviour to the tests, however it is clear that further refinement is now necessary to ensure accuracy of the predictions and in all cases it is preferable to be able to model the actual test value, but in reality to ensure a conservative prediction.

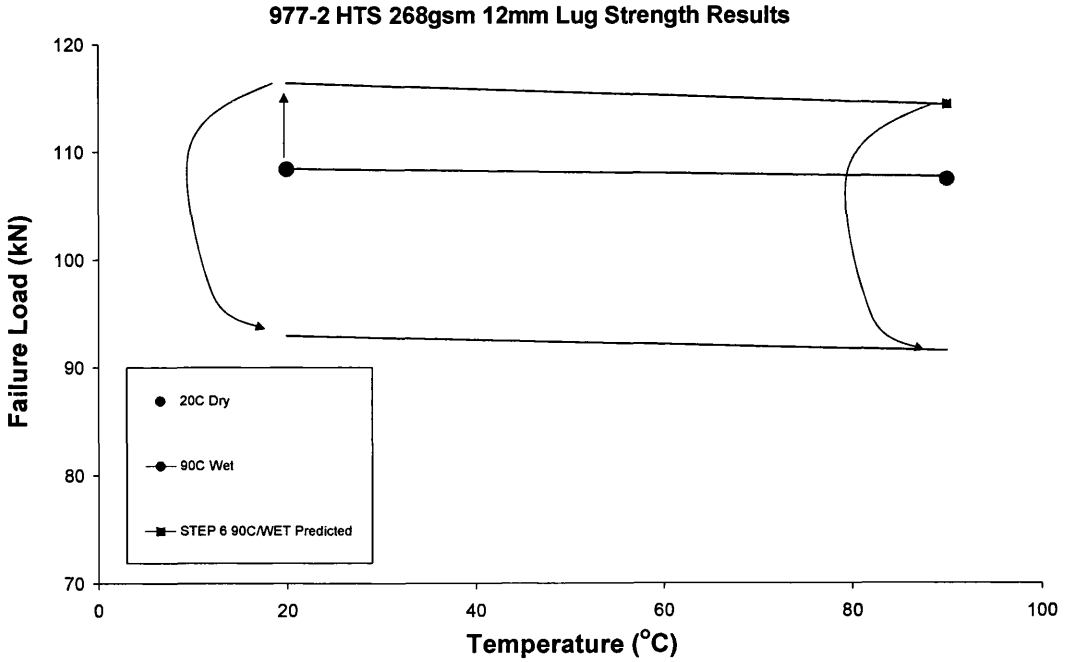

Figure 105 Shows a Comparison between the Predicted Load and Actual Test Load of the 12mm Thick 977-2 Lugs

When comparing the initial sizing calculations to the mean load obtained from testing it can be seen that the predictions are in good agreement (see figure 106), however the predictions are non-conservative predicting slightly higher failure load by 2.5%. However when using a conservative B-basis factor of 0.8, the pre-sizing produced a conservative estimate, which is 18% below the actual mean failure load value. In reality the test results showed little scatter and as such the knock down over the mean load was only 5.5%.

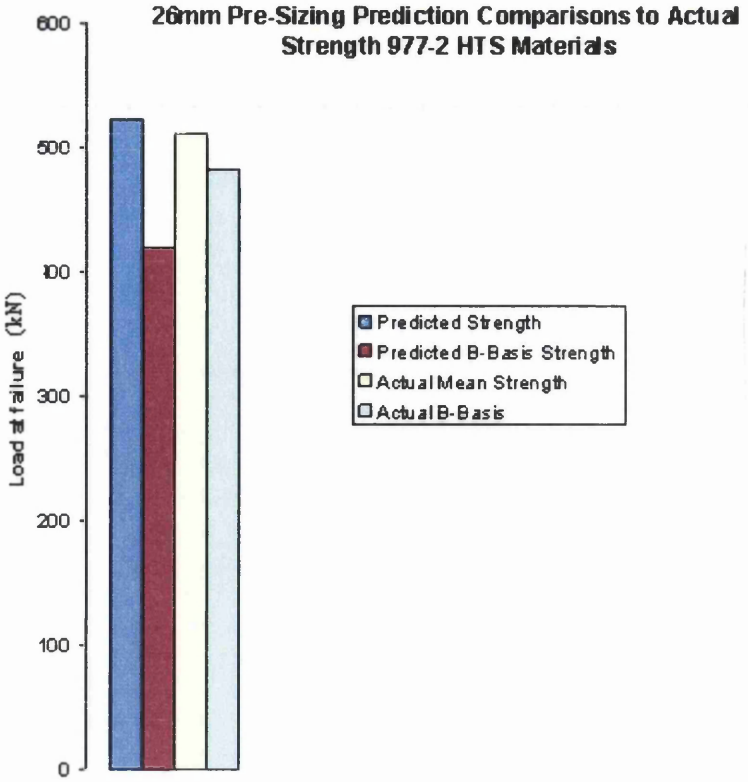

Figure 106 26mm Thick Lug Conditioned for 1000 hours at 70°C/85%RH, Tested at 90°C Comparing Test Data and Actual B-values Generated from Test Data to Pre-Test Predictions

6.6 EMOC Material Properties

The mean data is presented in this section for each mechanical property generated. The overall moisture uptake curves for the specimens can be found in Appendix A, figure A27. For an assessment of scatter all data points for each test type are presented in Appendix A, figures A.22-A.26. These mechanical properties have been used for the lug case study previously discussed. For the actual ELAP 1D tool it will be necessary to use the mean data based on the EMOC test data available. However for aircraft structure sizing the B-basis values will be required to ensure statistical conservatism. Typically B-basis values are not used in this thesis as it has been necessary to replicate actual performance of the parts tested and secondly budget constraints resulting in relatively small sample sizes, it was not always possible to produce robust B-values, without further testing.

In terms of moisture uptake, three samples of each condition were monitored until saturation occurred (no further noticeable increase in moisture recorded over three week period). The results of this are shown in the Appendix, figure A27. It should be noted that the time scale used is the square root of time, which indicated that the coupons may not be at saturation. This is likely to be due to non-Fickian behaviour, not specifically considered by this project. When plotting moisture uptake over time the coupons all appear to have all reached saturation.

Figure 107 shows the in-plane shear modulus of the 977-2 HTS material tested. It can be seen that there is a clear drop off in strength through the application of moisture, which becomes significantly more pronounced with increased temperature. The equations produced shall be used by the EMOC modelling tool and for the hand calculations carried out for the lug case study, to define mechanical properties. These linear equations have been generated and used in the same way for all mechanical properties investigated herein. In this case there is good fit between the test results and the linear profile.

Figure 108 shows a good fit to the linear trend lines added to the dataset, especially for the typical design temperature of 90°C, giving confidence in the resultant equations. In this instance overall there is a significant drop in mechanical performance with moisture and temperature, however the results are not as consistent, mainly due to scatter in the dataset (see Appendix A, A.23), this scatter means that the B-basis numbers generated would be too conservative and therefore additional tests are required to enhance the results.

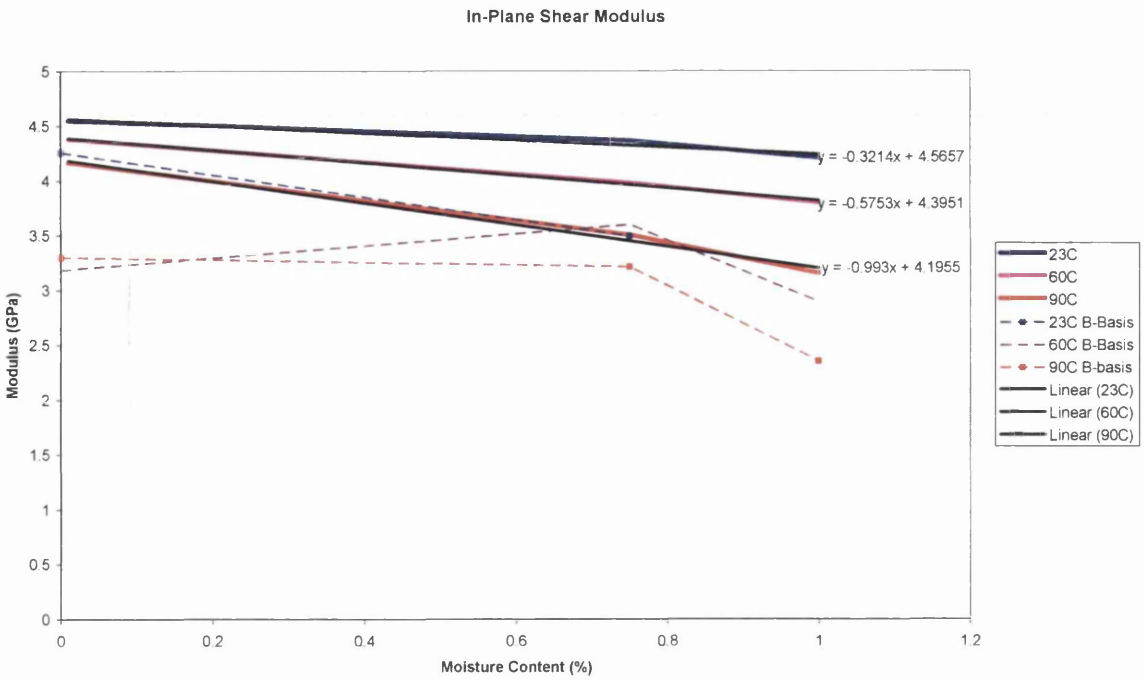

Figure 107 EMOC In-Plane Shear Modulus Data for 977-2 HTS Material Showing Modulus reduction for Increasing Moisture Content Investigated at Three Different Operating Temperatures

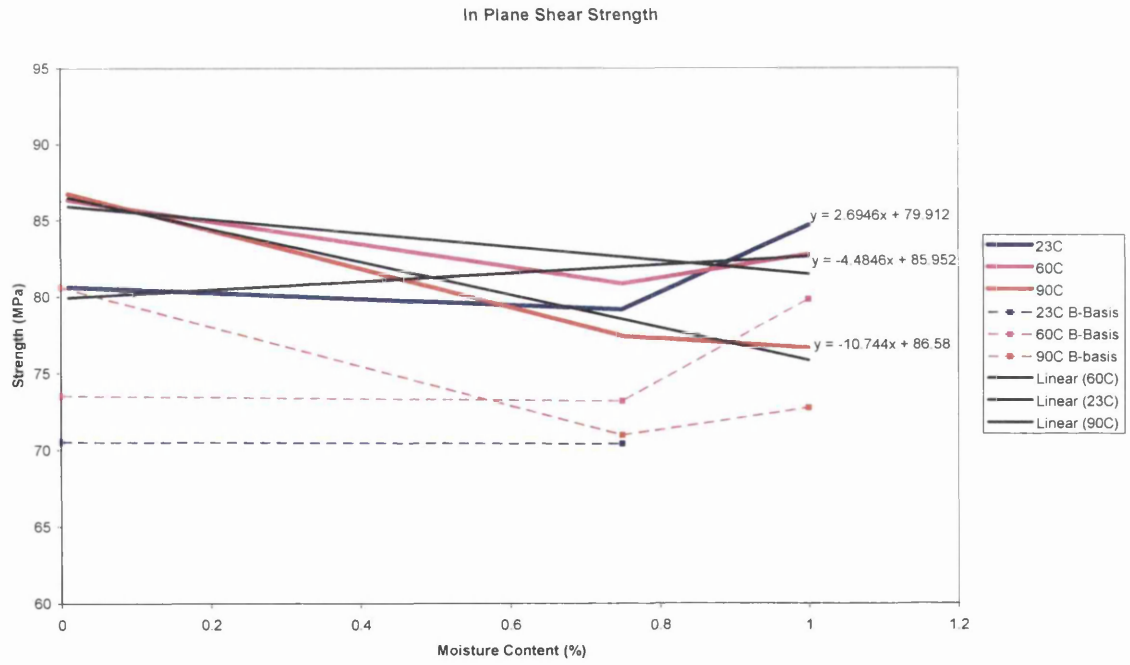

Figure 108 EMOC In-Plane Shear Strength Data for 977-2 HTS Material Showing Strength reduction for Increasing Moisture Content Investigated at Three Different Operating Temperatures

Figure 109 shows the 90° tensile modulus. With the exception of the 90°C tests, a linear reduction in strength is observed with increasing moisture levels at all temperatures tested. Generally when no moisture is present at all three temperatures tested the coupons appear to be of similar strength, this is taking into account the outlier on the 90°C sample set, which has artificially increased (see Appendix A, figure A.24) the mean strength in this case. B-basis values have been generated; however the numbers generated do not represent the material behaviour observed using the mean values, which can be attributed to the small sample size tested.

Figure 110 shows the perpendicular tensile strength, which clearly shows a marked drop in performance even at room temperature, which is extenuated further as temperature is increased. The decrease in properties generally follows a linear degradation, again with the exception of the 90°C batch at 0.75% moisture, which can be attributed to an outlier in the batch, which again will affect the generation of B-basis values. Again the B-basis values are misleading showing an enhancement in material performance, attributed to small batch size.

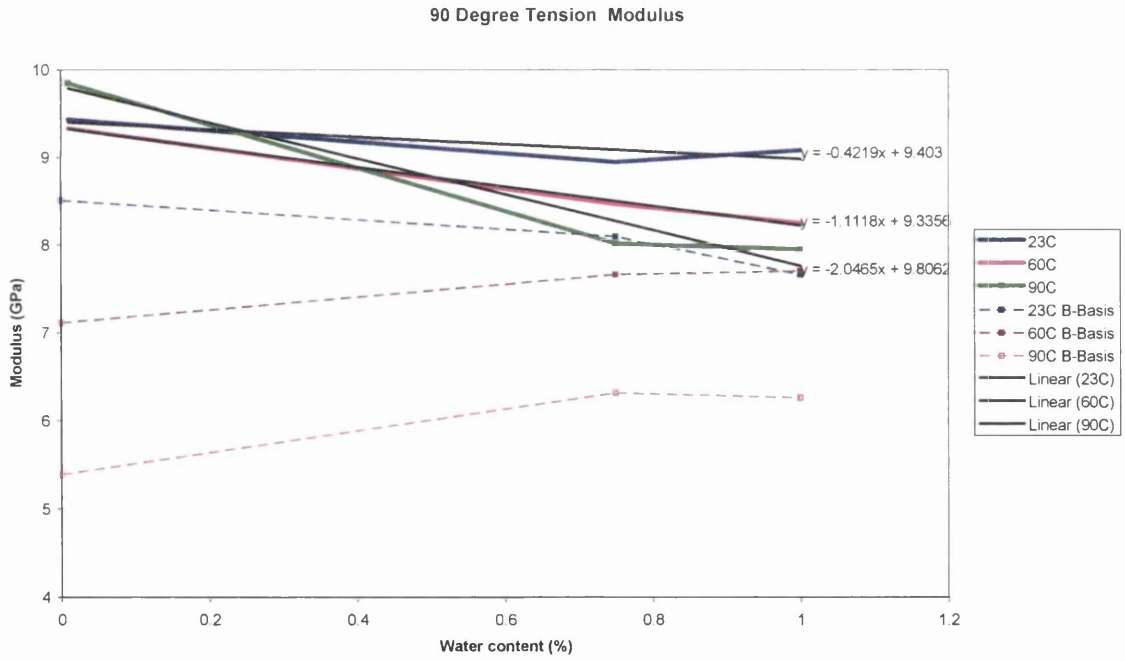

Figure 109 EMOC 90° Tensile Modulus Data for 977-2 HTS Material Showing Modulus reduction for Increasing Moisture Content Investigated at Three Different Operating Temperatures

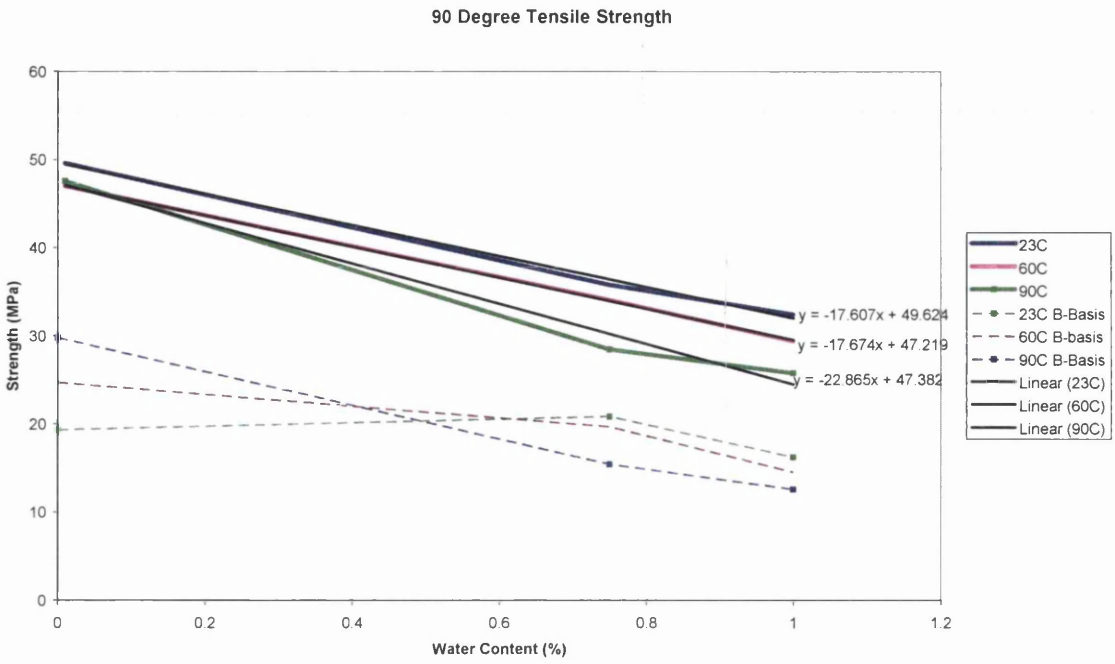

Figure 110 EMOC 90° Tensile Strength Data for 977-2 HTS Material Showing Strength reduction for Increasing Moisture Content Investigated at Three Different Operating Temperatures

With the limited number of coupons available, it was not possible to determine the compressive modulus, as this requires a separate set of coupons to be manufactured [13]. The mean compressive strength dataset (shown in figure 111) appears to show a good correlation to degradation of mechanical performance with temperature and moisture content. However 5 specimens had problems such as poor tab alignment, which appears to have affected individual results (see Appendix, A.26). In terms of B-Basis numbers the small single batch size of six does not allow the degradation of the material properties to be accurately tracked for the 60°C batch and therefore the B-basis numbers could not be used for analysis. However the room temperature and 90°C samples, appear applicable in this instance.

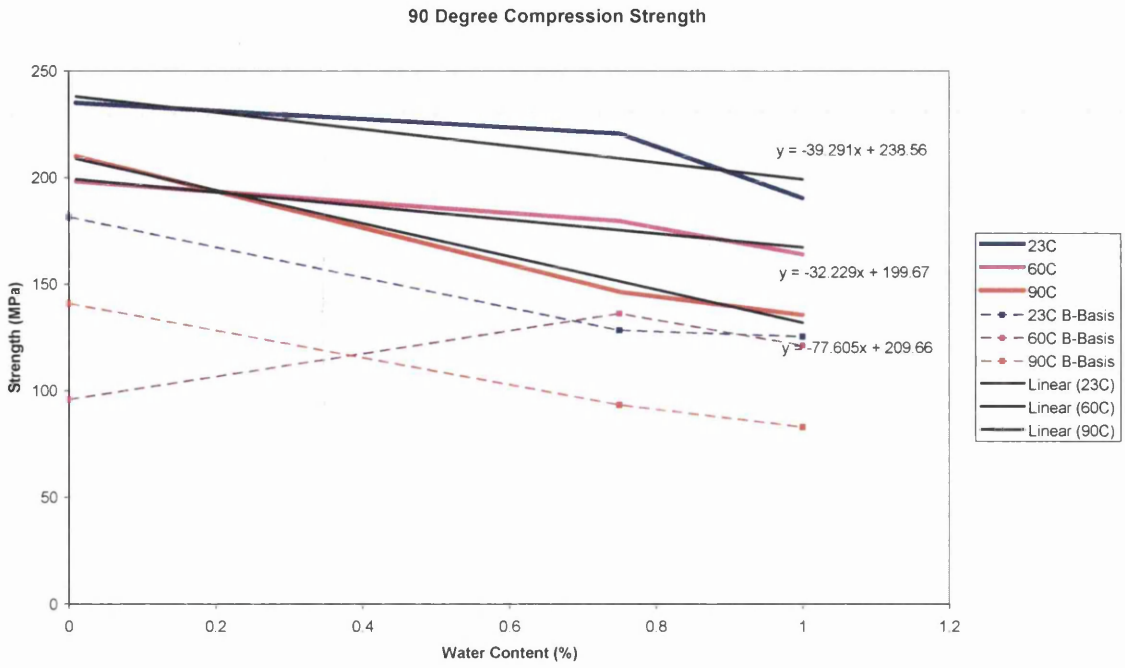

Figure 111 EMOC 90° Compression Strength Data for 977-2 HTS Material Showing Strength reduction for Increasing Moisture Content Investigated at Three Different Operating Temperatures

6.7 ELAP 1D Model Validation Results

The results of the calculations are shown in tables 32-35. As both LAP and ELAP agree to within two decimal places only the results of the ELAP model are shown.

Table 32 Effective Membrane Stiffness for Three Test Cases

	Case 1	Case 2	Case 3	Units
E_{xx}	63262.9	74354.1	84410.8	N/mm^2
E_{yy}	63262.9	49874.1	54167.2	N/mm^2
G_{xy}	24094.6	23070.5	20271.7	N/mm^2
V_{xy}	0.3128	0.36601	0.31331	
V_{yx}	0.3128	0.24552	0.20105	

Table 33 Expected Strengths for Test Case 1. Load (N/mm)

	Failure	Max Stress[1]	Max Strain[2]	Hoffman[2]	Tsai-Hill[1]	Tsai-Wu[2]	Layers
+Nx	1st ply	1617.77	1458.77	1444.46	1565.37	1376.18	2,6,11,15
	Ultimate	3194.84	3260.48	3201.67	3194.58	3196.43	
+Ny	1st ply	1617.77	1458.77	144.46	1567.37	1376.18	4,8,9,13
	Ultimate	3194.84	3260.48	3201.67	3194.58	3196.43	
-Nx	1st ply	1981.92	1982.49	2006.32	1982.76	2016.24	1-16
	Ultimate	1981.92	1982.49	2006.32	1982.76	2016.24	
-Ny	1st ply	1981.92	1982.49	2006.32	1982.76	2016.24	1-16
	Ultimate	1981.92	1982.49	2006.32	1982.76	2016.24	
Nxy	1st ply	1527.19	1111.19	932.217	1110.41	862.451	1-16[1]
	Ultimate	1527.19	1261.52	1234.88	1110.41	920.791	1,2,4-6,8,9,11-13,15,16[2]

Table 34 Expected Strengths for Test Case 2. Load (N/mm)

	Failure	Max Stress[1]	Max Strain[1]	Hoffman[1]	Tsai-Hill[1]	Tsai-Wu[2]	Layers
+Nx	1st ply	1454.54	1285.89	1261.32	1386.34	1194.6	4,9
	Ultimate	2881.68	2878.4	2981.95	2842.08	28882.23	
+Ny	1st ply	933.43	862.53	855.98	912.60	823.30	1,5,8,12
	Ultimate	1800.44	1827.28	1679.57	1736.16	1745.03	
-Nx	1st ply	1748.59	1747.54	1696.98	1739.31	1680.79	1-12
	Ultimate	1748.59	1747.54	1696.98	1739.31	1680.79	
-Ny	1st ply	1170.54	1172.19	1233.86	1167.38	1266.21	1-12
	Ultimate	1170.54	1172.19	1233.86	1167.38	1266.21	
Nxy	1st ply	947.54	941.12	699.61	820.60	654.62	1-12[1]
	Ultimate	947.54	941.12	699.61	820.60	823.03	3,10[2]

Table 35 Expected Strengths for Test Case 3. Load (N/mm)

	Failure	Max Stress[1]	Max Strain[2]	Hoffman[2]	Tsai-Hill[1]	Tsai-Wu[2]	Layers
+Nx	1st ply	1349.36	1216.51	1204.51	1305.51	1147.5	5,6
	Ultimate	2795.48	2795.33	2801.27	2795.26	2796.83	
+Ny	1st ply	831.54	780.65	780.13	820.73	755.07	2,3,8,9
	Ultimate	1674.64	1813.83	1526.54	1602.22	1626.7	
-Nx	1st ply	1652.79	1653.25	1672.54	1653.47	1680.56	1-10
	Ultimate	1652.79	1653.25	1672.54	1653.47	1680.56	
-Ny	1st ply	1058.63	1060.91	1156.76	1061.37	1206.57	1-10
	Ultimate	1058.63	1060.91	1156.76	1061.37	1206.57	
Nxy	1st ply	803.05	584.30	490.19	583.89	453.51	1-10[1]
	Ultimate	803.05	626.38	654.31	583.89	486.01	1-3,5,6,8-10[2]

6.8 ELAP 1D Lugs Prediction Results

The through thickness moisture profiles for the thick and thin lugs are shown in figure 112-113, which were produced directly by the EMOC model using the most accurate moisture diffusion parameters available from the EMOC project.

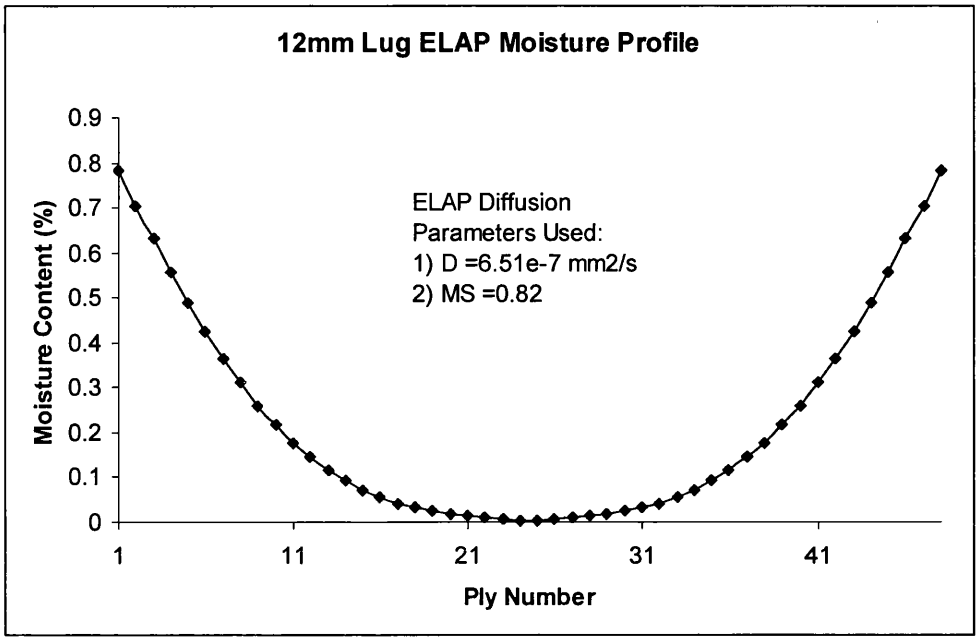

Figure 112 Showing the ELAP Predicted Moisture Distribution Cure for the 977-2 HTS 12mm Lug

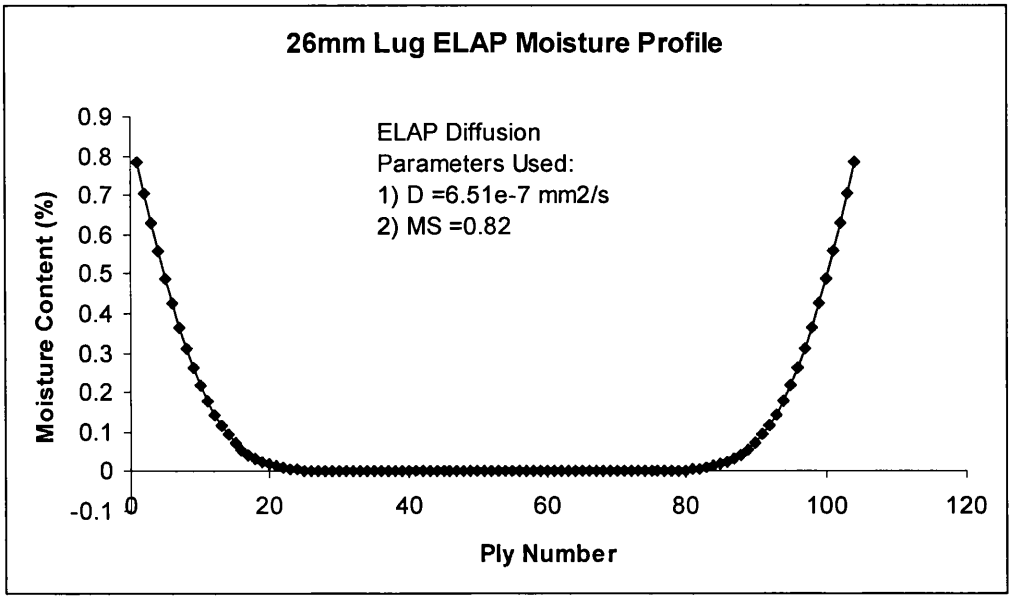

Figure 113 Showing the ELAP Predicted Moisture Distribution Cure for the 977-2 HTS 26mm Lug

Using the maximum stress criteria that was used to define previous laminate properties using LAP, the properties for 12mm & 26mm lug were generated, which are shown in table 36.

Table 36 ELAP Lug Material Properties Generated Using the Max Stress Failure Criteria

	12mm Lug (MPa)	26mm Lug (MPa)
Ex	54634	54809
Ey	54607	58821
Gxy	20655	20730
Vxy	0.32	0.32
Nx	798.53	798.53
-Nx	527.27	529.2
Ny	798.54	798
-Ny	527.27	529.34
Nxy	281.59	287.5

These material properties (table 36) combined with the same methodology for strength predictions allow the final strength predictions of the lugs to be made, which are shown in table 37. In this case each individual ply has its own unique set of mechanical properties based on its moisture level and can therefore be considered to be of the highest fidelity of all of the calculations performed. In both cases the calculations now fall slightly below the actual test value, which means they are slightly conservative.

Table 37 Lug Strength Predictions Using the ELAP tool

ELAP Lug Strength Predictions														
STEP Iteration Details	Iteration	Strength (LAP)			Stiffness (LAP)			Poissons Ratio Vxy	Geometry				Load (kN)	RF Shear Out
		Tensile (MPa)	Bearing (MPa)	Shear (MPa)	Ex (GPa)	Ey (GPa)	Gxy (GPa)		Edge Distance (mm)	Width (mm)	Thick-ness (mm)	Hole Diameter (mm)		
12mm ELAP 1000hrs 70C85%	2	798	737	281.59	54.634	54.607	20.655	0.3231	1D	48	12	24	104.9	1.000
26mm ELAP 1000hrs 70C85%	3	798	737	287.46	54.849	54.849	20.759	0.32	1D	156	26	52	502.5	1.000

6.9 Lug Weight Saving Identification Results

A summary of the mechanical properties can be seen in table 38. The first step shows the HOT/WET properties where the laminate is simulated in the fully saturated condition for both lugs. Using the derived thickness for HOT/WET properties a moisture profile was then generated simulating the aircraft life. This then produced the properties shown at 1000hrs, called iteration 1. A second iteration was then carried out for the

revised thickness to ensure that the modelling method had not resulted in an over optimistic thickness definition i.e. to ensure that the laminate was now not too thin to react the applied load. It is clear that there is significant improvement in the shear strength between the HOT/WET and derived ELAP property predictions, as would be expected, when considering the actual moisture profiles as shown in figures 114-115. A small improvement in the stiffness of the laminate is noted, although relatively insignificant, but this is likely to be due to the fact that the parallel and perpendicular compressive moduli of the lamina remain unchanged, due to the missing lamina properties that have not been generated by the EMOC project.

Table 38 ELAP Mechanical Property Results for Landing Gear (LG) and Thin Lug

STEP Iteration Details	Iteration	Strength	Stiffness ELAP		
		Shear (MPa)	Ex (GPa)	Ey (GPa)	Gxy (GPa)
LG HOT/WET	1	209	54.3	53.18	20.29
Thin HOT/WET	1	253	51.42	51.42	21.59
LG 1000hrs ELAP	1	290	54.89	54.88	20.75
Thin 1000hrs ELAP	1	307	52.37	52.35	20.56
LG 1000hrs ELAP	2	289	54.82	54.86	20.75
Thin 1000hrs ELAP	2	291	54	48	22.13

Figure 114 shows the derived moisture profile of the landing gear lug, starting with the thickness derived by HOT/WET properties. Clearly the lug remains largely unsaturated with only the outer plies of the material having any significant moisture concentration. This moisture profile was then used to derive the new mechanical properties and subsequent lug thickness shown in table 38 and 39.

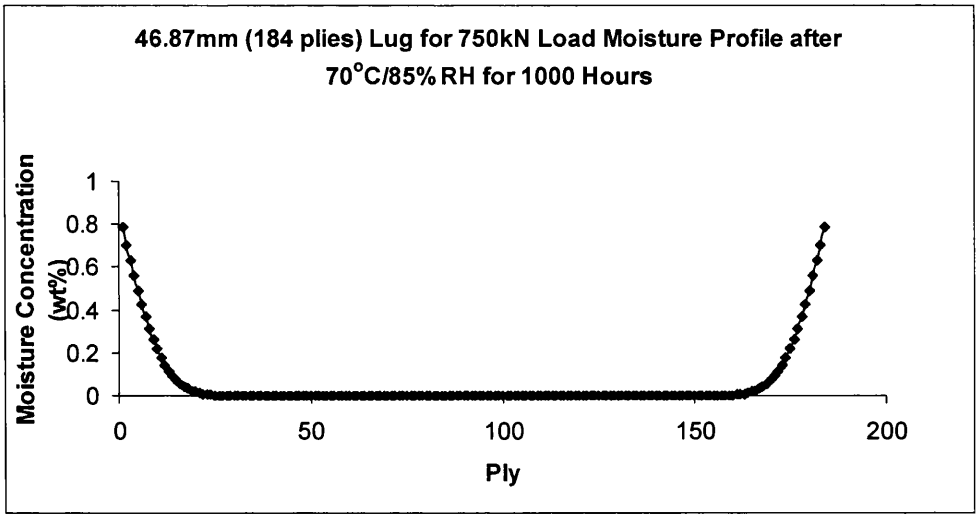

Figure 114 Through-thickness Moisture Distribution for Landing Gear Lug Based on the Thickness Initially Derived using HOT/WET Properties

The new derived thickness was then run through a second iteration, where the number of plies was determined by dividing the new thickness by the cure ply thickness. A new moisture profile was then produced for the reduced component thickness as shown in figure 115, with the new mechanical properties shown in iteration 2 in table 38.

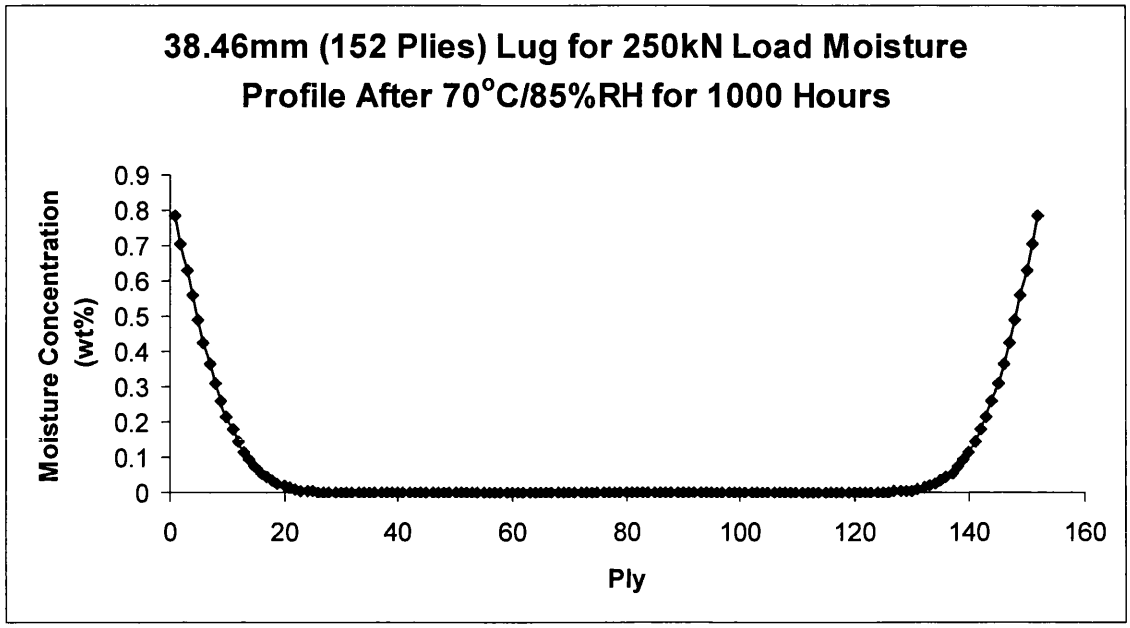

Figure 115 Through-thickness Moisture Distribution for Landing Gear Lug Based on the Thickness Derived Using ELAP Properties

Following the same process that has just been described for the landing gear lug two moisture profiles were produced for the small lug shown in figures 116-117. Clearly in this instance the amount of moisture in each ply is significant with even the core of the laminate having a significant moisture concentration that would affect the mechanical properties. That said the laminate can be considered to have a significantly lower moisture concentration through the thickness compared to a fully saturated laminate. The second iteration clearly shows an increased concentration, which was not so evident in the previous large landing gear lug simulation.

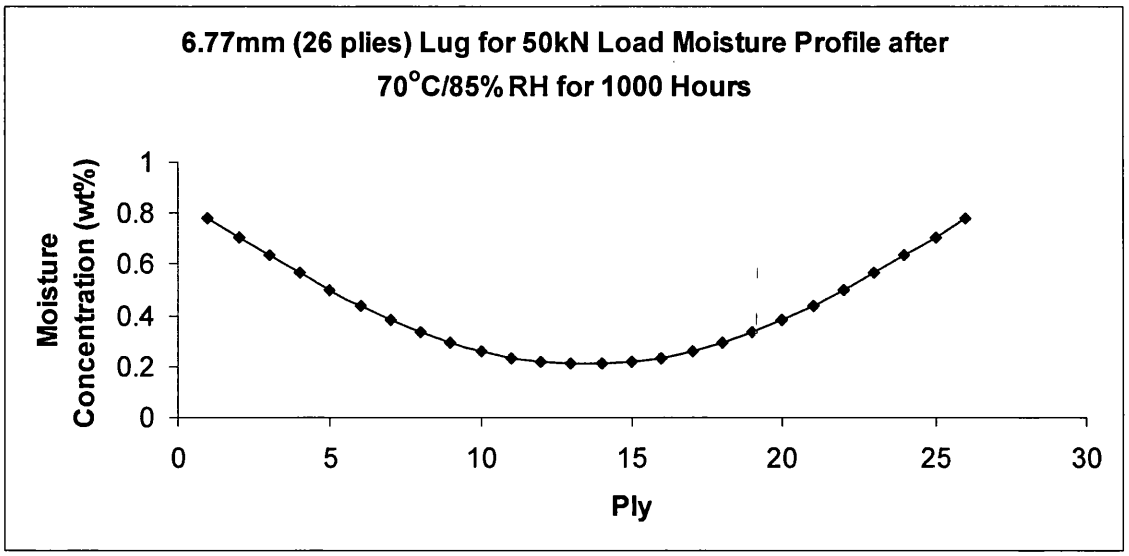

Figure 116 Through-thickness Moisture Distribution for Small Lug Based on the Thickness Initially Derived Using HOT/WET Properties

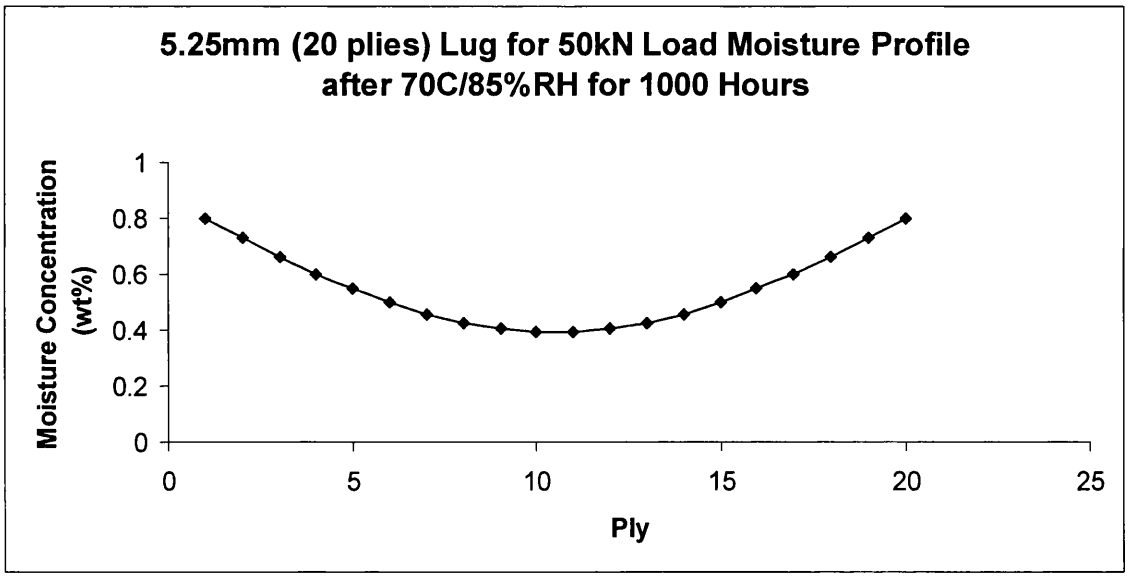

Figure 117 Through-thickness Moisture Distribution for Thin Lug Based on the Thickness Derived Using ELAP Properties

A summary of the geometric properties and thicknesses are shown for all iterations in table 39, these have been derived by the shear out sizing calculation used for the lugs case study.

Table 39 Geometric Properties & Thickness Results for Landing Gear (LG) and Thin Lug

STEP Iteration Details	Iteration	Geometry				Shear Stress (MPa)	Allowable Shear Out (MPa)	Load (kN)	RF Shear Out
		Width (mm)	No Plies	Thick-ness (mm)	Hole Diameter (mm)				
LG HOT/WET	1	156	184	53.37	52	209	209	750	1.000
Thin HOT/WET	1	72	26	6.37	24	253	253	50	1.000
LG 1000hrs ELAP	1	156	152	38.46	52	290	290	750	1.000
Thin 1000hrs ELAP	1	72	20	5.25	24	307	307	50	1.000
LG 1000hrs ELAP	2	156	152	38.54	52	289.4	289.4	750	1.000
Thin 1000hrs ELAP	2	72	22	5.54	24	291	291	50	1.000

Table 40 summarises the volume and subsequent mass calculations for each of the lug iterations. A typical CFRP laminate density was assumed. Clearly a reduction in mass is evident for both the thin and thick lug.

Table 40 Volume & Mass Estimations for All Sizing Iterations of the Landing Gear (LG) and Thin Lug

STEP Iteration Details	Iteration	Density (kg/m^3)	Volume (m^3)	Mass (kg)
LG HOT/WET	1	1650	1.19E-03	1.95610
Thin HOT/WET	1	1650	3.01E-05	0.04972
LG 1000hrs ELAP	1	1650	8.54E-04	1.40974
Thin 1000hrs ELAP	1	1650	2.48E-05	0.04097
LG 1000hrs ELAP	2	1650	8.56E-04	1.41266
Thin 1000hrs ELAP	2	1650	2.62E-05	0.04323

Table 41 shows the ELAP 1D weight savings achieved compared to using the HOT/WET approach, as derived from the mass calculations in table 40. Clearly the larger lug, having a significantly dry core has the greatest weight saving potential. The thin lug still showed a significant weight saving, showing that for a laminate of 6mm a significant weight saving is still achievable. For both the thin and thick lug, it was not necessary to iterate more than twice from the HOT/WET initial thickness as the solution appeared to converge on the optimal solution quickly to within one ply.

Table 41 ELAP Derived Weight Savings for Landing Gear (LG) and Thin Lug

Iteration 1	Large lug	**27.93%**
Iteration 1	Thin Lug	**17.59%**
Iteration 2	Large lug	**27.78%**
Iteration 2	Thin Lug	**13.06%**

7. DISCUSSION

7.1 Comparison of Material Properties

Figure 118 has been generated from an Airbus material Qualification report, and compares mean data for 977-2 material. The baseline for strength in this case is room temperature dry data with the plotted data points being material properties at full saturation (70°C/85%RH), tested at 120°C. Clearly the degradation on strength is clear for most properties, with f_{2t} the 90° tensile strength and in-plane shear modulus (G_{12}) being affected greatest by the presence of moisture. The key point to be made is that there is very little drop in both tensile strength F_{1t}, which proved at the beginning of the project that the key properties affected by the presence of moisture and temperature were the resin dominated properties.

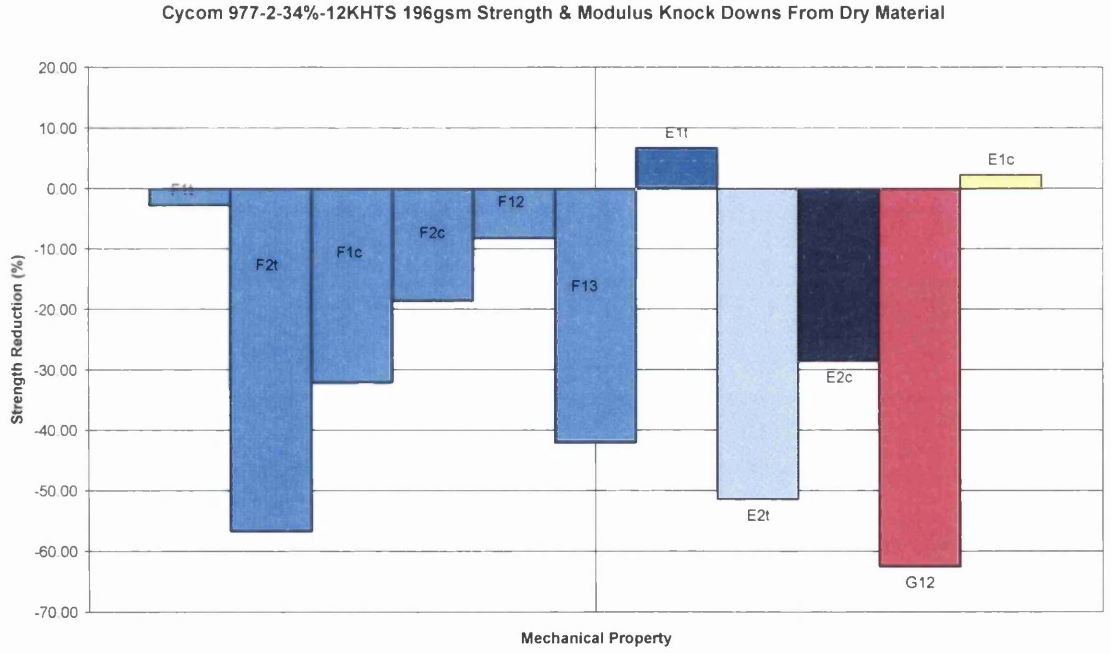

Figure 118 Comparison of Mechanical Properties using RT/DRY as the Baseline with HOT/WET Properties in this case Tested at 120°C Mean Values from Airbus Qualification Report Supplied by Material Supplier

Clearly there is a large drop in mechanical performance for many of the lamina properties, which is well understood. Classically when considering the design of a component, where laminates were relatively thin this approach appeared to be acceptable, where HOT/WET properties were used to size the structure in question. With Reference to figure 1, the ribs sizing tool has been used (discussed later), to

attempt to quantify the penalty of HOT/WET properties compared to RT/DRY. Clearly there is a weight penalty of 30% in this instance. This therefore provided the opportunity for the EMOC project to exploit this 30% penalty by applying more realistic mechanical properties and hopefully achieving a weight saving over the current philosophy. The opportunity for weight saving is obviously a function of the components' thickness, with the greater weight savings achievable as component thickness increases, because the amount of moisture through the thickness of the component will be less.

The basic principle of the project was to produce laminate properties at different levels of saturation that would be generated alongside a parallel programme to model the level of moisture through the thickness and assign these mechanical properties to each ply, thus producing laminate properties, which could be then used for structural sizing. The author of this thesis managed the overall programme and as the EMOC project continued, this led to a further number of small research packages designed to further investigate potential areas of weakness these included:

- MRes (Research Masters) 1, to investigate single & double lap bearing performance.
- MRes 2, to investigate Diffusion Coefficients of pure 977-2 resin and moisture diffusion in the x,y and z directions through the laminate.
- MRes 3 to investigate a new through thickness (F_{33}) test method that would be applicable to testing post moisture absorption.

Further to these smaller projects a Research Assistant (RA), was employed to develop the model produced by the complementary FE work. The RA would ensure that the models produced were to a commercial software standard and would allow the EMOC tool to have an interface with a mechanical property database, which would facilitate new materials being added at a later date. In parallel to this activity, Swansea University were contracted to generate further mechanical properties at elevated temperature that would supersede and improve on the initial mechanical property test programme that shall be discussed later.

7.2 Mechanical Testing Complementary PhD & MRes

As described previously an initial test programme was set up with a supporting PhD. This test programme, investigating all lamina properties, was very large, without

considering temperature. With such a large test programme and the PhD timescales for the student this restricted the investigation to room temperature testing only. The entire test data and material properties generated here are captured in [41], with a summary of the properties generated shown in Appendix A, figures A.28-A.34. Once the basic mechanical properties were determined the intention was to investigate directed laminates. In this case and for validation purposes the aim was to carry out quasi-isotropic tests with different amounts of dry core. Originally unidirectional coupons with a dry core were planned as well, however due to scatter in some of the UD results and problems during testing these samples were sacrificed for standard full saturation testing at different humidities. The model developed by PR1 [71], along with approximations made by PR2 were then expected to predict the mechanical performance of the OHC, OHT quasi-isotropic coupons. However, when the OHC & OHT coupons were manufactured, they were manufactured from a different version of the 977-2 HTS material, a woven 5-harness satin. The properties of this material are different to unidirectional tape and therefore it is not possible to accurately relate the mechanical performance to the UD laminate data, which was a major shortfall of the research built in by the Airbus team at the start of the programme, due to material availability.

Overall when considering the modelling tool validation at this stage it can be concluded that it was not possible to fully validate the model due to these shortcomings.

7.2.1 Material Property Degradation

Airbus typically tests the RT/DRY material in what is known as the as-received state. This means that coupons are tested once they are received from manufacture. As moisture absorption is a relatively slow process Airbus considers these coupons to be effectively dry. Therefore when planning PR2's supporting research no environmental control of the coupons was to be made. Furthermore, many of PR2's coupons were not scheduled for test on receipt of the coupons and in some instances coupons were left in an office environment for up to 18 months. Using humidity/temperature sensors in the office environment the temperature and humidity range the coupons were subjected to during this time was ~15 to 30°C and relatively humidity of ~30 to 90%RH.

On discovering these technical issues PR2 was instructed by the author to dry all further coupons prior to conditioning. Drying the coupons indicated that in the 18 month period up to 0.27% moisture [41] had been absorbed into the material, which as can be

seen from studying the results. Furthermore each batch of as-received coupons was tested at different times and as the test had already taken place there was no way to provide confidence in working out how much moisture was in each batch of coupons. Within all tests methods used there is a specific procedure to monitor the moisture absorption in specimens [9]. In all cases this procedure was not followed because it involves the manufacture of separate traveller specimens, which are then used to monitor moisture concentration for a batch of coupons. In hindsight if these procedures were followed this would have overcome many of the issues relating to measurement of moisture during and after conditioning. This method was deliberately ignored because it was felt that monitoring individual moisture uptake of each coupon would provide better fidelity, a decision made without considering end tab materials.

This error in coupon storage had a further knock on effect to all coupons that underwent conditioning. Although the diffusion value could be determined from the uptake of moisture overtime, it was not possible to have any confidence in the maximum moisture level achieved by each batch of coupons. Knowing the maximum moisture content at full saturation is critical to the success of the project, as it is essential when assigning material properties based on moisture content in each ply.

The application of Tufnol end tabs further added to the errors in understanding maximum moisture content. In all cases as instructed by Airbus test experts, Tufnol 10G/40 material was used to make the end tabs. This material is a precision made glass fibre woven material, which has an epoxy matrix. In most instances the end tab material forming part of the coupon exceeded the actual 977-2 test material in volume and mass. The epoxy used in the end tabs had its own unique diffusion characteristics and maximum moisture content and therefore in summary most of the uptake data in this instance is therefore specific to the Tufnol and not the 977-2 material. PR2 typically quoted maximum moisture content after conditioning at 70°C 85%RH of 0.87%, compared to the EMOC measured value of typically 0.82%. When considering the first error of poor storage of coupons, this further adds to the issue of measuring overall moisture concentration in the coupons.

Fibre volume fraction adds the final error to being able to accurately quote the moisture values in a material. The greater the amount of resin the greater the overall moisture uptake as a percentage weight of the coupon. Typically at Airbus and in published studies moisture values are quoted as a percentage weight of the coupon or component. However in this instance it is critical that the fibre volume fraction and

actual moisture content is known otherwise when material properties are assigned, based on moisture content there may be an error. Obviously this would be acceptable if an overestimate is made, however to ensure conservatism this would not be acceptable if the model were to underestimate the level of moisture in the structure as this would overestimate mechanical performance in this instance. Using 85, it is possible to mathematically take into account fibre volume fraction when calculating the maximum moisture content as a function of humidity, which shall be discussed along with the EMOC model later.

When talking to colleagues in the industry (Cytec and EADS Innovation Works in Toulouse France) the subject of non-Fickian diffusion arose. Residual moisture from non-Fickian diffusion is here defined as moisture chemically reacting with un-cured epoxy groups trapped within the matrix post cure. The water molecules react with the oxygen to produced OH groups as shown in figure 119.

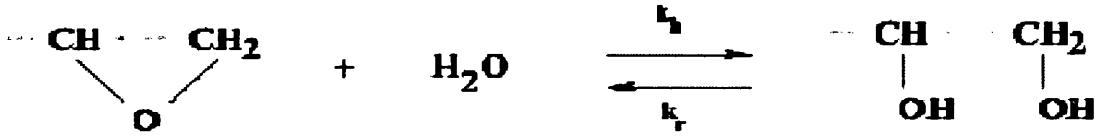

Figure 119 Typical Epoxy Group Reacting with Water Molecule Courtesy of EADS IW, Toulouse

It is possible to model this simplistically, however to do so would require the exact number of uncured epoxy groups to be known. As the mix of hardener (amine groups) and resin should be matched to ensure full cure of the epoxy it is not possible to determine this. However in a previous MRes project it was possible to quantify the amount of moisture taken into the material via this non-Fickian process [72]. In this instance the study included investigating residual strength after conditioning and drying. The conditioning cycle took coupons to saturation at 70°C/85%RH and then dried coupons in an oven until no further reduction in moisture was seen. These coupons followed [11,15] for perpendicular tensile and in-plane shear strength to quantify the non-Fickian moisture contents effect on strength. As can be seen from the results this was typically ~0.11% (see figure 120) and it was found that this level of moisture did have a small impact on strength. Ongoing unpublished work carried out by Swansea University on Airbus behalf verifies that over time this moisture is removed from the composite during prolonged drying cycles at a much slower rate, verifying that this process is reversible. For the purposes of this project and the finding of a relatively

small moisture content further work into modelling this phenomenon was not taken forward.

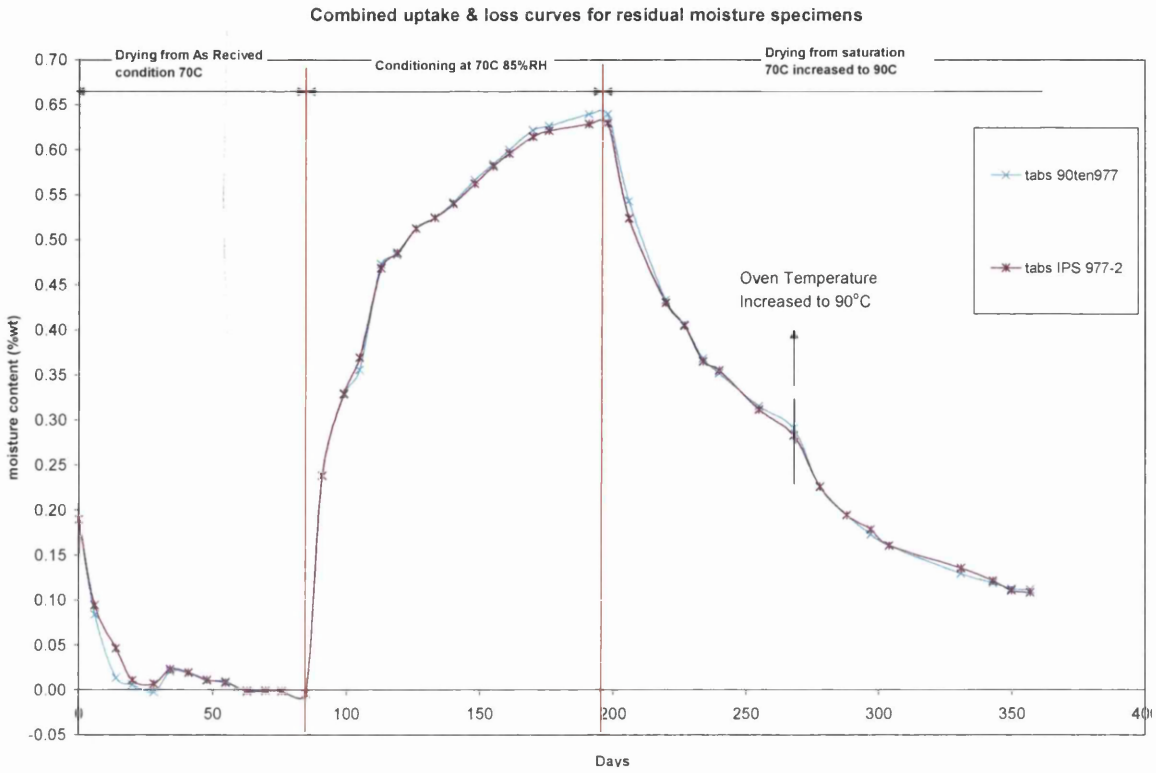

Figure 120 Supporting MRes Investigating Residual Moisture Trapped After Cycling to Saturation and Then Drying [72]

Figure 121, shows the results of the effect on strength due to residual moisture in the structure, with in-plane shear being more dramatically affected by the level of moisture. Another reason for discounting this effect is that even under accelerated conditioning at high temperature, the process is slow and would be insignificant when considering the worse case operating environment of 20°C 85% RH.

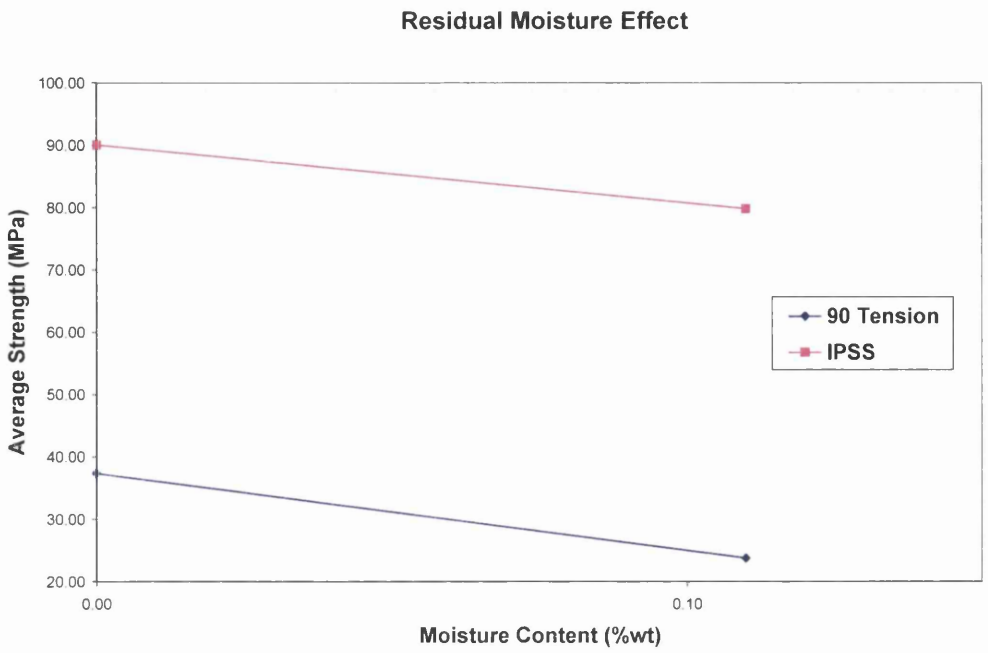

Figure 121 Supporting MRes Strength Affect Due to Residual Moisture [72]

Fibre volume fraction is another key factor that was previously not considered. It is clear from the literature [28,29,30,31,32,33] that it is the resin that absorbs moisture in the composite material. Therefore the greater the resins content within a manufactured laminate the greater the percentage of moisture that will appear to be absorbed by the laminate. Airbus manufacturing methods aim to achieve a fibre volume fraction of typically between 58 and 65%. Much greater than 65% fibre volume fraction results in not enough resin matrix to hold the fibres together. With this range in mind the measured amount of moisture at saturation would therefore be different for laminates with different fibre volume fractions. This will cause a problem when using the ELAP (EMOC Laminate Analysis Program) modelling tool because it assigns ply strengths based on the materials saturation level, which is based on mechanical tests for a dataset of a specific fibre volume fraction. If the component being modelled has a different fibre volume fraction for example a higher fibre column fraction, it would have less moisture as a percentage of its weight and therefore have optimistic material properties assigned to it. Therefore further development of the EMOC model is required to account for this to assign mechanical properties based on absolute moisture. To achieve this all assigned strength data needs to take into account fibre volume fraction when modelling, which can be done using equation 84. However when carrying out the structural analysis of a part not in production the exact fibre volume fraction would never be known and therefore a conservative approach would need to be adopted, perhaps assuming the lowest acceptable fibre volume fraction for

conservatism. In the initial studies no fibre volume fraction was measured, but this was implemented into all further testing to provide the data required during the modelling process.

The chambers used for the supporting PhD work, were supplied by Airbus throughout the duration of the project these chambers frequently broke down. To ensure the exact environmental history of the chambers was known humidity/temperature data loggers were employed to monitor the environmental history of the coupons. Typically, when a chamber breaks down the humidity drops within the chamber but the temperature is maintained, this results in drying and/or cycling of samples. When considering the phenomenon of non-Fickian diffusion, a key lesson is to ensure chamber redundancy and daily monitoring of equipment to help mitigate these risks.

7.2.2 Key Point Summary of Section 7.2

1. The initial supporting work (PR2) did not explore the effects of temperature in combination with moisture content, a key parameter that is required if this approach is to be adopted for aircraft structure.
2. No environmental control during coupon storage was enforced in PR2 leading to ambiguous moisture levels recorded post conditioning.
3. Uncontrolled moisture in coupons was quantified but could not be reliably accounted for as each batch of coupons had different storage time and therefore environmental exposure.
4. For PR1 modelling validation studies in association with PR2 the wrong material was used and therefore validation was not successful.
5. The usual traveller specimens used to monitor moisture uptake were not used instead favouring the measurement of each coupon compounded problems with determination of diffusion coefficients and maximum moisture due to end tab material.
6. Dissimilar end tab material, often summating to a greater volume and mass than the CFRP being tested led to the inability to reliably determine maximum moisture and diffusion coefficients for PR2.
7. Varying fibre volume fraction leads to different maximum moisture content across material batches, which should be taken into account in all future work.
8. Non-Fickian diffusion was observed within the test programme. It was discounted as significant due to the long conditioning times required to make it significant.

9. Non-Fickian diffusion leads to trapped moisture when drying samples, which appears to have a similar affect on strength as the moisture trapped by Fickian diffusion.
10. Chamber reliability was an issue during PR2, which could lead to undesirable cycling of samples, which should be avoided. Ensuring chamber redundancy in the future would prevent this.

7.3 Mechanical Property Investigations at Elevated Temperature

As previously discussed in section 6.2, an extensive test programme was undertaken, which was restricted to room temperature dry testing. Typically aircraft structures have to be designed to withstand higher operating temperatures. Airbus operating range for composites extends up to 120°C, although this is only in a few select areas such as along the leading edge of the wing, where bleed air ducting from the engines may subject the structure to these higher than average temperatures. When considering the temperature applicability for the EMOC programme, it was decided to restrict the applicability of the model to 90°C because in all materials considered within the programme their ceiling operating temperature for prolonged duration was 90°C. Long term exposure above this temperature can lead to material property degradation, such as micro cracking which was considered by the supporting PhD [41], As temperature is increased closer to the glass transition temperature these types of phenomenon begin to occur. This risk was also considered when setting the maximum conditioning temperature, where the temperature was restricted to 70°C in line with standard Airbus conditioning, rather than trying the accelerate conditioning time by increasing temperature.

7.3.1 Study into In-plane Shear Strength M21/T700 Material

As described earlier an initial investigation was carried out to consider the combined effect of temperature and moisture. Figures 93 & 94 show the effect on strength and modulus. As with PR2 data [41] when considering temperature without moisture the effect on the mechanical performance is relatively small, however it is clearly the combination of both moisture and temperature, which has a profound effect on mechanical performance. Although this was suspected from the beginning of the project, it highlighted that the only way the new modelling approach could be adopted would be to include the combined affects of temperature and moisture. Again ideally a large range of temperatures would be considered but due to the economics of the

project three temperatures were to be considered for all testing, namely 20°C or room temperature, 60°C & 90°C.

The combined moisture/temperature tests for strength and modulus show a clear linear degradation in mechanical performance, the linear equations are shown on the figures, which highlights the modelling principle that the EMOC modelling tool can use these equations to predict individual ply performance. For moisture tests without temperature the tests do not show a similar clear linear relationship, however the linear equations used could be considered conservative as the predicted mechanical performance would clearly be lower than reality. Again the use of end tabs clouds the true maximum moisture content.

7.3.2 New Control & Handling Procedures

From section 6.2, it can clearly be seen that there were issues with the control of specimens, which could lead to uncontrolled/unaccounted moisture diffusion before coupons were tested. Each step of the manufacturing process was evaluated and controls put in place as described in section 5.5. These procedures were then applied to the future EMOC test campaign discussed in section 6.3.4. The overall aim of these handling procedures was to ensure a traceable environmental history was maintained for all specimens in line with an auditable CAT 2 test programme. Enforcing such a procedure was a time-intensive and difficult exercise mainly due to the large number of stakeholders involved in the manufacturing process (Airbus manufacturing, materials and processes, design, stress), further complicated by the use of a subcontracting company for machining operations. One of the main controls was the environmental exposure of each batch of material, using vacuum bags, desiccant and humidity/temperature data loggers. The reality was that the vacuum bags failed to consistently maintain vacuum across batches and the data-loggers consistently showed high levels of humidity within the vacuum bags. The manufactures had not tested their data loggers in a vacuum environment so it is not possible to know if the readings taken by the data logging equipment were accurate. In summary the environmental control and recording of environmental history, especially when being handled by third party organisations was not practical. It was however possible to reduce the processing time of the coupons to limit exposure to the environment and weigh them at each stage to monitor moisture levels, which over a two week period appeared to be insignificant. As a clear recommendation and as a precaution during

the EMOC test campaign a drying cycle was applied to all coupons to ensure any moisture uptake as a result of the manufacturing process was removed.

It should be noted that water-jet cutting was used to extract coupons from laminates. This decision was made as the exposure to moisture is extremely brief; however it was reliant on the operator to ensure coupons were completely dried before returning them to a sealed environment.

It should be noted that data loggers were placed in the drying oven to monitor the ovens environmental parameters. The same loggers were placed in the desiccators where the coupons were stored prior to conditioning and in both cases humidity never reached zero. This could be down to the capability of the logging equipment at such low humidities, even though the logging equipment was claimed to be able to work from 0-95% RH. If the oven did in fact have humidity greater than zero, it would not have been possible to fully dry coupons and it may have actually led to some coupon pre-conditioning, however this was not observed during coupon weighing so was considered to be insignificant. Further investigation is necessary to fully understand whether any significant humidity existed in either the drying oven or desiccators, which would require the use of more sensitive sensors.

Having discussed the effects of non-Fickian moisture diffusion on the levels of moisture within the materials tested, attention should be drawn to the conditioning chambers. It was found throughout the test programmes that the chambers were typically used as storage buffers and it was assumed that once coupons had reached saturation, they could be stored in them until test. This seems to be a reasonable assumption as the non-Fickian uptake over short periods could be considered to be relatively slow and therefore insignificant (Appendix A, figure A.27 showing non-Fickian uptake continues over time). However in some instances due to other Airbus priorities coupons on occasion were sat at saturation for extended periods of time (up to a year). The extent of non-Fickian diffusion was not evaluated during this time as the test labs stopped monitoring coupon moisture levels once they reached saturation. The debate on the significance of this point would require further investigation and data generation, however none of the batches of coupons tested in this programme appeared to exhibit any unusual drop in mechanical performance, which could have been attributed to this. For future test programmes it would be prudent to avoid extended exposure to the conditioning environment, unless further investigations were conducted to investigate these parameters and define limits to ensure confidence.

Overall one of the best ways to limit moisture uptake was to ensure minimal time exposed to the environment between laminate cure in the autoclave and extraction of coupons. In all cases this was successfully limited to within two weeks thereby ensuring very little moisture uptake.

7.3.3 Removal of End Tabs

It has already been discussed that the end tabs caused significant problems with the derivation of both diffusion coefficients and also ascertaining maximum moisture content at a given relative humidity. For those test methods that require end tabs an alternative had to be found, as to ensure a successful valid test it is necessary to have the correct load introduction. The EMOC test programme followed an intermediate step, as instructed by the author, where the end tab material used was the same as the actual material being tested. This ensured that the measured moisture levels and diffusion coefficients were accurate for the material; however this methodology failed to deal with either an adhesive bond-line using a room temperature cure epoxy which was necessity for curing the tabs to the coupons. Furthermore when conditioning there was the added complication of material thickness, which was typically 2mm in the gauge section of the coupon and 6mm in the tabbed region, which will have had an effect on the time it takes for the material to reach saturation. Therefore when the test programme was commissioned to explore the M21/T800 material (outside the scope of this PhD) the removal of the end tabs, described earlier was used. Overall it can be concluded that where end tabs were removed the derived grips pressures etc, described in the results section were a success.

Overall the removal of end tabs for the M21/T800 material was extremely successful, with the exception of the 0°compression coupons, which failed in the tabbed region due to local crushing, which may have been attributed to the assembly of a non-bonded tab. The best way to overcome this would be to use end tabs as per the standards test specification and use traveller specimens to monitor moisture properties. Removal of the end tabs allowed the coupons to be manufactured more quickly than would have been otherwise possible and it did enable the moisture content of each individual coupon to be accurately measured. In terms of conditioning, it also offered the advantage of allowing the coupon to reach saturation in a more even manner than if any kind of tab had been bonded to the specimen. The alternative option would be to follow the mechanical test methods approach to conditioning and produce traveller

specimens of the same composite panel, thickness and fibre volume fraction to determine moisture uptake and the diffusion coefficient. Either methodology would appear applicable although following the tab removal approach would ensure improved accuracy as each coupon can be continuously monitored, although for large test programmes with large batch sizes, this is likely to be uneconomic.

7.3.4 Diffusion Values in Different Directions Relative to the Composite Fibre Orientation

The MRes student [73] successfully quantified the diffusion coefficient through the material in different fibre orientations. A summary of the findings can be seen in table 42. The fastest uptake of moisture is along the fibre ends 'D1', with the second fastest uptake being along the sides of the fibres. The slowest rate of uptake is therefore 'D3', which is typically the principal direction for diffusion in composite components. If these factors could be further proven, it would be possible to determine future diffusion values for the 'D1' & 'D2' relative to 'D3', which would reduce the amount of testing required to determine coefficients for 3D modelling purposes. Diffusion along fibre edges being typically 3.2 times faster in a humid atmosphere compared to the through thickness moisture update 'D3' indicates that where the edges of the composite are significant it would be necessary to take into account the faster rate of uptake, especially if only using a 1D simulation such as the 1D ELAP tool. It should be noted that when carrying out the lugs case study the fibre edges have not been taken into account, which may have accounted for the slightly optimistic sizing calculations (see section 6.3 & 6.5).

Table 42 Diffusion Comparison between Different Faces [73]

Condition	*D1/D2*	*D1/D3*	*D2/D3*
23°C Water	2.66	4.44	1.67
40°C Water	2.11	2.32	1.10
60°C Water	2.22	2.61	1.17
70°C Water	2.04	1.74	0.85
70°C 45% RH	1.79	3.45	1.92
70°C 60% RH	1.97	2.70	1.37
70°C 80% RH	2.08	3.45	1.66
Average	**2.13**	**2.96**	**1.39**

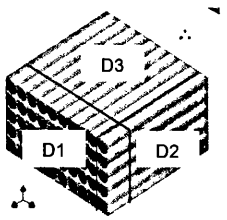

When comparing the diffusion parameters along the fibre ends to the pure resin samples, it appears that there is a good correlation, shown in table 43. It can be

hypothesised that this is due to the unrestricted diffusion path in both instances, which produces similar values compared to 'D1' & 'D3'. These comparable diffusion values were to be expected, with only the maximum moisture content being significantly different between the samples, which are a function of the fibre volume fraction of the material. Further work should be conducted to compare different D3 values for different lay-ups, continuing from these preliminary comparisons on discussed here.

Table 43 Diffusion Coefficient Comparison between 'D1' & the Neat Resin Samples Immersed in Water at Various Temperatures [73]

Condition	Cytec 977-2	
	Neat Resin	CFRP
	$D(x10^{-7}mm^2s^{-1})$	$D(x10^{-7}mm^2s^{-1})$
23°C Water	1.51	1.80
40°C Water	2.70	2.60
60°C Water	5.60	7.00
70°C Water	9.70	8.30

7.3.5 EMOC Material Properties

The commissioned EMOC test programme was designed to supersede the original supporting PhD firstly to overcome the shortcomings in the accurate measurement of moisture and secondly to allow the EMOC modelling tool to operate for the worse case high temperature operating conditions. As previously mentioned the maximum temperature investigated was 90°C, with various different moisture contents. The EMOC programme to date has not investigated the presence of moisture at temperatures below 20°C down to -55°C, which would be the full operating envelope of the aircraft. The reason for this is that all the work done so far by the EMOC project (and as found in the literature) shows that as temperatures increase up to the glass transition temperature of the material the stiffness and strength is reduced. As temperature is reduced the material becomes stiffer and more brittle. When considering the current aircraft design philosophy of utilising HOT/WET material properties, it would be prudent to carry out an investigation to study the effects of low temperature. Should such a mechanical testing programme be commissioned the EMOC modelling tool would easily be able to expand to cover a wider temperature range. No specific data was found in the literature on low temperature saturated testing, although data values for the COLD/WET case are typically generated by Airbus as part of the material

qualification programme, to ensure the full operating envelop of the material is understood.

The effectiveness of material handling parameters has already been discussed and as previously mentioned in this instance the end tabs were made of the same material as the composite being tested, to ensure an accurate moisture value at full saturation, which was 1% in this instance at 70°C 95% RH. Note that in ongoing research beyond this PhD it is the intention to start dealing in absolute moisture levels based on fibre volume fraction.

It should be noted that 0° Compression strength and modulus was not generated for the EMOC dataset. Due to resource limitations it was decided by the author that the critical properties needed were in-plane shear and 90° Tension, where the properties would be key in carrying out the lug predictions that would validate the modelling tool. Therefore a key mechanical property is missing from the dataset, 0° Compression. The absence of 0° was disappointing as the ribs sizing requires it to derive a shear strength based on shear stiffness, which is a function of the compressive modulus. Further complications with rib sizing shall be discussed in due course.

Firstly considering In-plane shear strength and modulus shown in figures 107-108, there appears to be a good linear fit in the reduction in modulus as moisture content increases for all temperatures with little scatter between coupons, however in this case it would not be appropriate to use the B-basis numbers because this would lead to an increase in mechanical performance, which clearly does not appear to be the case. Significant scatter was seen with regard to strength, which make the B-basis numbers invalid in this instance. Fortunately the dataset with least scatter was that generated at 90°C, which is what is used for the lug validation cases. Overall scatter wasn't significant, which means the only way to improve the B-basis values required for application to an aircraft component would be to conduct additional batches, with a rough order of magnitude of 30+ samples. Statistically using the methods described within the literature review, this would allow other methods besides the Weibull and Small samples methods to be utilised, thereby improving the fidelity of the B-basis results.

Comparisons were made for in-plane shear comparing M21 degradation to the 977-2 material focused on in the EMOC test campaign, shown in figure 103. Negating the small effect of temperature on dry material properties, it can clearly be seen that both

materials show a similar linear drop in performance, with the M21 material appearing to be affected to a greater extent by the combination of moisture and temperature. The aim of this comparison is to provide confidence that the modelling approach for strength reduction would be similar for different epoxies, which is clearly the case here. However it highlights that for EMOC to be a success, it will be necessary to develop material properties for the specific material being considered for any specific application. Airbus Composite Airframes typically use the same material for each component rather than adopting a cocktail of materials, which aids the EMOC principles in that it is unlikely that a huge array of materials would have to be tested to form an extensive database for modelling purposes. This is an important aspect when considering the huge amount of testing that this would otherwise imply.

For the 90^0 Tension Results shown in figure 109 & 110, the same situation occurs when considering the use of B-basis values. In this instance there is significant reduction in strength compared to modulus, in contrast to the in-plane shear tests previously discussed. When comparing to PR2 [41], it can be seen that there is significantly less scatter, especially in the room temperature dry condition. This is due to the way the coupons were machined, with the original supporting PhD utilising conventionally machined coupons, using a diamond tipped cutting saw. The EMOC coupons were machined using a water-jet cutting method, which made them significantly smoother. This particular test method is directly affected by the surface finish of the coupons, as discussed in [12] and therefore the EMOC coupons were deliberately machined using the water-jet cutting method to improve the scatter and produce a better data-set. Overall a linear equation provides a good fit for the use by the EMOC tool in terms of strength and modulus, with a slightly closer fit for strength.

Finally, 90^0 Compressive Strength also shows a good correlation to a linear reduction in strength (figure 111). In this instance it would be possible to use the B-basis data for 90°C & 23°C, as it mimics the overall mean performance of the data set. However in this case the 60°C test carried out in the dry state indicates a lower performance in the dry state, which leads to an exaggerated improvement in material performance as moisture content increases. As the dataset shows very little scatter, further testing would be required in the dry state to validate the results at 60°C. Note that as previously stated the compressive modulus is missing in this case, due to the lack of resources available at the time (a full extra set of coupons is required for the determination of modulus without end tabs). This was considered acceptable as the compressive modulus was not specifically required for the lug calculations.

The lack of compression strength when considering the sizing being conducted at first seems to be acceptable, however it adds risk, especially with the absence of CAI (compression after impact) data, which defines strain limits for ribs sizing. As mentioned previously one of the rib design drivers, which determines panel thickness is shear buckling, which uses a compression after impact strain allowable, as previously discussed. It would have been extremely useful to help set a strain limit for the shear buckling calculations, which could have been related to an undamaged strain allowable derived from compression data. Note that the use of CAI to determine an SAI (shear after impact) value is considered by Airbus to be conservative [51].

It should be noted that the lack of 90^0 Compressive Modulus and 0^o Compressive Strength/Modulus adds significant risk to this programme and it is highly recommended that these material properties are generated. The author has organised the generation of this data but unfortunately it will not be available before the submission deadline for this thesis. This could have further implications when using ELAP to predict overall laminate properties, which will be discussed later.

In terms of bearing performance [74] a clear degradation in mechanical performance was demonstrated for the double lap shear tests, clearly showing that the degradation in performance across all temperatures is significant. Overall bearing performance is reduced at all temperatures tested, as shown in figure 122.

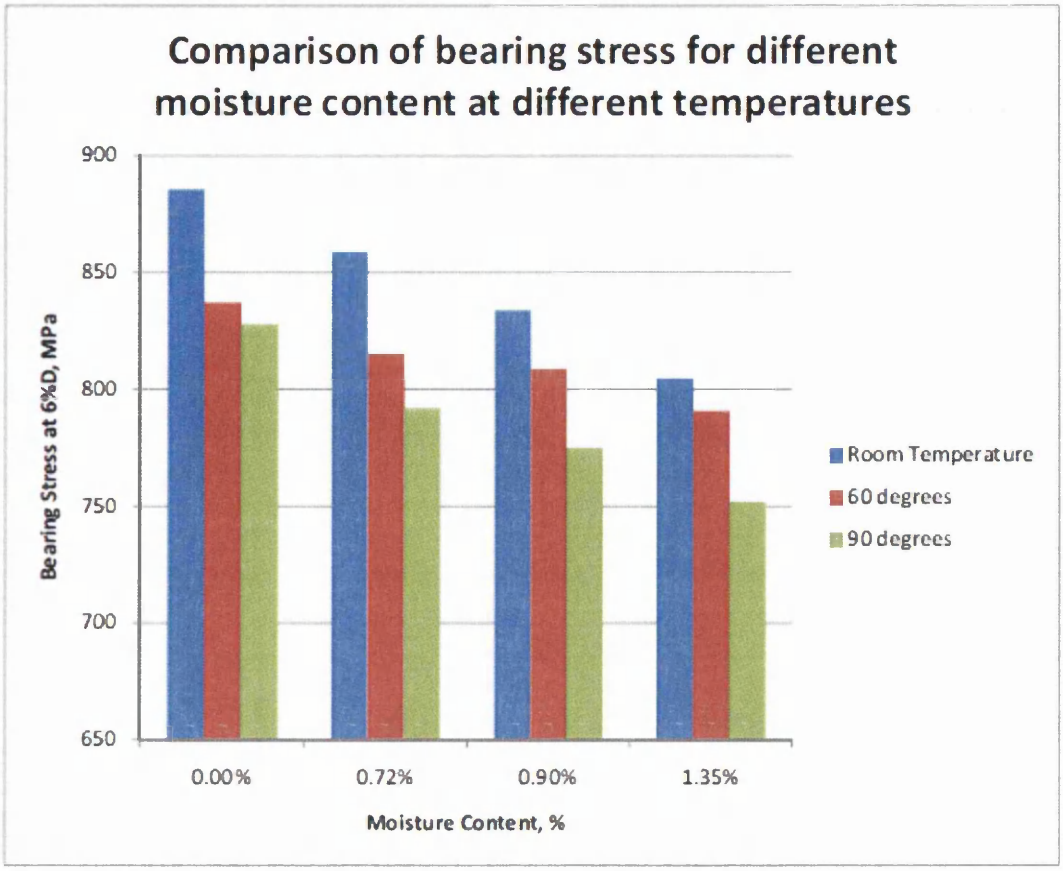

Figure 122 Double Lap Bearing Results [74]

Single lap bearing performance shows a similar linear reduction in strength due to temperature and moisture content, as shown in figure 123. The author's main aim in this work was to show that a similar degradation in mechanical performance existed for bearing failure as well as the basic mechanical properties of the laminate. However the data from the MRes student does not afford a definitive conclusion to be made, as it was not possible to extend the investigation to consider bearing performance after a realistic aircraft cycle (e.g. 1000hrs 70°C/85%RH). Also note that the 60°C data point for the dry condition is missing. These samples were used to generate the room temperature dry test point with 0% moisture as the original coupons were tested incorrectly.

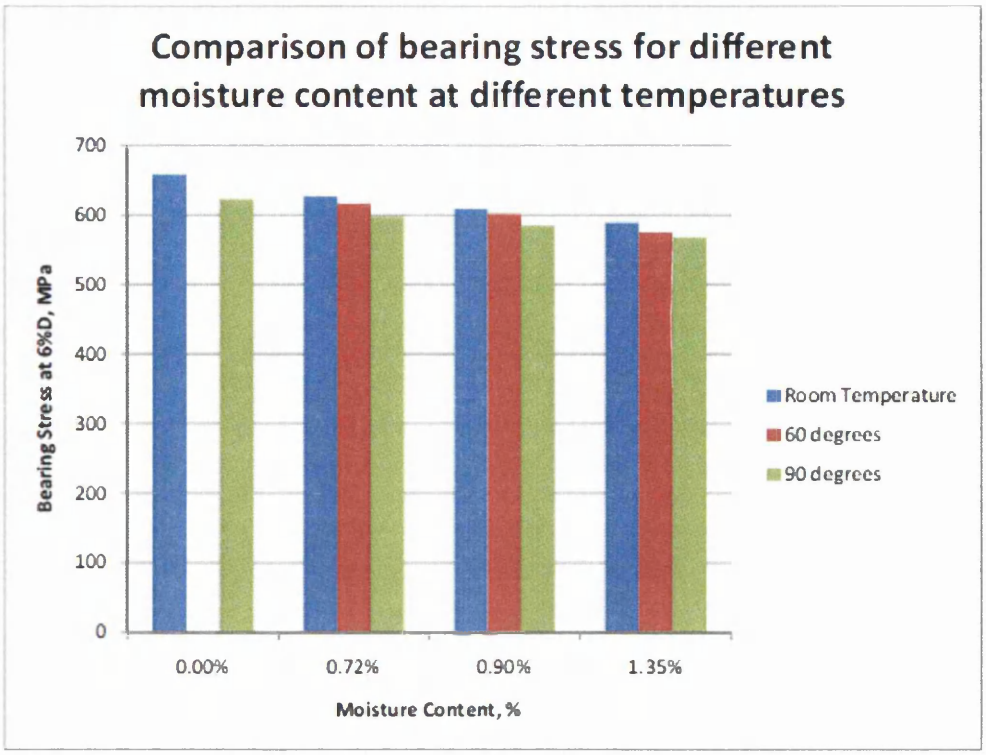

Figure 123 Single Lap Bearing Results [74]

To be able to consider using the ELAP modelling tool to predict a bolted joint bearing performance further work would be necessary to investigate partial saturation, especially for single lap shear where bearing failure is typically initiated at the surface of the composite, which would be in the saturated condition and hence little or no improvement in performance may be seen for this joint configuration. Should the outcome of the partial saturation study be positive it would then be necessary to investigate the feasibility of implementing these effects in the empirically driven analysis tool. The large test programme requires tests well in excess of 4mm to be tested and to do so for saturation would not be feasible due to the long conditioning times that these tests would require. The only way forward would be to investigate if it was possible to carry out thin (~4mm) laminate testing campaign and then apply the degradation in properties seen to larger thicker laminates. Further work is required to determine if this is a sensible way forward and it would inevitably require some validation testing, which could take in excess of 1 year to 18 months to complete.

Using the EMOC test campaign data it was possible to determine the diffusion coefficient of different samples utilising equation 86 and rearranging it to give equation 138. Table 44 shows some typical values derived during the EMOC programme, along with pure resin values. For the purposes of the lug case study when using the ELAP

tool it would appear to be appropriate to use a diffusion coefficient in line with the average of the three quasi-isotopic samples which equates to $6.1462X10^{-7}$ mm^2/s and a maximum moisture content of 0.83 assuming a fibre volume fraction of ~58%. Using equation 85, it would easily be possible to use this data to produce a maximum moisture level for a composite of a different fibre volume fraction. This is an important point to make as the definition of the correct maximum moisture content is related within the EMOC model to the assignment of mechanical property data. It should be noted that there is clearly lay-up dependency with regard to the diffusion coefficient, which in this case it is clear the pure resin samples tested have a higher diffusion coefficient in line with the MRes finding [73], where clearly the uptake of both the neat resin and fibres ends faster than through the thickness of the laminate.

$$D = \pi\left(\frac{h}{4M_{max}}\right)^2\left(\frac{M_2 - M_1}{\sqrt{t_2} - \sqrt{t_1}}\right)^2$$

(Equation 138)

Table 44 EMOC Material Properties Derived Diffusion Coefficients for Different Composite Panels with Different Fibre Volume Fractions & Ply Orientations

EMOC Database 977-2 Diffusion Coefficient Comparisons												
Panel Ref.	Fibre Orienation/ Layup	Thickness h (mm)	Material Specification	Conditioning Parameters		Fibre Volume Fraction (%)	M_{MAX} Maximum Moisture Content Weight (%)	T1 (s)	T2 (s)	M1(% Moisture)	M2 (% Moisture)	Diffusion Coefficient (mm^2/s)
				Temperature (°C)	Humidity (%RH)							
-	NA	5	977-2 Resin Only	40	85	0	2.65	36000	72000	0.054	0.108	3.3000E-07
-	NA	5	977-2 Resin Only	60	85	0	2.65	36000	72000	0.088	0.176	8.7638E-07
-	NA	5	977-2 Resin Only	70	85	0	2.64	36000	72000	0.098	0.196	1.0951E-06
7918	0/90	2	977-2-35KHTS 268gsm	40	85	56.46	0.88	36000	72000	0.022	0.044	7.9473E-08
7918	0/90	2	977-2-35KHTS 268gsm	70	85	56.46	0.94	36000	72000	0.039	0.078	2.1888E-07
8132	0	2	977-2-35KHTS 268gsm	40	85	63.16	0.86	36000	72000	0.017	0.034	4.9687E-08
8132	0	2	977-2-35KHTS 268gsm	60	85	63.16	0.82	36000	72000	0.022	0.044	9.1529E-08
8132	0	2	977-2-35KHTS 268gsm	70	85	63.16	0.8	36000	72000	0.027	0.054	1.4484E-07
8917	QI	4	977-2-35KHTS 268gsm	70	60	58.25	0.63	36000	72000	0.022	0.044	6.2024E-07
8916	QI	4	977-2-35KHTS 268gsm	70	60	57.58	0.62	36000	72000	0.024	0.044	5.2927E-07
8913	QI	4	977-2-35KHTS 268gsm	70	85	58.87	0.81	36000	72000	0.029	0.058	6.5197E-07
8912	QI	4	977-2-35KHTS 268gsm	70	85	58.41	0.81	36000	72000	0.029	0.058	6.5197E-07
8914	QI	4	977-2-35KHTS 268gsm	70	85	57.75	0.83	36000	72000	0.029	0.058	6.2092E-07

7.3.6 Key Point Summary of Section 7.3

1. Elevated temperature testing was limited to a maximum of 90°C, representing a typical wingbox components maximum operating temperature, which avoided phenomenon associated with the material, such as micro-cracking etc, that would have become more significant above this temperature.

2. Initial M21/T700 study at elevated temperature above ambient proved the requirement to tested at elevated temperature (up to 90°C), noting that a linear reduction in in-plane shear properties were observed.
3. New material handling procedures to limit moisture uptake during manufacture were partially successful, with one of the most effective control parameters being to keep the time between autoclave cure and specimen extraction and return to dessicator being kept to a minimum.
4. Removal of end tabs was successful except for 0° Compression coupons, where it is advised that tabs are utilised with the use of complimentary traveller specimens to measure moisture uptake and maximum moisture at saturation.
5. The removal of end tabs assisted in keeping manufacturing time to a minimum.
6. Fibre ends show the fastest rate of moisture uptake and are comparable to the uptake of pure resin samples, where it is hypothesised that this is due to unrestricted moisture paths.
7. Fibre ends typically absorb moisture at up to 3.2 times faster than through the thickness of the material.
8. Further work is required to investigate moisture uptake in a range of lay-ups both through the thickness and along the fibre ends.
9. An EMOC test campaign was set up to explore the combined affect of moisture and temperature and also to overcome shortcomings of PR2.
10. 90° Compressive Modulus and 0° Compressive Strength and Modulus to date have not been generated adding risk to the modelling process.
11. The properties generated typically show a linear degradation in performance the equations of which can be used by the ELAP modelling tool.
12. B-Basis numbers are generally poor due to small sample size.
13. Initial bearing studies show a linear drop in performance, most pronounced for double lap joints, however studies at partial saturation are required to quantify the applicability of the EMOC process.
14. Diffusion values from the EMOC tests and linear equations for mechanical property reduction are used for the ELAP modelling tool.

7.4 Lug Case Study

The main aim of this case study was to verify the EMOC modelling principles described in section 5.3.1. Pre-test sizing and predictions were carried out using these principles, which could then be compared to test. Once the EMOC tool was then available later in the project, the tool could then be used for post evaluation purposes where the numerical computer based modelling approach would theoretically offer improved fidelity, as well as allowing rapid iterations of component optimisation in the ribs sizing tool.

7.4.1 Lug Geometry

Firstly it is necessary to evaluate the lug geometry defined in section 4. The lug geometry was modified based on findings from [5,75] because there appeared from existing data to be a change in failure mode between a 'Shear Out Failure' and Net-section Failure', as discussed in the experimental procedures section. This geometry change does appear to have been a success as shown in figure 74, however with the benefit of hindsight it would have been beneficial to change the lug geometry further. The proposed geometry change is shown in figure 124:

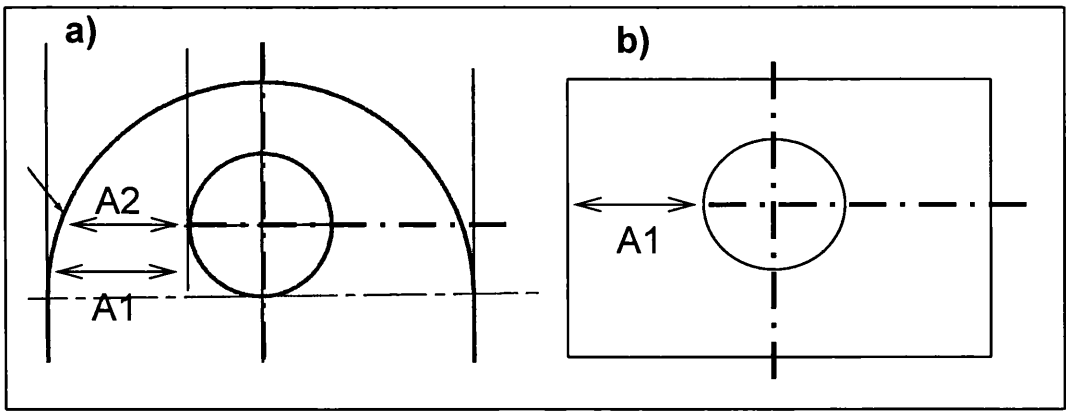

Figure 124 a) Showing Manufactured Lug Geometry and b) Proposed Improved Geometry

When defining the lug width to prevent shear out the decision was made based on the area 'A1', shown in figure 124a. However due to the radius of the end of the lug, this meant that in reality the shear out area, assuming the load acts along the horizontal centre line, is actually 'A2'. This can easily be taken into account and has been, when

carrying out the post sizing calculations using the EMOC tool. Although this may be accounted for it adds unnecessary complexity within the mechanics of the test, which may affect the calculation method used. The stress method assumes load is evenly distributed along the whole of the area on both sides of the hole; however the load introduction is applied around the edge of the hole, providing a local stress concentration, which is accounted for in the sizing calculations using a notch factor 'K_{so}'. This notch factor is not derived from this specific material, and is derived from Airbus carpet plots [78] although the material used to derive this factor is from the same Airbus Industry Specification (AISP). FE would offer a better understanding of load introduction, however the FE model was not able to predict the progressive failure of the lug in this instance, using the simplistic approach adopted. By changing the geometry to that shown in figure 124b would certainly remove any ambiguity resulting from the correct area assumed by which the load is transferred.

Despite the recommendation for further geometry changes, the observed failure mode does appear to be the derived shear out failure for the lugs specimens. Obviously the exact point of first failure will always be dependent on the exact geometry of the lug, which although appears to be fully symmetric will always have small geometric inconsistencies, leading to a slightly higher stress concentration on one side of the lug compared to the other. This is highlighted in figure 101, where a shear out failure has occurred on the right hand side of the lug. Once failed a bending moment then exists, which has led to what appears to be a net-section failure on the left hand side of the lug. Again the changes proposed to the lug geometry may have helped ensure a constant failure on both side of the lug and avoided any possible interaction between failure modes.

Overall the accuracy of the tests for both the 12mm and 26mm lugs appeared to be good in terms of the test parameters. There was no environmental chamber breakdown or failure during the 1000hour conditioning cycle. The weight of the 26mm lugs was the only parameter that could not be measured. Every effort was made to minimise any parameter that would affect the moisture level within each lug. The author constructed bespoke environmental heater boxes to place around the test rig for the 90°C tests, which were all tested before the lug tests were to begin. To prevent drying in the heater box while waiting for the lugs to reach temperature all equipment was pre-heated and the lugs were removed just before test from the environmental chamber to maintain as much residual heat as possible. Temperature control during test was to within ±4°C, all helping to prove that the test campaign was a success.

7.4.2 Pre-Sizing Laminate, Lamina Properties, Diffusion Moisture Values

Before discussing the material properties used and the validity of these properties, it is important to consider the laminate properties used for sizing purposes. Classical laminate theory via LAP, allows the first ply failure and ultimate ply failures (I.e. ultimate laminate) to be determined. With the knowledge that the sizing method discussed is classically conservative, using carpet plots from [78] and empirically derived reduction factors that further increase conservatism, it was decided by the author to utilise the ultimate strength in all calculations. As a general rule this would not be appropriate for aircraft structural sizing, where for composites a no crack philosophy exists and therefore the structure is designed for no failure at the desired operating load. However in this instance the author aimed to accurately predict what happens in reality and therefore wants to avoid unnecessary conservatism, to allow modelling approach validation.

Next to consider is the lamina mechanical properties which are then used to determine the mechanical properties of the laminate. The values assigned to each ply are fundamentally dependent on the diffusion value used and the maximum moisture content for each ply. It should also be noted that the edge effects, explored by the supporting MRes [73] indicated that the moisture diffusion along the fibre ends and sides of the composite can be typically much faster, leading to higher moisture content in the component than initially envisaged. The potential effects of this have not been taken into account.

At this pre-sizing stage an accurate diffusion coefficient and maximum moisture content was not available, with MRes studies to help provide confidence in these values still ongoing. For the sizing of the 12mm lugs the moisture profile shown in figure 78 was used and was generated using the Airbus 'Wet Aging Tool'. This used EMOC material properties at 90^{o}C, with a diffusion coefficient from existing Airbus data, having a maximum moisture value of 0.92%. Later on (step 10), a new moisture profile was generated using a diffusion coefficient and maximum moisture content of 0.6% from PR2, which was then used by the ELAP (noting that the laminate analysis part of the tool was not available at this time) modelling tool to provide a through thickness moisture distribution. Clearly there is a large difference in maximum moisture content and secondly the diffusion parameter has lead to moisture uptake almost twice as fast as the original profile. The original moisture profile discretised the lug into 3 parts

through the thickness, where an average moisture coefficient was then assigned for each section with ply properties assigned accordingly based on the mechanical property data. For the revised profile (figure 97) the author discretised the laminate into six discrete parts to improve the fidelity of each ply's assigned mechanical properties. When comparing the two moisture distribution curves (figure 78 & 97) analysis results there is only a small difference in the load carrying predictions (comparison of steps 6 & 10) of ~5.4kN. It would be expected that the new modelling approach, having lower maximum moisture content would predict a higher load carrying capability; however this appears to have been cancelled out. This is probably due to moisture penetrating deeper into the material, combined with the higher fidelity brought about by the increased through thickness discretisation apparently leading to a lower strength. Overall there appears to be good correlation from both approaches compared to test.

In both cases the prediction of lug strength, although modelled accurately, was optimistic compared to the actual tests (see figure 106). Furthermore when considering the B-values generated for the 12mm lugs (see table 30) the load for the conditioned (1000hrs) tests at 90°C, drop further to 101kN, meaning the predictions are optimistic by 8% for Step 10 and 12% for step 6. It was not possible to utilise B-basis values when deriving laminate strength for the reasons discussed in section 7.3.4, however if a B-basis knock down were applied, this would bring the predictions in line with the actual test data once more. Furthermore for aircraft sizing purposes the application of the knock-down factors, would further increase conservatism, ensuring that all predictions would be conservative compared to reality.

Although initial sizing appears to be a success, it highlights the importance of having a robust set of modelling parameters for the diffusion coefficient, maximum moisture content and a derivation of laminate properties with as high fidelity as possible, ideally calculating moisture content and subsequent properties for each ply, which is carried out using the EMOC model. Despite these potential shortcomings, the results appear to show that the modelling process adopted is robust, especially when the predicted load (step 4) using HOT/WET properties is only 78.6kN. Comparing this figure to both predictions and test prove that the HOT/WET approach is conservative for this thickness of lug by up to 45%. Assuming that all material parameters such as lay-up were to remain the same this would equate to a significant weight saving.

Finally comparing the 26mm lug performance to test, the same parameters for diffusion were used as in step 10. This resulted in a load carrying prediction of 523.6kN, with the average load carrying capability of the batch being 510kN, meaning that again there was good correlation comparing the modelling to tests. However, as with the 12mm lugs the calculations were slightly optimistic by 2.6% but again using the knock down factors in the method and the application of B-values this prediction could easily be made conservative. As both the small 12mm and thick 26mm lug predictions show good correlation to test the basis of the modelling principles appear to be an overall success.

The FE studies carried out on both lug thickness appear to give an indication of the point at which the first elements achieve the maximum allowable stress. As the FE is not a progressive failure model it is not possible to see what the ultimate strength of the lugs would be. Furthermore no failures were seen in the tests at these low loads indicating that the FE methodology was conservative for predicting the lug failure. An interesting point to consider that has not been taken into account with any of the predictions is that the moisture concentration around the hole where the load is applied will be greatest. This could lead to a theoretical lower failure load although this was not observed. As the FE suggests load is highest at the outmost edge, however the combined loss in stiffness as well as strength could have allowed re-distribution of the stress into the surrounding material, thereby reducing the local stress concentration and preventing failure. Using a 3D FE version of the code should allow such phenomenon to be accurately modelled and taken into account.

As was stated for all strength predictions and calculations the ultimate strength of laminate was used instead of first-ply in an attempt to accurately predict component strength, with first ply being considered to be a very conservative approximation. Clearly the approximations appear to be in good agreement, however it should be noted that many of the lugs were stopped as soon as the first significant drop in load was observed, to allow the failure mechanism to be identified. In some instances the lugs continue to take further additional load, however it is difficult to fully understand if this means the ultimate failure strength was higher, where the potential for a mixed mode failure appears to be evident after first failure. If more time were allowed, along with lug re-design as suggested it would be possible to further explore the relationship between predicted failure strength and actual failure strength.

7.4.3 Key Point Summary of Section 7.4

1. Modified lug geometry based on learning from historic Airbus tests appear to have led to the anticipated failure mode.
2. Further modification to the lug geometry may have prevented the secondary failure mode from occurring.
3. Lug tests can be considered a success with both the 12mm & 26mm failing consistently with low scatter.
4. In all calculations used to predict load carrying capability of the lugs the ultimate laminate strengths have been used, due to conservatism in first ply failure strengths. For aircraft sizing purposes first ply failure strength should be used.
5. Pre-sizing shows good correlation to test using the ultimate failure strengths for both the 12mm and 26mm lugs.
6. The effect of increased moisture concentration along the fibre edges has not been taken into account during this study, which would have resulted in higher moisture concentrations around the load introduction points of each lug.
7. The pre-sizing appears accurate despite the known inaccuracies in the moisture parameters used to determine the through thickness moisture profile and maximum moisture content.
8. In all cases the pre-sizing has produced slightly optimistic results.
9. FE studies only indicate first failure around the load introduction and does not allow for progressive failure modelling to determine ultimate strength.
10. Using full 3D moisture profiles and an FE failure model may allow accurate prediction of lug behaviour.
11. Lugs were typically stopped at the first significant failure defined by a drop in load at a given displacement, further studies would verify if this represents the ultimate lug strength, but with existing lug geometry this may be difficult when considering the secondary failure mode seen during some tests.

7.5 EMOC Tool & Lug Sizing Using ELAP 1D

The supporting project PR1 & PR2 were commissioned to enable moisture to be modelled and the properties to be assigned to the material based on the level of saturation at each ply. PR1 & 2 were successful in their own rights, however the final step for both projects was to produce joint predictions on the strength of a directed open hole coupon in compression. The main issue preventing success was that the material used in the open-hole test was different from that of the test campaign. All the

resin was the same but the fibre type used in the open hole coupons was of woven construction. None of the material used to generate moisture/properties data was of woven fibre, with all basic coupon tests comprising of unidirectional plies. Furthermore the weight of each ply was different with coupon tests in PR2 being of 196gsm and the woven material 268gsm. Negating the woven material for a moment, the different weight of material results in a different set of mechanical properties based on comparisons to existing Airbus data, despite the same fibre volume fraction after laminate manufacture. This fundamental difference in mechanical performance between materials meant that is was not directly possible to use the modelling approach and prediction made by PR2 to accurately make predictions of the OHC coupons. PR1 produced a functional prototype, however further development was required when considering laminate failure criteria to predict ultimate strength as well as first ply failure. PR1's goal was to produce a tool that could be used by any engineer, but having some sort of user interface or windows executable version of the code was not completed within the time frame. PR2 suffered from not taking into account properties at elevated temperature and also from the previously discussed flaws with regard to moisture levels etc.

These shortfalls were eradicated within the EMOC project where the ELAP 1D tool, combined with the EMOC material properties allowing accurate predictions of performance to be made. The ELAP 1D tool was designed to supersede the 'Airbus Wet Aging' tool as well as the LAP programme, used by Airbus. A Research Assistant, specialising in engineering software design was employed to develop the code on the behalf of Airbus to the author's specifications and requirements. Two versions of the tool were envisaged, both based on an FE approach. Version one of the ELAP 1D tool works on the principles previously discussed (laminate theory and moisture diffusion), with a 3D modelling capability still in development, where 3D moisture absorption and subsequent material properties could be modelled to provide a much more accurate prediction of actual components performance. If the 3D code is developed successfully, it will eventually be integrated into ABAQUS which is the Airbus standard non-linear solver. The 3D code development remains a much larger challenge and remains outside the scope of this project, which focuses on simple laminate theory and 1D modelling, which has been much more achievable within the project timescales. The 3D code provides a much greater challenge when considering that each ply needs to be modelled and for component studies this would result in extremely fine meshes requiring large amounts of computing power to converge on a solution. Furthermore each ply will no longer have a unique set of properties due to 3D moisture gradients.

3D solid modelling of composites remains a challenge in the composites industry without the complication of modelling 3D properties in the solid model, combined with the need to create failure models. The application of the approach created within this project may therefore be unachievable in the short term.

Although as previously seen the ELAP 1D tool appears to be in good agreement with the LAP tool, it has not been possible to validate the model against a simplistic coupon test. Some FHC samples have been manufactured to assess the model predictions against a basic test case, however these will not be available within the time frame of this project. It should be noted that PR1 successfully demonstrated that the ELAP modelling code matched the 'Airbus Wet Ageing Tool' for prediction of moisture diffusion. Further complication and risk has been added with the missing mechanical properties required for accurate laminate property prediction, namely 90° compressive modulus and 0° Compressive strength and modulus. With these properties missing arbitrary values have been used and fixed using Airbus databases. However as their degradation is not accounted for it adds significant risks to the ELAP 1D predictions at this time. It is essential that this data is acquired and tested with the tool. Hopefully combining this missing data with some basics coupon validation tests should allow confidence in the modelling capability.

As previously discussed diffusion values and maximum moisture content is critical to modelling the moisture distributions correctly. Further work is required to ensure the model corrects from the reference mechanical property data to a laminate of typical fibre volume fraction 'v_f' of 60%. Failure to do this could result in an incorrect material property assignment, based on an incorrect level of moisture, which would be a fundamental error. The lack of statistically robust datasets also adds risk; however this could be easily eradicated by further testing, which could easily be fed into the modelling process. So far and based on the data generated, linear equations have been used to show the degradation in property performance, this appears to hold true at the 90°C operating temperature, used for structural design. However some of the lower temperature curves do not show such a good linear relationship and it is therefore prudent to explore this further. The use of a polynomial equation may prove to be more accurate, but this would have to have clear operating limits to assure its applicability. It is recommended that further batches of mechanical property tests are conducted at 90°C to ensure tool robustness, ideally further studies would explore the full operating temperature range and this should also include -55°C tests as well. The current limits of the model applicability must be between 20°C & 90°C, with moisture

contents between 0% & 0.82% (utilising a maximum moisture content derived at 85% relative humidity, with reference to the fibre volume fraction of the test data).

The ELAP 1D tool was used to predict the material properties of the two lugs as a validation case study, which has helped mitigate risk with the lack of basic coupon validation tests cases. The maximum moisture level was increased to 0.82% at 85%RH compared to the previously used 0.6% value. A diffusion coefficient was used based on the EMOC test programme, which monitored the rate of uptake of a range of quasi-isotropic specimens, to provide what appeared to be the most accurate prediction possible. One risk to be identified here is that Airbus data would indicate a higher moisture content nearer to 0.92%, which would degrade the material properties further. However with this risk in mind the results are presented in table 45:

Table 45 ELAP Predictions, Compared to Pre-Test Hand Approach Predictions and Test Data

Lug Thickness (mm)	ELAP Load Prediction (kN)	Hand Approach (kN)	Test (kN)
12	104.9	109	107.4
36	502.4	523.6	510.6

Clearly, both the hand approach and ELAP 1D approach correlate well to test. However the main success is that the ELAP 1D program has predicted lug performance closer to test than the hand approach as expected. This is an excellent result. Also the ELAP 1D predictions show a lower performance than the tests and are therefore conservative. This has not only helped to validate the overall approach but shows that the ELAP 1D tool is clearly able to overcome the use of HOT/WET properties. This can be combined with excellent correlation of property predictions across a range of failure criteria with the LAP tool.

7.6 Lug Weight Saving Potential

It was initially envisaged to marry up the ELAP 1D modelling tool and ribs sizing tool, but as previously mentioned this was not possible because most of the ribs shear webs were not amenable to the new approach due to them typically having thicknesses of <6mm and compounded by foot flange having a through thickness lamina based strength dependency which cannot be predicted by the modelling tool. Therefore it was decided to use the lug case study in attempt to identify a weight saving based on the clear strength improvement over the original HOT/WET approach. This case study

considered a typical landing gear load of 1.5MN reacted around a lug to derive a lug thickness and hence weight for both the HOT/WET properties and ELAP predicted properties. In addition to this relatively thick lug a smaller load, resulting in a relatively thin lug was calculated to see if weight savings could still be achieved for a relatively thin laminate.

A weight saving of **27%** for the thick lug was achieved which can be attributed to the thick lug being in a mainly dry state, albeit operating at the same operating temperature as the fully saturated approximation. The thin lug also showed a significant weight saving of **13%** despite having a significant level of saturation through its thickness. Overall this represents an excellent success for the EMOC modelling approach, especially when considering that the approach can be applied with success to relatively thin laminates.

During the planning phase it was expected that a significant number of iterations might be required to converge on the true thickness solution, but for both the thin and thick lug cases the solution was arrived at after only two iterations to within 1 ply. At this point any further optimisation was unnecessary as the basic composite rules of achieving a balanced symmetric lay-up would be breached and therefore be undesirable.

Although for this strength based analysis a significant weight saving has been identified it should be noted that most Airbus structures are sized using a damage tolerance approach, where an assumed BVID (barely visible impact damage) amount of damage is present. The BVID approach means a strain limit is imposed on the structure to ensure no damage growth. For the lug case it would be appropriate when designing for damage tolerance to define the shear strength as a function of this strain limit, typically found to be 3500 to 4000$\mu\varepsilon$ from CAI tests. The shear modulus of the laminate is multiplied by this strain allowable to produce a strength property that can be used for the calculations. This approach was considered by the author; however the determination of an accurate shear modulus is dependent on both the perpendicular and parallel tensile and compressive lamina moduli. The EMOC project failed to derive the compressive lamina moduli and therefore an accurate shear modulus could not be derived. For laminate property determination in ELAP fixed compressive moduli were utilised based on existing Airbus data, which resulted in very little change in shear modulus despite significant changes in lamina shear modulus. Therefore to verify complete success of this project further work is required to define the missing

mechanical properties and assess the applicability to a stiffness-based design. However it can be speculated that as significant changes in modulus have been observed for perpendicular tensile and shear tests, the approach should be valid and significant weight savings would still be achievable.

As a final note it would be prudent to apply the EMOC modelling approach to a wide range of structural analysis methods for different areas of the wing to assess the potential benefits to a greater extent. Areas for consideration would include buckling of wing skin panels and associated stiffeners. The lugs represent a bolted joint, however for typical joints used to assembly different components, the structural driver would not be shear strength resulting in shear out, but bearing strength and as previously discussed further tests are required to determine the applicability of the EMOC approach to typical single and double lap bolted joints.

7.6.1 Key Point Summary Section 7.6

1. The initial modelling approach validation using PR1 & PR2 was unsuccessful due to incorrect material selection at the beginning of the project.
2. The ELAP tool uses material properties produced from the EMOC test campaign overcoming the technical issues discovered in PR2.
3. Two versions of the ELAP tool were perceived, 1D & 3D, with the 1D tool being completed within the timescales of this project and the 3D version requiring a significant amount of further development.
4. The 3D version of the tool is a much more complex problem as each individual ply in the modelled laminate will now have different properties per element due to 3D moisture diffusion. Fine meshes are required to capture this moisture absorption at a ply level, which at a structural level will require significant amount of computing power to converge on a solution.
5. 3D modelling is further complicated by the notoriously difficult challenge of modelling composites in 3D solid models, further complicated by the need to incorporate failure modelling.
6. ELAP 1D has been designed to supersede the 'Airbus Wet Ageing Tool' and the LAP programme combining the functionality of the two programs.
7. The ELAP 1D tool has been successfully validated against the 'Airbus Wet Ageing Tool' and LAP tool.

8. ELAP 1D predictions of stiffness properties with the presence of moisture are inaccurate due to the missing compressive moduli required to produce accurate stiffness predictions using classical laminate theory.
9. ELAP 1D utilises linear equations for mechanical property degradation, based on mean data generated by the EMOC testing programme.
10. ELAP 1D has environmental property limits for predicting mechanical properties, based on the mechanical test data generated, these range from 20-90°C operating temperatures and moisture levels between 0-0.82% (based on a humidity of 0-85%RH).
11. The full operating temperature has not been explored and it is recommended that some tests are conducted between 20°C & -55°C to allow the full operating envelope of the aircraft structure to be modelled using ELAP 1D.
12. The ELAP 1D programme showed excellent approximation to actual lug tests, offering a closer approximation than the conventional hand calculation method.
13. The Rib Sizing tool proved to be unsuitable for the calculation of weight savings due to the small rib thicknesses and therefore the lugs were revisited to determine a weight saving.
14. Both a large lug and a smaller thinner lug were investigated with both lugs offering significant potential weight savings, even for one component of less than 6mm thick.
15. Weight savings identified are valid for a strength based design, however for a stiffness based design to allow for damage tolerance the EMOC approach can not be validated due to missing mechanical property data required to generate the necessary laminate stiffness properties.

8. CONCLUSIONS RECOMMENDATIONS/FURTHER WORK

8.1 Conclusions

- The original supporting work in PR1 & PR2 was of limited success; however the short comings identified were addressed as this project progressed.
- Environmental control of coupons used to generate mechanical properties is essential to prevent inaccurate predictions of performance when using the developed modelling tool.
- Strict environmental control can be difficult to achieve in practice and the simplest way to prevent unnecessary exposure to environment resulting in inaccuracies in measured moisture content is to keep the exposure time to a minimum during manufacture.
- The ability to monitor each coupons individual moisture levels is unnecessary and the standard procedure of using traveller specimens manufactured from the same laminate negates the need to do this and further removes the complication of using end tabs of dissimilar material.
- Fibre volume fraction must be taken into account when quoting maximum moisture content used by the modelling tool. Without this incorrect moisture levels may be assigned to a component, which may affect the laminate strength predictions.
- Non-Fickian diffusion was observed and its effect on mechanical performance quantified to be the same as Fickian diffusion. The effects of the non-Fickian diffusion were discounted due to the large exposure times required to achieve significant moisture levels by this process, which would exceed a worst case aircraft life cycle.
- An initial study of in-plane shear performance proved that combining moisture and testing at elevated temperature dramatically enhances the reduction in mechanical performance, this led directly to the creation of EMOC test campaign to allow the model to account for typical aircraft operating temperature (90°C).
- Diffusion along fibre ends was proven to be significantly faster than through the thickness of the laminate. Typically fibre ends are insignificant in large composite structures, such as wing skins and have not been considered for the 1D modelling capabilities. When modelling the lugs the predictions were in good agreement with

tests despite the risk of increased diffusion around the load introduction point, resulting in further local property degradation.

- The generation of essential laminate compressive moduli was not achieved due to difficulties with test methods and insufficient resources to complete a full test campaign adding significant risk to the accurate modelling of laminate stiffness properties.
- Linear equations were derived from the EMOC test data, which were then utilised by the 1D tool to predict mechanical performance of each ply subject to moisture absorption. These equations were based on mean data as the small coupon sample sizes did not allow for statistical B-basis numbers to be accurately derived.
- Initial studies of both single and double lap bearing performance indicated that in both cases moisture and temperature degraded mechanical performance; however further testing is required with specimens containing moisture gradients through the thickness, to ensure the applicability of the modelling procedure. This is especially important for the single lap shear bearing tests, which typically exhibit surface dominated failures, which would coincide with the region of highest saturation.
- Initial pre-sizing of the lugs using a hand based approach, based on the derived principles for predicting the mechanical performance of the laminate was successful, although producing slightly optimistic results compared to the mean lug test values at each condition. This showed that the general principles of the project were sound in advance of the modelling tool becoming available.
- The application of the ELAP 1D modelling tool proved to improve the fidelity of the modelling procedure compared to hand based calculations and provided a slightly pessimistic prediction of lug performance.
- For all calculations the knock-down factors typically applied to ensure conservatism in the calculation methods were removed to ensure an accurate approximation to test. For aircraft structural sizing these would be re-instated, along with the use of statistical B-Basis values which would clearly ensure that all calculations remained considerably conservative, while still offering benefits over the use of HOT/Wet properties.
- The Lug tests appeared to fail in the expected failure mode; however after first failure a second net section failure mode became evident. Most lug tests were stopped at the first significant drop in failure load and it cannot be confirmed if this represents the ultimate strength of the lug. In all laminate strength predictions using

the modelling tool, the ultimate laminate strengths were used instead of first ply failure to allow good prediction to the lug tests. This would not be done for aircraft structure, which would work on a first-ply-failure no-crack philosophy.

- The ELAP 1D modelling tool was successfully validated against the 'Airbus Wet Ageing Tool' and LAP tool providing confidence in both moisture modelling capability and strength predictions via classical laminate theory.
- 3D modelling capability was not available within this project and continues to require significant development to allow it to model components successfully.
- The ELAP 1D tool was used to predict weight savings for a thick and relatively thin lug. In both cases this proved the potential benefits of the project offering a 27% weight saving for a component that would typically be ~50mm thick using the HOT/WET approach. Secondly the model appears to be applicable to laminate of around 5mm where a significant weight saving of 13% was achieved for a lug of 6.4mm initial thickness.
- For laminates of 5mm or less the weight saving potential would reduce because the ability to remove plies becomes even more difficult when taking into account standard stacking rules (e.g. the requirement for an equal number of plies to maintain symmetry).
- Due to the missing compressive moduli it was not possible to produce accurate stiffness predictions using the ELAP 1D tool, although it is expected that the ELAP tool would accurately model laminate stiffness properties should data be available. Assessment of this matter is therefore not conclusive. When sizing aircraft structure damage tolerance policy typically sets strengths based on stiffness properties and strain limits to ensure any undetected damage does not propagate within the limits of airframe operation. It is therefore critical that further work is carried out to validate the EMOC principles for a stiffness based design.

8.2 Recommendations/Further Work

- Overall the EMOC modelling process is robust, however the generation of missing mechanical properties is essential to ensure that the process is applicable to stiffness based design. Once the data is generated further studies will be required to ensure that weight savings benefits are achievable.

- An assessment of all standard Airbus sizing methods needs to be carried out to evaluate the applicability of the EMOC modelling process. It will then be necessary to develop and validate the modelling process for each of these sizing methods. An example of this would be the bearing sizing methods where further validation tests with partial saturation would be carried out to ensure applicability.
- To ensure the EMOC modelling process can be deployed for Airbus aircraft additional materials will need to be tested and validated against the modelling process. This should include all basic laminate properties, as well as moisture diffusion and maximum moisture values. It may be possible to reduce or limit the test campaign and only generate material property data at 90°C.
- Further work on 3D modelling is required as this version of the tool did not reach maturity within the project timescales. Although this represents a significant challenge it should be used to assess the effects of 3D diffusion on mechanical performance, especially around local load introduction points, to help ensure the 1D modelling processes remains conservative.

9. REFERENCES

1. Ever J. Barbero, 'Introduction to Composite Materials & Design' (Materials Science & Engineering Series, CRC Press, 1998, ISBN 1-56032-7014.
2. Bryan Harris, 'Engineering Composite Materials', IOM Communications Ltd, Second Edition, 1999, ISBN 1-86125-0320.
3. Michael C Y Niu, 'Composite Airframe Structures', Hong Kong Conmilit Press Ltd, Fourth Edition, 2005, ISBN 962-7128-06-6.
4. ASM International Handbook Committee, ' Volume 1 Engineered Materials Handbook, Composites', International Handbook Committee, TA403.E497, 1087, ASM International Materials Park, OHIO 44073, November 1987, ISBN 0-87170-279-7.
5. D Hull, T W Clyn, 'An Introduction to Composites', Press Syndicate University of Cambridge, Second Addition, 1996, ISBN 0-521-38190-8.
6. British Standard Aerospace Series, 'Glass Fibre Reinforced Mouldings and Sandwich Composites', BS EN2374:1991.
7. Association European des Constructeurs de Materiel Aerospace (AECMA) Standard, 'Preparation of Carbon Fibre Reinforced Resin Panels for Test Purposes', prEN2565, Edition 2, May 1993.
8. British Standard Aerospace Series. 'Reinforced Plastics – Standard Procedure for Conditioning Prior to Testing', BS EN2743:2002
9. Association European des Constructeurs de Materiel Aerospace (AECMA) Standard, 'Determination of the Effect of Exposure to Humid Atmosphere on Physical & Mechanical Characteristics', prEN2823, Edition 2, November 1998.
10. British Standard, 'Plastics – Determination of Tensile Properties', BS EN ISO527-5:1997.
11. British Standard Aerospace Series, 'Carbon Fibre Reinforced Plastics – Unidirectional Laminates – Tensile test Perpendicular to the Fibre Direction', BS EN2597:1998.
12. J M Hodgkinson, 'Mechanical Testing of Advanced Fibre Composites', Woodhead Publishing Ltd, 2000, ISBN 1-85573-312-9.
13. Association European des Constructeurs de Materiel Aerospace (AECMA) Standard, 'Aerospace Series Carbon Fibre Thermosetting Resin Unidirectional

Laminates Compression Test Parallel to Fibre Direction', prEN2850, Edition 2, November 1997.

14. Airbus Industrie Test Method (AITM), 'Fibre Reinforced Plastics Determination of In-plane Shear Properties ±45 Tensile Test', AITM1-002, Issue 3, November 1998.
15. British Standard, 'Fibre Reinforced Plastics Composites – Determination of the In-plane Shear Stress/Shear Strain Response, Including the In-Plane Shear Modulus and Strength by the ±45° Tension Test Method', BS EN ISO 14129:1998.
16. British Standard Aerospace Series, 'Carbon Fibre Reinforced Plastics – Unidirectional Laminates – Determination of the Apparent Interlaminar Shear Strength', BS EN2563:1998.
17. British Standard, 'Fibre-reinforced Plastic Composites – Determination of the Apparent Interlaminar Shear Strength by the Short-beam Method', BS EN ISO14130:1998
18. Airbus Industrie Test Method (AITM), 'Fibre Reinforced Plastics Determination of Bearing Strength by either Pin or Bolt Bearing Configuration', AITM1-0009, Issue 3, November 2003.
19. R Older, R Adams, ' Effectiveness of Using Double Sided Abrasive as a Replacement to Bonded End Tabs for CFRP Tensile Tests', Airbus Operations Document, RP0815822, 2008.
20. Airbus Industrie Test Method (AITM), 'Fibre Reinforced Plastics Determination of Compression Strength After Impact', AITM1-0010, Issue 3, October 2005.
21. American Society for Testing of Materials (ASTM), 'Standard Test Method for Measuring the Damage Resistance of Fibre-Reinforced Polymer Matrix Composite to a Drop-Weight Impact Event', D7136, October 2007.
22. Airbus Industrie Test Method (AITM), 'Fibre Reinforced Plastics Determination of Plain, Open Hole & Filled Hole Compression Strength', AITM1-0008, Issue 3, December 2004.
23. Airbus Industrie Test Method (AITM), 'Fibre Reinforced Plastics Determination of Plain, Open Hole & Filled Hole Tensile Strength', AITM1-0007, Issue 3, December 2004.
24. M desailloud, 'Composite Statistical Method to Determine B-Basis Value from Small Data Sets', Airbus Operations Document RP0300181, October 2004.
25. 'Military Handbook 17B', Army Materials Technology Laboratory, Plastics for Aerospace Vehicles, Part 1, Vol1, 1987.

26. Brian C Hoskin, Alan A Baker, 'Composite Materials for Aircraft Structures', Air Force Institute of Technology, Wright Patterson Air Force Base, OHIO, USA, 5th Addition, 1986.
27. W Hansel, M Jevons, M Desailloud, 'Composite Harmonised Plain Strength Failure Criteria', Airbus Operations Document, RP416030, 2005.
28. I G Hedrick, J B whiteside, 'Effects of Environment on Advanced Composite Structures', British Library, AIAA Paper, 1997.
29. J J Imaz, J L Rodriguez, A Rubio, I Mondragon, 'Hydrothermal Environmental Influence on Water Diffusion & Mechanical Behaviour of Carbon/Fibre Epoxy Laminates', Journal of Materials Science Letters 10, 1991, pages 662-665.
30. M D Cambell, D D Burleigh, 'Thermophysical Properties Data on Graphite/Polyamide Composite Materials', Composites for Extreme Environments, ASTM STP 768, 1982, pages 54-72.
31. S C Cruz, 'Thermo-mechanical Characterisation of Graphite/Polyamide Composites', Composites for Extreme Environments, ASTM STP 768, 1982, pages 33-53.
32. T T Aerafini, M P Hanson, 'Environnemental Affects on Graphite Fibre Reinforced PMR_15 Polymide', Composites for Extreme Environments, ASTM STP 768, 1982, pages 5-19.
33. S D P Garber, D H Morris, R A Everett Jr, 'Elastic Properties & Fracture Behaviour of Graphite/Polymide Composites at Extreme Temperatures', Composites for Extreme Environments, ASTM STP 768, 1982, pages 73-91.
34. H S Choi, K J Ahn, J D Ham, H J Chun, 'Hygroscopic Aspects of Epoxy/Carbon Fibre Composite Laminates in Aircraft Environments', AIAA 1633 Broadway, New York, NY 10019, 5th Edition, 1986.
35. C Shen, G S Springer, 'Moisture Absorption & Desorption of Composite Materials', Journal of Composite Materials, 10, 1976, pages 2-20.
36. G S Springer, 'Environmental Effects on Glass Fibre Reinforced Polyester & Vinylester Composites', Journal of Composite Materials, 14, 1980, pages 213-232.
37. S Hen, G S Springer, 'Environmental effects on the Elastic Moduli of Composite Materials', Journal of Composite Materials, 11, 1977, page 250.
38. O M K Joshi, 'The Effect of Shear Properties on Carbon Fibre Composites', Composites Volume 14, No. 3, 1982, Pages 196-200.

39. A J Barker, V Balasundaram, 'Compression Testing of Carbon Fibre-Reinforced Plastics Exposed to Humid Conditions', Composites Volume 18, No. 3, 1987, pages 217-225.
40. R Sizer, K Friedrich, 'Mechanical Properties & Failure Behaviour of Carbon Fibre-reinforced Polymer Composites Under the Influence of Moisture', Elsevier Composites Part A, 28A, 1997, pages 595-604.
41. J Ryan, 'Relating Moisture Ingress to Component Strength for Carbon Fibre Composites' PhD Thesis, Swansea University, 2009.
42. C Shen, G S Springer, 'Effects of Moisture & Temperature on the Tensile Strength of Composite Materials', Environmental Effects on Composite Materials, Westpoint CT: Technomic Publishing Company Inc., 1981, pages 79-93.
43. W L Bradley, T S Grant, 'The Effect of Moisture Absorption on the Interfacial Strength of Polymeric Matrix Composites', Journal of Materials Science, Vol. 30 (21), 2000, pages 5537-5542.
44. S B Kumar, I Sridhar, S Sivashanker, 'Influence of Humid Environment on the Performance of High Strength Structural Carbon Fibre Composites', Materials Science & Engineering Journal A, October 2008, pages 174-178.
45. M Shang, S E Mason, 'The Effects of Contamination on the Mechanical Properties of Carbon Fibre Reinforced Epoxy Composite Materials', Journal of Composite Materials, Vol. 33 (14), 2000, pages1363-1374.
46. E C Botelho, L C Pardini, M C Rezende, 'Evaluation of Hygrothermal Effects on the Shear Properties of Carall Composites', Elsevier Materials Science & Engineering, 18th October 2006 (article in press).
47. R D Adams, M M Singh, 'The Dynamic Properties of Fibre Reinforced Polymers Exposed to HOT/WET Conditions', Elsevier Composites Science & Technology 56, 1996, pages 977-997.
48. O Gillat, L J Broutman, 'Effect of an External Stress on the Moisture Diffusion and Degradation in a Graphite Reinforced Epoxy Laminate', Advanced Composite Materials environmental Effects, ASTM STP 658:61, 1978.
49. L E Asp, 'The Effects of Moisture & Temperature on the Interlaminar Delamination Toughness of a Carbon/Epoxy Composite', Elsevier Composites Science & Technology 58, 1998, pages 697-977.

50. S Ravi, N G R Iyenger, B D Faidi, 'Influence of Moisture Absorption on the Fracture Toughness of Kevlar Fabric/Epoxy Composite', Journal of the Institute of Engineers (India), Vol. 76, 1995, pages 23-28.
51. E A Adda-Bedia, M Bouazza, A Tounsi, A Benzair, M Maachou, ' Prediction of Stiffness Degradation in Hygrothermal Aged Composite Laminates with Transverse Cracking', Journal of Materials Processing Technology 199, 2008, pages 199-205.
52. K Ogi, H S Kim, T Maruyama, Y Takao, 'The Influence of Hygrothermal Conditions on the Damage Process in Quasi-isotropic Carbon/Epoxy Laminates', Elsevier Composites Science and Technology 59, 1999, pages 2375-2382.
53. P Shyprykevich, W Wolter, 'Effects of Extreme Aircraft Storage and Flight environments on Graphite Epoxy', Composites for Extreme environments ASTM STP 268, 1982, pages 118-134.
54. Z Youssef, F Jacquemin, D Gloaguen, R Guillen, 'A Multi-scale Analysis of Composite Structures: Application to the Design of Accelerated Hygrothermal Cycles', Elsevier Composite Structures 82, 2008, pages 302-309.
55. J Mercier, A Bunsell, P Castaing, J Renard, 'Characterisation and Modelling of Ageing Composites', Composites Part A 49, 2008, pages 428-438.
56. Y Y Yu, K Pochiraju, 'Modelling Long-term Degradation Due to Moisture & Oxygen in Polymeric Matrix Composites', Materials Science & Engineering A 489, 2008, pages 162-165.
57. Ming-Hwa Jen, Yu-Chung Tseng, Huang-Kuang Kung, J C Huang, 'Fatigue Response of APC-2 Composite Laminates at Elevated Temperatures', Composites Part B 39, 2008, pages 1142-1146.
58. G A Schoeppner, D B Curliss, 'Model Based Design For Composite Materials Life Management', Materials Directorate Air Force Research Laboratory, WPAFB, OHIO 45433, USA.
59. G S Springer, 'Moisture Absorption in Composites', Journal of Composite Materials, 14, 1980, pages 236-248/
60. E L Cussier, 'Diffusion Mass Transfer in Fluid Systems', Cambridge University Press, 2nd Edition, 2003, ISBN 0-521 56447-8.
61. A Vincent, 'Wet Ageing Software Model', EADS/Airbus Document.
62. C Parkin, 'Modelling Moisture Ingress In Composite Materials', Master of Research (MRes) Thesis, Swansea University, 2005.

63. M C Y Niu, 'Airframe Structural Design', Adaso Adastra engineering Centre, 2nd Edition, 2006, ISBN: 978-6927128090.
64. L williams, ' Wing Load distribution Guide', Airbus Operation Document FN01/B78-01/99/GEN/LLW/3468, 2004.
65. Airbus Operation Composite Stress Manual, Issue A, 2000.
66. R Adams, R Older, ' ALCAS Calculations for Spars & Ribs', Airbus Operations Document, RP0502016, 2005.
67. M Funnell, R Older, 'ALCAS Covers Sizing Tool Theory', Airbus Operations Document, RP0502013, 2005.
68. R Adams, M, Funnell, R Older, M Cantrell, 'ALCAS Sizing Tool Evaluation', Airbus Operations Document, RP0502011, 2005.
69. M Funnell, ' TANGO RF Summaries', Airbus Operations Document, TANGO-02-000558-WWP4.0-RPT-A, 2004.
70. Engineering Science Data Unit (ESDU), 'Shear Buckling Method', ESDU71005.
71. C Parkin, 'FE Transient Diffusion Model for Moisture Ingress Into Composite Components', PhD Thesis, Swansea University, 2009.
72. R Older, 'Environmental Effects on the Mechanical Properties of Carbon Fibre Reinforced Plastic (CFRP)', Master of Research (MRes) Thesis, Swansea University, 2007.
73. S Dauhoo, 'Determination of Diffusion Coefficients for Water in CFRP in Different Orientations', Master of Research (MRes) Thesis, Swansea University, 2009.
74. S Paddea, 'The Effect of Absorbed Moisture on the Bearing Strength of Carbon Fibre Composites', Master of Research (MRes) Thesis, Swansea University, 2009.
75. R Salisbury, 'Analysis of CASCADE/CT7 Carbon Lugs Under Tensile Testing', Airbus Operations Document, 2006.
76. B Kirby, 'Proposal for CASCADE Large Scale Lug Test', Airbus Operations Document, CAS-1053-WP3-MEM, 2003.
77. M C Y Niu, 'Airframe Stress Analysis & Sizing', Hon Kong Commilit Press Ltd, 1st Edition, 1997, ISBN962-7128-07-04.
78. British Aerospace PLC, 'Stress Manual' British Aerospace PLC Warton Division, August 1985, REF8343/PM/SC/B11/5.
79. Tufnol 10G/40 Epoxy Glass Fabric Data Sheet, Tufnol Ltd. Information Sheet FR39, Tufnol Ltd, PO BOX 374, Perry Barr, Birmingham, B42 2BD, 2006.

80. A Lombardi, C Fauure, M Werner, G Lopez-Martinez, 'ESAC Harmonised Analysis Method for Residual Strength After Impact', Airbus Operations Document, RP0309419, 2006.

APPENDIX A.

Table A.1 Summary of ALCAS Rib Loads Used for Rib Sizing Tool Iterations

Rib No.	Pull-Off Load Na (N/mm)	Max Applied Shear Flow 'q' in web (N/mm)
1	444.64	2242.76
2	720.12	1781.95
3	314.14	760.45
4	744.51	626.52
5	819.51	221.33
6	712.47	238.35
7	700.96	187.28
8	774.62	111.23
9	781.73	170.25
10	745.13	113.50
11	751.16	136.20
12	758.69	113.50
13	768.09	96.48
14	590.58	113.50
15	386.17	107.83
16	386.55	147.55
17	375.50	90.80
18	327.51	88.53
19	299.53	79.45
20	292.25	85.13
21	281.51	63.56
22	256.07	56.75
23	225.16	56.75
24	237.77	48.81
25	233.93	68.10
26	231.44	69.23
27	128.34	74.91
28	101.27	77.56
29	120.33	80.96
30	167.66	84.37

Note: sheer flows are not stress, to produce stress divide by unit width in mm which converts to N/mm^2

Table A.2 Sizing Tool Results for RT/DRY Material Properties

RT/DRY

	FOOT FLANGE SIZING						WEB SIZING			T' STIFFENER SIZING				RIB CONFIGURATION MASS COMPARISON			
	Through Thickness Corner Radius CSM 20.4-15						Shear Plain Panel	ESDU 71005 Shear Buckling									
		C-SECTION		I-SECTION				UN-STIFFENED	STIFFENED								
Rib No	Krt applied	Flange Thickness t_a	Flange Thickness t_b	t_a	t_b	Rib No	WEB Thickness t_w	WEB Thickness t_w	WEB Thickness t_w		Stiffener Mass (kg)	Mass of Nuts and Bolts (kg)	Total Mass of Stiffener Assembly (kg)	C Section Total Mass (kg)	C-Section Stiffened Total Mass (kg)	I-Section Total Mass (kg)	I-Section Stiffened Total Mass (kg)
1	1.40	21.65	16.35	11.46	9.69	1	11.90	20.16	7.28	108.15	30.240	0.146	30.386	177.06	168.41	144.56	135.91
2	1.30	27.41	19.25	14.90	12.00	2	9.46	17.14	6.78	131.35	24.636	0.138	24.774	145.20	140.01	116.73	111.54
3	1.30	15.34	12.18	7.80	6.83	3	4.04	12.21	4.93	64.89	8.051	0.122	8.173	75.25	61.55	58.67	44.98
4	1.30	26.43	18.20	14.31	11.39	4	3.32	10.31	4.65	48.94	5.155	0.114	5.268	68.22	60.06	52.57	44.42
5	1.30	27.23	18.26	14.79	11.58	5	1.17	6.57	3.32	26.22	2.757	0.106	2.863	46.01	42.79	34.36	31.14
6	1.30	24.09	16.48	12.91	10.25	6	1.26	6.11	3.46	21.65	1.944	0.097	2.042	32.52	30.61	24.21	22.30
7	1.30	23.02	15.67	12.27	9.72	7	0.99	5.09	3.08	14.07	1.352	0.097	1.450	22.99	22.07	16.99	16.08
8	1.30	23.67	15.65	12.66	9.84	8	0.59	3.92	2.62	15.18	1.087	0.089	1.176	16.60	16.55	12.24	12.19
9	1.30	22.89	14.96	12.19	9.42	9	0.90	4.39	3.06	14.27	0.929	0.081	1.010	13.95	13.84	10.53	10.42
10	1.30	21.26	13.89	11.23	8.69	10	0.60	3.76	2.56	10.21	0.822	0.081	0.904	11.56	11.53	8.64	8.60
11	1.30	20.42	13.17	10.74	8.25	11	0.72	3.92	2.77	10.28	0.732	0.073	0.805	9.78	9.75	7.43	7.40
12	1.30	19.56	12.44	10.24	7.80	12	0.60	3.62	2.66	12.44	0.681	0.065	0.746	7.99	8.10	6.11	6.21
13	1.30	19.72	12.51	10.33	7.85	13	0.51	3.37	2.57	14.86	0.611	0.057	0.668	6.87	7.07	5.24	5.44
14	1.35	16.94	11.30	8.72	6.86	14	0.60	3.50	2.56	4.78	0.441	0.057	0.498	5.71	5.72	4.32	4.34
15	1.35	12.56	9.12	6.24	5.20	15	0.57	3.39	2.57	4.00	0.357	0.049	0.406	4.35	4.39	3.23	3.27
16	1.35	12.57	9.13	6.24	5.20	16	0.78	3.72	2.94	4.31	0.294	0.041	0.335	3.92	3.94	2.95	2.97
17	1.35	12.31	8.98	6.10	5.10	17	0.48	3.12	2.33	3.46	0.277	0.041	0.318	3.15	3.19	2.32	2.37
18	1.35	11.14	8.33	5.45	4.63	18	0.47	2.94	2.24	2.87	0.244	0.041	0.285	2.44	2.52	1.80	1.88
19	1.35	10.43	7.91	5.06	4.34	19	0.42	2.69	2.36	2.96	0.174	0.032	0.206	1.84	1.97	1.36	1.49
20	1.35	10.24	7.80	4.96	4.27	20	0.45	2.59	2.33	2.51	0.150	0.032	0.182	1.41	1.53	1.06	1.19
21	1.35	9.96	7.63	4.81	4.15	21	0.34	2.23	2.03	4.37	0.070	0.032	0.102	1.00	1.07	0.76	0.83
22	1.35	9.27	7.21	4.44	3.87	22	0.30	2.04	1.88	3.69	0.060	0.032	0.093	0.71	0.78	0.55	0.62
23	1.35	8.40	6.66	3.98	3.51	23	0.30	1.95	1.95	3.68	0.040	0.024	0.064	0.51	0.58	0.41	0.47
24	1.35	8.76	6.89	4.17	3.66	24	0.26	1.78	1.78	2.98	0.035	0.024	0.059	0.36	0.41	0.30	0.36
25	1.35	8.65	6.82	4.11	3.61	25	0.36	1.91	1.91	3.14	0.031	0.024	0.055	0.25	0.31	0.24	0.29
26	1.35	8.58	6.77	4.07	3.58	26	0.37	2.36	1.98	4.36	0.056	0.024	0.081	2.25	2.28	1.37	1.40

Note: All values in mm unless otherwise stated.

Table A.3 Sizing Tool Results for HOT/WET Material Properties

HOT/WET

	FOOT FLANGE SIZING					WEB SIZING			T' STIFFENER SIZING				RIB CONFIGURATION MASS COMPARISON			
	Through Thickness Corner Radius CSM 20.4-15					Shear Plain Panel	ESDU 71005 Shear Buckling									
		C-SECTION		I-SECTION			UN-STIFFENED	STIFFENED								
Rib No	Krt applied	Flange Thickness t_a	Flange Thickness t_b	t_a	t_b	Rib No	WEB Thickness t_w	WEB Thickness t_w	WEB Thickness t_w		Stiffener Mass (kg)	Mass of Nuts and Bolts (kg)	Total Mass of Stiffener Assembly (kg)	C Section Total Mass (kg)	C-Section Stiffened Total Mass (kg)	I-Section Total Mass (kg)	I-Section Stiffened Total Mass (kg)
1	1.40	40.62	25.45	22.94	17.10	1	12.32	20.39	7.36	109.59	30.567	0.146	30.713	220.78	213.33	181.71	174.26
2	1.30	50.41	28.29	28.98	20.03	2	9.79	17.33	6.86	136.48	25.443	0.138	25.582	179.73	175.87	148.93	145.07
3	1.30	29.76	20.08	16.31	12.80	3	4.18	12.35	4.99	65.77	8.130	0.122	8.252	99.08	85.21	77.55	63.68
4	1.30	48.74	26.53	27.95	18.92	4	3.44	10.43	4.70	49.61	5.201	0.114	5.315	86.45	78.18	70.10	61.84
5	1.30	50.10	26.21	28.79	18.96	5	1.22	6.65	3.36	26.59	2.777	0.106	2.883	58.95	55.69	47.32	44.06
6	1.30	44.78	24.09	25.50	17.14	6	1.31	6.18	3.50	21.95	1.957	0.097	2.054	41.87	39.93	33.46	31.52
7	1.30	42.95	22.91	24.37	16.30	7	1.03	5.15	3.11	14.27	1.359	0.097	1.457	29.58	28.65	23.66	22.72
8	1.30	44.05	22.49	25.05	16.25	8	0.61	3.97	2.65	14.44	1.067	0.089	1.156	21.13	21.05	17.07	16.98
9	1.30	42.73	21.41	24.24	15.53	9	0.94	4.44	3.10	13.49	0.910	0.081	0.991	17.43	17.29	14.33	14.18
10	1.30	39.95	19.99	22.53	14.43	10	0.62	3.81	2.59	9.53	0.806	0.081	0.888	14.57	14.50	11.88	11.82
11	1.30	38.51	18.88	21.64	13.68	11	0.75	3.97	2.80	9.58	0.717	0.073	0.790	12.16	12.11	10.04	9.99
12	1.30	37.05	17.75	20.75	12.92	12	0.62	3.66	2.69	11.72	0.668	0.065	0.733	9.87	9.96	8.20	8.29
13	1.30	37.33	17.81	20.92	12.99	13	0.53	3.41	2.60	14.12	0.600	0.057	0.657	8.47	8.66	7.05	7.24
14	1.35	32.53	16.68	17.99	11.77	14	0.62	3.54	2.59	4.88	0.442	0.057	0.499	7.16	7.17	5.87	5.88
15	1.35	24.89	14.43	13.39	9.56	15	0.59	3.43	2.60	4.09	0.358	0.049	0.407	5.68	5.71	4.49	4.52
16	1.35	24.90	14.44	13.39	9.56	16	0.81	3.76	2.98	4.40	0.295	0.041	0.336	5.06	5.08	4.04	4.06
17	1.35	24.44	14.28	13.12	9.42	17	0.50	3.15	2.36	3.55	0.278	0.041	0.319	4.11	4.16	3.25	3.29
18	1.35	22.36	13.54	11.89	8.75	18	0.49	2.98	2.26	2.97	0.245	0.041	0.286	3.20	3.27	2.52	2.59
19	1.35	21.09	13.05	11.13	8.32	19	0.44	2.72	2.38	3.05	0.174	0.032	0.207	2.40	2.52	1.90	2.02
20	1.35	20.75	12.92	10.93	8.21	20	0.47	2.62	2.35	2.61	0.150	0.032	0.183	1.79	1.91	1.45	1.58
21	1.35	20.24	12.72	10.63	8.03	21	0.35	2.25	2.06	4.44	0.070	0.032	0.102	1.24	1.30	1.03	1.10
22	1.35	19.00	12.20	9.91	7.60	22	0.31	2.06	1.90	3.75	0.060	0.032	0.093	0.84	0.91	0.73	0.80
23	1.35	17.41	11.51	8.99	7.03	23	0.31	1.97	1.97	3.74	0.040	0.024	0.065	0.58	0.64	0.52	0.59
24	1.35	18.07	11.81	9.37	7.27	24	0.27	1.80	1.80	3.04	0.035	0.024	0.059	0.35	0.41	0.36	0.42
25	1.35	17.87	11.72	9.25	7.20	25	0.37	1.93	1.93	3.20	0.031	0.024	0.055	0.20	0.25	0.26	0.31
26	1.35	17.74	11.66	9.18	7.15	26	0.38	2.39	2.00	4.43	0.057	0.024	0.081	3.54	3.56	2.36	2.39

Note: All values in mm unless otherwise stated.

Table A.4 Moisture Uptake Results for In-Plane Shear Tests of M21/T700 Material to Be Tested at Temperature of Ambient & Above

Moisture Ingress Tracker 85%RH 70C																				
Date	Days	Coupon No. M21/T700 268gsm																Mean	Mean Increase (%)	Corrected (residual Moisture %)
		Dummy 1	Dummy 2	A1	A2	A3	A4	A5	A6	A7	A8	A9	A10	A11	A12	A13	A14	A15			
17/11/2006	0	59.42	53.39	48.96	48.73	49.05	48.29	48.56	47.99	48.7	47.8	48.44	48.33	48.5	48.45	48.61	47.81	48.09	49.36	0	0.248576785
24/11/2006	7	59.62	53.56	49.08	48.88	49.17	48.41	48.68	48.1	48.82	47.92	48.56	48.45	48.63	48.56	48.71	47.92	48.21	49.48706	0.257412527	0.505989312
05/12/2006	18	59.67	53.59	49.15	48.93	49.23	48.46	48.74	48.16	48.87	47.97	48.59	48.5	48.68	48.62	48.78	47.98	48.26	49.54	0.364667747	0.613244532
12/12/2006	25	59.7	53.63	49.17	48.96	49.26	48.49	48.76	48.18	48.9	47.98	48.64	48.52	48.7	48.65	48.8	48	48.29	49.56647	0.418295357	0.666872142
02/01/2007	46	59.71	53.67	49.24	49.01	49.3	48.53	48.82	48.24	48.96	48.04	48.69	48.56	48.73	48.68	48.85	48.05	48.33	49.61235	0.511249881	0.759826665
08/01/2007	53	59.71	53.67	49.22	49.01	49.31	48.53	48.8	48.22	48.94	48.02	48.68	48.57	48.74	48.7	48.85	48.04	48.34	49.60882	0.504099533	0.752676317
16/01/2007	60	59.71	53.67	49.24	49.02	49.31	48.55	48.82	48.25	48.96	48.05	48.69	48.58	48.76	48.71	48.86	48.05	48.35	49.62235	0.5315092	0.780085985
23/01/2007	67	59.72	53.69	49.25	49.03	49.35	48.56	48.84	48.25	48.99	48.07	48.72	48.61	48.76	48.72	48.88	48.07	48.36	49.63941	0.566069215	0.814646
05/02/2007	74	59.72	53.69	49.27	49.05	49.37	48.58	48.85	48.27	49	48.09	48.73	48.63	48.8	48.74	48.91	48.09	48.38	49.65706	0.601820955	0.85039774
14/02/2007	83	59.74	53.7	49.29	49.05	49.37	48.6	48.88	48.29	49.02	48.1	48.75	48.63	48.8	48.75	48.92	48.11	48.39	49.67	0.628038898	0.876615683
19/02/2007	88	59.74	53.72	49.29	49.07	49.37	48.6	48.88	48.28	49	48.09	48.74	48.63	48.81	48.75	48.91	48.11	48.39	49.66941	0.626847173	0.875423958
26/02/2007	95	59.73	53.7	49.3	49.08	49.38	48.59	48.87	48.27	49.02	48.1	48.75	48.63	48.8	48.76	48.92	48.1	48.39	49.67	0.628038898	0.876615683
05/03/2007	102	59.73	53.7	49.3	49.07	49.38	48.6	48.88	48.28	49.01	48.09	48.76	48.62	48.81	48.76	48.92	48.1	48.4	49.67118	0.630422347	0.878999132
12/03/2007	109	59.74	53.7	49.29	49.08	49.38	48.59	48.88	48.27	49.01	48.1	48.75	48.63	48.81	48.75	48.91	48.09	48.39	49.66882	0.625655449	0.874232233
16/04/2007	144	59.71	53.69	49.3	49.07	49.39	48.58	48.89	48.3	49.03	48.11	48.76	48.63	48.82	48.75	48.93	48.11	48.4	49.67471	0.637572695	0.88614948
PERCENT INCREASE/ per coupon		0.488051161	0.561902978	0.694	0.698	0.693	0.601	0.68	0.646	0.678	0.649	0.661	0.621	0.66	0.619	0.658	0.627	0.645			

Note: All values in g unless otherwise stated.

Table A.5 Moisture Drying Results for In-Plane Shear Tests of M21/T700 Tested at Temperature of Ambient & Above

Moisture Drying Tracker 70C 0%RH					
Date	Days	Coupon No. M21/T700 268gsm		Mean	Mean Increase
		A21	A18		
23/01/2007	0	48.78	47.78	48.28	0
29/01/2007	7	48.71	47.71	48.21	-0.144988
05/02/2007	14	48.69	47.7	48.195	-0.176056
14/02/2007	23	48.68	47.68	48.18	-0.207125
19/02007	28	48.67	47.68	48.175	-0.217481
26/02/2007	35	48.66	47.66	48.16	-0.24855
05/03/2007	42	48.66	47.66	48.16	-0.24855
12/03/2007	49	48.66	47.66	48.16	-0.24855
16/04/2007	84	48.64	47.65	48.145	-0.279619
22/04/2007	91	48.64	47.65	48.145	-0.279619
29/04/2007	98	48.64	47.65	48.145	-0.279619
PERCENT INCREASE/per coupon		-0.28700287	-0.272080368		

Note: All values in g unless otherwise stated.

A.1 In-Plane Shear Testing At Elevated Temperatures Method Summary

An appropriate tensile test machine was used to test the coupons in accordance with ISO 7500/1 class 1. However the addition of a heating chamber or furnace was required around the test rig for controlling the temperature of the coupons. This chamber was removable to allow the coupons to be inserted into the test frame at room temperature. The chamber was then placed around the test frame to heat the coupon to the required temperature. The requirements of the chamber [14], state the chamber shall be controllable to <±3°C. Ordinarily the temperature measuring equipment must be accurate to <±2°C. However in this case the thermocouple placed within the 'Dummy' coupons was used to measure the temperature, having significantly greater accuracy than the specified equipment.

A dwell time was required to enable the coupon to be of the required uniform temperature through its thickness. This dwell time was unknown, so to enable the core temperature of the coupon to be determined, the author has engineered a dummy coupon, having thermocouples located between the centre line of the material (see figure A.1).

To carry out the mechanical tests a summary of the apparatus is as follows:

- Tensile Test Machine calibrated to ISO 7500/1.
- Chamber compatible with test machine to permit tests at specified temperatures (controllable to within 3°C).
- Flat Face Micrometer accurate to nearest 0.01mm.
- Vernier Calliper (Dial Calliper) accurate to nearest 0.1mm.
- Equipment to measure longitudinal and transverse strain to < ± 1% in the applied load range. In this case this will be via the provision of bi-axial strain gauges, 2 off located on each face of the coupon to be tested (gauge length 5 to 10mm) and appropriate data logging equipment.

All coupons were 'C-Scanned' (Ultra sound Non Destructive Testing (NDT)) prior to testing to ensure the material was correctly consolidated and free from defects. In all cases the coupons were manufactured from unidirectional material with fibres orientated at +45° & -

45° to that will be the longitudinal axis of the test specimens (0°). This lay-up is fully symmetrical. The panels used for manufacture of the coupons were prepared in accordance with [7], method 'B'. All coupons required end tabs to be bonded to both ends and both sides of the coupon. The coupon requirements are detailed in [14], however in summary these were made from Tufnol 10G, a high quality commercially available glass fibre material infused with epoxy resin. In this case the end tabs material had a thickness of 2mm and has been bonded to the surface of the coupon using a suitable epoxy resin, by the coupon manufacturer.

a)

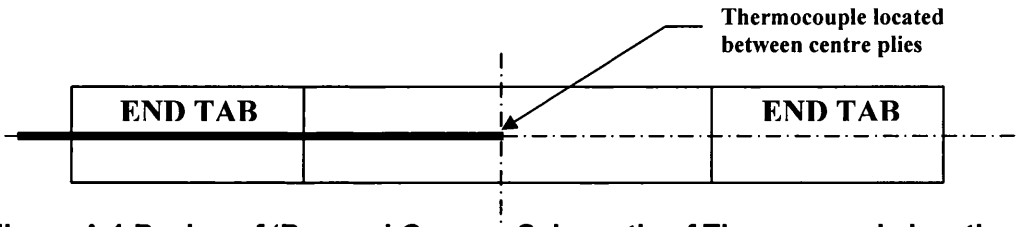

Figure A.1 Design of 'Dummy' Coupon Schematic of Thermocouple location in Coupon

This 'Dummy' coupon has been manufactured with a thermocouple located within its core. This is placed into the coupon at the centre ply during the manufacturing process. This coupon is to act as a 'dummy coupon' during the testing processes and was not subjected to mechanical test. Besides being able to determine the coupons core temperature had equalised with the surrounding atmosphere, the 'dummy coupons' primary roll was to ensure the test could be conducted in the shortest time possible.

For each condition six coupons were tested to ensure a large enough sample batch to reduce the effects of scatter, while keeping the number of tests to a minimum, taking into account cost considerations.

The storage of coupons prior to testing, once they have left the conditioning chamber, was in accordance with [8]. Before each test was conducted the coupons were measured for dimensional accuracy, specifically width at three points in the gauge length and thickness which was then recorded. For reference figure A.2 shows a schematic of the coupon geometry. Dimensions for the coupon are as follows:

- t = 8 times cure ply thickness of material used.

- w = 25.00 ± 0.25mm
- L_1 = 130 ± 1mm
- L = 230 ± 1mm
- g = 50 ± 1mm

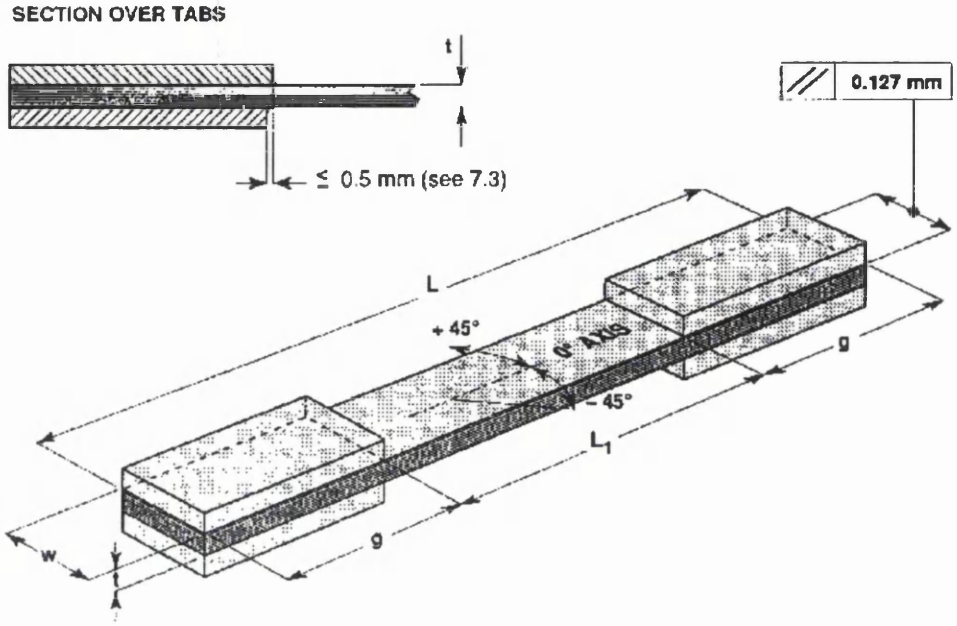

Figure A.2 In-Plane Shear Coupon [14]

The coupon is placed in the jaws of the machine. Care was taken to ensure that the coupon was accurately aligned in the 0° direction with the test machine axis. The tensile load was then applied at the machine crosshead at a speed of 1mm/minute and the 0 & 90° strains continuously recorded against load until 2% longitudinal strain was reached. Beyond 2% longitudinal strain the crosshead speed was increased to 10mm/minute until failure. On failure of the coupon the maximum load was recorded. In all cases the time taken to reach test temperature was recorded.

From testing shear strength can be determined as shown in equation A.1:

$$\tau = \frac{P_{\max}}{2wt} \ (\text{N/mm}^2) \qquad \textbf{(Equation A1)}$$

Where: P_{max} is the maximum tensile load during the test (N).

w is the average of the three width measurements (mm)

t is the average of the three thickness measurements (mm)

The shear modulus of the coupon can then be defined by equation A.2:

$$G = \frac{\Delta P}{2wt(\Delta\varepsilon_o - \Delta\varepsilon_{90})} = \frac{\Delta\tau}{(\Delta\varepsilon_o - \Delta\varepsilon_{90})} \text{ (N/mm}^2\text{)} \qquad \textbf{(Equation A2)}$$

Where: ΔP is the difference in tensile loads at the longitudinal strains.

$(\varepsilon_o)_1 = 500 \text{ X } 10^{-6}$ & $(\varepsilon_o)_2 = 2500 \text{ X } 10^{-6}$ (N)

$\Delta\tau$ is the difference in shear strength at:

$(\varepsilon_o)_1 = 500 \text{ X } 10^{-6}$ & $(\varepsilon_o)_2 = 2500 \text{ X } 10^{-6}$ (N).

$\Delta\varepsilon_o$ is the difference in longitudinal strains.

$(\varepsilon_o)_2 - (\varepsilon_o)_1 = 2000 \text{ X } 10^{-6}$ (N)

$\Delta\varepsilon_{90}$ is the difference in transverse strain corresponding to

$(\varepsilon_o)_2 = 2500 \text{ X } 10^{-6}$ & $(\varepsilon_o)_1 = 500 \text{ X } 10^{-6}$

Note: If $\Delta\varepsilon_o - \Delta\varepsilon_{90}$ is measure directly then:

$(\varepsilon_o - \varepsilon_{90o})_2 = 4500 \text{ X } 10^{-6}$ & $(\varepsilon_o - \varepsilon_{90o})_1 = 900 \text{ X } 10^{-6}$

$\Delta\varepsilon_0$-$\Delta\varepsilon_{90}$ $(\varepsilon_o - \varepsilon_{90o})_2 - (\varepsilon_o - \varepsilon_{90o})_2 = 3600 \text{ X } 10^{-6}$

The above strains were used unless otherwise specified.

Table A.6 In-Plane Shear Results of M21/T700 Material (RT/DRY)

Specimen ID	Test Environment	Width (mm)	Thickness (mm)	Axial Modulus (GPa)	Pmax (N)	Failure stress (MPa)	Shear Modulus G) (GPa)	Shear strength (τ) (MPa)
"B2"	RT - Dry	25.03	2.19	14.1	10607	194	4.0	96.8
"A24"	RT - Dry	24.93	2.08	15.8	10657	206	4.6	102.8
"B1"	RT - Dry	25.40	2.10	15.4	10714	201	4.5	100.4
"A19"	RT - Dry	25.01	2.04	16.1	10931	214	4.6	107.1
"A20"	RT - Dry	25.10	2.14	15.2	10731	200	4.4	99.9
			Average	*15.3*	-	*202.8*	*4.4*	*101.4*
			Std Dev	*0.8*	-	*7.7*	*0.2*	*3.9*
			C of V	*5.1*	-	*3.8*	*5.6*	*3.8*

Table A.7 In-Plane Shear Results of M21/T700 Material (60°C/DRY)

Specimen ID	Test Environment	Width (mm)	Thickness (mm)	Axial Modulus (GPa)	Pmax (N)	Failure stress (MPa)	Shear Modulus G) (GPa)	Shear strength (τ) (MPa)
"A17"	60 - Dry	25.02	2.00	15.5	10573	211	4.4	105.6
"A21"	60 - Dry	25.04	2.05	15.1	11074	216	4.4	107.9
"A22"	60 - Dry	24.99	2.09	14.9	10056	193	4.3	96.3
"A23"	60 - Dry	25.06	2.03	15.3	10744	211	4.4	105.6
			Average	*15.2*	-	*207.7*	*4.4*	*103.8*
			Std Dev	*0.3*	-	*10.3*	*0.1*	*5.2*
			C of V	*1.7*	-	*5.0*	*1.7*	*5.0*

Table A.8 In-Plane Shear Results of M21/T700 Material (DRY/90°C)

Specimen ID	Test Environment	Width (mm)	Thickness (mm)	Axial Modulus GPa)	Pmax N)	Failure stress MPa)	Shear Modulus G) GPa)	Shear strength ν) MPa)
"A18"	90- Dry	25.02	2.11	13.1	9993	189	3.7	94.6
"B4"	90- Dry	25.00	2.00	14.4	10206	204	4.1	102.1
"B5"	90- Dry	24.98	2.05	14.0	10331	202	4.0	100.9
"B6"	90- Dry	24.98	2.11	13.4	10251	194	3.8	97.2
"B7"	90- Dry	25.00	2.00	14.1	10401	208	4.0	104.0
			Average	*13.8*	-	*199.5*	*3.9*	*99.8*
			Std Dev	*0.5*	-	*7.6*	*0.2*	*3.8*
			C of V	*3.8*	-	*3.8*	*3.9*	*3.8*

Table A.9 In-Plane Shear Results of M21/T700 Material (RT/WET)

Specimen ID	Test Environment	Width (mm)	Thickness (mm)	Axial Modulus GPa)	Pmax N)	Failure stress MPa)	Shear Modulus G) GPa)	Shear strength ν) MPa)
"A1"	RT - Wet	25.02	2.01	15.0	10989	219	4.2	109.3
"A2"	RT - Wet	25.00	2.00	14.9	11163	223	4.3	111.6
"a3"	RT - Wet	24.87	2.02	15.0	10987	219	4.3	109.4
"a4"	RT - Wet	24.80	2.01	14.9	11016	221	4.2	110.5
"a5"	RT - Wet	24.96	2.10	14.4	11121	212	4.1	106.1
			Average	*14.9*	-	*218.7*	*4.2*	*109.4*
			Std Dev	*0.2*	-	*4.1*	*0.1*	*2.1*
			C of V	*1.7*	-	*1.9*	*1.7*	*1.9*

Table A.10 In-Plane Shear Results of M21/T700 Material (60°C/WET)

Specimen ID	Test Environment	Width (mm)	Thickness (mm)	Axial Modulus GPa)	Pmax N)	Failure stress MPa)	Shear Modulus G) GPa)	Shear strength ν) MPa)
"a6"	60- Wet	24.95	2.11	13.0	10400	198	3.7	98.8
"a7"	60- Wet	24.85	2.20	12.7	10195	186	3.6	93.2
"a8"	60- Wet	24.99	2.02	13.3	9940	197	3.8	98.5
"a9"	60- Wet	24.95	2.09	13.0	9876	189	3.7	94.7
"a10"	60- Wet	24.95	2.05	13.2	10078	197	3.7	98.5
			Average	*13.0*	-	*193.5*	*3.7*	*96.7*
			Std Dev	*0.2*	-	*5.2*	*0.1*	*2.6*
			C of V	*1.9*	-	*2.7*	*2.1*	*2.7*

Table A.11 In-Plane Shear Results of M21/T700 Material (90°C/WET)

Specimen ID	Test Environment	Width (mm)	Thickness (mm)	Axial Modulus GPa)	Pmax N)	Failure stress MPa)	Shear Modulus G) GPa)	Shear strength ν) MPa)
"A12"	Wet- 90°C	24.96	2.02	12.0	8829	175	3.4	87.6
"A13"	Wet- 90°C	24.97	2.04	11.7	8707	171	3.1	85.5
"A14"	Wet- 90°C	25.00	2.06	11.1	8700	169	3.1	84.5
"A15"	Wet- 90°C	24.99	2.06	11.7	8748	170	3.2	85.0
			Average	*11.6*	-	*171.2*	*3.2*	*85.6*
			Std Dev	*0.4*	-	*2.7*	*0.1*	*1.4*
			C of V	*3.2*	-	*1.6*	*3.7*	*1.6*

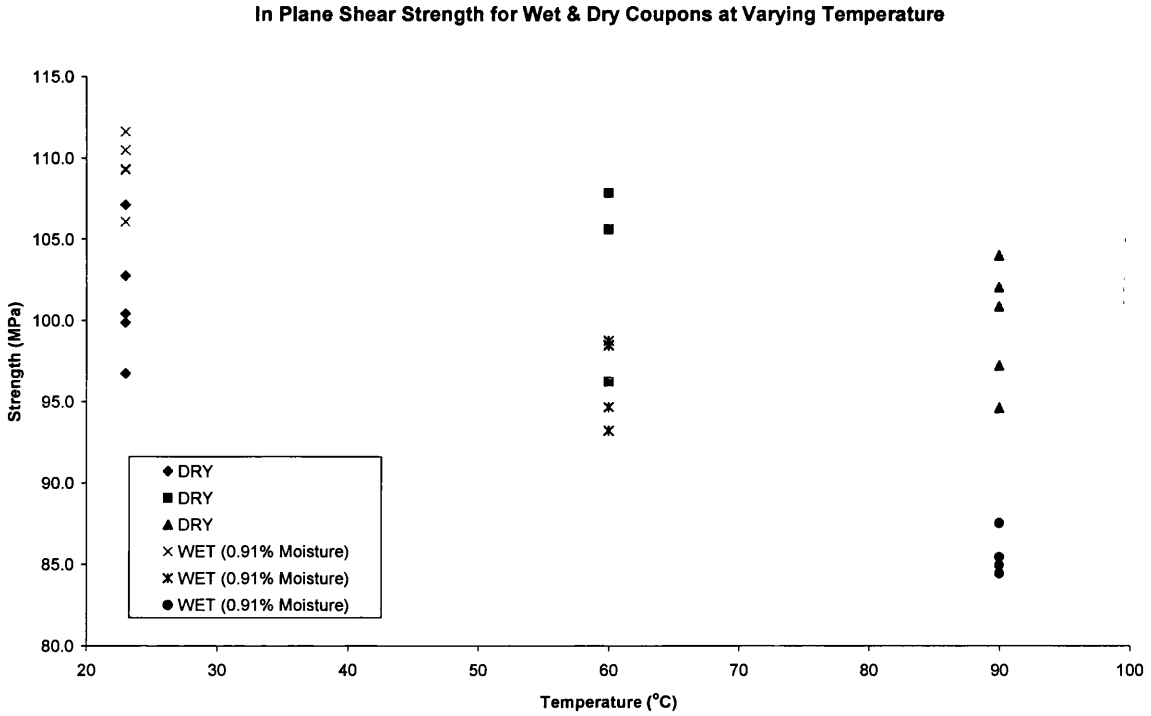

Figure A.3 M21/T700 Individual Coupon Test Results for In-Plane Shear Strength

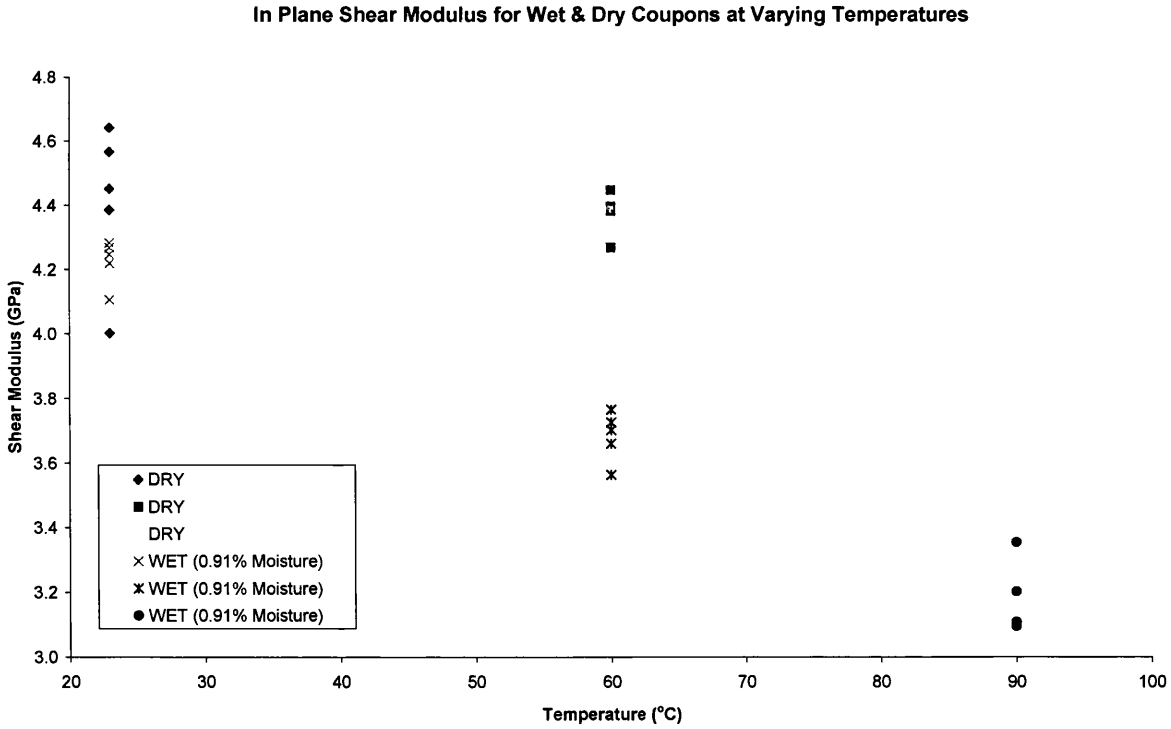

Figure A.4 M21/T700 Individual Coupon Test Results for In-Plane Shear Modulus

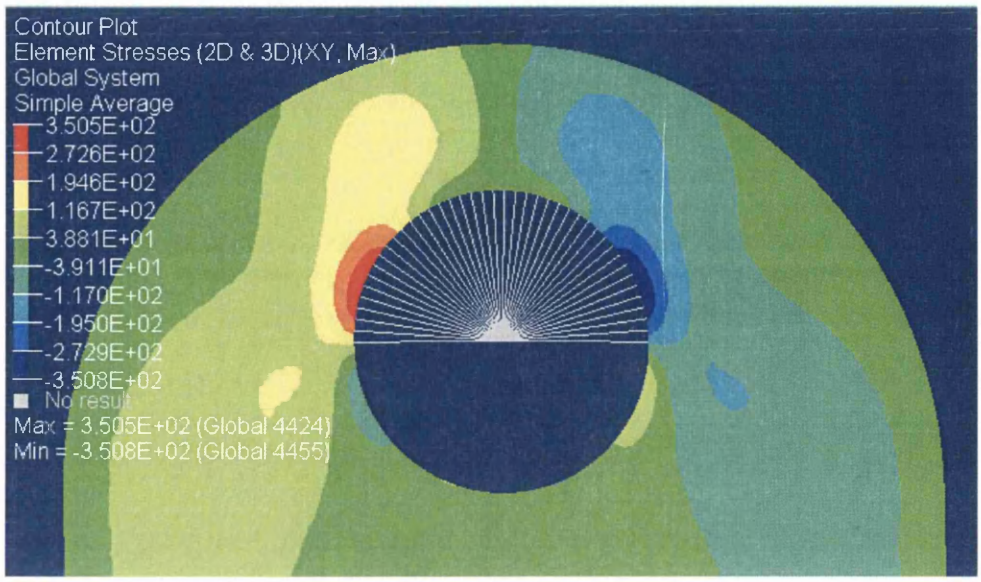

Figure A.5 Shear Stress (XY) Results for 26mm Lug at 470kN Load and a Shear Stress Failure at 350MPa

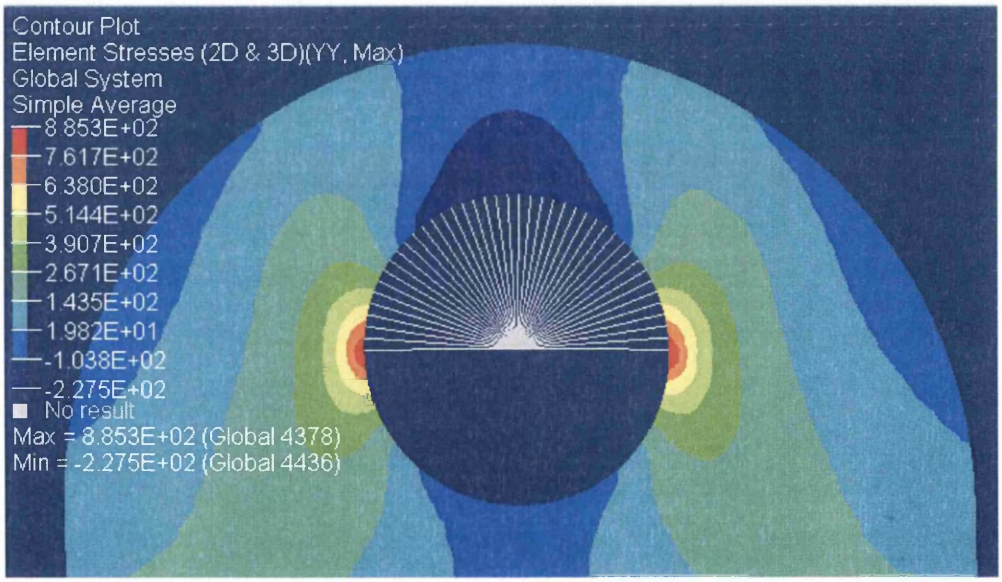

Figure A.6 Tensile Results for 26mm Lug at 470kN Load and a Shear Stress Failure at 853MPa

A.2 Environmental Control of Specimens

A.2.1 Specimen Manufacturing

The manufacture of panels for the creation of test specimens was carried out following the normal methods, as defined by the test leader, for the manufacture of composite components e.g. hand lay-up. As the resin was in the uncured state, standard procedures for handling and manufacture were followed.

The panels were considered to leave the Autoclave in a dry state (as the autoclave cure was carried out for both M21 & 977-2 resin systems at 180°C) and the aim was to preserve this dry state. Panels spend the shortest time possible going through the NDT process, and in most instances this was achievable within 2 days. **Seven days is considered the maximum** time allowed between removal from the autoclave and specimen cutting. During this time material was stored in a controlled environment which in this case was sealed bag containing desiccant.

As well as taking care to limit exposure to the ambient environment, it was also important to capture the conditions that the panel/specimens are exposed to. To achieve this, a data logger monitoring temperature and humidity was included with each batch of panels when it left the autoclave until it returned from specimen cutting and placed into the oven for drying. When the specimens were dried in the oven the humidity of the oven was also monitored, however the accuracy of the loggers used was in question, meaning that it was not possible to have confidence in the recorded data at this stage.

To limit exposure to the environment, the external machining company were then allowed seven days (5 working days), to extract coupons from the panels and were responsible for the control of the panels whilst in their care.

A2.2 Specimen Cutting

To further ensure a reduced exposure to ambient conditions all preparation for the cutting of specimens was in place prior to the completion of the panel from which they were to be cut. Specimens were returned in a controlled environment using sealed containers containing desiccant, provided by the author with an accompanying environmental data logger, originally supplied with the panels.

This control gave two weeks exposure to the ambient environment between leaving the autoclave and receiving the specimens back from being cut. Specimens were then weighed within one day after being received from the machining company. It should be noted that in reality some batches were delayed by up to a week, which didn't appear to increase the drying time required before conditioning, showing that this process can be considered more than adequate.

Where water jet cutting was utilised for coupon extraction as it provides relatively short cutting times to other methods and provides a good surface finish, critical to come test methods used. The use of the water jet was not considered to increase the level of moisture in the coupons, supported by negligible drying times required on receipt of the coupons.

A2.3 Oven drying

Upon receiving the specimens after machining they were weighed, then placed straight into an oven to remove any moisture absorbed during the NDT and cutting processes. Humidity in the oven was continually monitored. The specimens were then weighed weekly until there was no further decrease in weight, indicating that all absorbed moisture had been lost. The samples were then ready to be placed into desiccators so that they remained dry. In many cases the storage of specimens for testing was not required with coupons being delivered straight to conditioning chambers.

A.2.4 Storage

Once the specimens were dry they were be taken from the oven and placed in desiccators so that they remained dry until they were required for conditioning. The humidity and temperature inside the desiccators was logged, however the equipment that was used could not be considered to be accurate as humidity lower than 10%RH was lower than the calibrated range of the equipment. To overcome this weighing of coupons periodically and before testing proved that no moisture uptake had taken place, while coupons were in the desiccators.

A.2.5 Conditioning

Conditioning took place in accordance with [9]. Specimens were weighed prior to the start of conditioning and compared against the weight take prior to storage and drying. During the conditioning process the specimens were weighed weekly and the results recorded. This deviates from the standard, where coupons should be weighed daily for the first week of conditioning, an oversight by the author. Specimens were deemed to have reached equilibrium when their weight remained constant for a period of three weeks.

It was also important to check the functionality of the conditioning chambers regularly. Failure of the chamber can lead to unwanted drying which not only increases the time required for conditioning but also results in unwanted cyclic conditioning of the specimen. For this reason it was important to ensure that the environmental history of the chambers is recorded independently.

Once coupons reached equilibrium it was permitted for coupons to spend time in the chamber until test. For specimens that underwent only partial saturated (lug validation tests) coupons were removed from the chamber and tested within 1% of the desired conditioning time. This 1% was defined by the author, based on what was achievable during testing. Any further exposure would have led to an undesired increase in moisture content. The effect of any excess exposure will be dependent on the temperature and humidity levels i.e. the higher the temperature or humidity the faster the rate of diffusion or the higher the level of moisture that will get driven into the coupons.

All tests were conditioned without bonded end tabs allowing moisture uptake to be measured directly and with testing being carried out in accordance with reference [80]. End tabs (where required) were then assembled when putting the coupons into the test frame using the results from section 4.6.

A.2.6 Testing

Specimens were weighed as they were removed from the chamber and tested within 30 minutes to limit any drying during expose to the test lab environment.

For testing in conditions other than ambient it was important to ensure that an environmental cabinet was set up around the load frame and that it had reached the desired levels of temperature (and humidity where possible) before placing specimen in

grips ready for test. Specimens remained in the conditioning chamber until this has occurred.

When testing specimens that are partially saturated it was important to be aware that these specimens are particularly sensitive to time spent in environments other than that to which they were conditioned in. Therefore the procedures defined in this section are particularly important.

A.2.7 Remarks

In conclusion the overriding driver behind the control process is to limit the exposure to environment and monitor undefined environmental conditions. Using this control removes the possibility of any conditioning of the specimens occurring, other than that specified for the test. This removes any ambiguity in the level of moisture contained within a specimen, allowing confidence in the results.

A.3 End Tab Removal Study

The double-sided abrasive selected took the form of dry wall sanding screen. This is a double-sided abrasive mesh, Figure A.7. The sanding screen was supplied in packets containing two grades, medium 220 Grade and course 120 Grade. Both types were used interchangeably in the trial with no apparent difference being seen between the two.

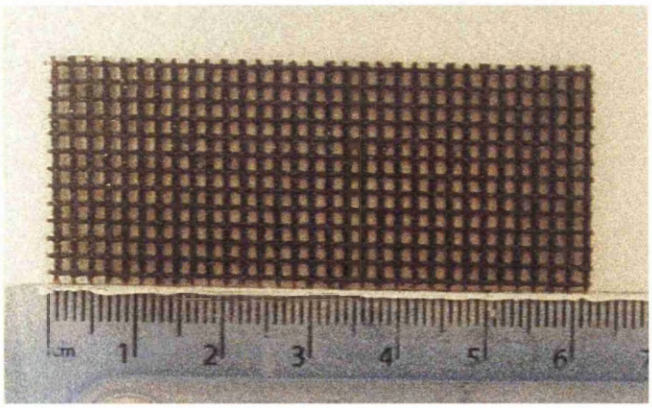

Figure A.7 Example of Sanding Screen Cut to Size

Two specimens were cut from surplus material, Figure A.8. They had the dimensions 270x25x9mm and a nominal lay-up of 44/44/11. Specimen configuration was selected

based on the requirements of all the previous test standards employed on the project with a large thickness in excess of the standards being used to ensure that high failure loads could be achieved using the chosen abrasive. This would provide a wide range over which to assess the effectiveness of using the abrasive as a replacement to bonding and easily encompasses the failure loads associated with thinner 2-4mm thick specimens usually specified in test standards. Work being carried out under EMOC concentrates on resin dominated failure modes with coupons having small amounts of 0° fibres compared to specimens used in these trials. Therefore the failure loads seen during this trial will be greater than anything likely to be seen during EMOC testing.

Figure A.8 Example of Specimen

End tabs were cut from Tufnol 1040G glass/epoxy and had a length of 60mm, Figure A.9. Although 50mm end tabs are generally the minimum requirement for tensile testing, 60mm is typically used by Airbus test labs.

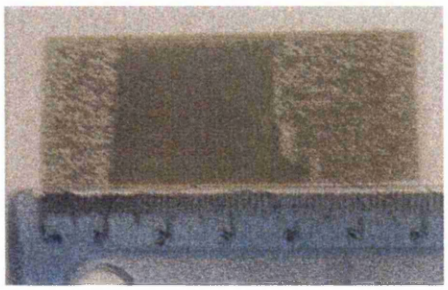

Figure A.9 Tufnol End Tab

Load was applied using a 250kN Zwick test frame in conjunction with MTS hydraulic grips.

A.3.1 Procedure

After all components had been cut to the right dimensions the specimen, abrasive and end tab were assembled and held together using sticky tape to enable easy assembly into the grips, Figure A.10.

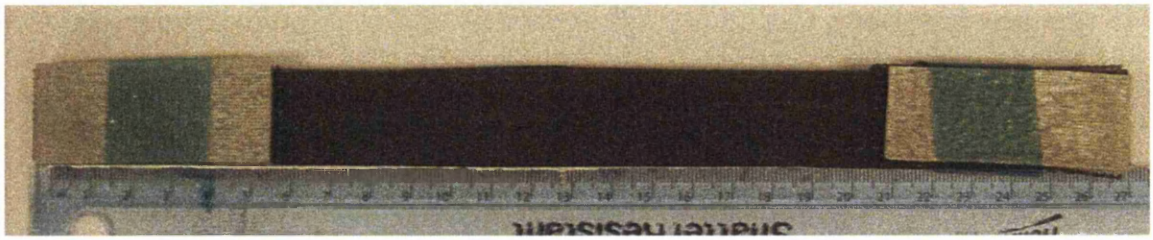

Figure A.10 Specimen With End Tabs and Abrasive Attached

The specimens were assembled into the grips and load was applied at a rate of 1mm/min. An initial grip pressure of 20.68MPa (3000psi) was applied. The output plot of stress versus displacement was monitored closely for signs of slippage i.e. when displacement increased without a corresponding increase in stress slippage was said to have occurred. As slippage was seen to occur the grip pressure was increased incrementally.

A.3.2 Results

A plot of Stress versus displacement is presented in Figure A.11. Points where slippage has occurred can be seen clearly.

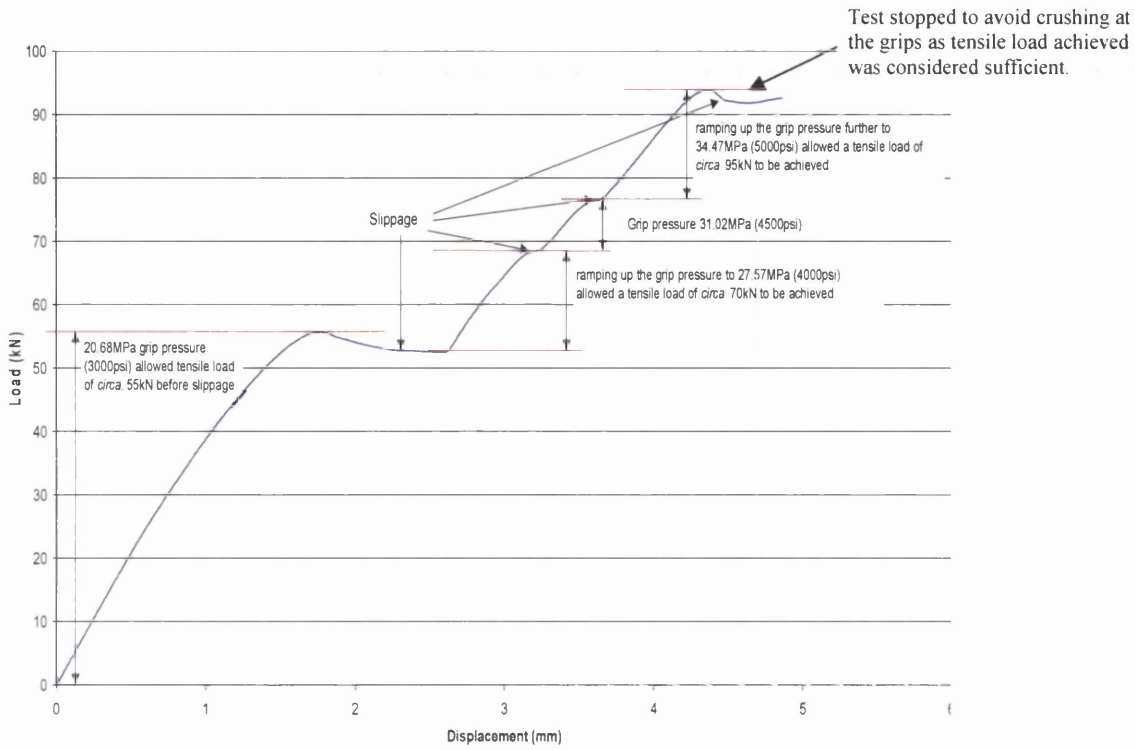

Figure A.11 Load Versus Displacement Plot Showing Slippage

Grip pressure was taken as the hydraulic pressure from the grip system. The initial grip pressure of 20.68MPa (3000psi) allowed the specimen to be loaded to 55kN before slippage began to occur. The grip pressure was then increased to 27.57MPa (4000psi) this allowed an increase in load up to about 66kN before slippage again began to occur. Grip pressure was then increased to 31.02MPa (4500psi) allowing an increase in load to about 77kN. A further and final increase in grip pressure to 34.47MPa (5000psi) allowed a load of around 93kN to be induced in the specimen. As a guideline these results have been tabulated in Table A.12.

Table A.12 Tensile Stress Achievable at Each Grip Pressure

Applied Load (kN)	Tensile Stress (MPa)	Grip Pressure (MPa)
55	250	20.68
66	300	27.57
77	350	31.02
93	425	34.47

A Graph of Tensile stress as a function of grip pressure is presented in Figure A.12.

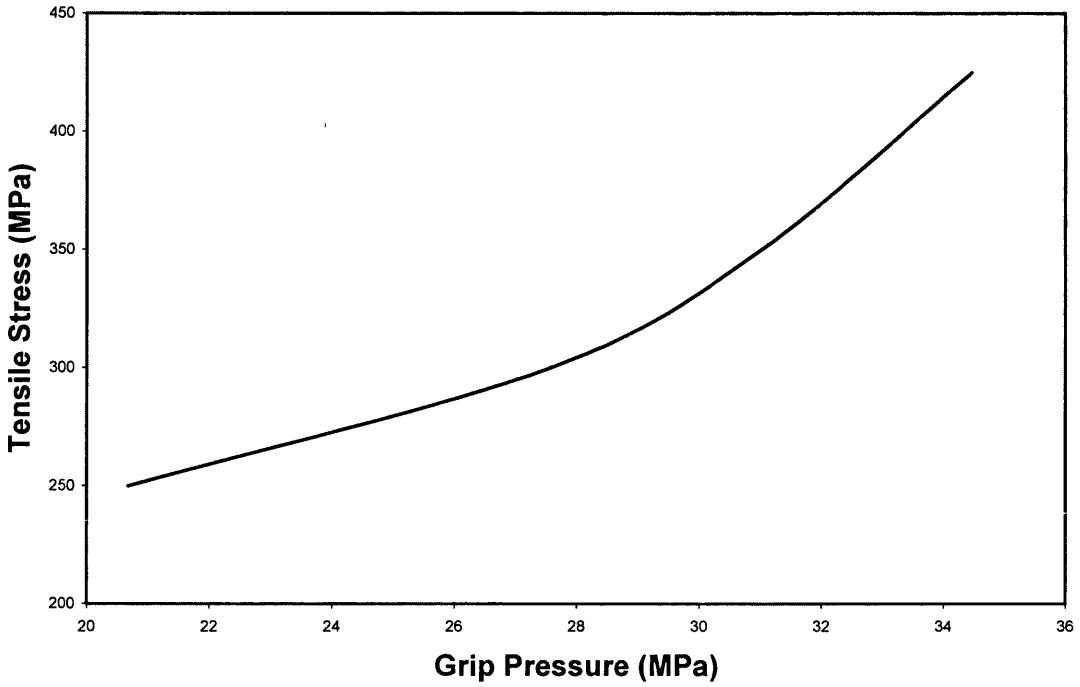

Figure A.12 Allowable Tensile Stress as a Function of Grip Pressure

An approximate shear stress at the coupon/end tab interface was calculated. It was assumed that the load is being put into the specimen via the two tabs at one end and taken out again via the two tabs at the other. Therefore each pair of tabs sees the total applied load. A schematic of the coupon/end tab configuration is shown in Figure A.13.

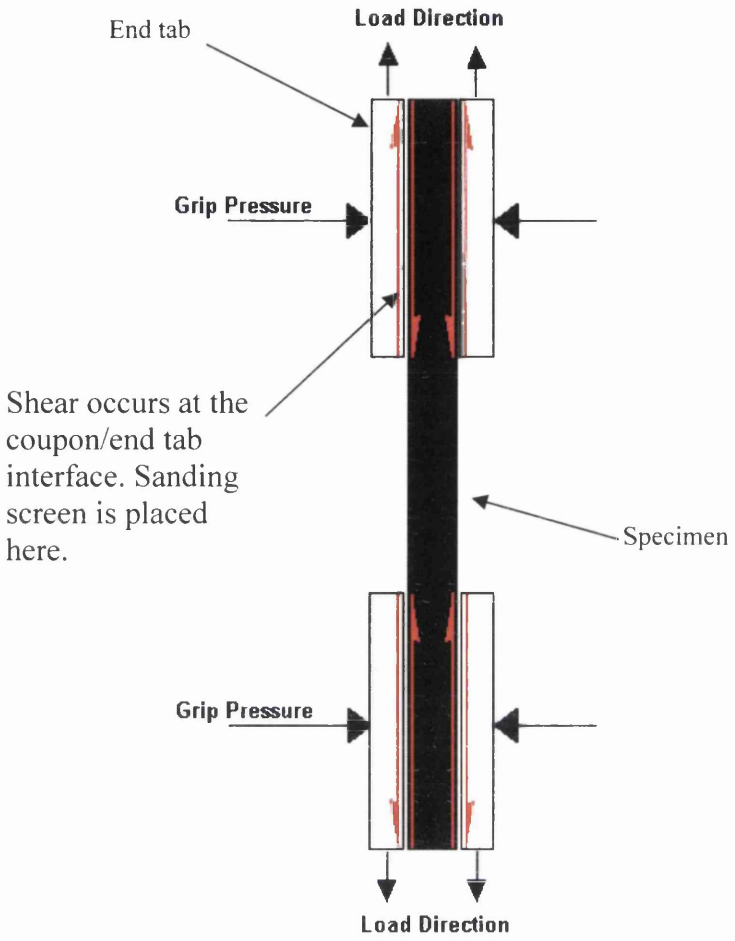

Figure A.13 Schematic of Coupon/End Tab Interface

The area of the end tabs can be calculated as follows:

Area (A) = 25x60mm = 1500mm^2 (for each end tab)

Loads (F) = 55kN, 66kN, 77kN, 93kN

And,

$$\tau = \frac{F}{A}$$ **(Equation A.3)**

Therefore as the stress is assumed to be split evenly between two end tabs:

$$\tau = \frac{F}{(A \times 2)}$$ **(Equation A.4)**

The loads selected give the shear stress for the maximum applied tensile load achievable for each incremental increase in pressure. These are shown in table A.13. It should be noted that in reality the actual shear stress distribution is not uniform across each tab face.

Table A.13 Shear Stress at Coupon/End Tab Interface Achievable at Each Grip Pressure For a Given Applied Load

Tensile Stress (MPa)	Shear Stress (MPa)	Grip Pressure (MPa)
250	18.3	20.68
300	22	27.57
350	25.7	31.02
425	31	34.47

A plot of the shear stress at the coupon/end tab interface versus grip pressure is also provided in figure A.14

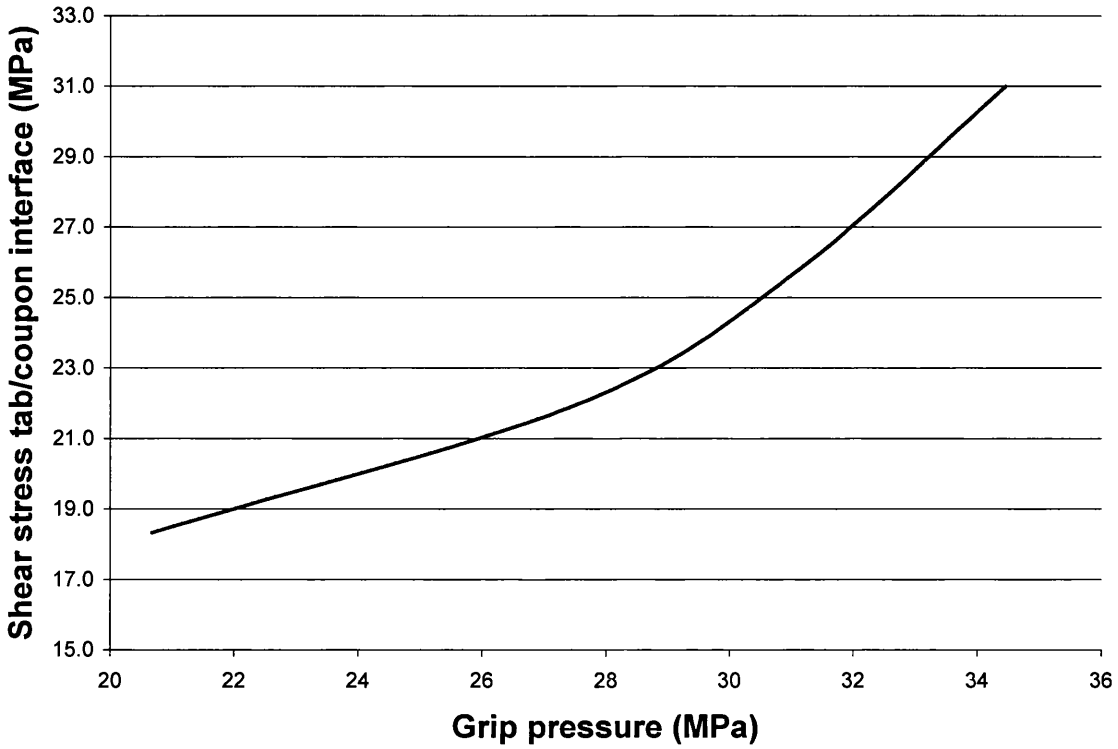

Figure A.14 Shear Stress at Tab/Coupon Interface versus Grip Pressure

Considering figure A.14 it is important to note that reducing the tab length will raise the shear stress at the tab/coupon interface while increasing it will reduce the shear stress. But as previously mentioned the shear stress distribution across the tab face is not likely to be uniform therefore the increase in grip strength with increasing tab length is not likely to be linear. Extrapolating the grip length and corresponding pressure may well lead to errors.

A.3.3 Remarks

The results show that the use of double-sided abrasive as a replacement to bonding for end tabs during CFRP tensile tests can be used successfully. Many of the standard specimen tests used by Airbus UK have failures stresses well within the maximum of 425MPa seen in this test. Upon inspection of the specimen after the test it can be seen that the abrasive has embedded itself quite considerably into both the specimen and the end tab, Figure A.15. This provided a very effective friction layer. Which, given the correct level of grip pressure, can be successfully used in preventing slippage of the specimen in the grips.

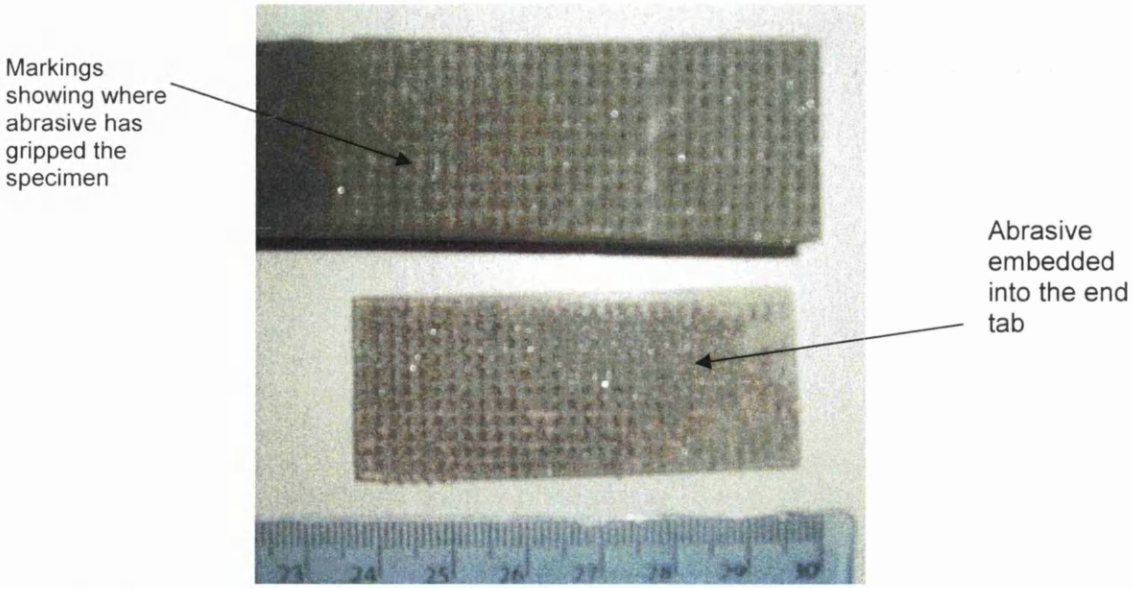

Figure A.15 Evidence of Abrasive Embedding into Both the Specimen and End Tab

It is recommended that some caution be used when applying this knowledge to thin specimens as they may be more susceptible to crushing in the grips. Increasing the size of the end tabs will lower the shear stress and therefore reduce the required grip pressure which should help to alleviate this. That said they will also fail at a low load and so it should be possible to reduce the grip pressures used in comparison to this test. It is advised that some trials are carried out before commencing testing.

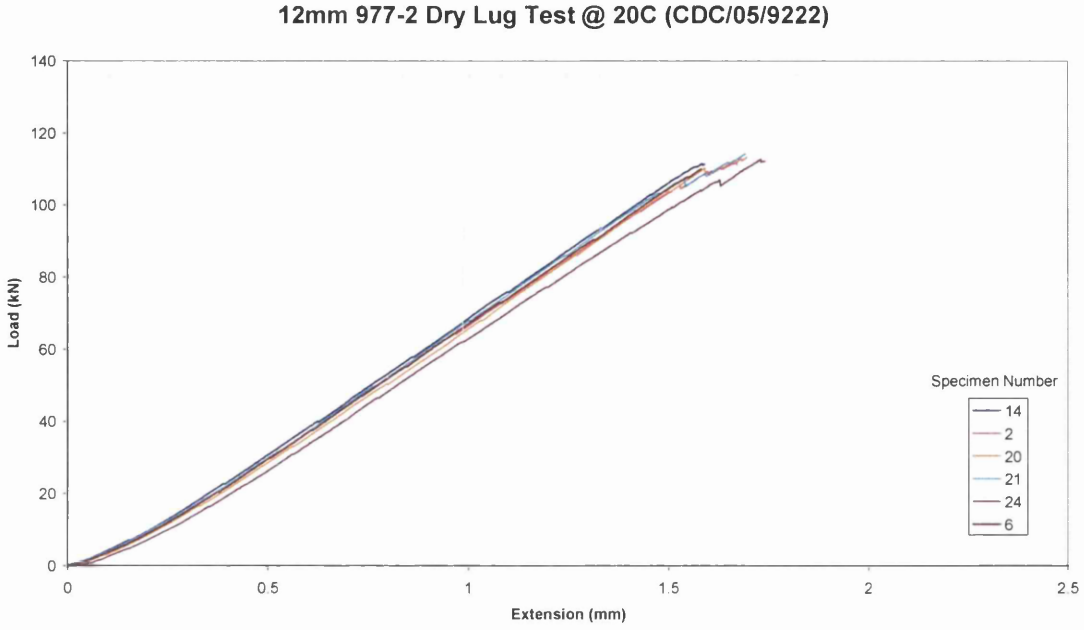

Figure A.16 Individual 12mm Lug Tests in the Dry State Tested at 20°C

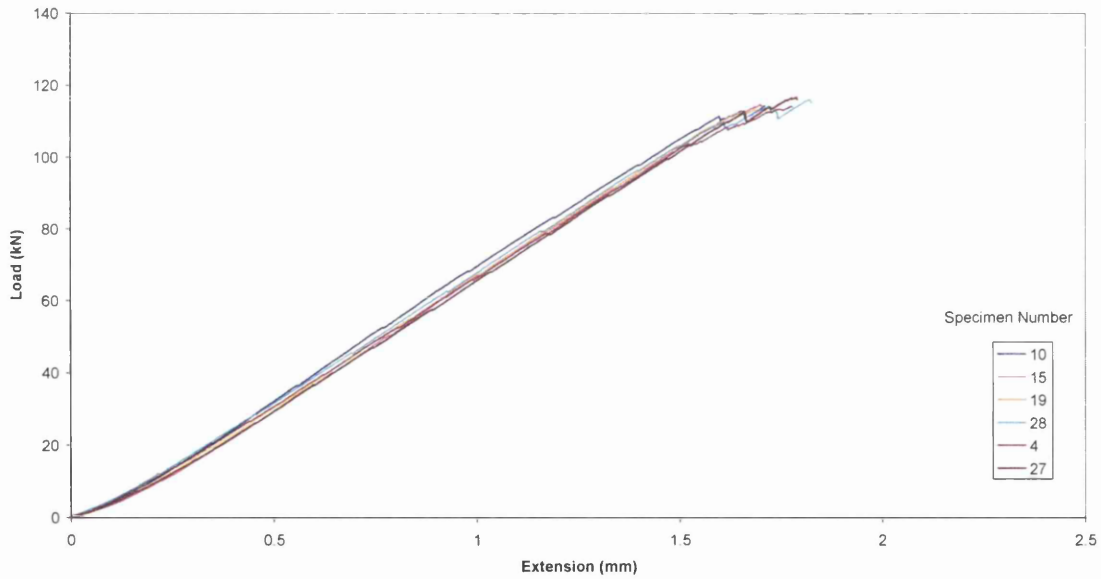

Figure A.17 Individual 12mm Lug Tests in the Dry State Tested at 90°C

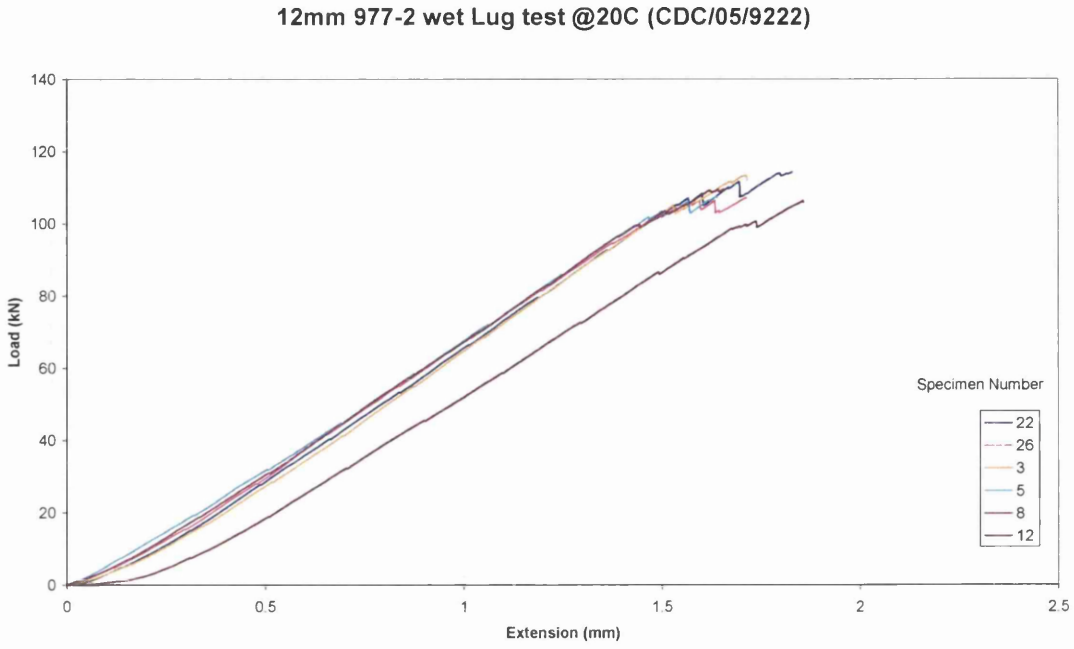

Figure A.18 Individual 12mm Lug Tests in the WET State Tested at 20°C

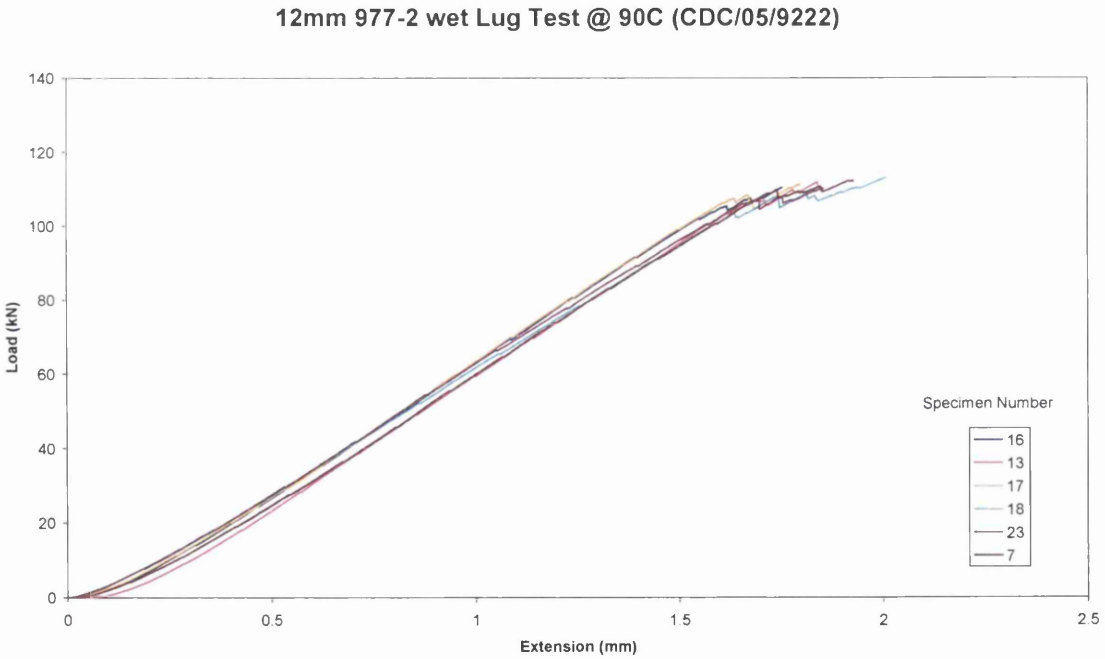

Figure A.19 Individual 12mm Lug Tests in the WET State Tested at 90°C

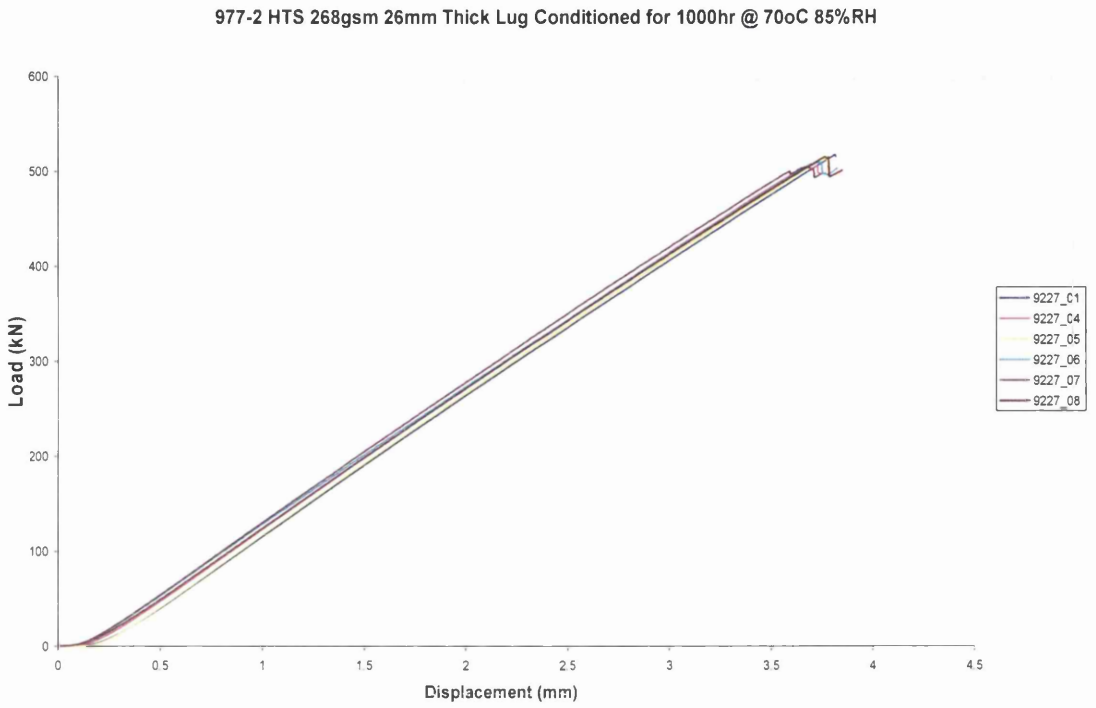

Figure A.20 Individual 26mm Lug Tests Conditioned for 1000hrs at 70°C/85%RH Tested at 90°C

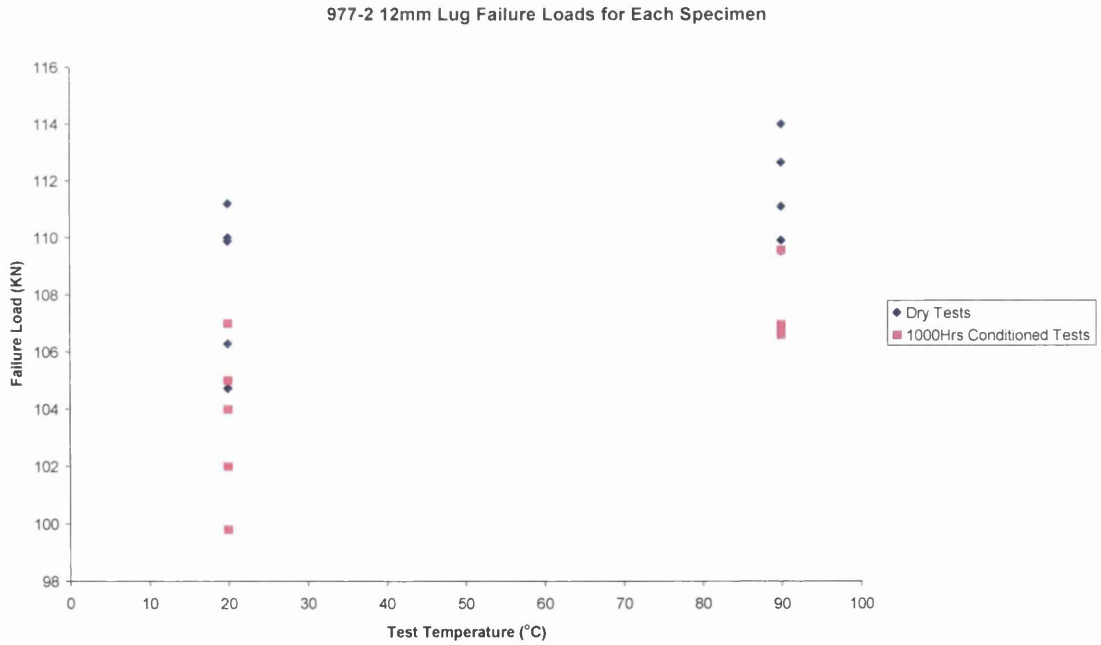

Figure A.21 Individual 12mm Lug Failure Load for Dry & WET Specimens

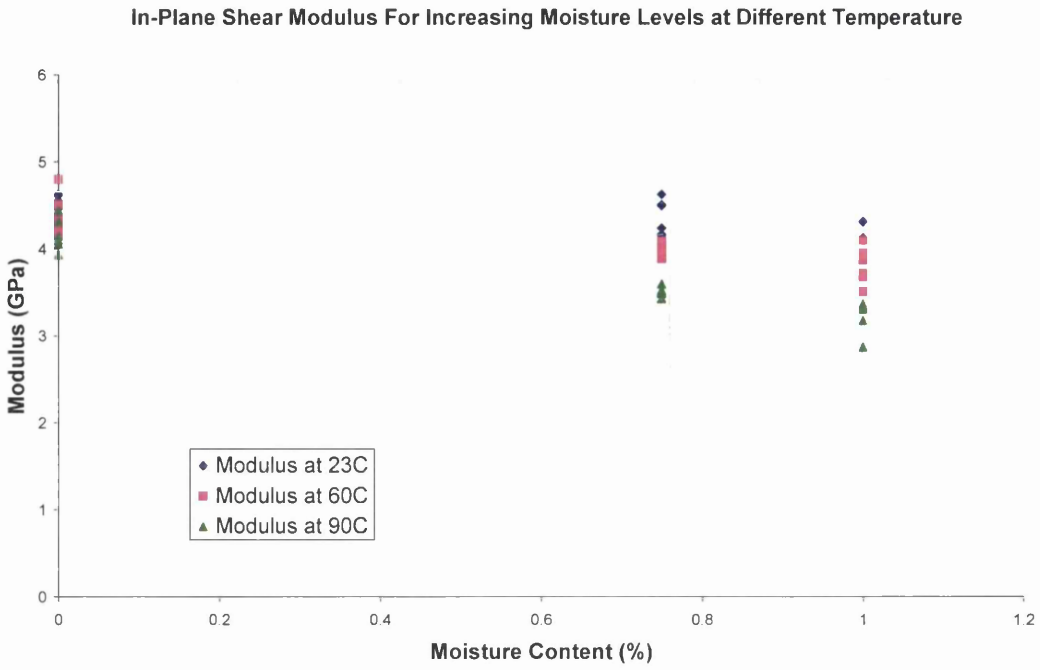

Figure A.22 EMOC In-Plane Shear Modulus Data for 977-2 Showing Individual Coupon Tests

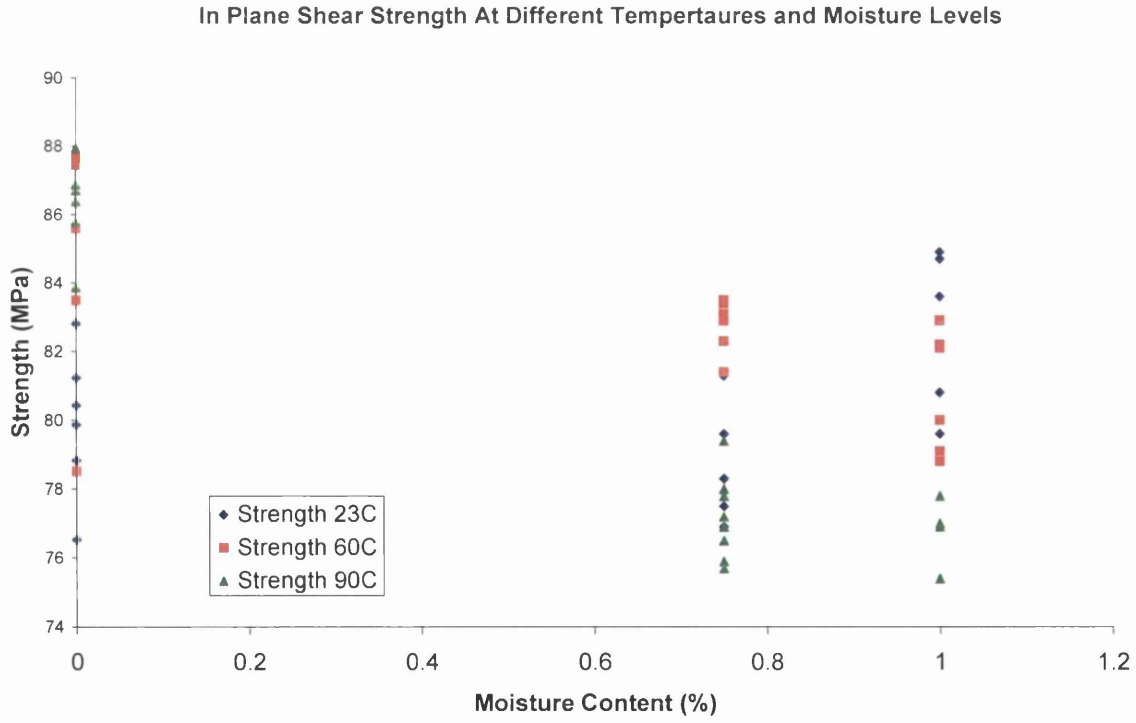

Figure A.23 EMOC In-Plane Shear Strength Data for 977-2 Showing Individual Coupon Tests

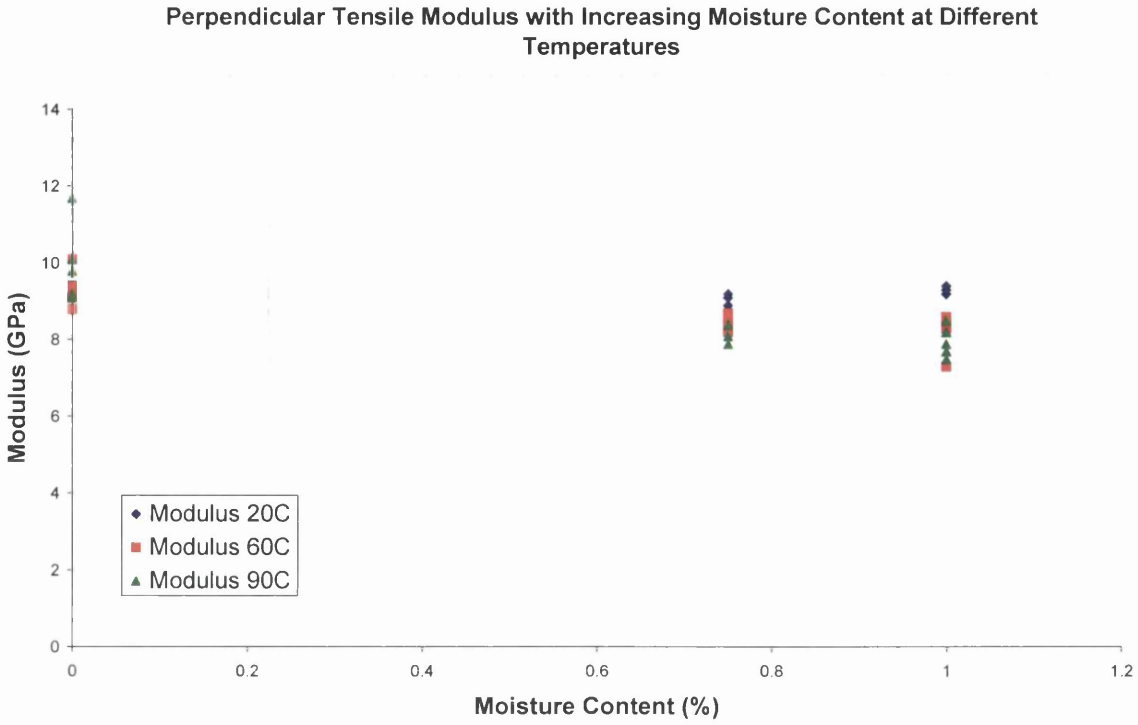

Figure A.24 EMOC 90° Orientation Lamina Tensile Modulus Data for 977-2 Showing Individual Coupon Tests

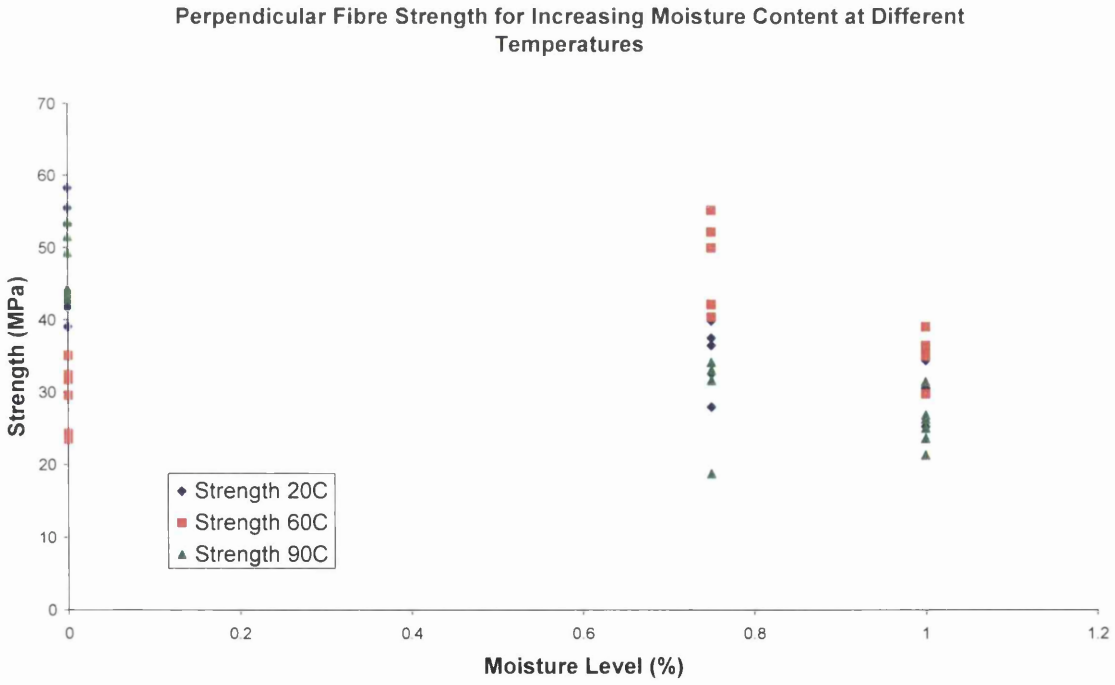

Figure A.25 EMOC 90° Orientation Lamina Tensile Strength Data for 977-2 Showing Individual Coupon Tests

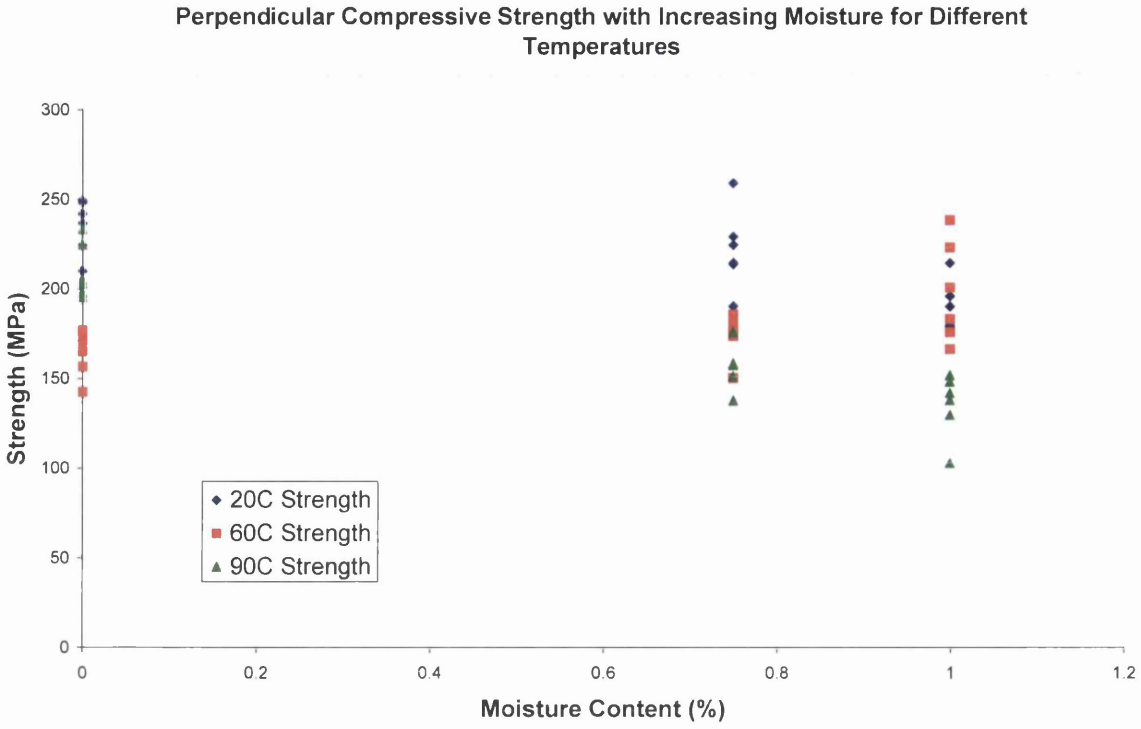

Figure A.26 EMOC 90° Orientation Lamina Compressive Strength Data for 977-2 Showing Individual Coupon Tests

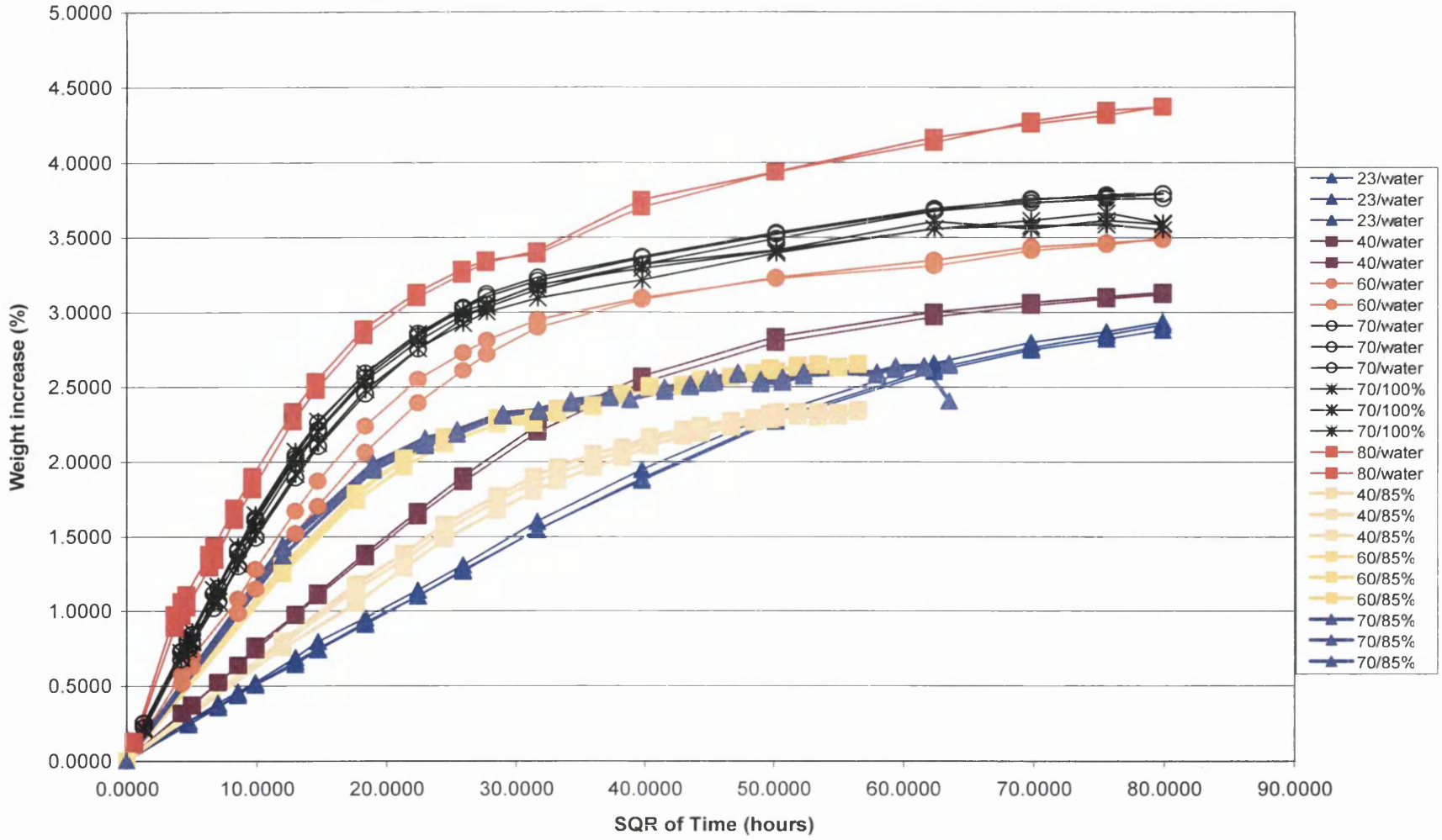

Figure A.27 EMOC Moisture Uptake Curves for 977-2 Material at Different Temperature & Humidities

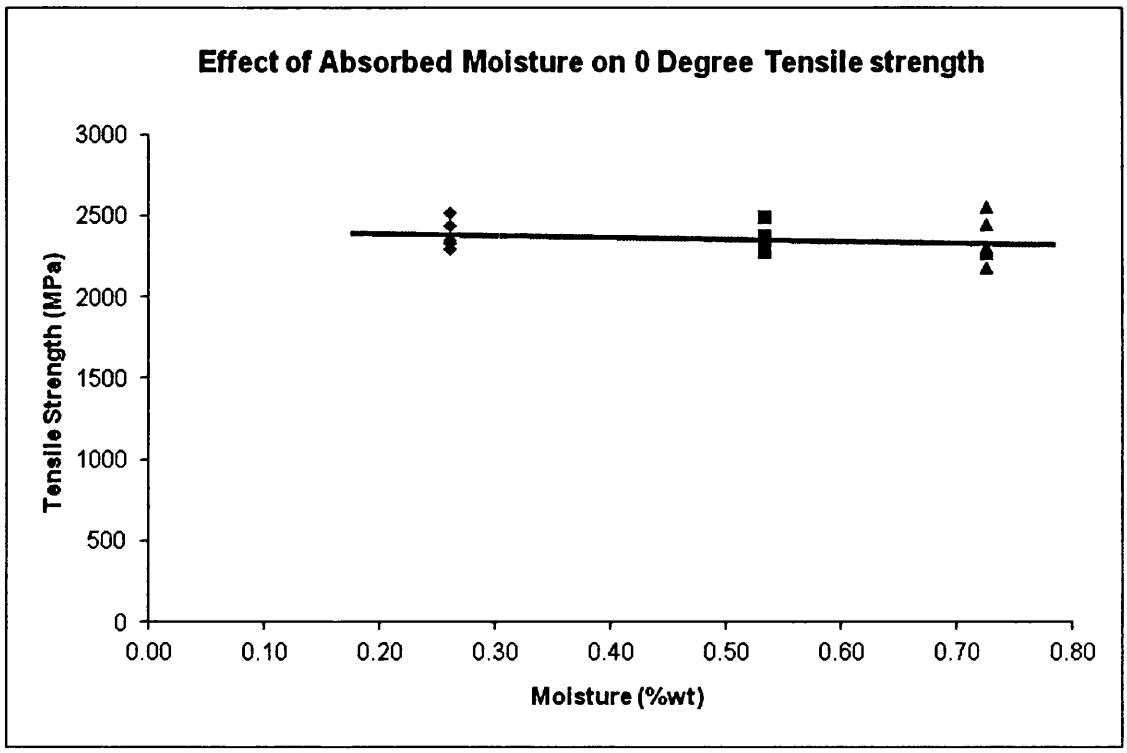

Figure A.28 PR2 Supporting PhD 0 Degree Tensile Strength Data at Room Temperature [41]

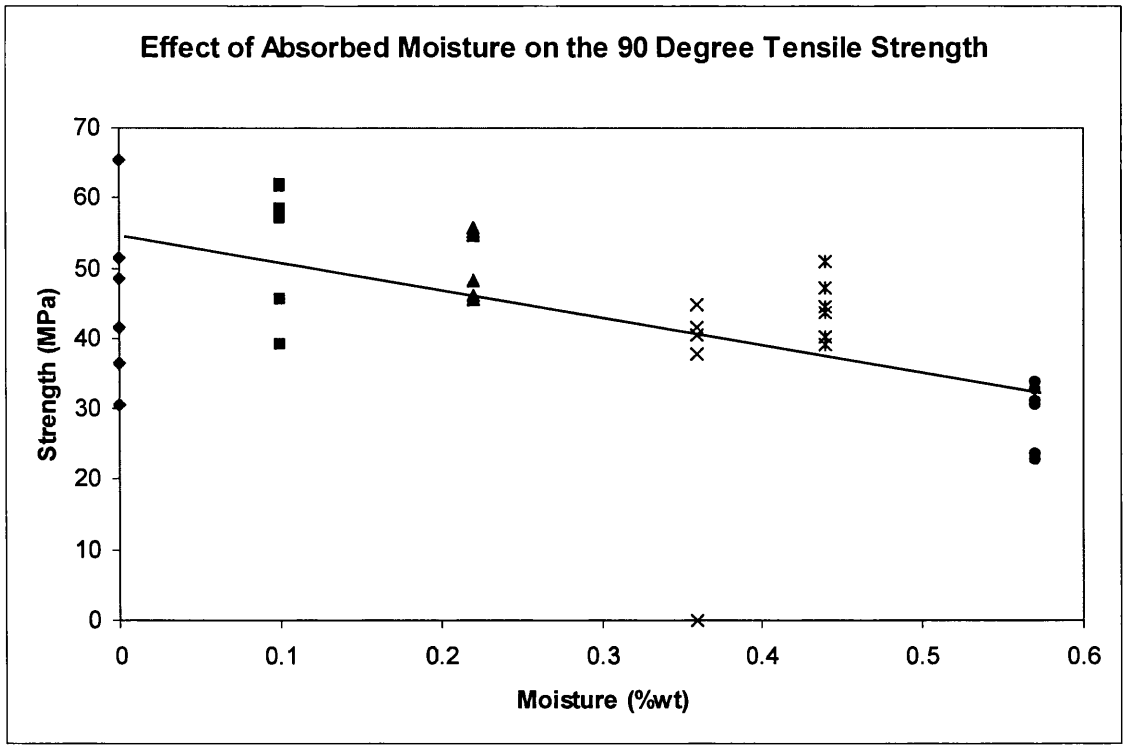

Figure A.29 PR2 Supporting PhD 90 Degree Tensile Strength Data at Room Temperature [41]

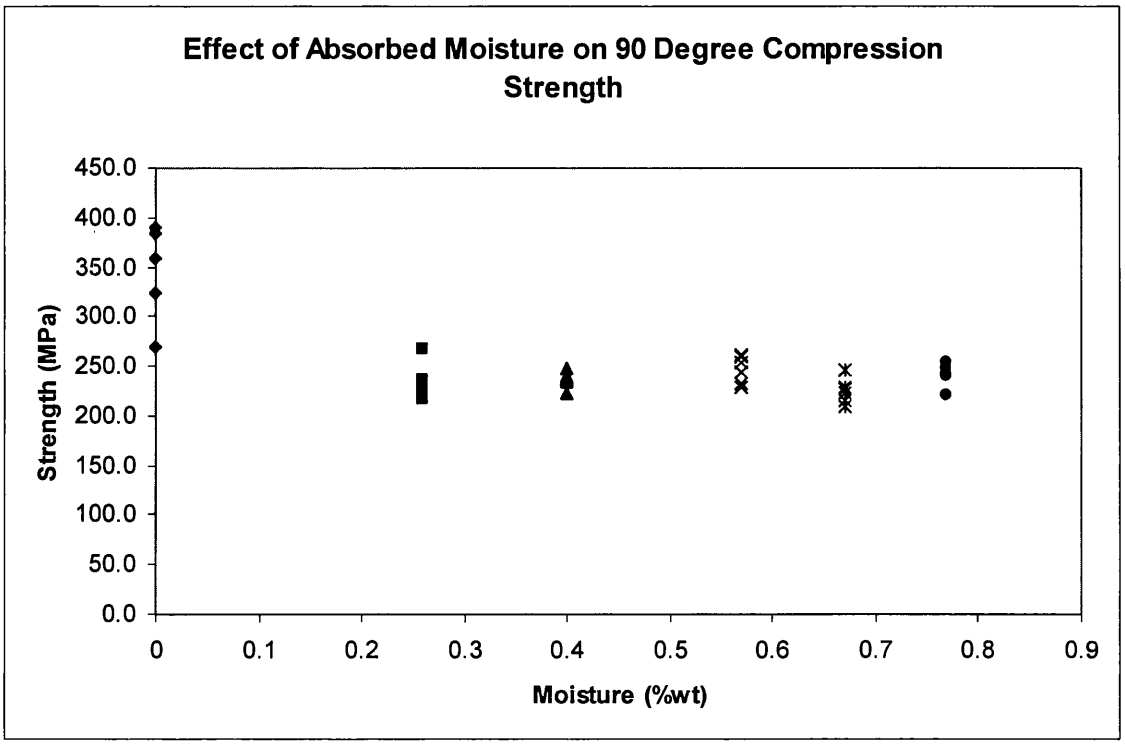

Figure A.30 PR2 Supporting PhD 90 Degree Compressive Strength Data at Room Temperature [41]

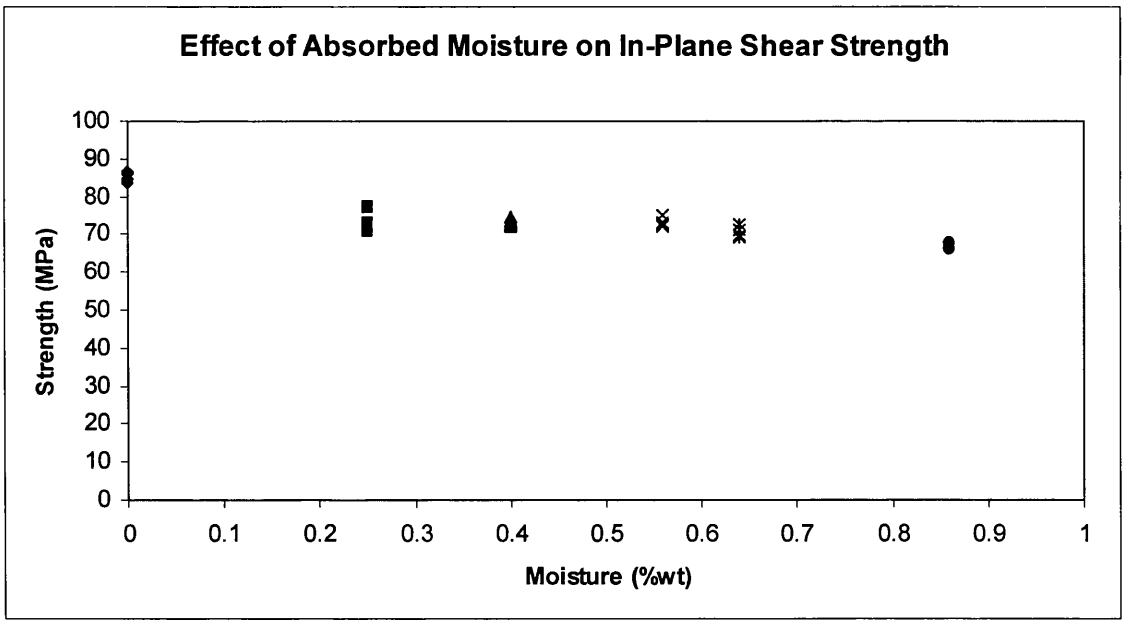

Figure A.31 PR2 Supporting PhD In-Plane Shear Strength Data at Room Temperature [41]

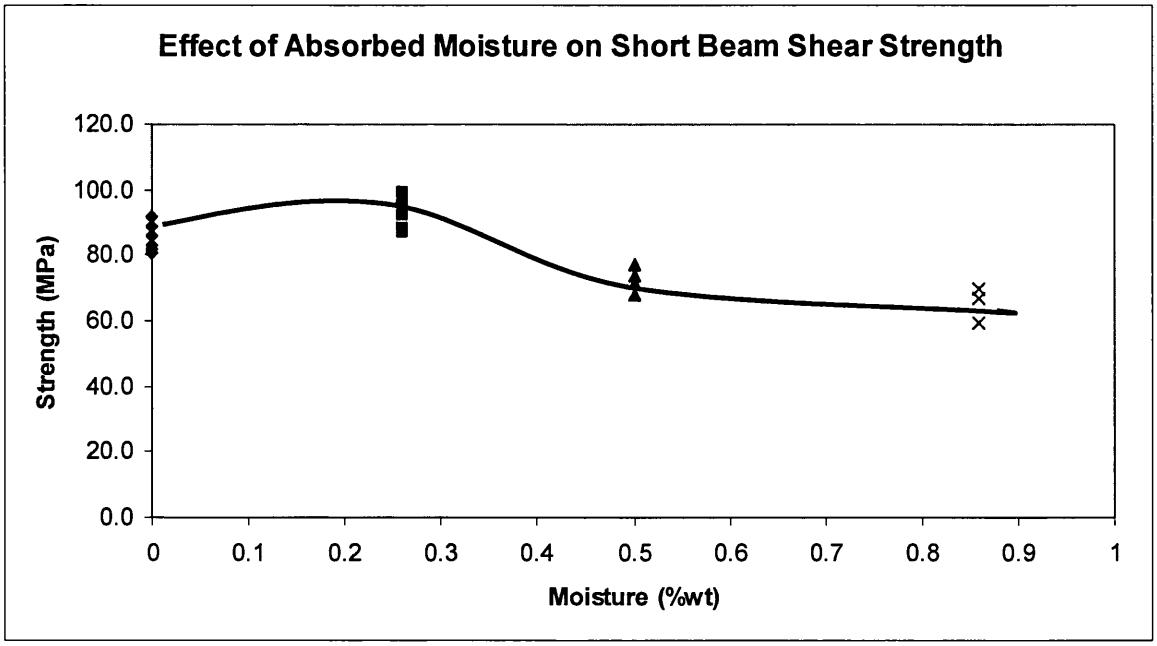

Figure A.32 PR2 Supporting PhD Inter-lamina Shear Strength Data at Room Temperature [41]

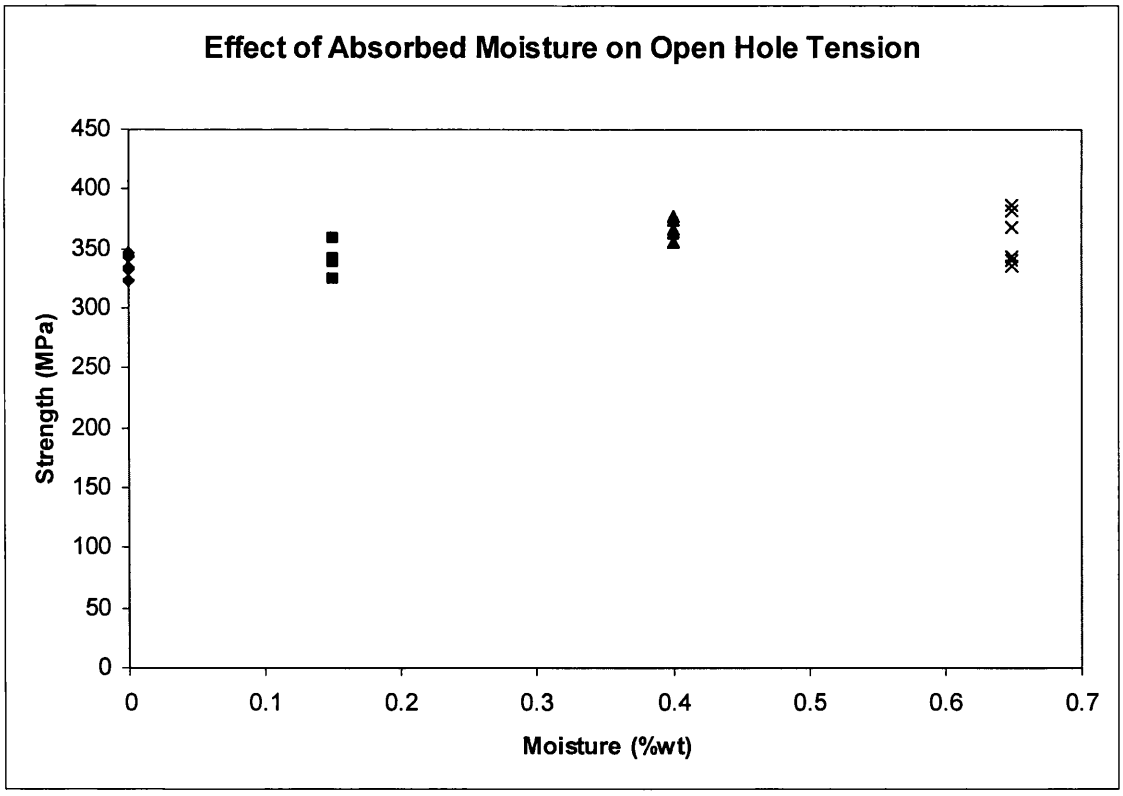

Figure A.33 PR2 Supporting PhD Open Hole Tensile Strength Data at Room Temperature [41]

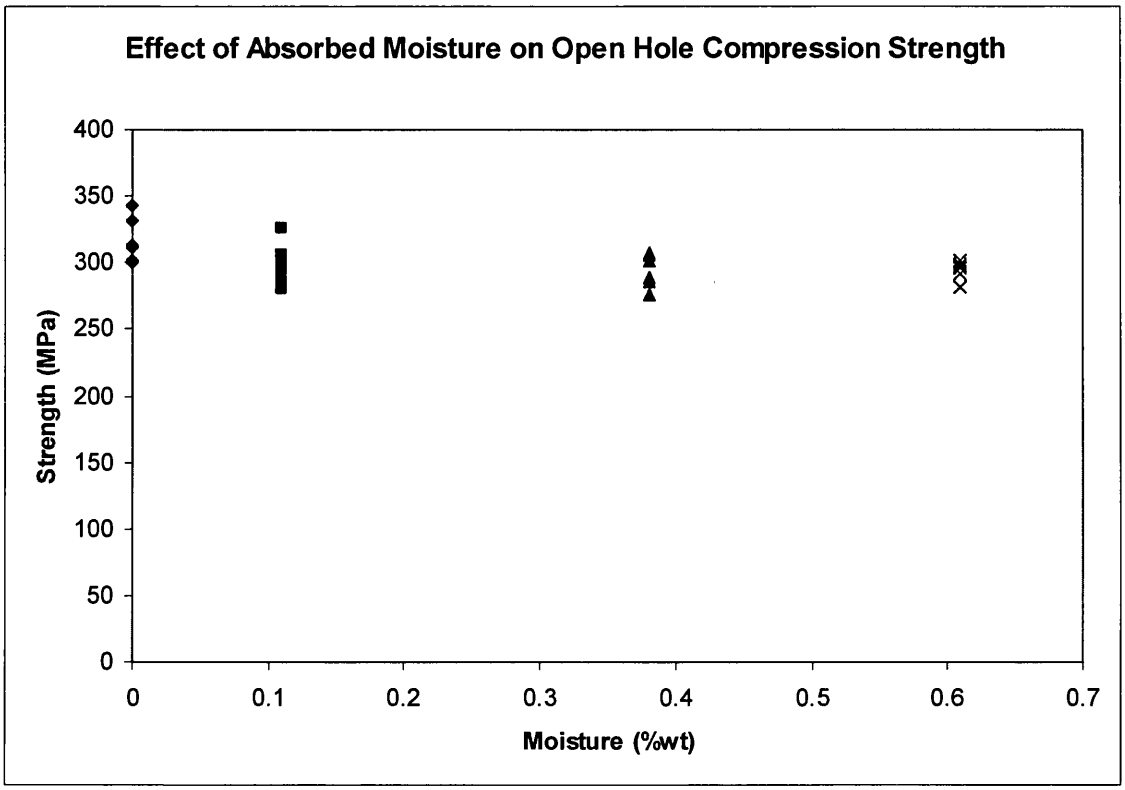

Figure A.34 PR2 Supporting PhD Open Hole Compression Strength Data at Room Temperature [41]